NUMERICAL STUDY OF THE IN-PLANE BEHAVIOUR OF CONCRETE MASONRY INFILLS BOUNDED BY STEEL FRAMES

by

Xi Chen

Submitted in partial fulfilment of the requirements
for the degree of Doctor of Philosophy
at

Dalhousie University
Halifax, Nova Scotia
August 2016

DEDICATION PAGE

This thesis is dedicated to my parents and my wife, who patiently supported me throughout and beyond measure. Thank you.

TABLE OF CONTENTS

LIST OF TABLES

LIST OF FIGURES

ABSTRACT

A finite element study was conducted to investigate the in-plane behaviour and strength of masonry infills bounded by steel frames with the focus on the effect of several influential parameters. In this study, two finite element models were developed using commercial software ANSYS adopting the simplified micro-modelling approach. The main difference of two models resided in the modeling technique used for simulating the mortar effect. The first model adopted a user-defined linkage element for mortar effect simulation whereas this was modelled by cohesive zone interface contact pairs in the second model. Both models were validated against experimental results available in the literature. Following the validation, the models were used in a series of studies to investigate the effect of several parameters on the stiffness and strength of infilled steel frames.

For the infill opening study, it was found that the presence of openings decreased the in-plane stiffness and strength of the infill, and the degree of this reduction was associated with the location of the opening. For the vertical loading study, it was found that when applied as a uniformly distributed load on the frame beam, the vertical load had an optimal load level and within this level, the vertical load was found to be beneficial to the lateral stiffness and strength of the infilled frame. When applied as point loads on columns, the vertical load was shown to reduce the lateral strength of the infilled frame. For the interfacial gap study, it was found that the top beam-infill gap was more detrimental to the stiffness and strength of infill than the side column-infill gaps. Gap(s) had less effect on infills bounded by weak frames than strong frames. In most cases, the reduction factor for the gap effect specified in the American masonry standard (MSJC 2013) produced conservative estimates for both the stiffness and strength. For the material and geometric property study, it was found that while grouting was beneficial to both the stiffness and strength of the infill, the loaded corner cells need to be grouted to achieve the maximum benefit. In terms of increasing stiffness and strength of the infills, the joint reinforcement showed a noticeable effect while the vertical reinforcement had almost negligible effect. Frame column stiffness had a greater effect on the behaviour of infilled system than the frame beam stiffness. However, the net strength of infill was less affected by either column or beam stiffness. Compared with the finite element results, the American masonry standard (MSJC 2013) generally underestimated the stiffness and strength of infills while the Canadian masonry standard (CSA S304-14) achieved a much better agreement.

Simplified analytical equations to account for the effect of the size and location of window openings; the uniformly distributed vertical load; and the size and location of gaps have been proposed respectively based on the regression analysis on finite element results. The proposed methods were shown to provide good agreement with both experimental and finite element results.

LIST OF SYMBOLS USED

A_b: cross-section of beam
A_c: cross-section of column
A_d: total cross-sectional area of the diagonal strut
A_{ni}: area of net mortared/grouted section across infill panel
A_0: area of opening
A_p: area of infill panel
A_w: cross-section of the masonry shear wall
C: an empirical constant that depends on the displacement of the infill and the damage the infill sustained
d: diagonal length of the infill
E_c: elastic modulus of concrete frame
E_d: Young's modulus of the infill along the diagonal direction which can be taken as E_m for simplicity
E_f: elastic modulus of frame
E_m: elastic modulus of masonry
E_{mortar}: Young's Modulus of mortar
e_c: eccentricity of the opening, measured from the center of opening to the center of infill panel
F_v: vertical load applied at columns;
f_1: Rankine tensile failure factor
f_2: Hill type compressive failure factor
f'_m: compressive strength of infill, unless otherwise specified, it is the compressive strength of masonry prism loaded parallel to the head joint
f'_{m0}: masonry strength when loaded in compression parallel to the head joint
f'_{m90}: masonry strength when loaded in compression parallel to the bed joint
f_{mx}: uniaxial compressive strengths of infills in x- direction
f_{my}: uniaxial compressive strengths of infills in y- direction
f_{tx}: uniaxial tensile strengths of infills in x- direction
f_{ty}: uniaxial tensile strengths of infills in y- direction
f_{vie}: expected shear strength of infill which shall not exceed the expected bed-joint shear strength.
G_m: shear modulus of masonry units, 0.4 E_m
G_{mortar}: shear modulus of mortar, 0.4 E_{mortar}
G_w: shear modulus of masonry wall
H: height of the column
H_{cr}: first cracking strength of infill
H_0: height of opening
H_u: horizontal ultimate load of infill for corner crushing mode
H_{ult}: total horizontal ultimate load of infilled frame

h: height of the infill
h_m: thickness of mortar joint between infill and frame
I_b: moment of inertia of beam
I_c: moment of inertia of column
K_{ana}: design stiffness obtained using analytical method
K_{CSA}: lateral stiffness calculated based on CSA S304
K_{FEM}: stiffness at crack load obtained from finite element analysis
K_{MSJC}: lateral stiffness calculated based on MSJC 2013
K_{col}: lateral stiffness of column
K_{cr}: lateral cracking stiffness of infill, the secant stiffness obtained at the crack load
K_{exp}: lateral stiffness obtained from the experimental tests
K_i: initial lateral stiffness of the test specimens
K_1: shape coefficient of the cross section
K_w: lateral stiffness of the masonry shear wall
k: factor to account for the presence of vertical load
k_n: unit area stiffness of a normal spring
k_{nf}: unit area normal stiffness of a contact element between frame and infill
k_{ns}: unit area stiffness of a shear spring
L: length of the beam
L_0: length of opening
l: length of the infill
M_F: modification factor applied to strut width to account for the presence of vertical load
M_{pb}: plastic moment capacity of beam.
M_{pj}: minimum value of the plastic moment capacity of beam or column,
M_{pc}: plastic moment capacity of column.
m: non-dimensional frame-to-wall strength ratio
P_{FEM}: ultimate load obtained from finite element analysis
P_{EXP}: lateral strength of infilled frame obtained from experimental tests
P_{net}: the net lateral strength of infills, which is calculated as the ultimate strength of the infilled system, subtracted by the corresponding load for a bare frame at the same displacement
P_u: ultimate lateral strength of infilled frame obtained from the either design standard or finite element model
p: vertical load ratio, calculated as the vertical load divvied by the total axial capacity of infills and columns
R_c: ultimate diagonal load of infill for corner crushing mode
R_F: reduction factor on the diagonal strut width to account for the presence of opening
$R_{F(\mathrm{ana})}$: reduction factor obtained from analytical methods

$R_{F(\exp)}$: reduction factor obtained from test results
r: aspect ratio, h/l
t: thickness of infill
t_{eff}: effective thickness of infill
t_{net}: net thickness of infill
V: vertical load level, taken as percentage of the axial capacity of two 350W W250x58 columns
V_c: vertical load transferred by through two columns
v: Poisson's ratio of infill
w: width of diagonal strut
w_{ec}: effective width of diagonal strut at first cracking load
w_{et}: effective width of diagonal strut at ultimate load
z: aspect ratio coefficient
α: weight of the shear stress contribution to the tension failure, taken as 1.25 in this study
α_b: ratio of the beam contact length to the length of the beam
α_c: ratio of the column contact length to the height of the column
α_h: contact length between infill and column
α_l: contact length between infill and beam
β: coupling factor between normal stresses in x- and y- directions, taken as -1.0 in this study
β_o: a nominal reduction factor to account for non-ideal plasticity of the frame, $\beta_o \leq 0.2$
γ: weight of the shear stress contribution to the compression failure, taken as 5.5 in this study
γ_p: masonry compressive strength penalty factor
ε_v: axial strain in column caused by vertical load
ε_m: infill failure strain
θ: angle whose tangent is the infill height-to-length aspect ratio, radians
θ_0: aspect angle of opening
λ: relative infill-to-frame stiffness coefficient used to determine equivalent width of infill strut
λ^*: a generalized correlation parameter to defines the ratio w/ d proposed by Papia et al. (2003)
λH: dimensionless relative infill-to-frame stiffness factor determined from column properties
λL: dimensionless relative infill-to-frame stiffness factor determined from beam properties
μ: coefficient of friction of the frame/infill interface
σ_b: normal contact stress along the beam
σ_{bo}: upper bound of normal contact stress along the beam

σ_c: normal contact stress along the column

σ_{co}: upper bound of normal contact stress along the column

σ_x: normal stress in the x- direction

σ_y: normal stress in the y- direction

τ_b: shear stress along the beam, $\tau_{b=}\mu\sigma_b$

τ_{xy}: shear stress at the node

τ_t: shear strength of the cohesive interface

φ: internal friction angle of the cohesive interface

φ_{st}: strut width reduction factor when calculating stiffness issued by CSA S304-14, $\varphi_{st} = 0.5$

ACKNOWLEDGEMENT

Sincere thanks to my supervisor Dr. Yi Liu, who provided valuable guidance and insights throughout the course of this research. Her encouragement and support has helped me through research challenges and to ultimately complete this work. Thanks to my committee members Dr. Newhook and Dr. Garagash and external member Dr. Shrive for reading my thesis and provide constructive comments and suggestions. I would also like to thank my friends Chris Mantha, Brittany McCallum, Phil Vickers and Vahid Farajkhah who helped me every step of the way of my life here in Canada. The finical support of this research was provided by the Canadian Concrete Masonry Producers Association, the Natural Sciences and Engineering Research Council of Canada and Dalhousie University. Their financial contributions are gratefully acknowledged. At last and definitely not the least, thanks to my mom and dad and my wife for believing in me and for their continuous support and encouragement throughout my study.

Chapter 1 Introduction

1.1 Background

Masonry walls built inside concrete or steel frames are commonly referred to as masonry infills. Different from individual masonry shear walls, the in plane lateral load resisting behaviour of infills is dependent on the interaction between the bounding frame and the infill. In general, masonry infills have been shown to contribute significantly to the lateral stiffness, strength, ductility and energy dissipation of the frame system. However, due to the complexity in determination of the exact extent of interaction between the infill and its bounding frame, the current design practice has been to treat infills as non-load bearing elements and design bounding frames for both gravity and lateral load. To reflect this design intention in construction, the infill has to be properly isolated from the bounding frame so it will not participate in the load sharing, and the lateral load resistance has to be realized using other structural elements. The resulting design may not be an economic one. When the infill is built in tight contact with the bounding frame with an intention for it to participate in the load sharing, its inherently large in-plane stiffness will attract additional forces to the frame area and change the behaviour and dynamic characteristics of the entire structure. If not designed properly, the strength and stability of the frame will be adversely affected. Thus, it is crucial to quantify the interaction between the masonry infill and its bounding frame so that the stiffness and strength contribution of the infill to the frame system can be accurately evaluated.

1.2 Research Overview and Design Practice

Both experimental and finite element studies have been conducted in an effort to better understand the infill-frame interaction and to provide some rational design approaches. A detailed literature review is presented in Chapter 2. Most of these studies focused on the development of the "diagonal strut method". This method treats the masonry infilled frame as a braced frame with the masonry infill replaced by an equivalent diagonal strut acting in compression to resist the lateral loading. Once the strut width is known, the stiffness of the system can be determined through a frame analysis and the strength of the infill can also be formulated as a function of the width. Since its inception, much research has been dedicated to proposing equations for the diagonal strut width that can simulate the actual stiffness of the infilled frames. Most of these equations were expressed as a function of some form of relative infill-to-frame stiffness ratio and infill geometry. These studies also showed that infills are capable of developing a number of possible failure mechanisms, depending on the strength and stiffness of the bounding frames with respect to those of the infills and the geometric configuration of the framing system. However since these equations were calibrated using experimental results to a specific set of testing parameters, none was found to provide universally satisfactory estimates for various infill and frame material and geometric properties. These studies did, however, show the complexity of masonry infilled systems as they are affected by material and geometric properties of both the frame and infill, the stiffness ratio of the frame and infill, and loading conditions. Largely scattered and even conflicting results were reported among some studies. In recent

years, finite element modelling has been increasingly used in the study of infilled frames in an effort to cover a wide range of parameters that often beyond the scope of experimental programs.

For design practice, the Canadian masonry design standard CSA S304 and the Masonry Structure Joint Committee standard MSJC 2013 are two governing standards for the design of infills in Canada and the United States respectively. Both standards adopted the diagonal strut method but with different formulations in calculating the strut width and infill strength. For the 2004 edition of the Canadian masonry standard CSA S304.1 (2004) on infill design in particular, design stiffness equations were based on studies conducted 40 years ago (Stafford-Smith, 1962, 1966; Stafford-Smith & Carter, 1969). On the other hand, the MSJC 2013 equations were largely based on the study conducted by Flanagan and Bennett (1999, 2001) on steel frames infilled with structural clay tiles. Performance assessment of the standard equations by Tucker (2007) and Liu and Soon (2012) indicated that the values obtained using CSA S304.1 and MSJC 2013 equations were in disparity with each other and with those obtained from experimental testing to different degrees. At the time of writing this thesis, CSA S304 was in the process of upgrading the infill design provision for the new edition to be published in 2014. This study thus served as a background research for the upgrade which has since been adopted in the latest edition of CSA S304 (2014). The upgrade is discussed in detail in Chapter 3.In addition, the guidelines contained in both standards are only intended for design of infills of simple situations. For more

complex cases such as gaps existing between the infill and the frame members, openings in the infill or combined lateral and vertical loading, the design standard provides no guidelines. The design methods contained in both standards are in need of validation with results covering a wide range of material and geometric parameters which are encountered in masonry infill construction as well as an upgrade to provide guidelines on the treatment of infills in those more complex situations.

1.3 Research Objectives

In view of the lack of comprehensive design guidelines of masonry infills in general, this research is designed to investigate the in-plane behaviour and strength of infilled steel frames with the focus on the infill itself. Early results from this study have already contributed to the upgrading of the infill design section in the CSA S304-14 edition, and it is expected that the rest of this study will further supplement the understanding of infill behaviour and result in the proposal of analytical methods.

A detailed description of objectives is as follows:

a) To compile and summarize results from existing experimental studies reported in the literature on masonry infills subjected to in-plane lateral loading, and to examine the validity of several analytical methods proposed by different researchers as well as standard design equations for the infill stiffness and strength calculation using the experimental results.

b) To develop a robust finite element model that is capable of simulating the in-plane behaviour and predicting the stiffness and the strength of masonry infills.

c) To conduct a series of in-depth parametric studies on the effect of several influential parameters on the stiffness and strength of infills. These parameters include masonry compressive strength, grouting extent and configuration, reinforcement, bounding frame stiffness, infill openings, frame-to-infill interfacial gaps, and the presence of vertical loading.

d) To assess the performance of design methods in the current standards for the infill design using the finite element results covering a wide range of material and geometric properties.

e) To propose analytical equations that can be adopted to consider the effect of the aforementioned parameters in the infill stiffness and strength calculation.

The contribution of this research will lie in the compilation of existing test results and the assessment of the current design standards of Canada and the United States; a comprehensive numerical study covering a wide range of parameters; and proposal of analytical equations that can be adopted for design.

1.4 Scope of the Thesis

This thesis is divided into nine chapters. Chapter 1 includes an introduction to the topic, description of research objectives and scope of the thesis. Chapter 2 presents a comprehensive literature review of various methods for infill stiffness and strength

calculations, North American masonry design standards and numerical modelling techniques. Chapter 3 compiles and summarizes results from existing experimental studies reported in the literature on masonry infills subjected to in-plane lateral loading; and assesses the validity of analytical equations proposed by several researchers as well as those specified in both CSA S304.1 and MSJC 2013 standards for the infill stiffness and strength calculation. Chapter 4 provides details of the two finite element models developed in this study and their validation using existing experimental results in the literature. Chapters 5 to 8 present a series of parametric studies using the models on the in-plane behaviour of concrete masonry infills bounded by steel frames. Chapter 5 studies the effect of infill opening size and location. Chapter 6 studies the effects of infill aspect ratio, masonry compressive strength, grouting extent and configuration, vertical and joint reinforcement, and the bounding frame stiffness. Chapter 7 investigates the effect of vertical load and its application manner. Chapter 8 investigates the effect of interfacial gaps between the infill and the bounding frame. The summary, main conclusions and recommendations from this study are given in Chapter 9.

Chapter 2 Literature Review

The available literature on the in-plane behaviour of infilled frames is high in volume. For clarity, this chapter is divided into three main sections. The first section provides a summary of available analytical methods proposed by various researchers for both stiffness and strength evaluation of the infilled system; the second section describes infill design guidelines contained in the current Canadian and American masonry standards; the third section is a review of state-of-the-art numerical techniques used in the analysis of masonry infilled frames. Each of Chapters 5 to 8 is dedicated to a numerical study conducted on a specific parameter or a group of parameters. Thus, a literature review on studies more pertinent to those parameters is included in each chapter for ease of reference.

2.1 General Behaviour

The mechanism of interaction between the infill and its bounding frame described by Holmes (1961) provided the theoretical background for "diagonal strut" method. At the initial loading stage, the frame and infill work together as a whole. As the lateral load increases, the infill and frame begin to separate due to the different deformation modes of the infill and frame but with a certain area remaining in contact. A further increase in the lateral load results in the development of cracks and changes in the contact area. At failure, two diagonal corners where the compression force is transferred remain in contact with the frame forming an equivalent diagonal strut action. Based on this observation, the "diagonal strut" method was proposed to consider the infill as a strut connecting two diagonal corners

of the frame as shown in Fig. 2.1.

The infill stiffness and strength can then be determined based on the width and the thickness of the strut where the thickness of the strut is often simply taken as the thickness of the infill. The width of the strut was found to be dependent on many factors such as infill and frame material and geometric characteristics, presence of gaps between the infill and frame, openings in the infill, and frame-to-infill stiffness ratio. Effects of these factors are interactive and complex and this, coupled with the high variability of masonry properties, makes the stiffness and strength evaluation of an infilled frame a challenge. The following section presents analytical methods proposed by various researchers for evaluating the stiffness and strength of infilled frames.

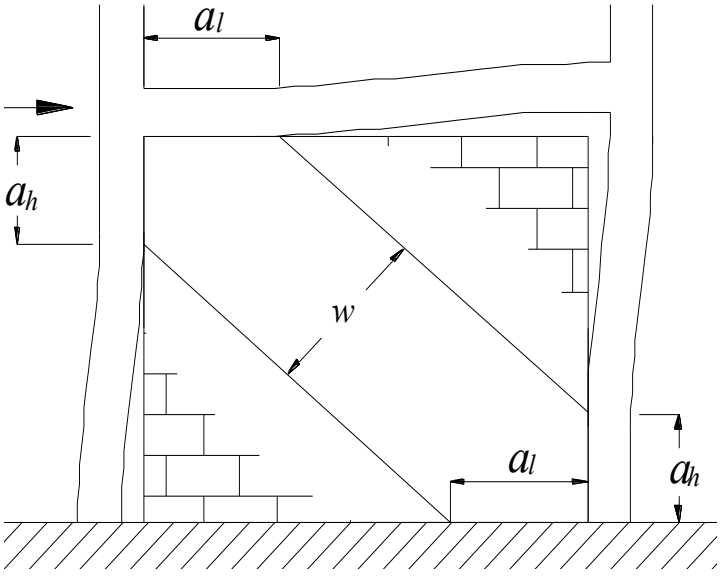

Fig. 2.1: "Diagonal strut concept" for in-plane behaviour of masonry infilled frames

2.2 Analytical Methods for Stiffness and Strength Consideration

2.2.1 Stiffness Models

Much research has been dedicated to proposing equations for the diagonal strut width, *w*,

that can simulate the stiffness of the infilled frames. Most of these equations expressed the strut width as a function of some form of the relative infill-to-frame stiffness ratio and infill geometry.

Based on the diagonal strut model and the results of seven series of experiments, Stafford-Smith (1966) proposed the equation to determine the contact length between the infill and frame column as:

$$\frac{\alpha_h}{H} = \frac{\pi}{2\lambda H} \tag{2.1}$$

In which λ is the relative stiffness of the infill to the frame and can be calculated as (Stafford-Smith & Carter, 1969):

$$\lambda = \sqrt[4]{\frac{E_m t \sin(2\theta)}{4E_f I_c H}} \tag{2.2}$$

where E_m and E_f are the elastic moduli of masonry and frame material respectively, t is the infill thickness, H is the height of the frame, I_c is the moment of inertia of the frame column, and $\theta = \tan^{-1}(h/l)$.

The parameter λ is often combined with H to form a non-dimensional parameter λH to express the relative stiffness of the infill to the frame. Curves for w/d as a function of λH were provided for determination of the width of strut w, where d is the diagonal length of the infill panel.

Mainstone (1971) conducted experiments on small-scale concrete and brick masonry

infilled frames and developed two sets of equations for the initial strut width w based on the curve-fitting of test results to predict the initial stiffness.

For brick infill:

$$\frac{w}{d} = 0.175(\lambda H)^{-0.4} \qquad 4 \le \lambda H \le 5 \tag{2.3}$$

$$\frac{w}{d} = 0.16(\lambda H)^{-0.3} \qquad \lambda H > 5 \tag{2.4}$$

For concrete infill:

$$\frac{w}{d} = 0.115(\lambda H)^{-0.4} \qquad 4 \le \lambda H \le 5 \tag{2.5}$$

$$\frac{w}{d} = 0.11(\lambda H)^{-0.3} \qquad \lambda H > 5 \tag{2.6}$$

where λ is defined as in Eqn (2.2) and H is the height of the frame.

Based on experimental results of Barua and Mallick (1976) and non-linear finite element analysis, Liauw and Kwan (1984) suggested that the width of strut be expressed as the lesser of the following:

$$w = \frac{0.86H\cos(\theta)}{\sqrt{\lambda H}} \tag{2.7}$$

$$w = 0.45H\cos(\theta) \tag{2.8}$$

Flanagan and Bennett (1999) proposed an empirical equation to calculate the width of the diagonal strut as:

$$w = \frac{\pi}{C\lambda\cos(\theta)} \tag{2.9}$$

where C is an empirical constant that depends on the displacement of the infill and the damage the infill has sustained. Flanagan and Bennett (2001) provided a table of values of

C for different infill and frame materials. Based on the various experimental results, a *C* value of 5 was proposed for all types of masonry infilled frames (SCT, CMU infills and RC frames) with a lateral displacement lower than 4 mm; a *C* value of 10 was proposed for infilled frames with a lateral displacement between 4 mm and 12 mm.

Some research has shown that single-strut models were inadequate in accurately predicting the force and moment in members of the bounding frame around loaded corners. Multi-strut models have thus been proposed to overcome such limitations (Thiruvengadam, 1985; Hamburger & Chakradeo, 1993; Chrysostomou et al., 2002; El-Dakhakhni et al., 2003).

One example of the multi-strut model is the "three-strut model" proposed by El-Dakhakhni et al. (2003) as shown in Fig. 2.2. It was suggested that two additional off-diagonal struts are required at the point of maximum moments in the beam and columns to reproduce the moments in these members.

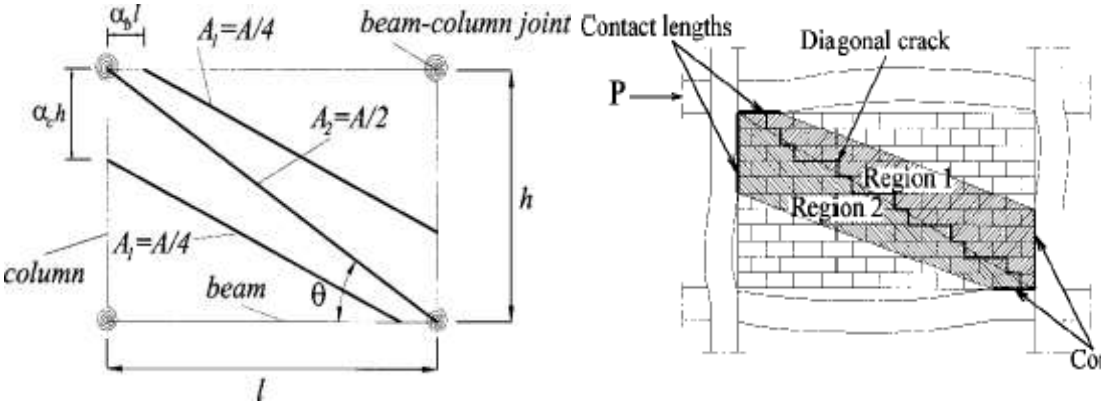

Fig. 2.2: Schematic view of the three-strut model (El-Dakhakhni et al., 2003)

The following equation was proposed for the total area of the struts:

$$A_d = \frac{(1-\alpha_c)\alpha_c Ht}{\cos(\theta)} \tag{2.10}$$

and α_c is defined as:

$$a_c H = \sqrt{\frac{2(M_{pj} + 0.2M_{pc})}{tf'_{m-0}}} \leq 0.4H \tag{2.11}$$

where f'_{m-0} is the compressive strength of masonry parallel to the bed joint, M_{pj} is the minimum value of the plastic moment capacity between the beam and column, M_{pc} is the plastic moment capacity of the column. The area A_d is split among three struts; the middle strut which connects two loaded corners took one-half of the area whereas the upper and lower strut took one-quarter of the area each.

Papia et al. (2003) proposed an analytical strut model for the stiffness of reinforced concrete infilled frame by introducing a correlation parameter λ^*, which can be calculated as:

$$\lambda^* = \frac{E_d}{E_f}\frac{tH}{A_c}\left(\frac{H^2}{L^2} + \frac{1}{4}\frac{A_c}{A_b}\frac{L}{H}\right) \tag{2.12}$$

where E_d is the Young's modulus of the infill along the diagonal direction which can be taken as E_m for simplicity, A_c and A_b are the cross-section areas of the column and beam respectively, and the rest of symbols are the same as previously defined. The ratio of strut width w to its diagonal length d is given by:

$$\frac{w}{d} = \frac{c}{z}\frac{1}{(\lambda^*)^\beta} \tag{2.13}$$

$$c = 0.249 - 0.0116v + 0.567v^2 \tag{2.14}$$

$$\beta = 0.146 + 0.0073v + 0.126v^2 \tag{2.15}$$

where z is the aspect ratio factor and $z = 0.75+0.25\times L/H$, v is the Poisson ratio of infill. Furthermore, Amato et al. (2008) and Campione et al. (2015) derived a vertical load factor k based on finite element results obtained by Cavaleri et al. (2004), which can be applied to Eq (2.16) to account for the presence of vertical loads applied at the beam-column joints. Eq (2.16) is then modified into

$$\frac{w}{d} = \frac{c}{z}\frac{k}{(\lambda^*)^{\beta}} \tag{2.16}$$

where $k = 1$ when there is no vertical load, and when vertical load exists:

$$k = 1 + (18\lambda^* + 200)\varepsilon_v \quad \text{(Amato et al., 2008)} \tag{2.17}$$

$$\text{or} \quad k = \frac{1}{z} + (18\lambda^* + 200)\varepsilon_v \quad \text{(Campione et al., 2015)} \tag{2.18}$$

where ε_v is the axial strain in column caused by vertical load, which can be calculated as $\varepsilon_v = \frac{F_v}{2A_cE_c}$ and F_v is the vertical load.

Based on regression analysis on the existing experimental data from steel frames infilled with CMU, Tucker (2007) proposed the following equation to determine the diagonal strut width, w and thus the stiffness of the masonry infilled system:

$$w = 0.25d(\lambda H)^{-1.15} \tag{2.19}$$

2.2.2 Strength Models

The strength of infills is shown to be dependent on failure modes of the system which are in turn affected by the geometric and configuration characteristics of the infill and the frame.

For in-plane lateral loaded infilled frames, five failure modes have been identified, and they are described as follows:

Corner Crushing Failure (CC) – Crushing at the two loaded corners of the infill.

Compression Strut (CS) – Crushing in the central region of the infill, which happens when the diagonal strut is slender that causes the out-of-plane buckling of the infill.

Sliding Shear (SS) – Sliding along the bed joints of the infill. This usually happens due to weak mortar joints and strong frame members.

Diagonal Tension Failure (DT) – Diagonal cracking along the two loaded corners of the infill. This failure mode is often associated with the weak frame and strong infill.

Frame Failure (FF) – Columns of the frame yielding in flexure or failed in compression due to an exceptionally strong infill.

For most tested steel and concrete infilled frames, the failure mode is characterized by the development of diagonal cracking and corner crushing at failure. The frame failure is the least likely failure mode. In view of this, most past research focused on the studies of first cracking strength and corner crushing strength and the analytical models reported in the literature reflected this focus.

Holmes (1961) gave the following formula to calculate the crushing load for infilled steel frames.

$$H_{ult} = \frac{24E_f I_c \varepsilon_m d}{H^3 (1 + \frac{I_c}{I_b} \cot(\theta)) \cos(\theta)} + A_d f'_m \cos(\theta) \tag{2.20}$$

where ε_m is the infill failure strain, d is the length of the diagonal strut, f'_m is the compressive strength of infill, and A_d is the strut area which is calculated as $A_d = t \times d/3$ and t is the thickness of the infill. The rest of symbols are the same as previously defined.

The ultimate diagonal load of infill for corner crushing mode given by Stafford-Smith and Carter (1969) can be described as:

$$R_c = \frac{tf'_m \pi}{2\lambda \cos(\theta)} \tag{2.21}$$

where f'_m is the compressive strength of infill, λ is defined in Eqn (2.2). The diagonal load R_c should be converted to corresponding lateral load by the following formula:

$$H_u = R_c \cos\theta \tag{2.22}$$

Mainstone (1971) proposed the formulas for first cracking strength H_{cr} and corner-crushing strength H_{ult} respectively as follows:

$$H_{cr} = f'_t w_{et} t \cos(\theta) \tag{2.23}$$

$$H_u = f'_m w_{ec} t \cos(\theta) \tag{2.24}$$

where t is the thickness of infill, f'_t is the tensile strength of infill, w_{ec} and w_{et} are the effective width of the diagonal strut at first cracking load and ultimate load respectively. According to the infill type and λH value, Mainstone has developed four equations to calculated w_{ec} and w_{et} respectively.

For brick infill:

$$\frac{w_{et}}{d} = 0.17(\lambda H)^{-0.4} \qquad 4 \le \lambda H \le 5 \tag{2.25}$$

$$\frac{w_{et}}{d} = 0.15(\lambda H)^{-0.3} \qquad \lambda H > 5 \tag{2.26}$$

$$\frac{w_{ec}}{d} = 0.56(\lambda H)^{-0.875} \qquad 4 \le \lambda H \le 5 \tag{2.27}$$

$$\frac{w_{ec}}{d} = 0.52(\lambda H)^{-0.8} \qquad \lambda H > 5 \tag{2.28}$$

For concrete infill:

$$\frac{w_{et}}{d} = 0.255(\lambda H)^{-0.4} \qquad 4 \le \lambda H \le 5 \tag{2.29}$$

$$\frac{w_{et}}{d} = 0.22(\lambda H)^{-0.3} \qquad \lambda H > 5 \tag{2.30}$$

$$\frac{w_{ec}}{d} = 0.84(\lambda H)^{-0.875} \qquad 4 \le \lambda H \le 5 \tag{2.31}$$

$$\frac{w_{ec}}{d} = 0.78(\lambda H)^{-0.8} \qquad \lambda H > 5 \tag{2.32}$$

Liauw and Kwan (1985) proposed a formula to calculate the lateral load H_u as follows for each failure mode:

For Corner Crushing/Column Failure:

$$H_{ult} = \sqrt{\frac{2(M_{pj} + M_{pc})}{f'_m \cdot t \cdot h^2}} f'_m \cdot t \cdot h \tag{2.33}$$

For Corner Crushing/Beam Failure:

$$H_{ult} = \sqrt{\frac{2(M_{pj} + M_{pb})}{f'_m \cdot t \cdot h^2}} \frac{f'_m \cdot t \cdot h}{\tan\theta} \tag{2.34}$$

Diagonal Crushing/ Beam-connection Failure:

$$H_{ult} = \frac{4M_{pj}}{h} + \frac{f'_m \cdot t \cdot h}{6} \tag{2.35}$$

Diagonal Crushing/ Column-connection Failure:

$$H_{ult} = \frac{4M_{pj}}{h} + \frac{f'_m \cdot t \cdot h}{6\tan^2(\theta)} \tag{2.36}$$

where, M_{pc} and M_{pb} are the plastic moment capacity of column and beam, respectively; M_{pj} is the plastic moment capacity of the joint, which is taken as the smaller value of M_{pc} and M_{pb} for the moment-resisting frame.

Wood (1978) suggested that due to the non-ideal plasticity of masonry, masonry cannot reach its full crushing stress at failure; a penalty factor γ_p should be applied to the masonry compressive strength. He proposed that the penalty factor γ_p be calculated as:

$$\gamma_p = 2.663m^2 - 1.371m + 0.406 \leq 0.45 \tag{2.37}$$

where m is the non-dimensional ratio for frame-to-wall strength which is calculated as:

$$m = \frac{8M_{pj}}{f'_m t L^2} \tag{2.38}$$

Some researchers (McBride, 1984; Flanagan & Bennett, 2001) found that using the penalty factor in conjunction with the method by Liauw and Kwan (1985) produced an accurate prediction of the ultimate load.

Based on the diagonal strut analogy, Stafford-Smith and Coull (1991) developed an empirical formula for the corner crushing strength of masonry infill as follows.

$$H_u = 1.12 f'_m ht \left(\frac{4E_f I_c}{E_m t h^3} \right)^{0.22} \cos^2 \theta \tag{2.39}$$

The symbols are the same as previously defined.

Saneinejad and Hobbs (1995) proposed a method which considered the inelastic behaviour of infills and steel frames to calculate the corner crushing strength of the infill.

$$H_u = \sigma_c t(1-\alpha_c)\alpha_c h + \tau_b t \alpha_b L \tag{2.40}$$

where σ_c is a normal contact stress along the column, $\alpha_c h$ is the contact length along the column, τ_b is the shear stress along the beam, and $\alpha_b L$ is the contact length along the beam. The shear stress along the beam is determined as:

$$\tau_b = \mu \sigma_b \tag{2.41}$$

where μ is the coefficient of friction of the frame/infill interface and σ_b is the normal contact stress along the beam.

The contact stress lengths are determined as follows:

$$\alpha_c h = \sqrt{\frac{2M_{pj} + 2\beta_o M_{pc}}{\sigma_{co} t}} \le 0.4h \tag{2.42}$$

$$\alpha_b L = \sqrt{\frac{2M_{pj} + 2\beta_o M_{pb}}{\sigma_{bo} t}} \le 0.4L \tag{2.43}$$

where β_o is a nominal reduction factor to account for non-ideal plasticity of the frame and an upper bound value of 0.2 for β_o was suggested. The column and beam normal contact stresses are determined from the upper bound contact stresses, σ_{co}, and σ_{bo}:

$$\sigma_{co} = \frac{f'_m}{\sqrt{1+3\mu^2 r^4}} \tag{2.44}$$

$$\sigma_{bo} = \frac{f'_m}{\sqrt{1+3\mu^2}} \tag{2.45}$$

where r is the aspect ratio ($h/l < 1.0$). The actual normal contact stresses can be obtained

as:

$$\sigma_b = \sigma_{bo} \text{ and } \sigma_c = \sigma_{co}\left(\frac{A_b}{A_c}\right) \text{ if } A_c > A_b \tag{2.46}$$

$$\sigma_b = \sigma_{bo}\left(\frac{A_c}{A_b}\right) \text{ and } \sigma_c = \sigma_{co} \text{ if } A_c \le A_b \tag{2.47}$$

$$A_c = r^2\sigma_{co}\alpha_c(1-\alpha_c-\mu r) \tag{2.48}$$

$$A_b = \sigma_{bo}\alpha_b(1-\alpha_b-\mu r) \tag{2.49}$$

From the formula of Mainstone (1971), the cracking load H_{cr} is expressed essentially as a product of the tensile strength of the masonry and the strut area. Since the tensile strength of masonry is often expressed in terms of $\sqrt{f'_m}$, a simplified cracking strength formula was developed by Flanagan and Bennett (1999) as:

$$H_{cr} = K_{cr} lt\sqrt{f'_m} \tag{2.50}$$

Flanagan and Bennett (1999) suggest that the frame properties and geometry have little effect on corner crushing strength, thus a simplified corner crushing strength formula is proposed as:

$$H_{ult} = K_u tf'_m \tag{2.51}$$

where K_{cr} and K_{ult} are empirical constants. Based on the tests of clay tile infilled steel frames, values of 0.066 mm and 246 mm for K_{cr} and K_{ult} respectively were suggested. Calibrated using 58 test results of both steel and concrete infill frames, Flanagan and Bennett (2001) proposed using of a K_{ult} of 243 mm to calculate the infill ultimate load.

Tucker (2007) compared the results from 13 analytical strength methods with test results

from 15 experimental programs at cracking load and ultimate load. Based on the comparison, Tucker proposed 6 new strength equations.

For concrete masonry units:

$$H_{cr} = 0.6wtf'_m\cos(\theta) \quad (2.52)$$

$$H_u = 1.05wtf'_m\cos(\theta) \quad (2.53)$$

For brick infill:

$$H_{cr} = wtf'_m\cos(\theta) \quad (2.54)$$

$$H_u = 1.9wtf'_m\cos(\theta) \quad (2.55)$$

For clay tile infill:

$$H_{cr} = 1.05wtf'_m\cos(\theta) \quad (2.56)$$

$$H_u = 2.4wtf'_m\cos(\theta) \quad (2.57)$$

where w is determined by Eqn (2.19) (Tucker, 2007).

2.3 Design Standards for the In-Plane Behaviour

2.3.1 Canadian Standard CSA 304.1

The Canadian masonry design standard, CSA S304.1, which adopts the semi-empirical formula proposed by Stafford-Smith (1966), suggests that the contact length between infill and frame column, α_h, and between infill and frame beam, α_l can be determined as:

$$a_h = \frac{\pi}{2}\sqrt[4]{\frac{4E_f I_c h}{E_m t \sin(2\theta)}} \quad (2.58)$$

$$a_l = \pi\sqrt[4]{\frac{4E_f I_b l}{E_m t \sin(2\theta)}} \quad (2.59)$$

Assuming a triangular stress distribution along the strut width, w (Hendry, 1981), the effective diagonal strut width shall be calculated as:

$$w = \frac{1}{2}\sqrt{\alpha_h{}^2 + \alpha_l{}^2} \le d/4 \tag{2.60}$$

The upper limit of *d/4* was prescribed empirically. It is noted that based on this research, an upgrade of the strut width calculation has been introduced in the latest Canadian masonry design standard CSA S304-14 where a reduction factor $\varphi_{st} = 0.5$ was adopted for the strut width when calculating stiffness.

The compressive strength of the diagonal strut shall be calculated using the compressive strength of masonry normal to the head face times the effective cross-sectional area of the diagonal strut. The effective cross-sectional area of the diagonal strut shall be the lesser of the effective cross-sectional areas parallel or normal to the bed-joints. Slenderness effects shall be included.

2.3.2 FEMA

The Federal Emergency Management Agency (FEMA) 273 (1997) NEHRP Guidelines for the Seismic Rehabilitation of Buildings and FEMA 356 (2000) Prestandard and Commentary for the Seismic Rehabilitation of Buildings provide following guidelines to evaluate the stiffness and strength of the infills. Both FEMA 273 and FEMA 356 adopted the diagonal strut method proposed by Mainstone (1971) as their evaluation model. The evaluation formula in the guideline is described as follows:

$$w = 0.175(\lambda H)^{-0.4} d \tag{2.61}$$

It should be noted that this formula is identical to Eqn (2.3) which was based on extensive experimental of brick infilled frames with $4 \le \lambda H \le 5$. The test results of Mehrabi et al.

(1996) suggested that this formula significantly underestimated the stiffness of concrete block infilled frames.

FEMA 273 (1997) and FEMA 356 (2000) do not provide a method to evaluate the corner crushing load of the infill. FEMA 306 (1998) Evaluation of Earthquake Damaged Concrete and Masonry Wall Buildings adopted the modified version of the method proposed by Stafford-Smith and Carter (1969) to calculate the corner crushing failure load. The lateral load H_u causing compression failure of the strut is calculated as:

$$H_u = wtf'_{m\text{-}90}\cos(\theta) \tag{2.62}$$

where w is the equivalent strut width calculated previously in Eqn (2.64) and f'_{m-90} is the masonry strength when loaded in compression parallel to the bed joint.

2.3.3 American Standard MSJC 2013

The American design standard MSJC 2013 adopts the method proposed by Flanagan and Bennett (1999, 2001) and the diagonal strut width is calculated as:

$$w = \frac{0.3}{\lambda \cos\theta} \tag{2.63}$$

The factor of 0.3 is used to account for the effect of damage sustained by the infills. It should be noted that in the calculation of λ, the MSJC 2013 specified that the thickness of the infill shall be taken as the effective thickness of the infill t_{net}. In the case of ungrouted infills, it is taken as the sum of the thickness of the faceshells of the block.

MSJC 2013 also provides an equation for corner crushing based on 68 test results of clay tile infilled steel frames. It is simple to use but seems to suggest that the strut width is a

constant term of 6 inches.

$$H_u = 6(\text{inch}) t_{net} f'_m \tag{2.64}$$

2.3.4 Eurocode 8

The European seismic design standard Eurocode 8 (1988) recommends that the equivalent diagonal strut width for determining stiffness shall be calculated as:

$$w = 0.15d \tag{2.65}$$

Eurocode 8 (2004) states that the strut width should take into account of the presence of openings and should not exceed $0.25l$ or $4t$ whichever is smaller. However, no provision on how to take openings into account was given.

For all design standards mentioned above, the design guidelines only apply for the ungrouted and fully grouted infill. All are silent on the treatment of partially grouted infills and none mention the effect of vertical or joint reinforcement. None of the standards provides any provisions on the effects of infill opening, interfacial gap(s) between the infill and the frame, and vertical load on the lateral resistance of the infill. It should be pointed out that all the proposed strength equations in Sections 2.2 and 2.3 are for the net strength of the infill except for the equations from Holmes (1961) and Liauw and Kwan (1985) which were intended for the total load capacity of the infilled frames.

2.4 Numerical Studies

In general, there are two main approaches that have been employed in the modeling of masonry infills, i.e. micro-modeling and macro-modelling. Micro-modelling focuses on

the modeling of discrete masonry components (i.e. masonry unit, mortar and the interface between them). Commonly, units and mortar joints are represented by continuum elements whereas the unit-mortar interface is represented by discontinuous elements. Micro-modeling studies are shown to give a better understanding of the local behaviour of masonry structures, and it allows the tracing of the developed stresses and cracks in the wall assembly. However, this type of modelling requires a detailed description of the material used and requires an excessively large number of elements and thus extensive computational time. Macro-modelling, on the other hand, considers the whole masonry assemblage as a composite continuum; units, mortar and unit-mortar interface are smeared out in one homogenous continuum. Macro-models are applicable when the structure is sufficiently large in dimensions so that the stresses along a macro-length are essentially uniform; however, it is not ideal in studying the failure patterns of masonry walls. The previously mentioned diagonal strut methods are examples of simple macro-models where the continuum infill is even further simplified by a truss element (strut). With the development of computer technology, the micro-modeling technique has been increasingly used in the numerical studies in the past 10 years.

Page (1979) was one of the first to use the micro-modeling approach to model plain masonry structures. Rectangular plane stress elements with isotropic properties were used to model the bricks in running bond. The bricks were bonded with joints that were modeled using a user-defined linkage element which has limited tensile strength, high compressive

strength, and nonlinear deformation characteristics. However this model was only developed for stiffness evaluation, and since it did not have a failure criterion for bricks, it cannot predict the ultimate load of the masonry structure.

Lourenço (1994, 1996) suggested that masonry micro-modelling has two forms: detailed micro-modelling and simplified micro-modelling. The detailed micro-modelling scheme requires the detailed knowledge of all material properties of masonry unit and mortar, especially the behaviour of the interface between the two materials whereas the simplified micro-modelling scheme simplifies the problem by lumping the mortar joint and the interface together. The finite element model proposed by Lourenço (1994,1996) modelled the mortar joint and interface using zero-thickness interface elements. All the damage and cracks that could occur in the head joints, bed joints, and masonry units were lumped in the weak interface elements; the geometry of the unit was expanded to include the thickness of the joint as shown in Fig. 2.3. This model was less accurate since the Poisson's ratio for mortar is ignored, but it improved the efficiency of the model significantly.

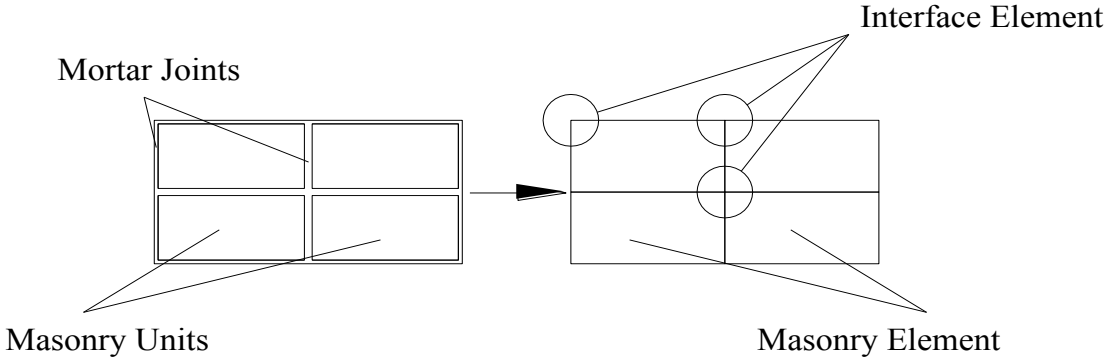

Fig. 2.3: Simplified micro-modeling approach (Lourenço, 1994)

Mehrabi and Shing (1997) developed a finite element model for the masonry infilled RC

frames. The smeared-crack finite element formulation proposed by Lotfi and Shing (1991) was employed to model concrete in the RC frame and masonry units in the infill panels and the cohesive crack formulation of Lotfi and Shing (1994) was adopted for interface elements. The mortar joints as well as the interfaces between infill and frame were modeled using two-node contact elements. A dilatant interface constitutive model for mortar was developed to account for the compressive hardening behaviour, the reversal of shear dilatancy, and the normal contraction of mortar interfaces. This model was successfully implemented for modeling the behaviour of a large variety of interfaces including rock joints and mortar joints. A bond-slip constitutive model was proposed and adopted for reinforced concrete structures. It was observed that although the bond-slip model improved the analytical response of a bare frame considerably, the influence of the bond-slip model on the behaviour of the infilled frames was insignificant.

Seah (1999) developed a simplified micro-model using a self-written C++ code which had the flexibility of considering a wide range of parameters. The masonry units were modeled as continuum connected by dimensionless joint elements. Joint elements consisted of rigid springs to force the nodes connected by joints to move in unison. Comparison of the numerical results with the results of 31 specimens conducted by Dawe et al. (2001) showed that the model was reasonably accurate. However, this mode only works for steel infilled frame and not RC frames.

Zucchini and Lourenço (2002, 2004, and 2007) adopted a homogenization technique

proposed by Lourenço (1995, 1996) and derived a basic periodic cell for modeling of masonry walls. The periodic cell then was homogenized into a continuum with appropriate deformation mechanisms which took into account the staggered alignment of the blocks. A damage model in tension and a Drucker–Prager plasticity model in compression for the homogenized wall were developed and incorporated into the iterative solution procedure to calculate the damage and the degradation and failure of masonry.

Al-Chaar and Mehrabi (2008) incorporated the modelling approach and the constitutive models proposed by Mehrabi and Shing (1997) with commercial software, DIANA for masonry infilled RC frames. Both the RC frame and the masonry infill wall were modelled as a smeared-crack continuum; the mortar joints were modelled using an interface model. To capture the cohesion, separation and shear degradation at the interface, Al-Chaar and Mehrabi (2008) proposed a Coulomb friction model combined with a tension cutoff and elliptical compression cap. One of the drawbacks of this modelling technique is that it cannot capture the cumulative damage in mortar joints when the infill is subjected to cyclic loading.

Stavridis and Shing (2010) adopted the model proposed by Mehrabi and Shing (1997) to capture different failure modes of the infilled system. Masonry infills and RC frames were modelled as rectangular smeared-crack continuum elements that were inter-connected with zero-thickness interface elements. In addition, interface brick elements were introduced at the middle of each block to account for possible splitting of each block. The comparison

of the numerical and experimental results indicated that the model is capable of capturing the highly nonlinear behaviour of the physical specimens and accurately predicting their strength and failure mechanisms. It showed that among all the material parameters, the mortar joint shear strength appeared to be the most influential in the accuracy of the model in simulating the behaviour around the cracking load.

In summary, although several finite element models have been proposed by various researchers, each has some limitations in its application. Mehrabi and Shing (1997)'s approach has the capability of simulating concrete frames and parameters of infills that were ignored by other researchers; however the resultant models (Mehrabi & Shing, 1997; Al-Chaar & Mehrabi, 2008; Stavridis & Shing, 2010) were too complicated and cumbersome to be used as a parametric study tool. They demand considerable computational time and consider factors such as the shear dilatancy of mortar joints and the bond-slip effect between rebar and concrete which have little impact on the behaviour of infilled frames. In addition, it required material properties input which are not commonly provided by engineering practice. The model from Dawe et al. (2001) was coded in C++, and it enabled the researcher to incorporate elements and failure criteria that commercial software does not support. But the source code is not in the public domain, which prevents its use by others. The model proposed by Zucchini and Lourenço (2002, 2004, and 2007) provided theoretical support for modeling the infill as a homogenized continuum. However, their homogenization method cannot be implemented using the elements and material

models provided by the commercial FE softwares (ANSYS, ABAQUS etc.). In addition, no attempts have been made in reported literature to adopt their algorithm to the modeling of infilled frames.

Chapter 3 Comparative Study of Existing Analytical Methods

3.1 Introduction

In the past six decades of research on masonry infilled frames, considerable experimental research has been conducted on masonry infills of various material and geometric properties. However, the results have, until recently, been scattered, and there is a lack of systematic summarization of these results in their categories of frame and infill material and geometric characteristics. This chapter is to compile and summarize results from existing experimental studies reported in the literature on masonry infills subjected to in-plane lateral loading; and to examine the validity of design equations proposed by several researchers as well as those specified in both CSA S304.1 and MSJC 2013 standards for the infill stiffness and strength calculation. Both steel and RC bounding frames were considered. Through this study, the performance of some existing analytical methods for infill design were examined and recommendations for the possible upgrading of design stiffness provisions in the Canadian standard were made.

3.2 Stiffness Method

In this section, the validity of several existing analytical stiffness equations was assessed with the available experimental results. These analytical equations include those suggested in the Canadian masonry design standard, CSA S304.1 and American standard MSJC 2013 as well as several proposed by researchers (Stafford-Smith, 1966; Mainstone, 1971; Liauw & Kwan, 1984; Eurocode 8, 1988; FEMA 356, 2000; Flanagan & Bennet, 2001; El-

Dakhakhni et al., 2003; Papia et al., 2003; Tucker, 2007). The design equations given by CSA S304.1 were described in Eqn (2.58) to Eqn (2.60) whereas the design equation given by MSJC 2013 was described in Eqn (2.63). As mentioned earlier, this study has resulted in an upgrade in the infill design provisions which were incorporated in the latest version of CSA 304-14. To demonstrate the rationale for this upgrade, the comparison study was made using CSA S304.1 (2004). The equations of other analytical methods were also described in Section 2.2 to 2.3. For the design equations given by Flanagan and Bennet (2001), a C value of 5 was adopted for the initial stiffness calculation since this value was obtained from the test results of infilled frames at a low displacement (4 mm); a C value of 10 was adopted for the cracking stiffness calculation since it was obtained from the test results of infilled frames experiencing diagonal cracking.

3.3 Strength Method

As mentioned in Chapter 2, compression strut failure or corner crushing has been identified to be the predominant failure mode for steel and RC infilled frames of typical material and geometric properties encountered in practice. Most analytical models were thus developed to predict the ultimate strength of infills corresponding to this failure mode. In both CSA S304.1 and MSJC 2013, compression failure strength or corner crushing strength is essentially a function of diagonal strut width and material compressive strength f'_m except that CSA S304.1 also considers the slenderness effect. While MSJC 2013 proposes a constant term of 152.4 mm (6 inches) for diagonal strut width in the strength calculation,

CSA S304.1 uses the strut width determined by Eqn (2.60) for strength calculation.

In addition to the standard equations, several strength methods proposed by various researchers are also evaluated. These methods included Mainstone (1971), Liauw and Kwan (1985), Stafford-Smith and Coull (1991), Saneinejad and Hobbs (1995), FEMA 306 (1998), Flanagan and Bennett (2001), and Tucker (2007). All methods were based on diagonal strut concept except for those proposed by Liauw and Kwan (1985) and Saneinejad and Hobbs (1995) which were based on the plastic collapse theory. The equations of above-mentioned methods were described in Section 2.2 to 2.3.

3.4 Experimental Studies

A total of 15 experimental studies were considered, which resulted in 66 specimens including 30 steel frames with concrete masonry unit (CMU) infills, 18 steel frames with structural clay tile (SCT) infills, and 18 concrete frames with brick or CMU infills. The experimental results are summarized in Tables 3.1 and 3.2 for steel infilled frames and in Table 3.3 for concrete infilled frames. Details of these specimens are listed in Table 3.4 for frames and in Tables 3.5 to 3.7 for infills. In the case of studies conducted by Henderson (1994) and Flanagan (1994) shown in Table 3.2, cyclic static displacements were applied to the specimens. The displacements were increased in amplitude to investigate the response throughout the full range of loading. In Table 3.2, the ultimate loads obtained from the hysteresis curves in both the pull and push directions were reported where the specimen designation ending with L indicates the pull direction results and the other

specimen in the pair show the push direction results. For other studies, a static loading or quasi-static loading was used where an in-plane lateral load was applied gradually to the frame top beam to the failure of the specimen.

Table 3.1: Experimental results – steel frames infilled with CMU

Author	ID	Experimental Results		
		K_i (kN/mm)	K_{cr} (kN/mm)	P_{exp} (kN)
McBride (1984)	WA1	72.9	54.9	471.0
	WA2	81.6	51.8	440.0
	WA3	73.8	69.0	463.0
	WA4	62.9	63.0	476.0
Yong (1984)	WB1	72.0	-	448.8
	WB2	74.0	74.0	556.0
	WB3	67.0	54.0	538.2
Riddington (1984)	2a	32.0	29.0	210.0
	2b	61.0	60.0	410.0
Amos (1985)	WC7	71.0	71.0	534.0
	WC8	65.0	65.0	445.0
	WC9	54.0	45.0	400.0
	WC10	68.0	53.0	458.0
Richardson (1986)	WD1	55.0	53.0	378.0
	WD2	63.0	44.0	445.0
	WD3	110.0	31.0	356.0
	WD4	73.0	43.0	467.0
	WD7	123.0	56.0	494.0
	WD8*	17.0	14.0	156.0
	WD9*	55.0	30.0	237.0
	WD10*	56.0	25.0	245.0
Hendry & Liauw (1991)	HN1	15.8	-	260.0
El-Dakhakhni (2002)	SP2	30.4	-	450.0
Liu & Soon (2012)	P1NA	27.1	19.9	111.0
	F1NA	38.8	22.7	156.9
	P3NA	35.4	24.9	93.8
	P3NI	17.9	13.1	78.9
	F3NA	56.4	26.9	131.7
	F3NI	21.4	18.4	121.9
	P6NA	29.7	23.4	104.2

*Pinned connection frame

Table 3.2: Experimental results – steel frames infilled with SCT

Author	ID	Experimental Results		
		K_i (kN/mm)	K_{cr} (kN/mm)	P_{exp} (kN)
Henderson (1994)	HW2		87.4	200.0
	HW2L		87.3	200.0
Flanagan (1994)	F1		14.7	122.0
	F1L		11.7	165.0
	F2		10.9	166.0
	F2L		17.8	183.0
	F3		-	158.0
	F3L		-	168.0
	F4		26.7	228.0
	F4L		13.7	149.0
	F5		23.2	191.0
	F5L		28.3	168.0
	F9		28.7	220.0
	F9L		32.0	207.0
	F17		18.5	212.0
	F17L		16.0	206.0
	F21		12.7	180.0
	F21L		13.2	203.0

Table 3.3: Experimental results – RC frames

Author	ID	Experimental Results		
		K_i (kN/mm)	K_{cr} (kN/mm)	P_{exp} (kN)
Fiorato et al. (1970)	S2B	-	-	41
	S2H	-	-	22
	S2I	-	-	28
Mainstone & Weeks (1972)	a1	135.0	65.0	440
	a2	75.0	55.0	480
	a3	50.0	25.0	310
	a4	315.0	265.0	1620
Angel (1994)	2a	46.9	-	-
	3a	47.6	-	-
	4a	68.3	-	209
	5a	219.9	-	-
	6a	38.2	-	-
	7a	89.1	-	-
	8a	44.5	-	-
Crisafulli (1997)	C1	-	27.3	43
	C2	-	-	95
Al-Chaar (1998)	2	95.8	-	84
	3	71.8	-	89

Table 3.4: Details of frames used in the experimental studies

		Frame		Moment of inertia	
		Height (mm)	Length (mm)	I_c (mm^4)	I_b (mm^4)
McBride (1984) Yong (1984) Amos (1985) Richardson (1986)	all	2800	3600	1.87E+07	4.58E+07
Riddington (1984)	2a	2710	2710	1.78E+07	1.78E+07
	2b	2485	2485	1.24E+08	1.24E+08
Hendry & Liauw (1991)	HN1	2375	2600	3.80E+06	3.80E+06
El-Dakhakhni (2002)	SP2	2874	3670	4.92E+07	4.92E+07
Liu & Soon (2012)	P1NA	1080	1080	4.77E+06	4.77E+06
	F1NA	1080	1080	4.77E+06	4.77E+06
	P3NA	1080	1351	4.77E+06	4.77E+06
	P3NI	1080	1351	1.61E+06	4.77E+06
	F3NA	1080	1351	4.77E+06	4.77E+06
	F3NI	1080	1351	1.61E+06	4.77E+06
	P6NA	1080	1758	4.77E+06	4.77E+06
Henderson (1994)	HW2	6223	7315	1.51E+07	1.86E+08
Flanagan (1999)	F1	2240	2240	9.13E+05	1.19E+08
	F2	2240	2240	7.03E+06	1.19E+08
	F3	2240	2240	2.22E+07	1.19E+08
	F4	2240	2240	4.04E+06	5.56E+08
	F5	2240	2240	1.20E+07	2.97E+08
	F9	2240	2240	7.17E+07	1.19E+08
	F17	2240	3450	7.03E+06	1.19E+08
	F21	2240	2840	7.03E+06	1.19E+08
Fiorato et al. (1970)	al	381	762	2.81E+06	2.25E+07
Mainstone & Weeks (1972)	al	2770	3360	8.48E+08	4.29E+08
Angel (1994)	all	1626	2438	7.20E+08	9.63E+08
Crisafulli (1997)	all	2000	2516	4.22E+07	1.00E+08
Al-Chaar (1998)	all	1327	1829	8.85E+07	8.09E+07

Table 3.5: Details of CMU infills used in the experimental studies

		Infill			
	ID	Thickness Infill/Faceshell (mm)		f'_m (MPa)	E_m (MPa)
McBride (1984)	WA1	190	66	27.4	23290
	WA2	190	66	27.7	23545
	WA3	190	66	26.5	22525
	WA4	190	66	24.4	20740
Yong (1984)	WB1	190	66	23.7	
	WB2	190	66	33.3	
	WB3	190	66	31.4	
Riddington (1984)	2a	100	62	18.1	15400
	2b	100	62	18.1	15400
Amos (1985)	WC7	190	66	33.4	19000
	WC8	190	66	33.3	17500
	WC9	190	66	21.7	17400
	WC10	190	66	23.5	13200
Richardson (1986)	WD1	190	66	25.9	10060
	WD2	190	66	24.8	13000
	WD3	190	66	23.1	13000
	WD4	190	66	22.6	8000
	WD7	190	66	25.4	18000
	WD8	190	66	28.1	17700
	WD9	190	66	24.6	19800
	WD10	190	66	25.3	17000
Hendry & Liauw (1991)	HN1	100	62	11.2	9520
El-Dakhakhni (2002)	SP2	140	64	13.4	11390
Liu & Soon (2012)	P1NA	64	43	8.6	10496
	F1NA	64	64	9.6	14430
	P3NA	64	43	7.3	10496
	P3NI	64	43	10.3	10496
	F3NA	64	64	10.3	14430
	F3NI	64	64	7.3	14430
	P6NA	64	43	10.3	10496

Table 3.6: Details of SCT infills used in the experimental studies

	ID	Thickness (Solid infills) (mm)	f'_m (MPa)	E_m (MPa)
Henderson (1994)	HW2	325	4.1	5300
Flanagan (1994)	F1	195	3	2300
	F2	195	3	2300
	F3	195	3	2300
	F4	325	2.6	2800
	F5	325	2.6	2800
	F9	195	3	2300
	F17	195	3	2300
	F21	195	3	2300

Table 3.7: Details of infills in the concrete infilled frame tests

	ID	Infill			
		Thickness (mm)	f'_m (MPa)	E_m (MPa)	Infill type
Fiorato et al. (1970)	S2B	22.2	26.5	15858	Brick
	S2H	22.2	26.5	15858	Brick
	S2I	22.2	26.5	15858	Brick
Mainstone (1971)	a1	110.0	9.0	6600	Brick
	a2	110.0	9.0	6600	Brick
	a3	70.0	9.0	6600	Brick
	a4	340.0	9.0	6600	Brick
Angel (1994)	2a	47.6	10.9	8046	Brick
	3a	47.6	10.1	5212	Brick
	4a	92.1	22.9	12438	CMU
	5a	142.9	21.5	11625	CMU
	6a	98.4	4.6	2137	Brick
	7a	98.4	11.0	2923	Brick
	8a	187.3	3.5	2358	Brick
Crisafulli (1997)	C1	75.0	19.3	11500	Concrete Brick
	C2	75.0	19.3	11500	
Al-Chaar (1998)	2	95.0	18.2	15470	CMU
	3	58.0	26.7	22695	Brick

The typical test set-ups used in these studies are shown in Fig. 3.1 (a) for infilled steel frames and in Fig. 3.1 (b) for infilled RC frames. In both cases, the frame connections were considered to be rigid.

a)

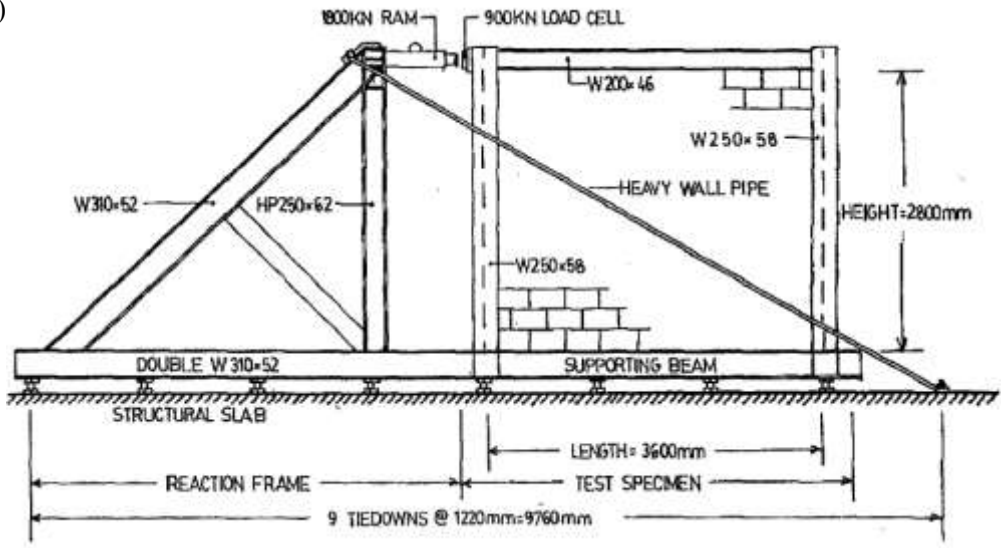

b)

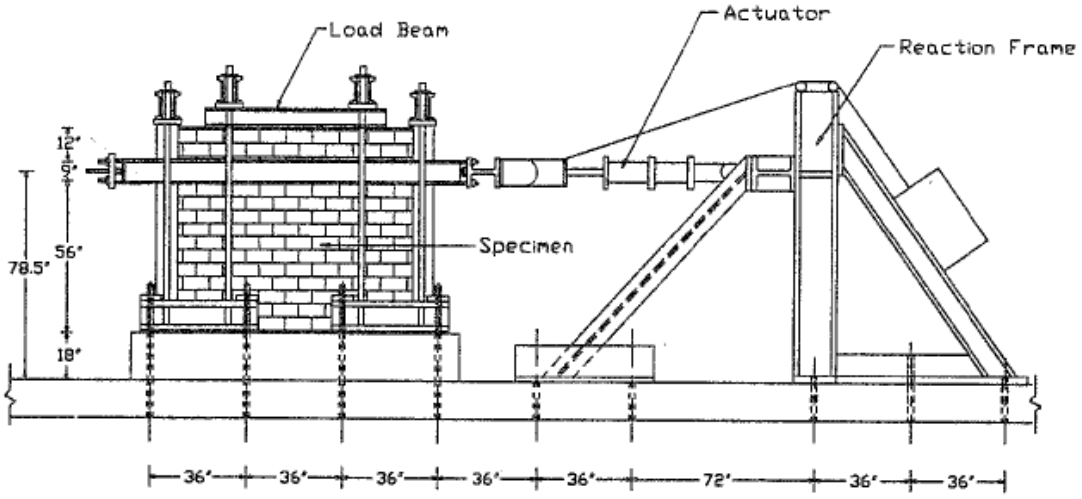

Fig. 3.1: Typical test setup used in the experimental studies: (a) steel frames (McBride, 1984); (b) RC frames (Mehrabi & Shing, 1996)

3.5 Stiffness Comparison

3.5.1 Comparison of Standard Stiffness Equation

Tables 3.8 to 3.10 present the comparison of experimental and design stiffness calculated based on CSA S304.1 and MSJC 2013 for steel and RC infilled frames. For most studies, both initial lateral stiffness (K_i) and secant lateral stiffness at the first cracking load (K_{cr}) were reported, and they are then included in the table while in some cases, only one

stiffness value was reported.

In the calculation of design stiffness, the diagonal strut width was first determined, and a frame analysis was then carried out using commercial software ANSYS®. The thickness of infill used was consistent with the manner in which the f'_m was determined in the studies. The experimentally determined properties of frames and infills were used as input in the computer analysis.

As shown in Tables 3.8 and 3.9, the CSA S304.1 overestimates the stiffness of steel infilled frames regardless of whether the initial stiffness or cracking stiffness is concerned. The degree of overestimation by S304.1 for CMU and SCT infills is comparable. The average K_i/K_{CSA} for steel infilled frames is around 0.51 with a coefficient of variation (COV) of 40.0%, and the average K_{cr}/K_{CSA} is 0.39 with a COV of 45.0%. A similar performance by CSA S304.1 is observed for RC infilled frames with an average K_i/K_{CSA} of 0.49 with a COV of 33.8% as shown in Table 3.10. It can be concluded that in general, the design stiffness of infilled frames by CSA S304.1 was 2 to 2.5 times the experimental stiffness.

Table 3.8: Stiffness comparison - steel frames infilled with CMU

Author	ID	CSA			MSJC		
		K_{csa} (kN/mm)	K_i / K_{CSA}	K_{cr} / K_{CSA}	K_{MSJC} (kN/mm)	K_i / K_{MSJC}	K_{cr} / K_{MSJC}
McBride (1984)	WA1	149.2	0.49	0.37	32.0	2.28	1.72
	WA2	150.2	0.55	0.35	32.2	2.55	1.61
	WA3	146.3	0.51	0.47	31.3	2.36	2.20
	WA4	139.1	0.45	0.45	29.6	2.13	2.13
Yong (1984)	WB1	136.6	0.53	-	29.1	2.47	-
	WB2	167.6	0.44	0.44	36.4	2.03	2.03
	WB3	161.9	0.41	0.33	35.0	1.91	1.54
Riddington (1984)	2a	70.9	0.45	0.41	23.1	1.39	1.27
	2b	93.0	0.65	0.65	47.7	1.27	1.26
Amos (1985)	WC7	131.8	0.54	0.54	28.0	2.54	2.54
	WC8	125.2	0.52	0.52	26.5	2.45	2.45
	WC9	124.8	0.43	0.36	26.4	2.05	1.70
	WC10	104.8	0.65	0.51	22.1	3.08	2.40
Richardson (1986)	WD1	87.9	0.63	0.60	18.6	2.96	2.85
	WD2	103.8	0.61	0.42	21.9	2.88	2.01
	WD3	103.8	1.06	0.30	21.9	5.02	1.42
	WD4	72.6	1.01	0.59	16.1	4.53	2.67
	WD7	127.4	0.97	0.44	27.0	4.56	2.07
	WD8	123.8	0.14	0.11	24.1	0.71	0.58
	WD9	132.9	0.41	0.23	26.1	2.11	1.15
	WD10	120.6	0.46	0.21	23.4	2.35	1.07
Hendry & Liauw (1991)	HN1	47.7	0.33	-	12.2	1.30	-
El-Dakhakhni (2002)	SP2	83.4	0.36	-	25.1	1.21	-
Liu & Soon (2012)	P1NA	54.7	0.50	0.36	26.3	1.03	0.76
	F1NA	92.5	0.42	0.25	37.4	1.04	0.61
	P3NA	64.0	0.55	0.39	25.6	1.38	0.97
	P3NI	59.1	0.30	0.22	16.6	1.08	0.79
	F3NA	114.8	0.49	0.23	37.2	1.52	0.72
	F3NI	106.0	0.20	0.17	25.2	0.85	0.73
	P6NA	78.3	0.38	0.30	24.5	1.21	0.96
AVG			0.51	0.38		2.14	1.56
COV (%)			40.0	36.6		51.1	44.6

Table 3.9: Stiffness comparison - steel frames infilled with SCT

Author	ID	CSA			MSJC		
		K_{csa} (kN/mm)	K_i / K_{CSA}	K_{cr} / K_{CSA}	K_{MSJC} (kN/mm)	K_i / K_{MSJC}	K_{cr} / K_{MSJC}
Henderson (1994)	HW2	91.6		0.95	17.0		5.14
	HW2L	91.6		0.95	17.0		5.14
Flanagan (1994)	F1	34.3		0.43	6.0		2.45
	F1L	34.3		0.34	6.0		1.95
	F2	41.8		0.26	11.6		0.94
	F2L	41.8		0.43	11.6		1.53
	F4	63.9		0.42	13.7		1.95
	F4L	63.9		0.21	13.7		1.00
	F5	71.4		0.32	19.6		1.18
	F5L	71.4		0.40	19.6		1.44
	F9	57.9		0.50	33.4		0.86
	F9L	57.9		0.55	33.4		0.96
	F17	65.6		0.28	11.9		1.55
	F17L	65.6		0.24	11.9		1.34
	F21	54.7		0.23	11.9		1.07
	F21L	54.7		0.24	11.9		1.11
AVG				0.42			1.85
COV (%)				54.5			73.3

In the case of MSJC 2013, since the diagonal strut width equation is intended to consider the damage that may have been sustained by the infill, the following discussion is focused on the comparison with the cracking stiffness. In contrast to CSA S304.1, MSJC 2013 underestimates the cracking stiffness for both steel and concrete infilled frames with the average K_{cr}/K_{MSJC} of 1.67 with a COV of 59.1% for steel frames and 1.33 with a COV of 42.6% for RC frames. An anomaly is observed for results by Henderson (1994) where K_{cr}/K_{MSJC} ratios reached as high as 5. This is due to an unusually high experimental stiffness. If results by Henderson are excluded from the calculation, the average of K_{cr}/K_{MSJC} is

changed to 1.50 for steel frames with a much-improved COV of 41.8%.

Table 3.10: Stiffness comparison - RC frames

Author	ID	CSA			MSJC		
		K_{csa} (kN/mm)	K_i / K_{CSA}	K_{cr} / K_{CSA}	K_{MSJC} (kN/mm)	K_i / K_{MSJC}	K_{cr} / K_{MSJC}
Mainstone & Weeks (1972)	a1	181.5	0.74	0.36	51.1	2.63	1.26
	a2	181.5	0.41	0.30	51.1	1.46	1.07
	a3	115.5	0.43	0.22	36 .6	1.37	0.68
	a4	492.1	0.64	0.54	120.0	2.63	2.21
Angel (1994)	2a	130.4	0.36		95.6	0.49	
	3a	109.8	0.43		89.0	0.54	
	4a	242.8	0.28		125.9	0.54	
	5a	315.4	0.70		143.1	1.54	
	6a	104.1	0.37		87.0	0.44	
	7a	115.8	0.77		91.0	0.98	
	8a	143.8	0.32		98.4	0.45	
Crisafulli (1997)	C1	84.9		0.32	19.5		1.40
Al-Chaar (1998)	2	178.4	0.54		52.2	1.84	
	3	164.5	0.44		49.2	1.46	
AVG			0.49	0.35		1.26	1.33
COV (%)			33.8	34.1		61.9	42.6

The drastic difference between CSA S304.1 and MSJC 2013 design stiffness is a result of the difference in the diagonal width value. For all specimens considered, the average strut width calculated by CSA S304.1 is 840 mm which was about 5 times the width determined by MSJC 2013.

3.5.2 Comparison of Other Stiffness Equation

Tables 3.11 to 3.13 compare the experimental stiffness of the reported tests with the design stiffness based on analytical methods (K_{ana}) proposed by several researchers. Presented in the tables are the stiffness ratio values averaged over the experimental results in the specific

frame and infill category.

In the case of steel frames infilled with CMU (Table 3.11), four methods underestimate the initial stiffness (Mainstone, 1971; FEMA 356, 2000; Flanagan & Bennet, 2001; Tucker, 2007) with the method by Flanagan and Bennet (2001) having the average K_i/K_{ana} ratio of 1.09 which is closest to unity with a high COV (50%). In the case of cracking stiffness, only three methods (Mainstone, 1971; Flanagan & Bennet, 2001; and Tucker, 2007) give a conservative estimation of the cracking stiffness. The method by Mainstone (1971) provides the best estimation with an average K_{cr}/K_{ana} of 1.04 with a COV of 39.7%. It seems that most methods overestimate the stiffness especially the cracking stiffness for steel frames infilled with CMU.

In the case of steel frames infilled with SCT (Table 3.12), only the method by Tucker (2007) provides a conservative estimation of the cracking stiffness with a K_{cr}/K_{ana} close to unity (1.08) but with the highest COV of 41.2%. The method by Flanagan and Bennet (2001) is ranked the second with an average K_{cr}/K_{ana} of 0.68 and a COV of 28.8%.

Table 3.11: Stiffness comparison - steel frames infilled with CMU

Methods	Average K_i/K_{ana}	COV (%)	Average K_{cr}/K_{ana}	COV (%)
Stafford-Smith (1966)	0.61	46.9	0.45	41.2
Mainstone (1971)	1.43	45.9	1.04	39.7
Liauw & Kwan (1984)	0.59	44.3	0.43	38.6
Eurocode 8 (1988)	0.69	44.4	0.51	39.1
FEMA 356 (2000)	1.11	46.4	0.81	40.3
Flanagan & Bennet (2001)	1.09	50.0	1.44	46.2
El-Dakhakhni et al. (2003)	0.84	52.8	0.61	48.9
Papia et al. (2003)	0.49	45.5	0.36	40.4
Tucker (2007)	2.62	52.0	1.91	47.1

Table 3.12: Stiffness comparison - steel frames infilled with SCT

Methods	Average K_i/K_{ana}	COV (%)	Average K_{cr}/K_{ana}	COV (%)
Stafford-Smith (1966)			0.23	29.7
Mainstone (1971)			0.36	28.2
Liauw & Kwan (1984)			0.21	29.2
Eurocode 8 (1988)			0.23	34.0
FEMA 356 (2000)			0.39	27.0
Flanagan & Bennet (2001)			0.68	28.8
El-Dakhakhni et al. (2003)			0.25	35.4
Papia et al. (2003)			0.17	35.6
Tucker (2007)			1.08	41.2

In the case of RC frames (Table 3.13), except for methods by Flanagan and Bennet (2001) and Tucker (2007), all methods overestimate both the initial stiffness and cracking stiffness. The method by Flanagan and Bennet (2001) overestimates the initial stiffness with an K_i/K_{ana} of 0.64 but achieved an K_{cr}/K_{ana} of 1.00. The method by Tucker (2007) produces an average K_i/K_{ana} of 1.28 and an average K_{cr}/K_{ana} of 1.39. The methods by FEMA 356 (2000) and Mainstone (1971) show the same average test-to-analytical ratios since the two methods are the same for brick infills. These two methods produce an average K_i/K_{ana} of 0.86 and an average K_{cr}/K_{ana} of 0.75.

In summary, no method is found to provide accurate stiffness estimate for all infill specimens. The methods by FEMA (2000) and Flanagan and Bennet (2001) perform well for the initial stiffness of CMU infills while the methods by Mainstone (1971), Flanagan and Bennet (2001) and Tucker (2007) perform well for the cracking stiffness of CMU, RC frame, and SCT infills respectively. In terms of the overall performance of all infill types, the methods by Mainstone (1971), Flanagan and Bennet (2001) and Tucker (2007) have achieved a relatively good overall performance.

Table 3.13: Stiffness comparison – RC frames

Methods	Average K_i/K_{ana}	COV (%)	Average K_{cr}/K_{ana}	COV (%)
Stafford-Smith (1966)	0.38	37.4	0.27	47.8
Mainstone (1971)	0.86	46.2	0.75	34.2
Liauw & Kwan (1984)	0.47	34.3	0.33	34.9
Eurocode 8 (1988)	0.69	39.0	0.53	31.2
FEMA 356 (2000)	0.86	46.2	0.75	34.2
Flanagan & Bennet (2001)	0.64	41.7	1.00	43.8
El-Dakhakhni et al. (2003)	0.73	48.3	0.61	62.5
Papia et al. (2003)	0.45	34.9	0.32	37.2
Tucker (2007)	1.28	62.7	1.39	45.2

3.6 Strength Comparison

Tables 3.14 to 3.16 compare the experimental ultimate loads of the reported tests with the design strengths based on various analytical methods. Presented in the tables are the strength ratio average value and indicators of the scatter of the value for all experimental results considered. The comparison shows again, that there is no one method that performs well for all infill specimens.

In the case of steel frames infilled with CMU (Table 3.14), five methods underestimate the ultimate strength (CSA S304.1, 2004; MSJC, 2013; Tucker, 2007, FEMA 306, 1998; Liauw & Kwan, 1985; Liauw & Kwan, 1985 in combination with Wood, 1978) with P_{exp}/P_u ratios greater than unity while the remaining methods overestimate the strength. The overestimation is observed in methods based on the diagonal strut concept as well as those based on plastic collapse theory (Liauw & Kwan, 1985; Saneinejad & Hobbs, 1995). For the five methods that underestimate the strength, the method by FEMA 306 provides the best estimation with an average P_{exp}/P_u of 1.01 with a COV of 38.7%. The method by Liauw and Kwan (1985) in combination with Wood (1978) is ranked the second with an average P_{exp}/P_u of 1.09 and a COV of 35.8%. It confirms that the method of Liauw and Kwan (1985) needs to be modified by the reduction factor γ_p applied to f'_m to achieve a better comparison with the test results. CSA 304.1 provides the third best estimation with an average P_{exp}/P_u of 1.39 but with a higher COV of 44.0%. This is followed by MSJC 2013 while the method by Tucker (2007) provides the most significant underestimation. In the case of steel frames

infilled with SCT (Table 3.15), Liauw and Kwan (1985) in combination with Wood (1978) provides a strength estimation closest to the test results with an average P_{exp}/P_u of 1.04. CSA 304.1 and FEMA 306 show similar average P_{exp}/P_u ratios (1.07 vs. 1.08) but CSA S304.1 seems to perform better with a lower COV of 25.7%. The P_{exp}/P_u ratio based on MSJC 2013 is comparable with that for CMU infills.

Table 3.14: Strength comparison - steel frames infilled with CMU

Methods	Average P_{exp}/P_u	Standard Deviation	Standard Error	COV (%)
Mainstone (1971)	0.45	0.16	0.03	36.0
Liauw & Kwan (1985)	0.61	0.24	0.04	39.6
Liauw & Kwan (1985) in combination with Wood (1978)	1.09	0.39	0.07	35.8
Stafford-Smith & Coull (1991)	0.76	0.28	0.05	36.7
Saneinejad & Hoobs (1995)	0.69	0.25	0.05	36.7
FEMA 306 (1998)	1.01	0.39	0.07	38.7
Flanagan & Bennet (2001)	0.96	0.27	0.04	28.5
CSA S304.1 (2004)	1.39	0.61	0.11	44.0
Tucker (2007)	2.28	0.86	0.16	37.5
MSJC 2013	1.44	0.46	0.08	31.8

In the case of RC frames (Table 3.16), except for methods by Liauw and Kwan (1985) in combination with Wood (1978) and MSJC 2013, all methods overestimate the strength. In

particular, CSA S304.1 overestimates the strength by 21% with an average P_{exp}/P_u of 0.79. The average P_{exp}/P_u ratios by Liauw and Kwan (1985) in combination with Wood (1978) and MSJC 2013 are 1.53 and 1.03 respectively but both with high COV and high standard error, which indicates a significant scatter of experimental results. One factor to be attributed to the overall large scatter may be the experimental inaccuracies which may include variation in the quality of construction, loading procedures, and definition of stiffness and strength in the experimental studies (different studies may have defined stiffness differently). As reinforced concrete has inherently higher variation in qualities than steel, the results of RC infilled frames are thus more scattered than those of steel infilled frames. Another factor for the high scatter may be due to the inherent limitations in the analytical methods. Most analytical models have some constants that were calibrated using empirical curve-fitting with their own test results. Most analytical models were developed based on steel infilled frames where more results were available. Before more RC infilled frame results become available, using the current strength equations for the design of infills in the RC infilled frames should then be cautioned.

Table 3.15: Strength comparison - steel frames infilled with SCT

Methods	Average P_{exp}/P_u	Standard Deviation	Standard Error	COV (%)
Mainstone (1971)	0.76	0.30	0.07	39.6
Liauw & Kwan (1985)	0.56	0.21	0.05	36.9
Liauw & Kwan (1985) in combination with Wood (1978)	1.04	0.38	0.09	36.4
Stafford-Smith & Coull (1991)	0.81	0.30	0.07	37.0
Saneinejad & Hoobs (1995)	0.58	0.22	0.05	39.0
FEMA 306 (1998)	1.08	0.33	0.08	30.5
Flanagan & Bennet (2001)	0.96	0.24	0.06	24.8
CSA S304.1 (2004)	1.07	0.28	0.07	25.7
Tucker (2007)	1.14	0.58	0.14	51.4
MSJC 2013	1.43	0.33	0.08	23.5

Table 3.16: Strength comparison - concrete frames

Methods	Average P_{exp}/P_u	Standard Deviation	Standard Error	COV (%)
Mainstone (1971)	0.70	0.72	0.21	103.6
Liauw & Kwan (1985)	0.57	0.24	0.07	42.5
Liauw & Kwan (1985) in combination with Wood (1978)	1.53	1.12	0.32	73.7
Stafford-Smith & Coull (1991)	0.38	0.23	0.07	61.6
Saneinejad & Hoobs (1995)	0.50	0.20	0.06	40.2
FEMA 306 (1998)	0.62	0.41	0.12	67.3
Flanagan & Bennet (2001)	0.65	0.66	0.19	101.2
CSA S304.1 (2004)	0.79	0.49	0.14	61.8
Tucker (2007)	0.70	0.45	0.13	64.7
MSJC 2013	1.03	1.07	0.31	103.0

3.7 Diagonal Strut Width Study on Stiffness

As discussed earlier, the significant overestimation in stiffness by CSA S304.1 indicates that the diagonal strut width equation provides unrealistically high values. A reasonable approach to improve the performance of the design equation is to keep the current methodology and to simply reduce the strut width by dividing the originally determined effective strut width (Eqn (2.60)) by a factor greater than one. In this section of the study, three strut widths, i.e. $w/1.5$, $w/2$, and $w/3$ were considered where w is the effective strut

width determined based on Eqn (2.60). The resulting stiffness values based on the three widths are compared with the experimental results in Table 3.17. The values in the table are the average for each experimental study. The overall K_i/K_{CSA} ratios for $w/1.5$, $w/2$, and $w/3$ are determined to be 0.67, 0.84, and 1.17 respectively. The use of widths $w/2$ and $w/3$ provide a significant improvement in the initial stiffness estimate. The width $w/2$ is recommended since the estimation still remains somewhat conservative with an average experiment-to-design ratio less than unity. This recommendation has been adopted in the latest Canadian masonry standard S304-14 for the strut width when calculating stiffness.

For strength calculation using CSA S304.1, it is recommended that the original strut width is used. Since S304.1 provides an underestimate of strength with the original strut width, the use of a reduced strut width will make the underestimation more severe, rather than improving the strength value. Considering that the underestimation of the strength is not as significant as the overestimation of the stiffness, and it is also desirable to be on the conservative side on strength calculation, it is, therefore, reasonable to keep the original strut width for strength design.

Table 3.17: The in-plane design stiffness for varying strut width based on CSA S304.1 (2004)

Authors	No. of Specimens	w/1.5		w/2		w/3	
		K_i /K_{CSA}	K_{cr} /K_{CSA}	K_i /K_{CSA}	K_{cr} /K_{CSA}	K_i /K_{CSA}	K_{cr} /K_{CSA}
McBride (1984)	4	0.70	0.58	0.90	0.74	1.28	1.06
Yong (1984)	3	0.64	0.54	0.82	0.69	1.18	0.99
Riddington (1984)	2	0.64	0.62	0.79	0.75	1.05	1.01
Amos (1985)	4	0.76	0.68	0.98	0.88	1.40	1.26
Richardson (1986)	8	0.92	0.51	1.19	0.66	1.71	0.94
Hendry& Liauw (1991)	1	0.49		0.64		0.93	
El-Dakhakhni (2002)	1	0.49		0.62		0.85	
Liu & Soon (2012)	7	0.54	0.29	0.68	0.36	0.92	0.49
Henderson (1994)	2		1.26		1.56		2.16
Flanagan (1994)	14		0.41		0.52		0.72
Mainstone (1971)	4	0.74	0.48	0.98	0.64	1.48	0.96
Angel (1994)	7	0.46		0.48		0.56	
Crisafulli (1997)	1		0.44		0.56		0.85
Al-Chaar (1998)	2	0.65		0.81		1.12	
AVG		0.67	0.48	0.84	0.62	1.17	0.85
COV (%)		44.9	51.3	47.6	52.9	50.7	53.2

Chapter 4 Finite Element Study

4.1 General

This chapter describes the two finite element modelling techniques used in this study. Both techniques were developed and implemented using software ANSYS® 13.0. The major difference between these two models is the treatment of interface between the masonry blocks. Model I adopted user-defined joint elements to model the interface between blocks. A Rankine type criterion was adopted to model failure in joint elements while a Hill type yield criterion was adopted to model compression failure in masonry elements. After validating the model with existing test results, Model I was used to investigate the effects of infill openings on the behaviour of infilled frames (Chapter 5). However, during the process, the author realized some drawbacks and limitations with Model I which reduced its efficiency (discussed in detail in Section 4.3). Although these limitations did not impact the study of the openings, it was felt that in order to conduct further parametric studies, a new model with the desired efficiency was necessary. Model II was then developed where cohesive zone interface contact pairs were adopted for simulation of the interface between blocks. The tension and shear failure in interface elements were realized by the traction–separation law that follows the bilinear material model. This modification has greatly increased the efficiency and robustness of the model since it made detection and realization of tension and shear failure an integral part of the solution. After validating the model with existing test results, the Model II was used to conduct parametric studies on the effects of

several material and geometric properties (Chapter 6), vertical load (Chapter 7) and interfacial gaps (Chapter 8) on the behaviour of infilled frames.

4.2 Model I

4.2.1 General Description

For the infill, a simplified micro-modeling approach which is similar to the method used by Seah (1999) was adopted. The infill was represented by homogeneous continuum elements. The mortar joints were omitted, and each masonry unit was expanded to its nominal size to account for the mortar thickness. The bond between the unit and mortar was modeled using user-defined joint elements which are capable of simulating the orthotropic characteristics of infill due to the presence of mortar and the unit-mortar interfacial connection. The interfacial connection between frame and infill was modeled using contact elements. A schematic representation of an infilled frame model is shown in Fig. 4.1.

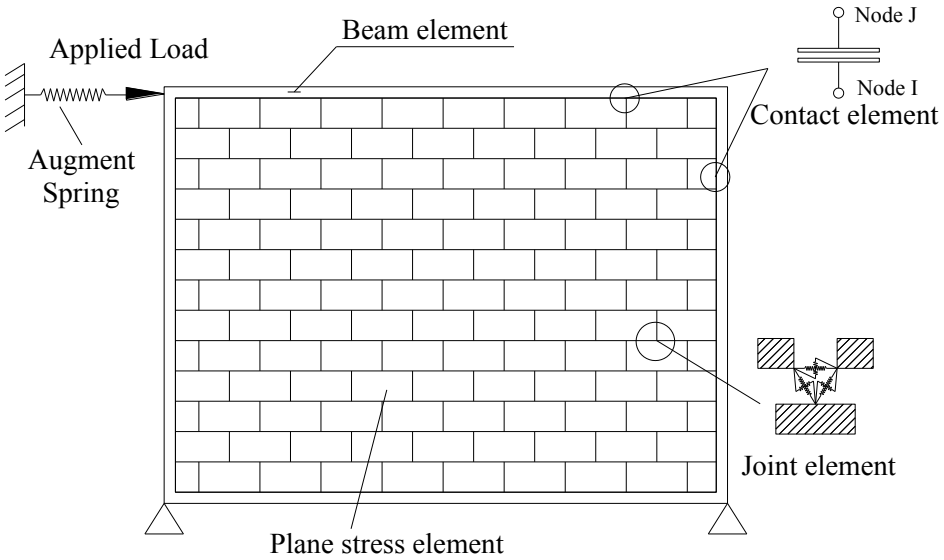

Fig. 4.1: In-plane finite element model of infilled frame

The infill in this study was modeled by masonry units placed in running bond. Each unit was meshed into 2x2 plane-stress elements. A convergence study on infills under in-plane loading was conducted and results presented in Table 4.1 showed that 2x2 meshing for each unit provides sufficient accuracy.

Table 4.1: Convergence study results

Meshing	Max Displacement (mm)	Max. Tensile Stress (MPa)	Max. Compressive Stress (MPa)
1x1	4.189	1.02	2.86
2x2	4.307	0.99	2.79
3x3	4.302	0.99	2.74
4x4	4.323	0.99	2.72

4.2.2 Element Description

Several types of finite elements available in ANSYS were used in this modeling. The steel frame members were modeled using 3-D beam elements having six degrees of freedom per node and stress stiffening, and large deflection and strain capabilities. These features enable the simulation of inelastic behaviour and potential formation of plastic hinges of bounding frame members.

The two-dimensional 4-node plane-stress element, PLANE42 was used to model the masonry infill continuum. As shown in Fig. 4.2 (a), PLANE42 has two degrees of freedom at each node: translations in the nodal x and y directions. The element has plasticity, creep, swelling, stress stiffening, large deflection, and large strain capabilities.

The interface between the infill and the frame was modeled using 2-D point-to-point

contact elements, CONTAC12. Shown in Fig. 4.2 (b), CONTAC12 represents two surfaces which may maintain or break physical contact and may slide relative to each other. For CONTAC12, only compression in the direction normal to surface and shear in the tangential direction are supported; no propagation of tensile force is allowed. In addition, gaps between the infill and the frame can be introduced in CONTAC12 as an initial condition.

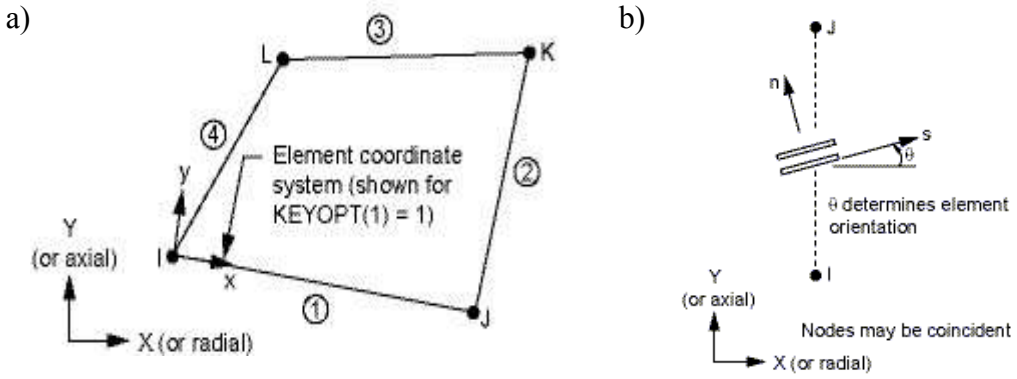

Fig. 4.2: a) ANSYS PLANE42 element, b) ANSYS CONTACT12 element

The stiffness of a contact element at the infill-frame interface needs to be assumed with a reasonable value. A low contact stiffness will cause the frame to penetrate the contact element and result in errors in displacements. However, an unreasonably high stiffness will result in ill-conditioning of the stiffness matrix of the model and then difficulties in convergence. If the stiffness is within a reasonable range, variation in the value does not cause much difference in results. In this study, the contact stiffness of each contact element was set as the contact area times the unit area normal stiffness. The unit area normal stiffness of a contact element at the infill-frame interface was calculated by the following

equation proposed by Lourenço (1994).

$$k_{nf} = \frac{E_m E_f}{h_m (E_f - E_m)} \tag{4.1}$$

where k_{nf} is the unit area normal stiffness; E_m and E_f are the moduli of masonry and frame respectively; h_m is the thickness of the mortar joint.

The connection between masonry blocks was modeled using user-defined joint elements. The configuration of a joint is shown in Fig. 4. 3. Each joint consists of three nodes with six springs of zero length. The purpose of springs 1 to 6 is to transfer normal and shear stress between the masonry units and to ensure that nodes of the plane stress elements connected by the joint move in unison. It should be noted that the distances between masonry units are zero, the springs 1, 2 and 3 are normal to the bed joint and head joint; springs 4, 5 and 6 are shear springs which are parallel to the bed joint and head joint. When a failure occurred in the form of tensile cracking or sliding shear along joints, the stiffness of one or more springs was set to zero to reflect the corresponding failure.

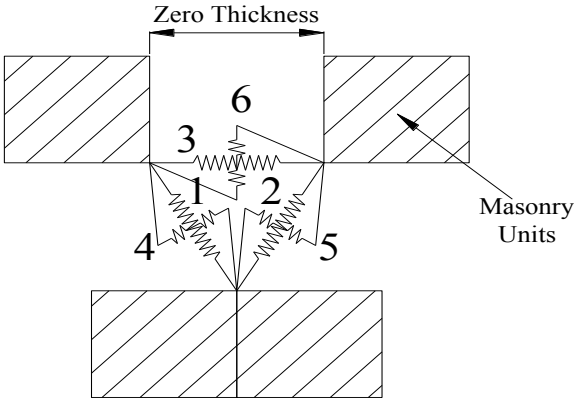

Fig. 4.3: Configuration of a joint

The springs in a joint were modeled using MATRIX27 elements specified in ANSYS. A

MATRIX27 element represents an arbitrary element whose geometry is undefined but whose elastic behaviour can be specified by stiffness, damping, or mass. The unit area stiffness of a normal spring, k_n, and a shear spring, k_s, in a joint element were determined by the following expressions proposed by Lourenço (1996).

$$k_n = \frac{E_m E_{mortar}}{h_m (E_{mortar} - E_m)} \tag{4.2}$$

$$k_s = \frac{G_m G_{mortar}}{h_{mortar} (G_m - G_{mortar})} \tag{4.3}$$

where E_m and E_{mortar} are the moduli of masonry units and mortar respectively; and G_m and G_{mortar} are the shear moduli of masonry units and mortar respectively. In lieu of experimental data, E_{mortar} was taken as 0.1 times E_m; G_m and G_{mortar} were taken as 0.4 times E_m and E_{mortar}, respectively where the Poisson's ratio, v, for masonry was assumed as 0.25. The Poisson's ratio for masonry in reported experimental studies varies from 0.15 to 0.25. A sensitive study of the Poisson's ratio was then conducted and the results are presented in Table 4.2. It shows that the variation of the Poisson's ratio from 0.1 to 0.25 results in no significant change in the behaviour of infilled frames.

Table 4.2: Sensitivity study of the Poisson's ratio

Poisson's ratio	Stiffness (kN/mm)	Ultimate Strength (kN)	Displacement at the Ultimate Load (mm)	Max. Compressive Stress (MPa)
0.10	43.2	239.5	19.53	16.3
0.15	43.0	240.5	19.89	16.7
0.20	43.1	240.1	19.49	16.4
0.25	43.4	239.0	19.73	16.2

4.2.3 Material Model and Failure Criteria

The masonry units were assumed to be linear elastic with a modulus of elasticity of $850f'_m$ based on CSA S304-14 (2014). The compression failure of masonry infill was monitored through the masonry unit element using a Hill type yield criterion (f_1) while the tension failure of masonry infill was monitored through the joint element using a Rankine type criterion (f_2). These two failure criteria are defined in the following expressions which were originally proposed by Lourenço and Rots (1997).

$$f_1 = \frac{\sigma_x^2}{f_{mx}^2} + \beta\frac{\sigma_x\sigma_y}{f_{mx}f_{my}} + \frac{\sigma_y^2}{f_{my}^2} + \gamma\frac{\tau_{xy}^2}{f_{mx}f_{my}} - 1 \le 0 \tag{4.4}$$

$$f_2 = \frac{(\sigma_x - f_{tx}) + (\sigma_y - f_{ty})}{2} + \sqrt{(\frac{(\sigma_x - f_{tx}) - (\sigma_y - f_{ty})}{2})^2 + \alpha\tau_{xy}^2} \le 0 \tag{4.5}$$

where σ_x and σ_y are the normal stresses in the x- and y- directions at the node, respectively; τ_{xy} is the shear stress at the node; f_{tx} and f_{ty} are the uniaxial tensile strengths in x- and y- directions of the infill, respectively; f_{mx} and f_{my} are the uniaxial compressive strengths in x- and y- direction of the infill, respectively. In general, x- direction means the direction parallel to the bed joint and y- directions means the direction normal to the bed joint. The value of f_{my} was taken as the compressive strength of masonry f'_m. In lieu of experimental data, f_{mx} can be taken as $0.7f'_m$, and f_{ty} and f_{tx} can be taken as 1/10 of f_{my} and f_{mx}, respectively. The factor α accounts for the shear stress contribution to tension failure; the factor β controls the coupling between normal stresses in x- and y- directions; and the factor γ accounts for the shear stress contribution to compression failure. These factors may be determined experimentally (Lourenço & Rots, 1997). In this study the values of α, β and γ

were taken as 1.25, -1.0 and 5.5 respectively as suggested by Seah (1999).

The failure detection process followed in the model is described as follows. Examining Eqn (4.5), if f_2 was greater than zero and σ_x was positive in a joint, then a tensile failure in the x- direction was detected in that joint. The stiffness of normal spring in the x- direction (spring 3) and shear spring parallel to the joint (spring 6) were then reduced to zero. If f_2 was greater than zero and σ_y was positive in a joint, then a tensile failure in y- direction was detected in that joint. The stiffness of normal spring in the y- direction (springs 1 and 2) and shear spring parallel to the joint (springs 4 and 5) were then reduced to zero. If f_2 was greater than zero and both σ_x and σ_y were negative in a joint, then the shear stress was the main contributor to the failure; the normal spring stiffnesses were then assumed to remain unchanged while a reduced shear stiffness was assigned to the shear springs. This reduced shear stiffness was to account for the frictional resistance of the joint even after shear crack occurred. If f_2 was greater than zero and both σ_x and σ_y were positive, all spring stiffnesses were reduced to zero. Examining Eqn (4.4), when f_1 was greater than zero, a compressive failure was detected in the masonry unit which was then deactivated to represent masonry crushing.

4.2.4 Boundary Conditions and Loading Procedure

The frame beam was modelled as rigidly connected to the columns and the columns were fix-supported at the ends. To obtain the falling branch in the load vs. lateral displacement response, an augmented spring was implemented as shown in Fig. 4.1. In a load controlled

analysis, the infill cracking and crushing could lead to sudden loss of infill stiffness which may in turn result in convergence difficulty. The spring was then implemented to regulate the load when the infill suddenly cracked or crushed so that the load vs. lateral displacement curve can reflect this load drop. The stiffness of this spring was set to be equal to the initial stiffness of the infilled frame.

A monotonically increased load with a defined load increment was applied at the frame beam level. At each load step, stresses in the structure were checked for failure using the failure criteria described in Eqns (4.4) and (4.5). If a failure was detected, the stiffness of the joint element or masonry element associated with the failure was modified according to the rules described above; and the analysis was rerun with the updated system stiffness matrix until no new failure was detected. Then another increment of the load was applied, and the process was repeated. The analysis was terminated when an irreversible load drop was observed.

4.3 Limitations of Model I

The key characteristic of this Model I was the user-defined joint elements for simulating the bond between the mortar and the masonry unit. The advantage of this modeling technique over a detailed micro-modeling one was its simplicity for computer implementation. However, the simplicity has some inherent limitations as discussed as follows.

1. Although the user-defined joint element can offer great flexibility in simulation, the

failure of a joint was realized by reducing the stiffness of springs according to the failure criteria and user-defined rules. The failure detection and stiffness modification of a failed joint can only be processed through user-developed programming at the end of each load step, and then the model restarted the solution to repeat the analysis until no new failure was detected. The whole process was time-consuming.

2. By adopting the user-defined joint elements, the behaviour of interface is then concentrated at each nodes connected by joint elements instead of the surface, which is physically inaccurate.

3. The model adopted a Rankine type criterion (f_2) to monitor the joint failure as described in Eqn (4.5). However, this criterion was originally developed for smeared-crack continuum instead of a discrete model. In addition, the value of α needs to be determined by various tests proposed by Lourenco (1994, 1996) and was not explicitly given in the literature.

4. When the Rankine type criterion ($f_2 \leq 0$) was violated, a failure was detected, however whether the failure was tensile cracking or sliding shear was unknown. A set of rules developed by the author (described in Section 4.2.3) was implemented to examine the stress state of the infill to determine the failure type by interpretation from the failure surface defined by f_2. Although this set of rules functioned well in achieving a good agreement with experiment results, it was based on simple mechanics principles and many may consider it over-simplifying.

4. At joint failure, the stiffness of springs was assigned with a residual value which was determined through calibration with available experiment results. For tensile failure, the residual stiffness of normal springs was determined as 0.01 times the original stiffness. For shear failure, the stiffness of normal springs remained the same while shear springs were given the residual stiffness of 0.05 times the original stiffness to account for the frictional resistance. Although this assumption achieved a good agreement with experiment results in terms of initial stiffness and strength, the model tended to underestimate the post-cracking stiffness of the infill.

4.4 Model II

4.4.1 Model Description

To overcome the above-mentioned modeling limitations, an improved model which implemented a traction–separation law for contact elements was developed. While Model II adopted the same meshing for masonry infills as shown in Fig. 4.4(a), the mortar joints were simulated using surface-based cohesive contact pairs to capture the cracking and sliding failure of the mortar joints. Each contact pair consists of a zero-thickness surface-to-surface cohesive zone interface element, CONTA171, and a zero-thickness target element TARGE169. The CONTA171 element was used to detect contact or separation between "target" surfaces (TARGE169) and a deformable surface defined by the CONTA171 element. These contact pairs were also used for the contact between the infill and the frame members. The geometry and configuration of inter-block contact pairs are shown in Fig. 4.4(b).

Detection of normal separation (tensile cracking) and/or tangential separation (shear sliding) in contact pairs was idealized by a traction–separation law that accounts for separations due to tension and shear cracks. The traction-separation law was represented by the bilinear cohesive zone material model of the contact pairs. The traction-separation law does not require the user-defined rules for normal or tangential separation detection, the value of constant α, or the user-defined constant residual stiffness for failed springs. The CONTA171 and TARGE169 contact pairs can integrate the softening of a failed joint with each iteration of the solution, thus increasing the efficiency of the model tremendously.

4.4.2 Material Model and Failure Criteria

The constitutive model for masonry adopted the one proposed by Priestley and Elder (1983) which was calibrated with experimental results, and it is expressed in Eqn (4.6). It should be pointed out that this model was assumed homogenous.

$$\varepsilon \le 0.0015, \qquad \sigma = \frac{f'_m}{0.9375}\left(\frac{2\varepsilon}{0.002} - \left(\frac{\varepsilon}{0.002}\right)^2\right) \tag{4.6a}$$

$$0.0015 \le \varepsilon \le 0.0025, \qquad \sigma = f'\left(1 - z_m(\varepsilon - 0.0015)\right) \tag{4.6b}$$

$$\text{where} \quad z_m = \frac{0.5}{\frac{3 + 0.29 f'_m}{145 f'_m - 1000} - 0.002} \tag{4.6c}$$

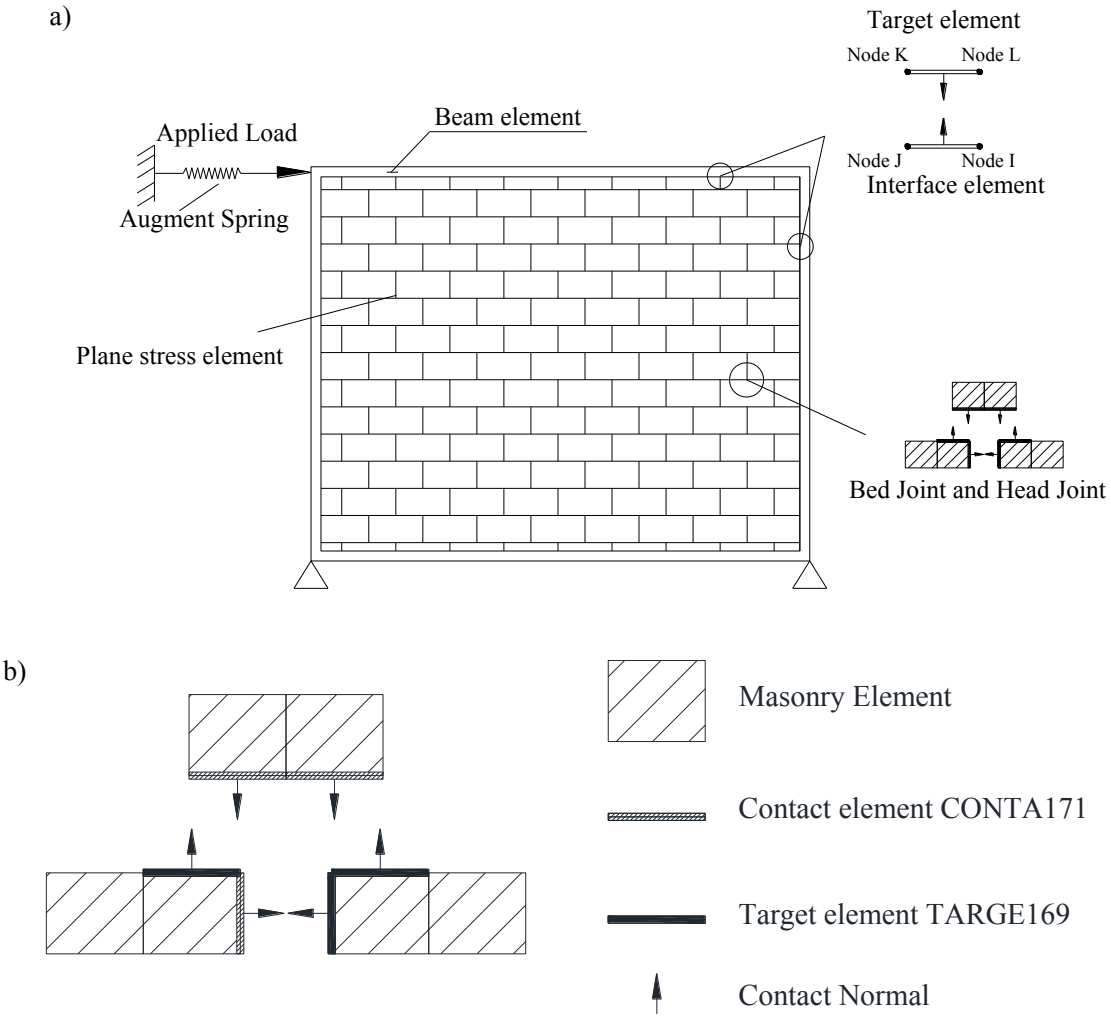

Fig. 4.4: a) Finite element model of the infilled frame, b) configuration of a joint

Cracking and sliding failures of mortar joints were monitored using the linear elastic traction-separation laws as shown in Fig. 4.5. Represented by the bilinear cohesive zone material model of the CONTA171 element, separation initiates when the maximum normal or shear stress in a contact pair reaches the corresponding strength. The shear stress and the relative slip behaviour is plotted in Fig. 4.5(a) which shows separation begins at point A where the shear strength (τ_t) is achieved and is completed at point C when the shear stress reaches zero. The softening stage provides mortar joints with a residual shear

strength for accounting for the frictional resistance of the joint after shear cracking has occurred. The ultimate slip at point C, u^c_t is set as a very large value (180 times the slip at the separation imitate point A, u^A_t) to provide a gradual and slow softening stage. It should be noted that u^c_t is set to be sufficiently large that it will never be reached in any contact pairs in this study. As a result, there will always be considerable residual shear strength to account for the frictional resistance. The resulting slip vs stress relationship achieved a good agreement with the shear behaviour of mortar joints experimentally obtained by Vasconcelos and Lourenco (2009).

For tension separation, a similar bilinear constitutive relationship but with a cut-off was adopted. As Fig. 4.5 (b) shows, once the tension stress in the contact pair reaches the tensile strength (f_t) of the mortar joint, the contact pair is considered separated to represent the tensile cracking of the mortar joint. The values of the normal and shear stiffness of the contact pairs were determined the same way as in Model I.

The damage initiation criterion was defined using a Mohr-Coulomb friction yield surface combined with a tension cut-off and elliptical compression cap as shown in Fig. 4.6 where f_t is the tensile strength of the mortar joint and φ is the friction angle. Note that the compression cap was defined using the same Hill type yield criterion (f_1) adopted in Model I to monitor compression failure of the masonry infill. This failure surface has been shown by Lourenço (1996) and Al-Chaar and Mehrabi (2008) to produce reasonably accurate estimates when compared with experimental results.

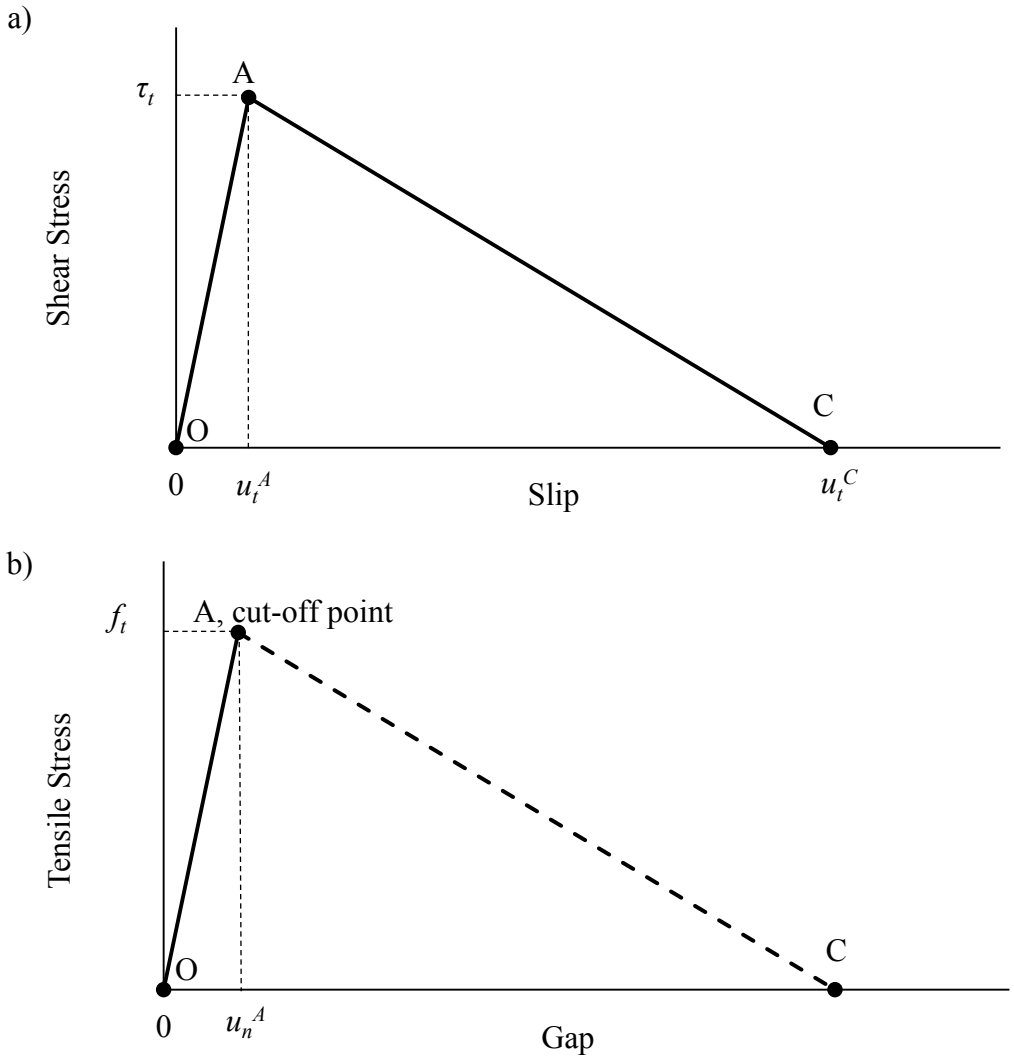

Fig. 4.5: Constitutive relationship for cohesive material, a) shear stress vs. slip, b) normal stress vs. gap

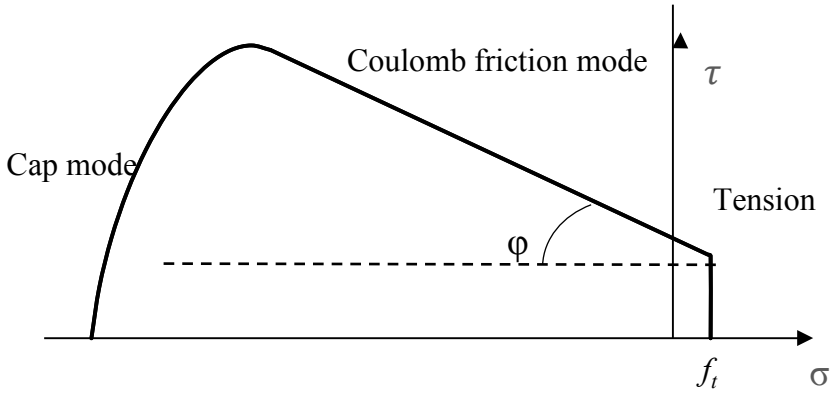

Fig. 4.6: Yield surface for mortar interface elements.

4.5 Verification of Model

A total of eight experimental studies were included in the verification of both models. It should be noted that only the infilled steel frames loaded statically or quasi-statically were considered. However, specimens used in the validation process covered a wide range of parameters including infill opening, reinforcement and interfacial gaps. The details of the specimens in these studies are summarized in Tables 4.3 to 4.5.

4.5.1 Model I

Since Model I was used in the study of infills with openings, the model was validated using experimental studies involving infills both with and without openings from the available literature (McBride, 1984; Yong, 1984; Amos, 1985; Richardson, 1986; Flanagan, 1994; Liu & Soon, 2012). The infills tested by McBride (1984), Yong (1984), Amos (1985), and Richardson (1986) were constructed using standard masonry units; those tested by Flanagan (1994) were constructed with structural clay tiles; and those tested by Liu and Soon (2012) were constructed with one-third scaled concrete masonry units. All mortar used were composed of cement, lime, and sand in specific proportions. A total of 26 specimens were considered, of which 18 specimens had infills without openings (referred to as solid infills) and eight specimens had infills with an opening.

Table 4.6 summarizes the comparison results where K_{exp} and P_{exp} are the initial stiffness and ultimate load obtained from experimental results whereas K_{FE} and P_{FE} are the corresponding results obtained from Model I. It should be noted that, due to the absence of

initial stiffness or highly scattered initial stiffness, in the case of infills tested by Flanagan (1994) and Liu and Soon (2012), the cracking stiffness was adopted as K_{exp} instead of the initial stiffness. The material properties reported in the original papers were also included in the table. It is noted that available f'_t values listed in the table are obtained as mortar tensile strength, and the mean value was approximately the 1/10th of the mean value for f'_m.

The table shows that the average test-to-FE ratios of the ultimate load for solid infills and infills with openings are 0.97 with a COV of 13% and 0.92 with a COV of 11%, respectively. In the case of stiffness, the average test-to-FE ratio is 0.99 with a COV of 16% for solid infills and 1.11 with a COV of 18% for infills with openings. Fig. 4.7 compares the experimental and numerical load vs. lateral displacement curves for a solid infill (specimen WB2) and an infill with an opening (specimen WD12) as well as the failure mode for specimen P3WA. The figure shows that the finite element model is capable of simulating the degradation of stiffness due to cracking as well as capturing the cracking and crushing of the infill similar to that obtained from the test.

Table 4.3: Details of specimens used in validation of FE model (Full-scale CMU)

		H (m)	L (m)	f'_m (MPa)	f'_t (MPa)	E_m (MPa)	t_e (mm)	Beam section	Column section	Opening size (hxl, m×m)
McBride (1984)	WA1[I, II]	2.8	3.6	27.4	2.65	23290*	66	W250x58	W200x46	
	WA2[I, II]	2.8	3.6	27.7	2.63	23545*	66			
	WA3[I, II]	2.8	3.6	26.5	2.10	22525*	66			
	WA4[I, II]	2.8	3.6	24.4	1.22	20740*	66			
	WA5[II]	2.8	3.6	25.6	2.11	21760*	66			
Yong (1984)	WB1[I, II]	2.8	3.6	23.7	2.55	20145*	66	W250x58	W200x46	
	WB2[I, II]	2.8	3.6	33.3	2.12	28305*	66			
	WB3[I, II]	2.8	3.6	31.4	1.90	26690*	66			
	WB4[II] ①	2.8	3.6	32.8	1.76	27880*	66			
	WB5[II] ①	2.8	3.6	31.0	2.41	26350*	66			
	WB6[II]	2.8	3.6	35.4	3.23	30090*	66			
Amos (1985)	WC1[I]	2.8	3.6	26.9	1.69	26945*	66	W250x58	W200x46	
	WC2[I]	2.8	3.6	27.7	0.97	11400	66			
	WC3[I]	2.8	3.6	30.9	1.82	26265*	66			2.2x0.8
	WC4[I]	2.8	3.6	33.1	1.45	21650	66			2.2x0.8
	WC5[I]	2.8	3.6	32.5	2.23	27625*	66			2.2x0.8
	WC6[I]	2.8	3.6	30.9	2.45	26265*	66			2.2x0.8
	WC7[I, II]	2.8	3.6	33.4	1.31	19000	66			
	WC8[II]	2.8	3.6	33.3	3.05	17500	66			
	WC9[II]	2.8	3.6	21.7	1.16	17400	66			
	WC10[II]	2.8	3.6	23.5	2.63	13200	66			

Table 4.3: Details of specimens used in validation of FE model (Full-scale CMU, Cont'd)

		H (m)	L (m)	f'_m (MPa)	f'_t (MPa)	E_m (MPa)	t_e (mm)	Beam section	Column section	Opening size (h×l, m×m)
Richardson (1986)	WD6 II	2.8	3.6	26.3	2.70	17300	66	W250x58	W200x46	2.2x0.8
	WD7 II	2.8	3.6	25.4	3.05	18000	66			
	WD5 I	2.8	3.6	29.4	2.87	19000	66			
	WD11 II ①	2.8	3.6	24.6	1.46	12400	66			
	WD12 I	2.8	3.6	24.2	2.40	15500	66			2.2x0.8
Riddington (1984)	R2a II	2.71	2.71	7.0	-	15400	100	152x152x30 UC*	152x152x30 UC*	
	R3a II ②	2.71	2.71	7.0	-	15400	100			
	R4a II ③	2.71	2.71	7.0	-	15400	100			
	R2b II	2.48	2.48	7.0	-	15400	100	406x140x39 UB*	406x140x39 UB*	
	R3b II ②	2.48	2.48	7.0	-	15400	100			
	R4b II ③	2.48	2.48	7.0	-	15400	100			

*E_m was not reported in the paper, a value of 850 f'_m was assumed

① 20mm top gap

② 3mm top gap

③ 3mm Top gap+ 1.5mm gap on each side

I : Specimen is used in verification of Model I

II: Specimen is used in verification of Model II

Table 4.4: Details of specimens used in validation of FE model (One-third scale CMU)

		H (m)	L (m)	f'_m (MPa)	E_m (MPa)	t_e (mm)	Beam section	Column section	Opening size ($h \times l$, m×m)
Liu & Soon (2012)	P1NA [II] **	1.08	1.08	8.6	10496	43	W100x19	W100x19	
	F1NA [II] **	1.08	1.08	9.6	14430	64			
	P3NA [II] **	1.08	1.35	7.3	10496	43			
	P3NI [II]	1.08	1.35	10.3	10496	43			
	F3NA [II] **	1.08	1.35	10.3	14430	64			
	F3NI [II]	1.08	1.35	7.3	14430	64			
	P3WA [I, II]	1.08	1.35	10.3	10496	43			0.28x0.5
	P3DA [I, II]	1.08	1.35	10.3	10496	43			0.64x0.4
	P6NA [II] **	1.08	1.76	10.3	10496	43			
									Vertical load (kN)
Liu & Manesh (2013)	CF-113 [II]	1.08	1.35	9.1	12800	64	W100x19	W100x19	111
	CF-213 [II]	1.08	1.35	9.1	12800	64			80
	CF-313 [II]	1.08	1.35	9.1	12800	64			49
	CP-113 [II]	1.08	1.35	9.4	10100	43			111
	CP-213 [II]	1.08	1.35	9.4	10100	43			80
	CP-313 [II]	1.08	1.35	9.4	10100	43			49

Table 4.5: Details of specimens used in validation of FE model (SCT)

		H (m)	L (m)	f'_m (MPa)	E_m (MPa)	t_e (mm)	Beam section	Column section
Flanagan (1994)	F1[I, II]	2.24	2.24	3.0	2300	195	W310x52	W250x18
	F2[I, II]	2.24	2.24	3.0	2300	195	W310x52	W250x45
	F3[I, II]	2.24	2.24	3.0	2300	195	W310x52	W250x67
	F4[I, II]	2.24	2.24	2.6	2800	325	W460x113	W410x39
	F5[I, II]	2.24	2.24	2.6	2800	325	W460x67	W410x60
	F9[I, II **]	2.24	2.24	3.0	2300	195	W310x52	W250x45
	F17[I, II]	2.24	3.45	3.0	2300	195	W310x52	W250x45
	F21[I, II]	2.24	2.84	3.0	2300	195	W310x52	W250x45

**Columns are strong-axis oriented

[I] : Specimen is used in verification of Model I

[II]: Specimen is used in verification of Model II

Table 4.6: Stiffness and strength comparison of the experimental and Model I results

		K_{exp} (kN/mm)	P_{exp} (kN)	K_{FE} (kN/mm)	P_{FE} (kN)	$\frac{K_{exp}}{K_{FE}}$	$\frac{P_{exp}}{P_{FE}}$
Infills with opening							
Amos (1985)	WC3	34	285	37	255	0.92	0.90
	WC4	34	335	32	307	1.06	0.91
	WC5	39	245	38	251	1.01	1.02
	WC6	50	365	37	358	1.35	0.98
Richardson (1986)	WD5	55	334	44	305	1.25	0.91
	WD12	22	196	25	189	0.88	1.07
Liu & Soon (2012)	P3WA	21	89	14	112	1.45	0.80
	P3DA	11	75	12	91	0.94	0.83
AVG						1.11	0.92
COV(%)						18	11
Solid infills							
McBride (1984)	WA1	73	471	75	476	0.97	0.99
	WA2	82	440	75	481	1.09	0.91
	WA3	74	463	75	460	0.99	1.01
	WA4	63	476	68	424	0.93	1.12
Yong (1984)	WB1	72	449	62	412	1.16	1.09
	WB2	74	538	81	581	0.91	0.93
	WB3	67	556	77	546	0.87	1.01
Amos (1985)	WC1	41	420	68	451	0.60	0.93
	WC2	46	310	37	403	1.24	0.77
	WC7	71	534	81	537	0.88	0.99
Flanagan (1994)	F1	15	122	18	125	0.80	0.98
	F2	11	166	15	145	0.74	1.15
	F3	-	158	21	140	-	1.13
	F4	27	228	30	211	0.90	1.08
	F5	23	191	25	225	0.92	0.85
	F9	29	220	30	330	0.94	0.67
	F17	19	212	17	226	1.10	0.94
	F21	13	180	14	196	0.88	0.92
AVG						0.94	0.97
COV(%)						16	13
Overall							
AVG						0.99	0.96
COV(%)						19	12

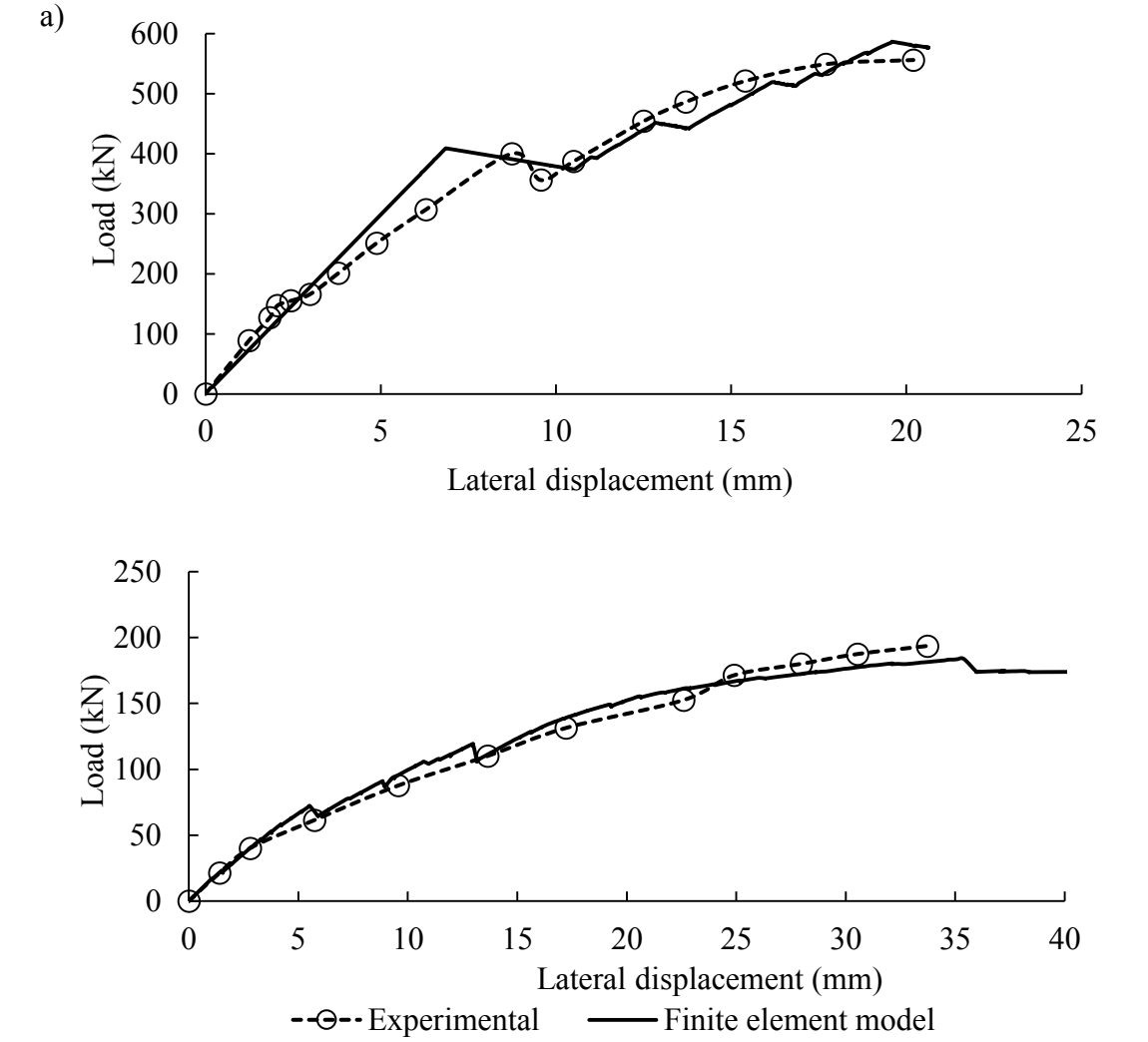

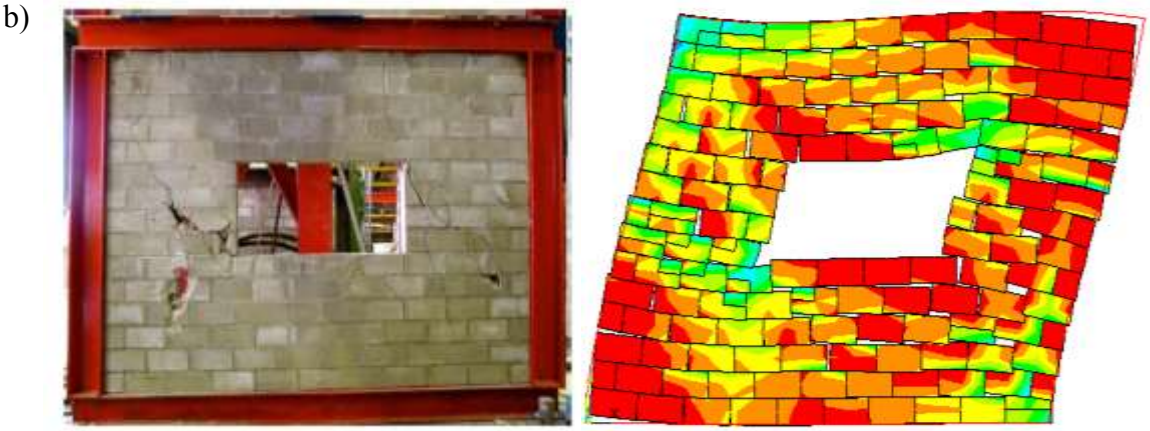

Fig. 4.7: Comparison of experimental and Model I results: (a) load vs. lateral displacement curves of WB2 and WD12; (b) cracking pattern of P3WA (the yellow/green area is stressed area whereas the red area is non-stressed area).

4.5.2 Model II

Model II was adopted for investigation of the effects of the following parameters: aspect ratio, masonry compressive strength, grouting extent and configuration, vertical reinforcement, joint reinforcement, relative infill-to-frame stiffness, vertical load, and interfacial gaps. In addition to those experimental studies used in the verification of Model I (McBride, 1984; Yong, 1984; Amos, 1985; Richardson, 1986; Flanagan, 1994; Liu & Soon, 2012) the studies conducted by Riddington (1984) and Liu and Manesh (2013) were also added in the verification of Model II. A total of 45 specimens were considered including 24 specimens infilled with full-scale CMUs, thirteen specimens infilled with one-third scale CMUs, and 8 specimens infilled with SCTs. In the case of full-scale CMU infilled specimens as shown in Table 4.3, specimen WA4, WC7, WD7, R2a and R2b were control specimens constructed without reinforcement, grouting, openings, or gaps, or ties; nine specimens (WA1, 2, 3; WB1, 2, 3 and WC8, 9, 10) had horizontal truss-type joint reinforcement (Blok-Trus BL30) placed in alternate bed joints starting at the second course from the bottom; two specimens (WA5 and WB6) had panel-to-column flat bar ties at alternate joints; WD6 had a 600 mm length of 20M rebar placed vertically in each cell along the compression diagonal. Seven specimens had a gap(s) between the infill and the frame, among which five specimens had a top beam-infill gap (WB4, WB5, WD11, R3a and R3b) and two specimens had both column-infill and beam-infill gap (R4a and R4b). In the case of one-third scale CMU infilled specimens (Table 4.4), seven specimens were partially grouted and vertically reinforced with steel rebar with a diameter of 6 mm (P1NA,

P3NA, P3NI, P6NA, CP-113, CP-213, and CP-313); six specimens were fully grouted (F1NA, F3NA, F3NI, CF-113, CF-213, and CF-313). The vertical reinforcement location and amount remained the same as their partially grouted counterparts. In addition to the grouting variation, specimen CF-113, CF-213, CF-313, CP-113, CP-213 and CP-313 were subjected to combined lateral and vertical load. Three vertical load levels including 111 kN, 80 kN, and 49 kN, applied at the two one-third points of the beam were considered. In the case of SCT infilled specimens (Table 4.5), F1, F2, F3, F4, F5, F9, F17 and F21 had frame members varies from W250x19 to W460x113. Tables 4.7 to 4.9 summarize the comparison results. All SCT specimens were subjected to cyclic static loading with increasing displacement amplitude in both directions and values for the stiffness and strength in both directions are listed. The FE values, however, were obtained from models loaded in one direction monotonically to failure, and this value was used for the other direction as well.

Tables 4.7 to 4.9 show that for either CMU infills or SCT infills, the average test-to-FE ratios of ultimate load and stiffness are all close to unity with an overall coefficient of variation (COV) of 16% for cracking stiffness and 15% for ultimate load. This suggests that the finite element model is accurate in providing the stiffness and strength estimates, and this accuracy is reasonably consistent for all specimens considered. Fig. 4.8 compares the experimental and numerical load vs. lateral displacement curves for two standard infill (WC7 and WB2), an infill with joint reinforcement (specimen WA2), three infilled frames subjected to combined loading (specimen CF-113, CF-213 and CF-313), a fully grouted

infill with vertical reinforcement (specimen F3NA), and two gapped infills (specimen R3a and R4a). The crack pattern and failure mode comparison of specimen WB2, R3a and R4a are presented in Fig. 4.9. These figures further illustrate that the finite element model can simulate the behaviour and failure mode reasonably well where the degradation of stiffness due to cracking in the infill and development of cracking and crushing as loading progressed is accurately captured.

Table 4.7: Stiffness and strength comparison of the experimental and Model II results (Full-scale CMU)

		K_{exp} (kN/mm)	P_{exp} (kN)	K_{FE} (kN/mm)	P_{FE} (kN)	$\frac{K_{exp}}{K_{FE}}$	$\frac{P_{exp}}{P_{FE}}$
McBride (1984)	WA1	73	471	68	475	1.07	0.99
	WA2	82	440	90	420	0.91	1.05
	WA3	74	463	87	455	0.85	1.02
	WA4	63	476	77	449	0.82	1.06
	WA5	78	445	83	445	0.94	1.00
Yong (1984)	WB1	72	449	80	409	0.90	1.10
	WB2	74	538	81	581	0.91	0.93
	WB3	67	556	80	549	0.84	1.01
	WB4	27	209	24	219	1.13	0.95
	WB5	34	231	29	254	1.17	0.91
	WB6	73	423	94	464	0.78	0.91
Amos (1985)	WC7	71	534	76	490	0.93	1.09
	WC8	65	445	81	578	0.80	0.77
	WC9	54	400	58	460	0.93	0.87
	WC10	68	458	62	487	1.10	0.94
Richardson (1986)	WD6	65	623	69	564	0.94	1.10
	WD7	56	494	61	457	0.92	1.08
	WD11	14	167	13	175	1.08	0.95
Riddington (1984)	R2a	30	209	36	226	0.83	0.92
	R2b	60	411	67	423	0.90	0.97
	R3a	29	199	23	189	1.26	1.05
	R3b	45	382	35	323	1.29	1.18
	R4a	7	170	7	167	0.97	1.02
	R4b	19	363	18	331	1.06	1.10
AVG						0.97	1.00
COV						14%	9%

Table 4.8: Stiffness and strength comparison of the experimental and Model II results (One-third scale CMU)

		K_{exp} (kN/mm)	P_{exp} (kN)	K_{FE} (kN/mm)	P_{FE} (kN)	$\frac{K_{exp}}{K_{FE}}$	$\frac{P_{exp}}{P_{FE}}$
Liu & Soon (2012)	P1NA	20	111	21	148	0.95	0.75
	F1NA	23	157	27	177	0.85	0.89
	P3NA	25	94	22	148	1.14	0.64
	P3NI	13	79	12	61	1.08	1.30
	F3NA	26	132	31	130	0.84	1.02
	F3NI	18	122	17	96	1.06	1.27
	P6NA	23	104	20	106	1.15	0.98
Liu & Manesh (2013)	CF-113	37	198	36	203	1.03	0.98
	CF-213	32	169	32	163	1.00	1.04
	CF-313	29	152	28	161	1.04	0.94
	CP-113	26	126	28	133	0.93	0.95
	CP-213	25	120	27	129	0.93	0.93
	CP-313	26	109	24	99	1.08	1.10
AVG						1.01	0.98
COV						10%	18%

Table 4.9: Stiffness and strength comparison of the experimental and Model II results (SCT)

		K_{exp} (kN/mm)	P_{exp} (kN)	K_{FE} (kN/mm)	P_{FE} (kN)	$\frac{K_{exp}}{K_{FE}}$	$\frac{P_{exp}}{P_{FE}}$
Flanagan (1994)	F1	14.7	122	14.3	134	1.03	0.91
	F1L	11.7	165	14.3	134	0.82	1.23
	F2	10.9	166	17.5	189	0.62	0.88
	F2L	17.8	183	17.5	209	1.02	0.88
	F3	-	158	20.9	134		1.18
	F3L	-	168	20.9	134		1.25
	F4	26.7	228	23.9	214	1.12	1.07
	F4L	13.7	149	23.9	214	0.57	0.70
	F5	23.2	191	25.5	172	0.91	1.11
	F5L	28.3	168	25.5	172	1.11	0.98
	F9	28.7	220	27.6	325	1.04	0.68
	F9L	32.0	207	27.6	325	1.16	0.64
	F17	18.5	212	22.6	228	0.82	0.93
	F17L	16.0	206	22.6	228	0.71	0.90
	F21	12.7	180	16.9	218	0.75	0.83
	F21L	13.2	203	16.9	218	0.78	0.93
AVG						0.89	0.94
COV						22%	20%

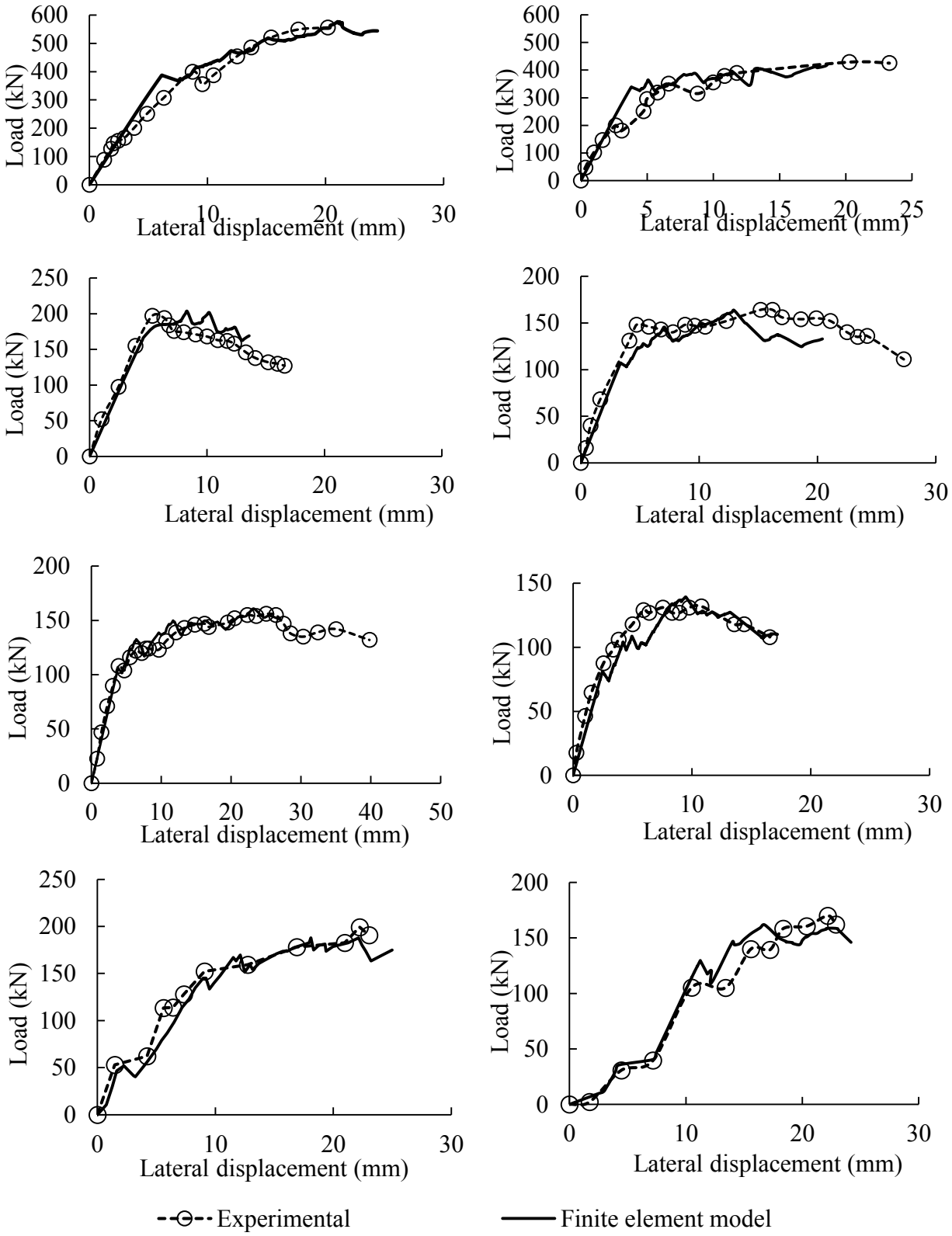

Fig. 4.8: Comparison between Model II and experimental load vs. lateral displacement curves: a) WB2, b) WA2, c) CF113, d) CF213, e) CF313, f) F3NA, g) R3a andh) R4a

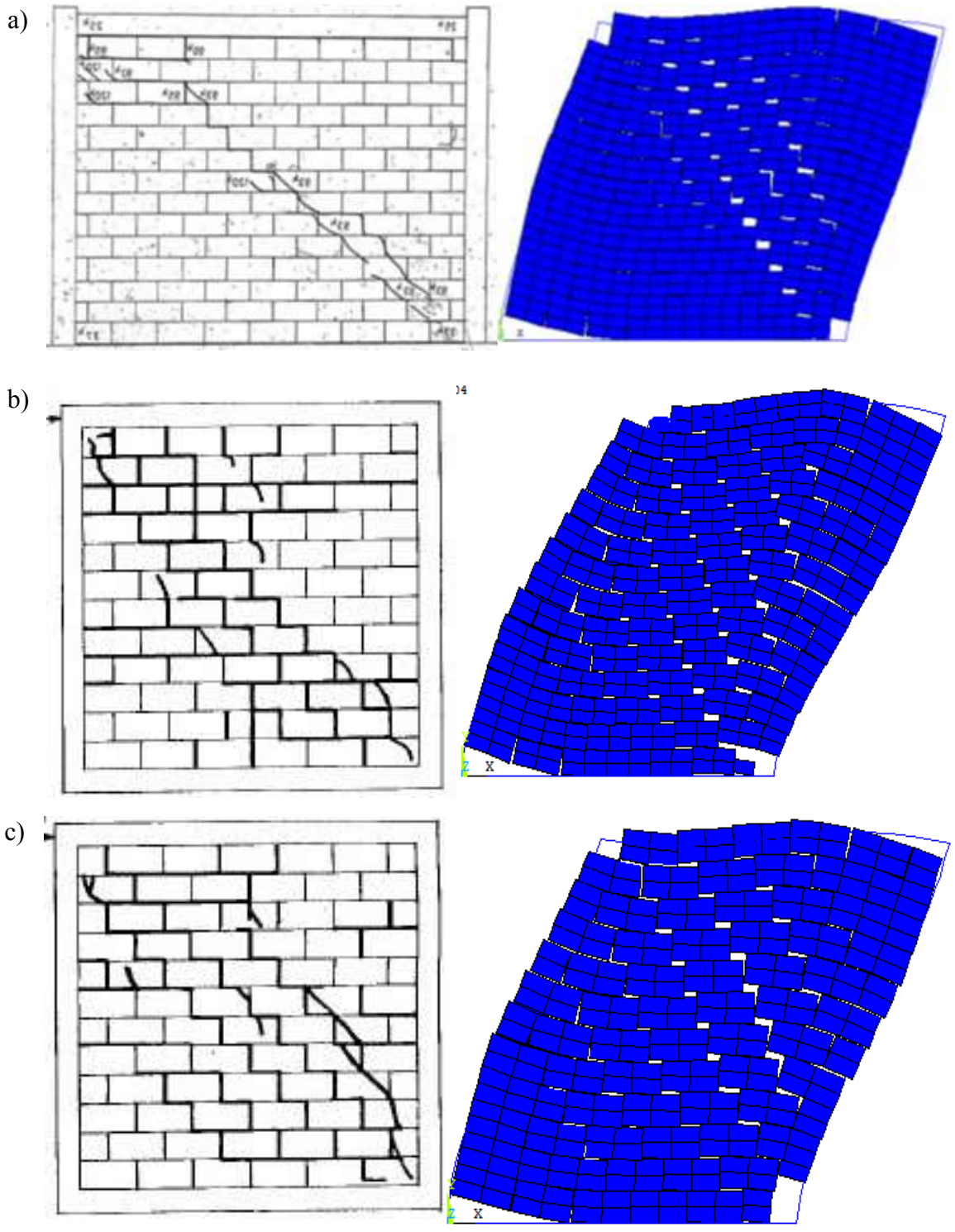

Fig. 4.9: Comparison of cracking patterns between Model II and experimental results: a) specimen WB2, b) specimen R3a, and c) specimen R4a

4.6 Comparison of Two Models

In comparison with the Model I, adoption of Model II reduces the computing time by about 30%. The saving mainly resulted from elimination of the need to examine the stress state of each element and modify the stiffness of each failed spring using user-defined macro commands at the end of each load step. In addition, the Model II requires no user-defined rules or user-assumed α value and thus requires less input. A comparison between the load vs lateral displacement curves produced by both models is shown in Fig. 4.10. It shows that while values for the initial stiffness as well as the ultimate load obtained from two models are comparable, the discrepancies are observed in the post-cracking behaviour. The Model I tends to underestimate the post-cracking stiffness of the infill due to user-defined rules and parameters whereas the Model II with cohesive zone interface element has a load vs displacement curve very similar to experimental results.

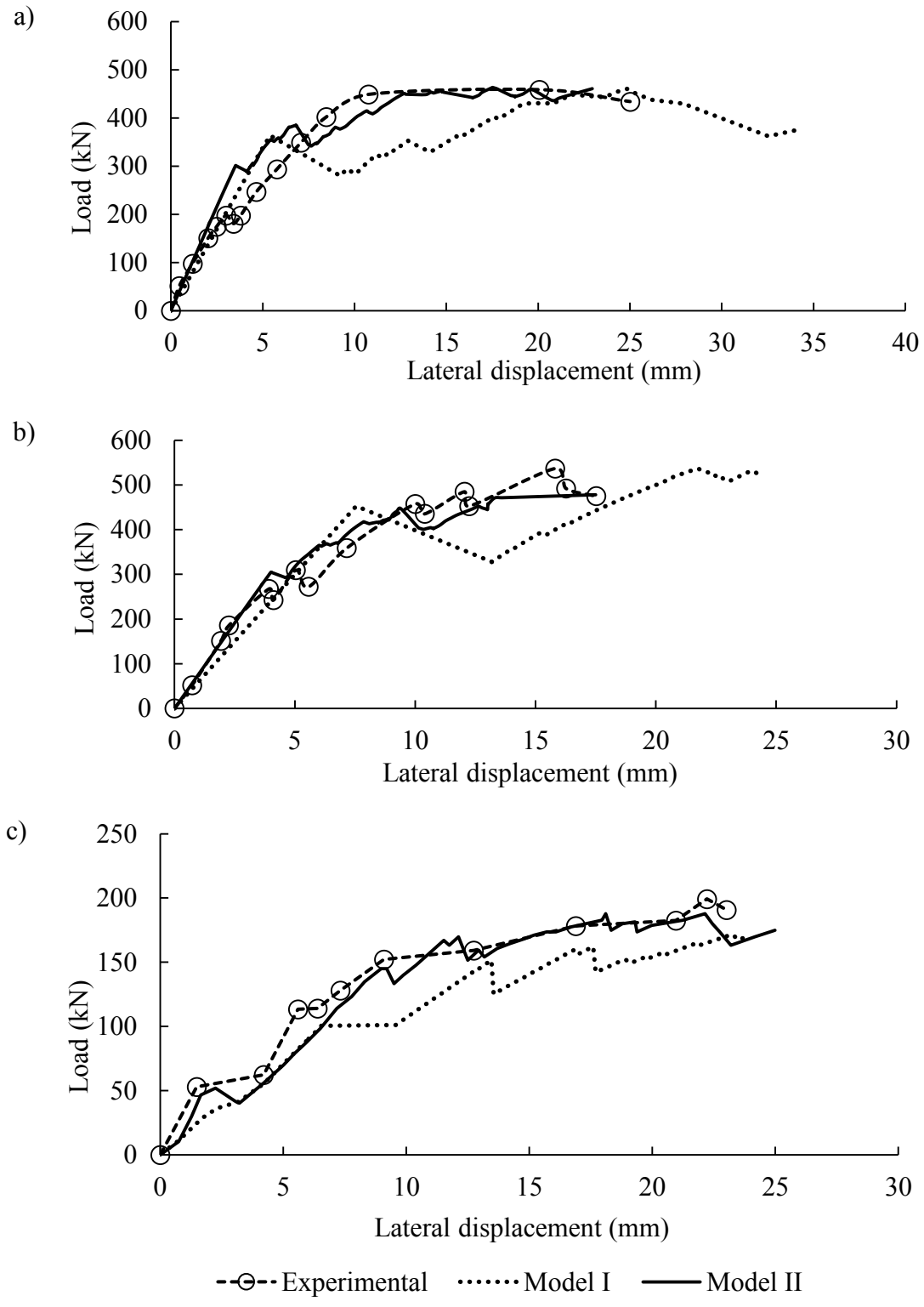

Fig. 4.10: Comparison of FE and experimental load vs. lateral displacement curves: a) WA3 (McBride, 1984) b) WC7 (Amos, 1986) and c) R3a (Riddington, 1984)

Chapter 5 Parametric Study on Infill Openings

5.1 Introduction

Door or window openings are often provided in masonry infills for either architectural or ventilation purposes. In comparison with extensive experiments on solid masonry infills, infills with door or window openings are less researched and even within the few available studies, limited parameters were considered. It is commonly accepted that the presence of infill openings reduces the lateral stiffness and strength of the infilled system (Mallick & Garg, 1971; Amos, 1985; Richardson, 1986; Schneider et al., 1998; Kakaletsis & Karayannis, 2008; Liu & Soon, 2012; Liu & Manesh, 2013). Liu and Soon (2012) further showed that the reduction in stiffness and strength is not proportional to the opening size and opening aspect ratio may be a factor as well.

Flanagan (1994) introduced a 600×600 mm opening placed in the corner of the clay tile infill wall within a steel frame. He reported that the opening on the loaded side of the panel reduced the in-plane capacity of the system by approximately 25% in the pull direction and over 50% in the push direction. Results of the experimental study conducted by Tasnimi and Mohebkhah (2011) indicated that infilled frames with openings are not always more ductile than the ones with solid infills. It seems that the ductility of such frames depends on the failure mode of infill piers. The infills in this experimental investigation experienced pier diagonal tension or toe crushing failure and had smaller ductility factors than those frames with solid infills. Tasnimi and Mohebkhah (2011) attributed such loss of ductility

to the brittle failure of the masonry piers having strong mortar as well as the out-of-plane instability of infill piers.

As for the location of the opening, conflicting findings have been reported. Kakaletsis and Karayannis (2008) suggested placing the opening near the edge of infill to achieve best improvement in the performance whereas others indicated that the openings be located at the center of the infill (Amos, 1985; Dawe & Seah, 1989; Mallick & Garge, 1971).

Due to the lack of technical information, the current Canadian and American masonry design standards (CSA S304-14, 2014; MSJC, 2013) do not contain design provisions for masonry infills with openings. In this chapter, a numerical study was conducted to investigate the effect of opening size and location on the in-plane behaviour and strength of masonry infills bounded by steel frames. An analytical method that take into account the effect of openings on the stiffness and strength of infills was proposed based on the finite element results, and the efficacy of the proposed method and other existing methods was assessed using available experimental results.

5.2 Existing Analytical Methods

Based on the diagonal strut approach for solid infills, the simple and practical way of taking into account of opening effect is to apply a reduction factor, R_F, to the width of the corresponding solid infill, w, resulting in an effective width of $R_F \times w$. The existing analytical methods adopted this approach and details of each method are summarized in the following sections. All existing methods expressed the reduction factor as some form

of a polynomial function of opening-to-infill area ratio. It is noted that some proposed equations are valid for only stiffness or strength reduction factors whereas others are intended for both.

5.2.1 Durrani and Luo (1994)

Durrani and Luo (1994) proposed the following empirical equations to calculate the reduction factor, R_F, for both stiffness and strength consideration based on a finite element study.

$$R_F = 1 - (\frac{A_d}{H \times L})^2 \tag{5.1}$$

$$A_d = H \times L - \frac{[R\sin(2\theta) - R_o \sin(\theta + \theta_o)]^2}{2\sin(2\theta)} \tag{5.2}$$

$$R_0 = \sqrt{H_o^2 + L_o^2} \tag{5.3}$$

$$R = \sqrt{H^2 + L^2} \tag{5.4}$$

where H_o and L_o are the height and length of the opening respectively; θ_o is calculated as $tan^{-1}(H_o/L_o)$, the rest of the symbols are the same as previously defined.

5.2.2 Al-Chaar et al. (2003)

Al-Chaar et al. (2003) developed an expression for the reduction factor as a function of the ratio of opening-to-infill area, A_o/A_p, to account for the effect of openings on both stiffness and strength by conducting a series of experimental tests and analytical studies.

$$R_F = 1 + 0.6(A_o / A_p)^2 - 1.6(A_o / A_p) \tag{5.5}$$

5.2.3 New Zealand Society for Earthquake Engineering (2006)

Based on the work of Dawe and Seah (1989), the New Zealand Society for Earthquake Engineering (NZSEE) recommends a simplified expression for R_F to account for the

reduction in stiffness and strength due to an opening.

$$R_F = 1 - \frac{1.5 \times L_o}{L} \tag{5.6}$$

This formula calculates the R_F factor solely based on the length of the opening and infill instead of the area of the opening and infill. When the length of opening exceeds 2/3 of the length of infill, the contribution of infill can be ignored.

5.2.4 Mondal and Jain (2008)

Based on finite element studies and experimental data of reinforced concrete infilled frames, Mondal and Jain (2008) proposed a linear relationship for stiffness reduction factor as follows:

$$R_F = 1 - 2.6(A_o / A_p) \tag{5.7}$$

It suggests that the contribution of the infill to the stiffness of the system can be neglected when the opening area is greater than 38% of the infill area.

5.2.5 Tasnimi and Mohebkhah (2011)

Based on a series of experiments on the in-plane seismic behaviour of steel frames with clay brick masonry infills having openings, Tasnimi and Mohebkhah (2011) proposed the following expression as the reduction factor in strength only where an upper limit of A_o/A_p is set to be 0.4.

$$R_F = 1 + 1.49(A_o / A_p)^2 - 2.238(A_o / A_p) \tag{5.8}$$

5.2.6 Asteris et al. (2012)

Asteris et al. (2012) proposed the following expression for reduction factor in stiffness only. The authors placed an upper limit of A_o/A_p of 0.5, above which the infill was considered

negligible.

$$R_F = 1 - 2(A_o / A_p)^{0.54} + (A_o / A_p)^{1.14} \tag{5.9}$$

5.2.7 Mohammadi and Nikfar (2013)

Through a statistical analysis using experimental data, Mohammadi and Nikfar (2013) concluded that the material of confining frames (steel or RC) affected the reduction in strength but not the stiffness due to openings. Reduction in the infill strength with RC bounding frames was less than that with steel bounding frames. Hence, Mohammadi and Nikfar (2013) proposed two separate sets of reduction factor expressions for strength and stiffness of infill with openings as follows:

For stiffness:

$$R_F = 1 + 1.1859(A_o / A_p)^2 - 1.6781(A_o / A_p) \tag{5.10}$$

For strength:

$$R_F = 1 - 2.122(A_o / A_p) \quad \text{for steel frames} \tag{5.11}$$

$$R_F = 1 - 1.085(A_o / A_p) \quad \text{for RC frames} \tag{5.12}$$

It is noted that none of the methods consider the eccentricity of openings; all openings are assumed to be located at the center of the infill.

5.3 Numerical Study of Openings

The Model I was adopted in this study. For the standard specimen, the bounding frame was made of W250x58 columns and W200x46 beams. The frame members were oriented such that the webs of the beams were in the plane of the infill while the webs of the columns

were perpendicular to the plane of the infill. This orientation was also used for parametric studies presented in Chapter 6 to 8. The infill was 2800 mm high by 3600 mm long. The infill compressive strength was assumed to be 25 MPa and the tensile strength was taken as the 1/10th of the compressive strength. Three variables, i.e., the size, location and the aspect ratio (H_o/L_o) of the opening in the infill were considered, and the resulting model specimens are summarized in Table 5.1.

Table 5.1: Infill opening study parameters

Nominal percentage of opening	A_o/A_p	H_o (m)	L_o (m)	H_o/L_o	H (m)	L (m)	e_c/L
Size and location of the opening							
10%	0.107	0.9	1.2	0.75	2.8	3.6	-1/6~1/6
20%	0.190	1.2	1.6	0.75	2.8	3.6	-1/6~1/6
30%	0.318	1.6	2.0	0.80	2.8	3.6	-1/6~1/6
40%	0.429	1.8	2.4	0.75	2.8	3.6	-1/6~1/6
50%	0.556	2.0	2.8	0.71	2.8	3.6	0
60%	0.611	2.2	2.8	0.79	2.8	3.6	0
Aspect ratio of the opening							
3%	0.032	0.8	0.4	2.00	2.8	3.6	0
13%	0.127	1.6	0.8	2.00	2.8	3.6	0
29%	0.286	2.4	1.2	2.00	2.8	3.6	0
3%	0.032	0.4	0.8	0.50	2.8	3.6	0
10%	0.071	0.6	1.2	0.50	2.8	3.6	0
15%	0.127	0.8	1.6	0.50	2.8	3.6	0
20%	0.198	1.0	2.0	0.50	2.8	3.6	0
30%	0.286	1.2	2.4	0.50	2.8	3.6	0

The opening was introduced in the infill by removing the plane stress elements and joint elements on the infill panel which were covered by the opening. The opening dimensions were then designed to be multiples of the mesh size of plane stress elements so no

complication in meshing would be caused by introducing openings. Since the model adopted a 2x2 meshing for each concrete block (0.2 m by 0.4 m), the height of the opening must be multiple of half of the height of block (0.1m) and the length of the opening must be multiple of half of the length of block (0.2 m). Due to this limitation, the A_o/A_p ratios in this study were not round numbers.

For the opening sizes study, six sizes of window opening which represent about 10 to 60% of the infill area were studied. The length of the opening ranged from 1200 to 2800 mm whereas the height of the opening ranged from 900 to 2200 mm, resulting in an standard aspect ratio (H_o/L_o) around 0.75. In the study of opening location, locations including central, left-leaned and right-leaned were considered for opening size less than or equal to 40% of the infill area,, as shown in Fig. 5.1. The eccentricity of the opening, measured from the centre of the infill is indicated by e_c. Eccentricity towards the left (loaded side) is taken as negative, and eccentricity towards the right is taken as positive. For each direction, three offset values of 0.2, 0.4, and 0.6 m were considered resulting in e_c/L of 1/18, 1/9 and 1/6. For openings greater than 40% of the infill area, offsetting the opening away from the center of the infill caused part of the opening to be outside of the infill panel. Thus, the study on eccentricity was only conducted on openings that are smaller than or equal to 40% of the infill area. In the study of aspect ratio of the opening, in addition to the standard ratio of 0.75, two aspect ratios, i.e., $H_o/L_o = 0.5$ and $H_o/L_o = 2.0$ were considered, corresponding to a range of A_o/A_p from 0.032 to 0.286.

Note that in this as well as the following chapters, the following terms are adopted for evaluation of the infill behaviour: the lateral cracking stiffness, K_{cr}, which is defined as the lateral stiffness at the first major cracking load; the lateral ultimate strength of the infilled system, P_u, which is defined as the highest point on the load vs. lateral displacement curve; the net lateral strength of infills, P_{net}, which is calculated as the ultimate strength of the infilled system, P_u, subtracted by the corresponding load for a bare frame at the same displacement.

5.4 Discussion of Results

5.4.1 General Behaviour

The load vs. lateral displacement curves of infills with central openings are plotted in Fig. 5.2. As expected, a bare frame has the lowest stiffness which is approximately 5% of an infilled frame with solid infill. The presence of openings reduces the K_{cr} and P_u of infilled frames, and this reduction is related to the size of the opening. However, the ductility seems to increase as the size of the opening increases. Also observed in the behaviour typical of most specimens is that in the rising branch of the curve, there might be a drop in the load which often corresponded to the first crack in the infill and the load continued to increase immediately thereafter at a reduced stiffness. This behaviour is an indication of the ability of the infill to realign itself and establish alternate load path and thus maintain some level of resistance even after the development of cracking. However, when the opening size exceeds 40%, the alternative failure paths diminish and after reaching the maximum load, the load vs. lateral displacement curve becomes almost flat which is similar to a bare frame.

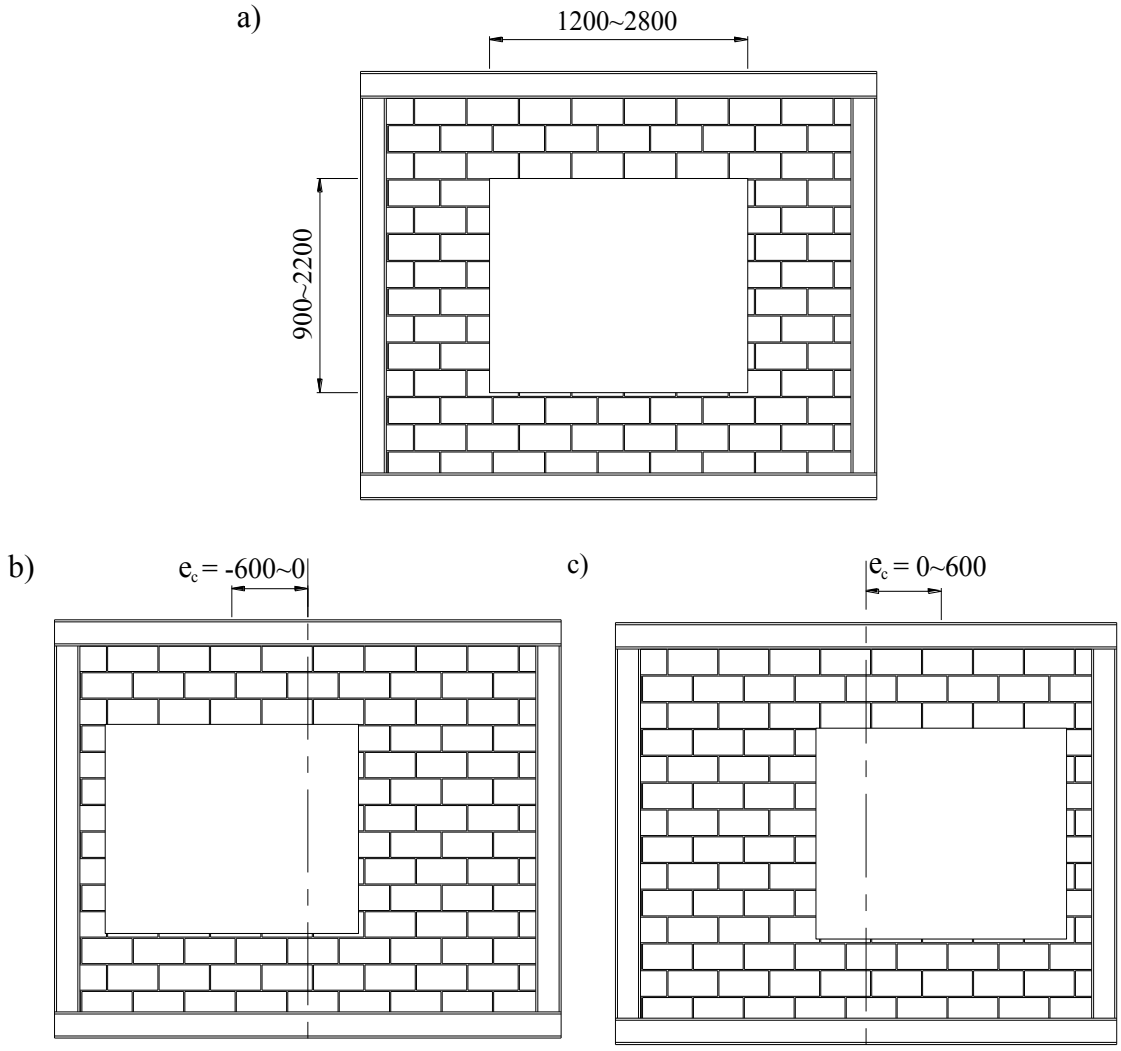

Fig. 5.1: Configuration of openings, unit (mm): a) central opening, b) left-leaned opening and c) right-leaned opening

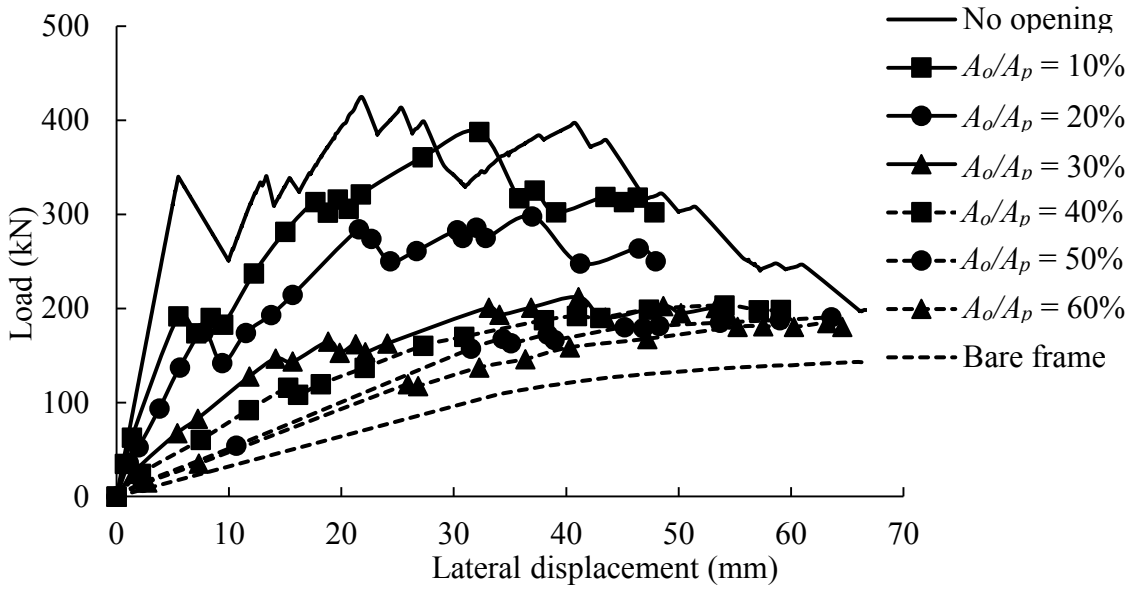

Fig. 5.2: Load vs. lateral displacement curves of Infills with different size of central opening

5.4.2 Effect of Opening Size

The effect of opening size is shown in Fig. 5.3 where the relationship between opening size and reduction factor R_F in the K_{cr}, P_u, and P_{net} for infills with a central opening is plotted. Two dotted lines in the figure mark the strength and stiffness of a bare frame as indicated.

Fig. 5.3 shows that the stiffness and strength of infills decrease drastically due to the presence of an opening. The rate of decrease slows down as the opening size increases. The overall relationship between the R_F in K_{cr} and P_{net} and the opening area ratio is approximately asymptotic, and for the opening area ratios considered in this study, the relationship can be approximated by a parabolic function. Comparison with the bare frame shows that when the opening area reaches 50% of the infill area, K_{cr} of the infilled frame is just slightly higher than the stiffness of a bare frame and P_{net} of the infill is less than 20% of the solid infill.

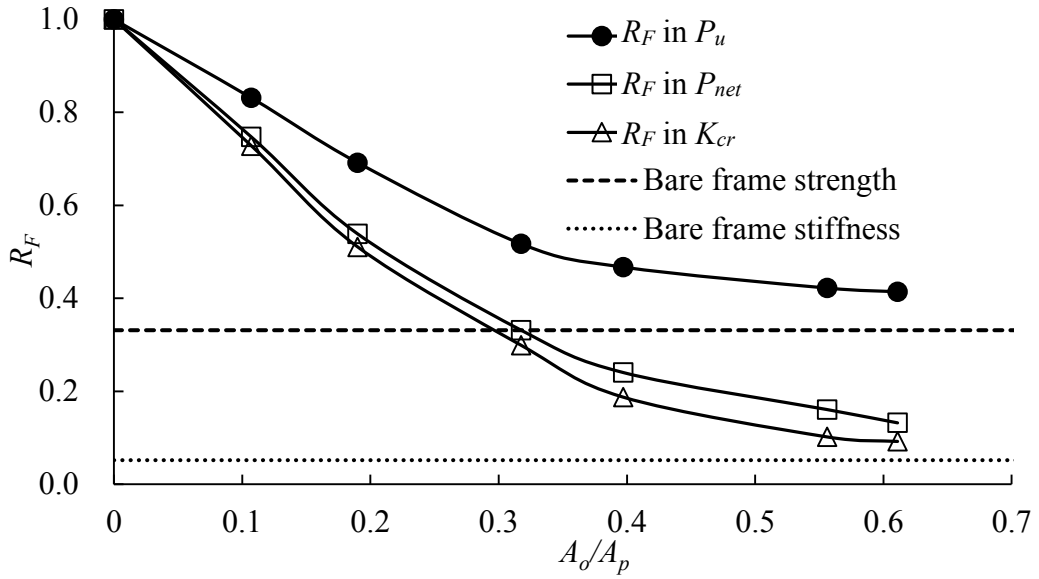

Fig. 5.3: The effect of openings sizes on the RF in stiffness and strength of the infill

5.4.3 Effect of Opening Location

The relationship between e_c/L and R_F in K_{cr} and P_{net} for infills with openings is presented in Fig. 5.4. Regardless of the location of the opening, an increase in the opening area results in reductions in both K_{cr} and P_{net} of infills. However, the rate of this reduction is associated with the opening location. In general, as the opening moves from the left off-centre to centre to right off-centre, the reduction lessens. In other words, when the opening offset is toward the loaded side, the K_{cr} and P_{net} are the lowest. As the opening offset moves away from the loaded side, the K_{cr} and P_{net} increase. This is more pronounced when the opening size becomes larger. Fig. 5.5 shows a finite element generated stress distribution in the infill. For an opening toward the loaded side, the pier on the loaded side becomes too thin to develop an effective strut while for an opening away from the loaded side, the pier on the loaded side is still capable of forming a strut resulting in an increase in K_{cr} and P_{net}. If the infill in a practical application is expected to resist lateral load in either direction, the

ideal location of the opening would, therefore, be at the centre of the infill.

5.4.4 Effect of Opening Aspect Ratio

The relationship between opening aspect ratio and R_F in K_{cr} and P_{net} is presented in Fig. 5.6. It can be observed that the aspect ratio of the opening does show some effect on the reduction in either K_{cr} or P_{net} while the effect of the latter is more pronounced. For a given A_o/A_p ratio, an opening aspect ratio decrease from H_o/L_o = 2.0 to 0.5, results in about 3% and 6% reduction in stiffness and strength respectively. It suggests that for a given A_o/A_p ratio, a narrow tall opening performs better than a narrow long opening, and the standard H_o/L_o = 0.75 is somewhat in between. However, the differences are only marginal.

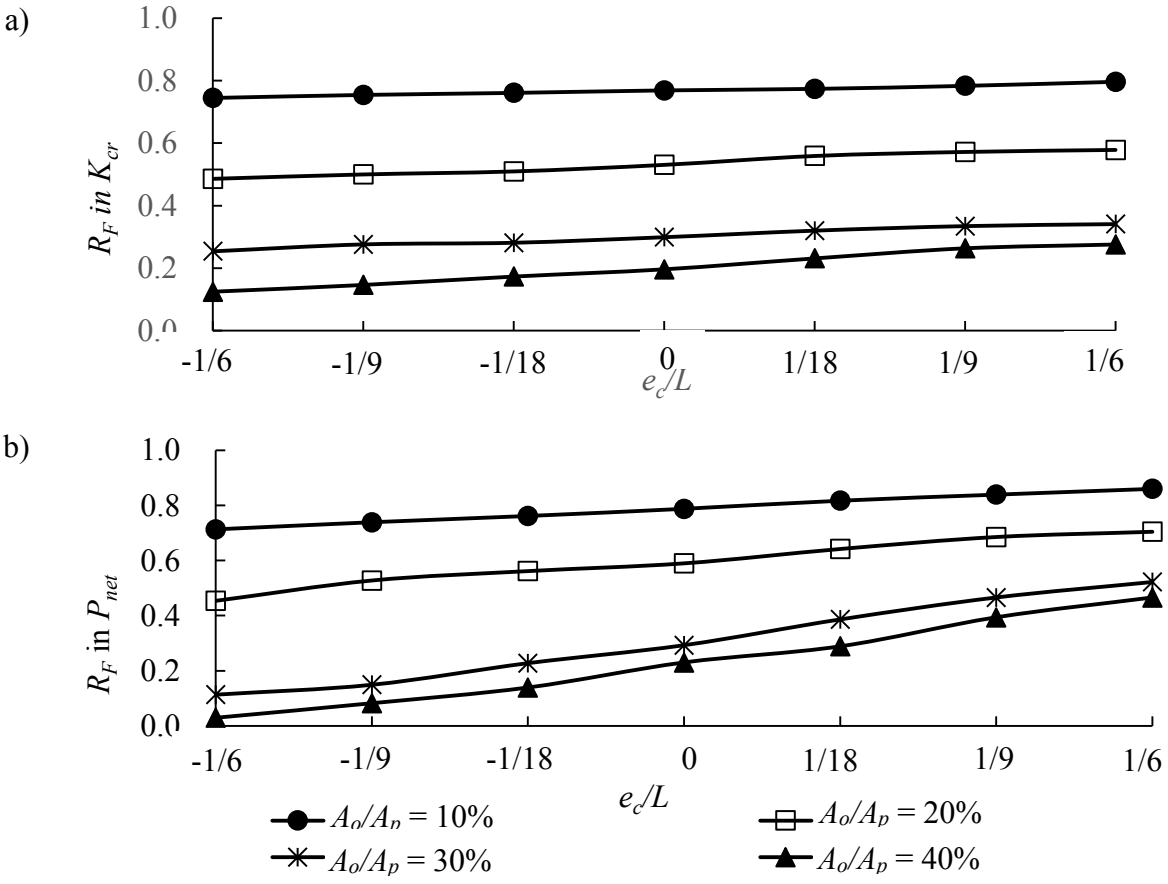

Fig. 5.4: The effect of opening location on a) the stiffness and b) the strength of infill

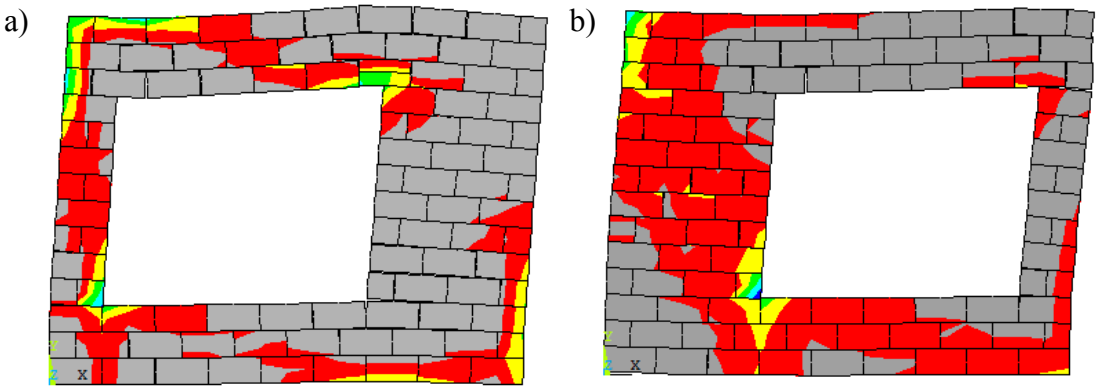

Fig. 5.5: Stress distribution and failure mode for infills with a) left-leaned opening; and b) right-leaned opening

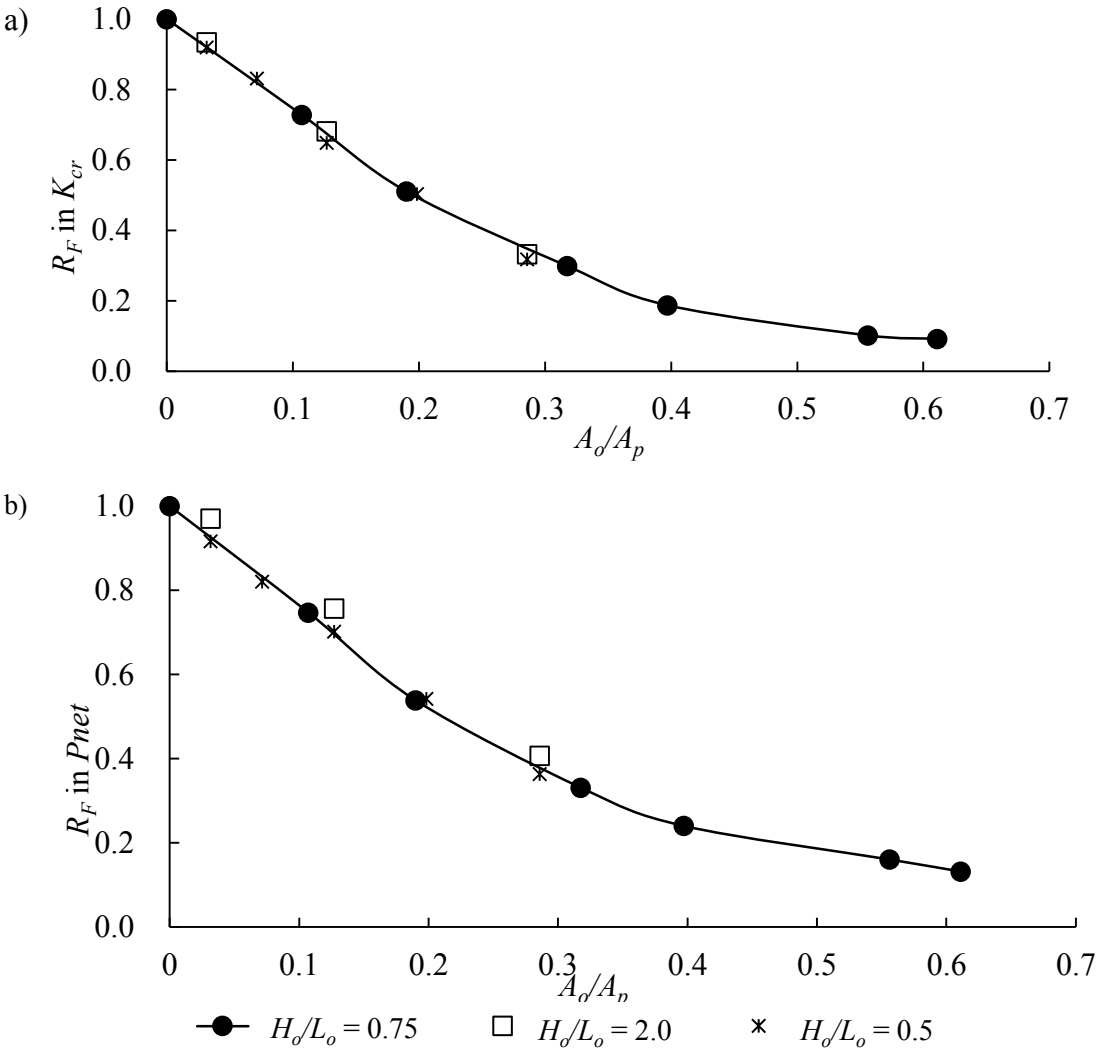

Fig. 5.6: The effect of opening aspect ratio on the reduction factor : a) K_{cr} and b) P_{net}

In order to further confirm the above finding for extremely wide or tall openings, studies on additional two series of specimens were conducted. As shown in Table 5.2, Series 1 consists of three specimens each with an extremely tall opening (H_o = 2.6m) while Series 2 consists of three specimens each with an extremely wide opening (L_o = 3.2m). The R_F(s) in K_{cr} and P_{net} for these two series of specimens are compared to the standard H_o/L_o = 0.75 cases, the comparison is presented in Fig. 5.7.

Table 5.2: Parameters of additional specimens

Nominal percentage of opening	A_o/A_p	H_o (m)	L_o (m)	H_o/L_o	H (m)	L (m)
Series 1						
20%	0.206	2.6	0.8	3.25	2.8	3.6
30%	0.310	2.6	1.2	2.17	2.8	3.6
40%	0.413	2.6	1.6	1.63	2.8	3.6
Series 2						
20%	0.190	0.6	3.2	0.19	2.8	3.6
30%	0.317	1.0	3.2	0.31	2.8	3.6
40%	0.444	1.4	3.2	0.44	2.8	3.6

It can be seen that for a given opening area, when an opening is either extremely tall or wide, the reduction in K_{cr} or P_{net} is generally larger than that of the standard H_o/L_o = 0.75 cases. This is expected since, in both series, the openings, running through almost the whole height or the whole width of the infill, divide each infill into either two vertical or two horizontal piers and completely disrupt formation of the diagonal strut in the infill. The remaining height or length that connects two piers of the infill is not stiff or strong enough to transfer lateral load from one pier to the other. Thus the resulted reduction is greater than other cases where an effective load transfer path can still be established despite of the

openings. It can also be observed that the reduction is more pronounced in Series 2 (L_o = 3.2 m) than in Series 1 (H_o = 2.6 m). Load transfer for these two specimens is shown in Fig. 5.8 where one may observe that in Series 1, the diagonal strut can still be relatively effectively established in the left pier of the infill which governs the behaviour of the infill (Fig. 5.8a) whereas in Series 2, the left pier is significantly weaker than in Series 1 and governs the failure of the whole infill (Fig 5.8b). It should be noted that while the openings of this configuration serve to complete a scientific discussion, they are not likely to occur in practice. For openings with aspect ratios within a realistic range (0.5~2.0), the variation in aspect ratio will not cause any significant change in R_F. This can be shown by the specimen with an opening of $H_o \times L_o$ = 2.6 m×1.2 m and the specimen with an opening of $H_o \times L_o$ = 2.6 m×1.6 m. These two specimens from Series 1 have an aspect ratio of 2.16 and 1.63, respectively. The resulted R_F in K_{cr} and P_{net} are very close to that of the standard H_o/L_o = 0.75 case.

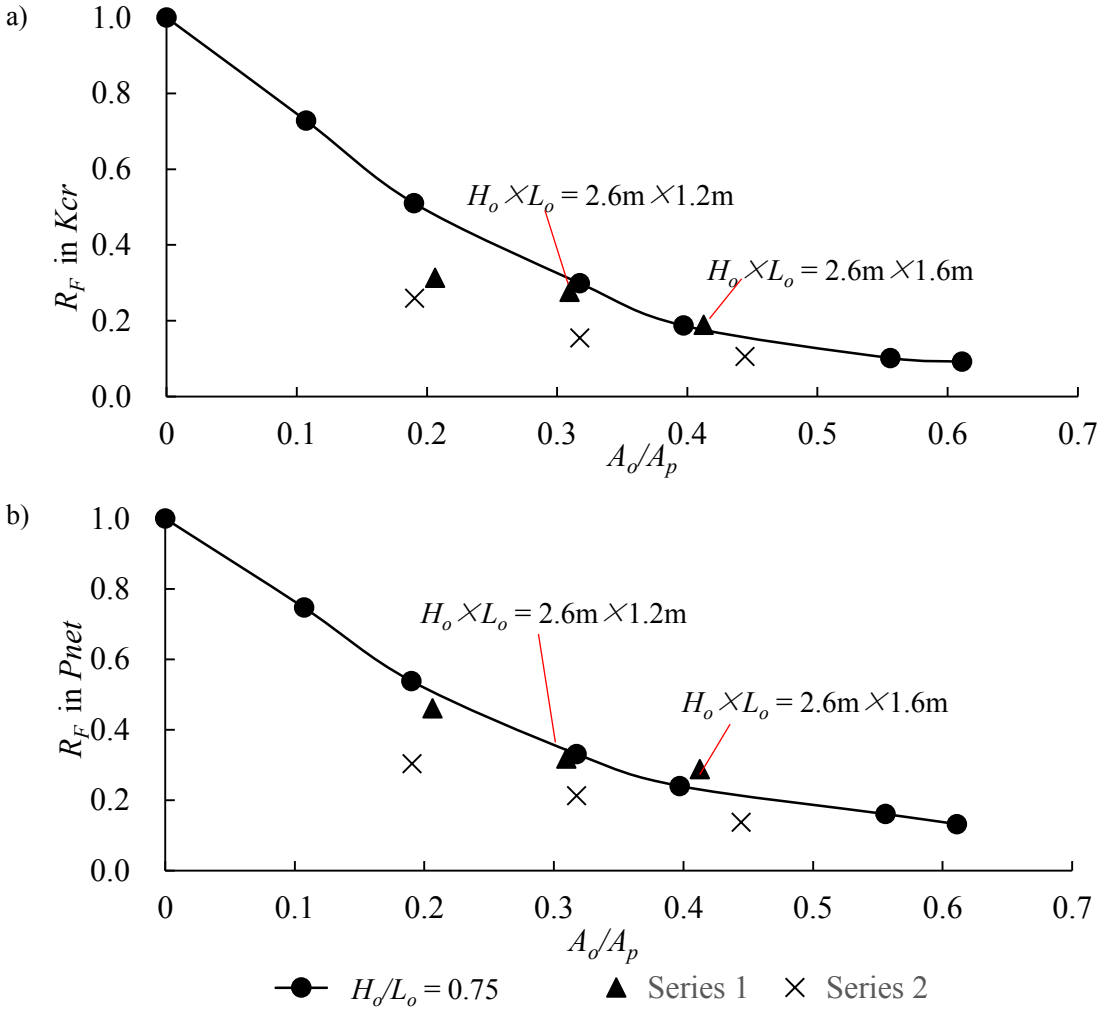

Fig. 5.7: Reduction factor in specimens with an extrmely tall opening or an extremly wide opening: a) K_{cr} and b) P_{net}

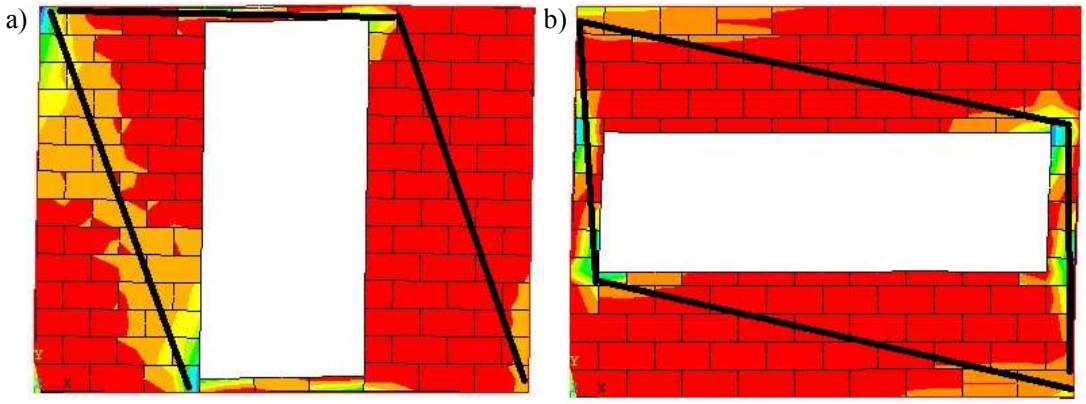

Fig. 5.8: Load transfer path in an infill with: a) a tall opening and b) a wide opening

5.4.5 Effect of Material and Geometric Input Properties

Recognizing that masonry infilled steel frames may have a large variability in the infill material properties and frame member sections, the effect of some input parameters on the trend of the reduction factor was studied, and results on infills with central openings are shown in Fig. 5.9. The line in the figure represents the trend determined from the standard model input values. Parameters considered were the masonry compressive strength f'_m, the Young's modulus of mortar E_{mortar}, and the infill-to-frame stiffness ratio

In each case, two additional values were considered to represent a range of masonry or frame properties that may be encountered in practice. The infill-to-frame stiffness ratio was considered using a factor λH where $\lambda = \sqrt[4]{\frac{E_m t \sin 2\theta}{4 E_f I_c H}}$ as defined in Eqn (2.2).

The figure shows that the change in masonry strength f'_m and mortar modulus E_{mortar} does not result in any significant variation in either the stiffness or strength reduction factor. Since both E_m and f_t are related to f'_m values, it is hence reasonable to deduce that variation on E_m and f_t input values will not result in any significant impact on the reduction factors either. The most marked variation on the strength reduction factor is observed when the infill-to-frame stiffness ratio was varied. As the infill-to-frame stiffness ratio decreases indicating a stiffer frame than the standard model, the same size of opening results in a greater reduction in strength. To account for the effects of all these parameters and aspect ratios, a lower bound reduction factor curve can be established using regression analysis as shown in Fig. 5.9.

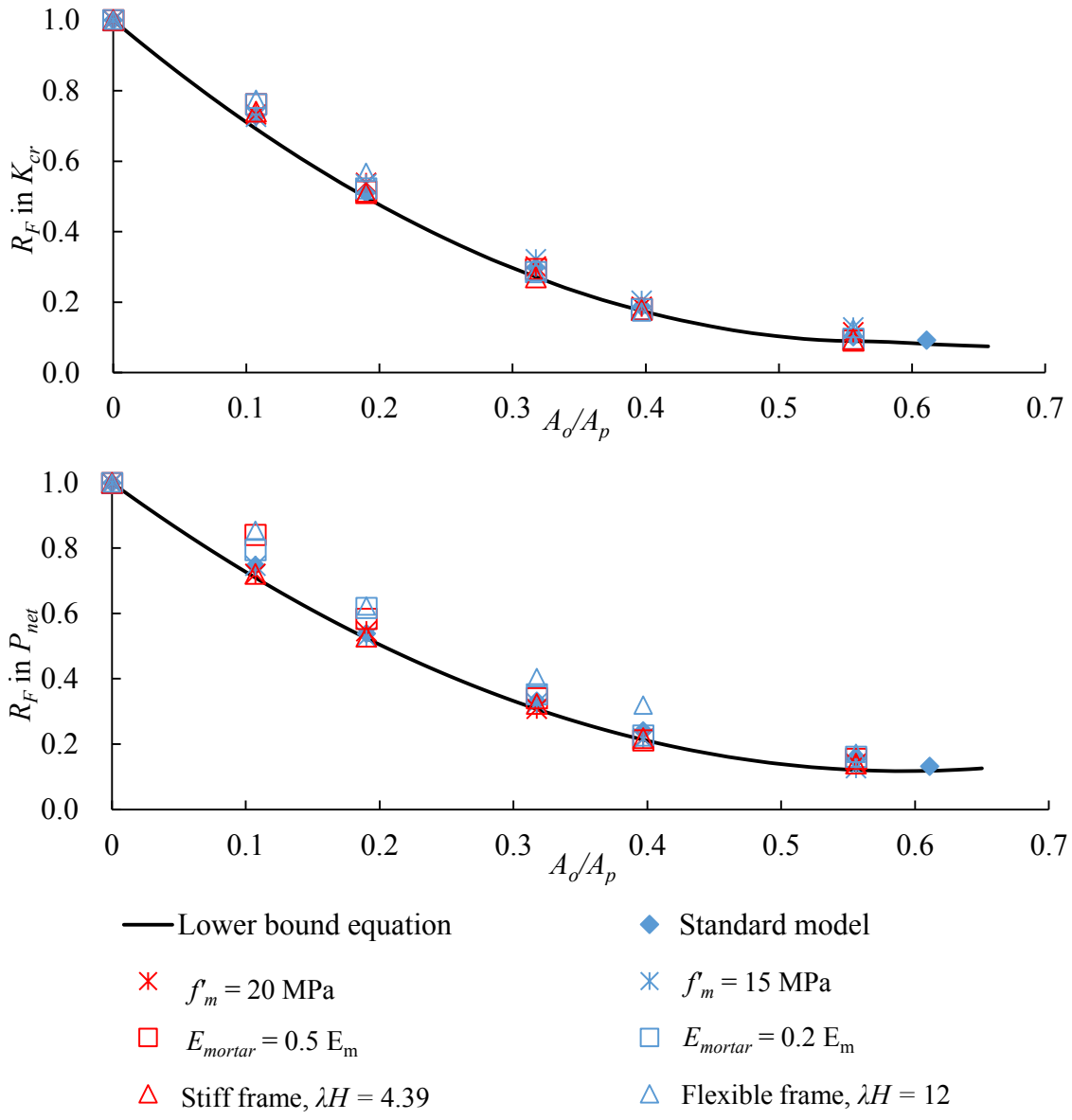

Fig. 5.9: The effect of material and geometric input properties on the reduction factor: a) K_{cr} and b) P_{net}

5.5 Proposed Analytical Method

The previous discussion shows that among the three parameters of the opening considered in this study, the size and location of the opening are two main factors influencing the K_{cr} and P_{net}. In the case of aspect ratios, within the practical range considered in this study (0.5~2.0), the effect of opening aspect ratio is marginal. Among the material input

parameters considered, frame stiffness has the greatest effect on the reduction in stiffness and strength. Keeping in line with the reduction factor approach, this study uses the following expression for determination of the reduction factor R_F:

$$R_F = 1 + f(A_o/A_p) \times g(e_c/L) \tag{5.13}$$

where $f(A_o/A_p)$ and $g(e_c/L)$ are two functions to account for the effects of size and location of the opening respectively. Through nonlinear regression analysis on the results of 61 finite element models, the expressions of $f(A_o/A_p)$ and $g(e_c/L)$ are determined as follows noting that the effect of material input parameters is accounted for using a lower bound approximation as described above.

For stiffness:

$$f(A_o / A_p) = 2.751(A_o / A_p)^2 - 3.170(A_o / A_p) \tag{5.14a}$$

$$g(e_c / L) = 1 - 0.533(e_c / L) \tag{5.14b}$$

For strength:

$$f(A_o / A_p) = 2.517(A_o / A_p)^2 - 2.981(A_o / A_p) \tag{5.15a}$$

$$g(e_c / L) = 1 - 1.738(e_c / L) \tag{5.15b}$$

The correlation between the equation and FE results is shown in Fig. 5.10 and a reasonably good correlation ($R^2 > 0.98$) for both K_{cr} and P_{net} is achieved. The equations show that the reduction factors in K_{cr} and P_{net} have a similar relationship with variables A_o/A_p and e_c/L. For simplicity, one general reduction factor is proposed as follows for both K_{cr} and P_{net}.

$$f(A_o / A_p) = 2.751(A_o / A_p)^2 - 3.170(A_o / A_p) \tag{5.16a}$$

$$g(e_c / L) = 1 - 1.121(e_c / L) \quad (5.16b)$$

The correlation of this set of equations with FE results is illustrated in Fig. 5.11. It shows that the use of a single reduction factor still achieves reasonable agreement with FE results, and the loss of accuracy is not significant.

5.6 Verification of Proposed Method

The efficacy of the proposed equations was assessed using existing experimental results on both solid and infills with openings (Amos, 1985; Richardson, 1986; Liu & Soon, 2012; Mondal & Jain, 2008; Mosalam et al., 1997). Detailed descriptions of these studies are available in the above-mentioned papers, and those key parameters are summarized in Table 5.3. It is noted that both window and door opening configurations were present in the studies. The A_o/A_p ratios covered by sample specimens ranged from 0.1 to 0.25, and the maximum aspect ratio was 2.75. The experimental reduction factors for both the stiffness, $R_{F,k}$, and strength, $R_{F,P}$, were calculated by dividing the stiffness and strength of specimens with openings by those of corresponding solid specimens. For experimental studies where the specimens with openings had different material properties from the solid counterpart (Amos, 1985; Richardson, 1986; Liu & Soon, 2012), the strengths of specimens with openings were first normalized using the material properties of solid infills.

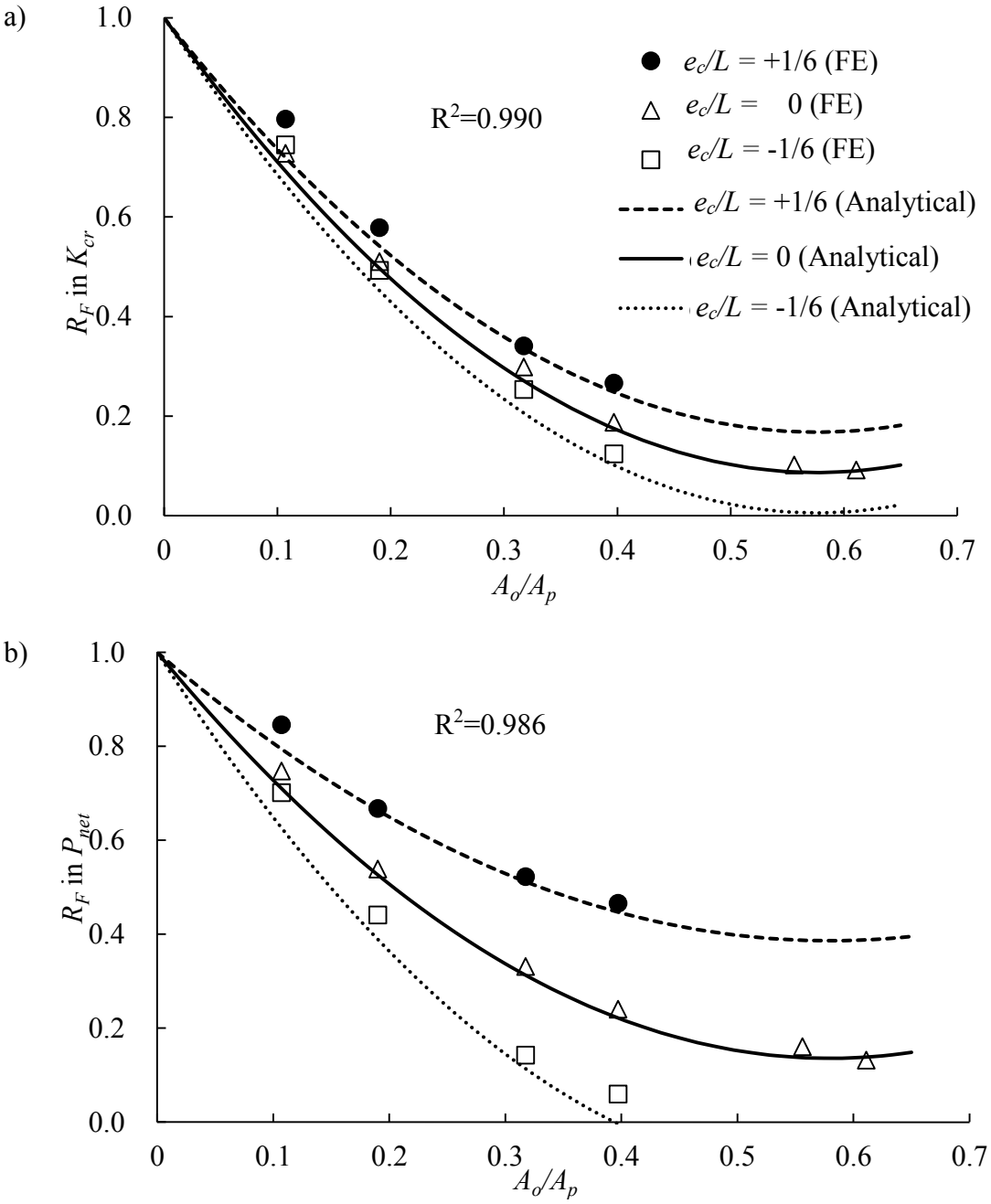

Fig. 5.10: Analytical values vs. FE results: a) K_{cr} and b) P_{net}

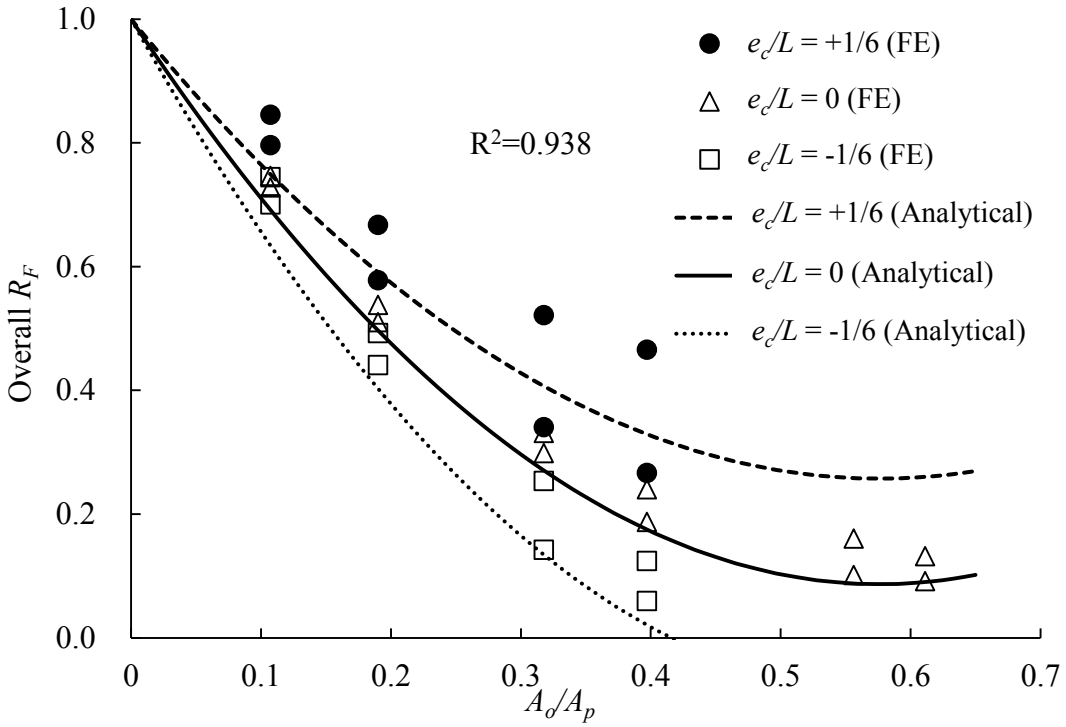

Fig. 5.11: Analytical values vs. FE results for both stiffness and strength

For example, WD5 had a door opening and an f'_m = 29.4 MPa and E_m = 19,000 MPa, its solid counterpart WD7 had an f'_m = 25.4 MPa and E_m = 18,000 MPa. The strength of WD5 was normalized by applying a factor of 25.4/29.4. The stiffness normalization was more complicated since the relationship between the stiffness of the infilled frame and E_m was not linear. It is reasonable to evaluate the stiffness of the diagonal strut as:

$$K_d = \frac{w \times t \times E_m}{d} \tag{5.20}$$

where d is the diagonal length of infill, and other terms are as defined before. Note that the diagonal strut width w is commonly accepted as a function of λH, and hence, K_d is dependent on $E_m^{0.75}$. Therefore, a factor of $(18{,}000/1900)^{0.75}$ was applied to the stiffness of WD5 before making a comparison with WD7.

Table 5.3: Experimental stiffness and strength reduction factors

	ID	A_o/A_p	H_o (m)	L_o (m)	H (m)	L (m)	f'_m (MPa)	E_m (MPa)	K_{exp} (kN/mm)	$R_{F,k}$	P_u (kN)	$R_{F,P}$
Amos (1985)	WC3#	0.175	2.2	0.8	2.8	3.6	30.9	26265*	34	0.47	285	0.58
	WC4#	0.175	2.2	0.8	2.8	3.6	33.1	21650	34	0.44	335	0.63
	WC5#	0.175	2.2	0.8	2.8	3.6	32.5	27625*	39	0.42	245	0.47
	WC6#	0.175	2.2	0.8	2.8	3.6	30.9	26265*	50	0.55	365	0.74
	WC7				2.8	3.6	33.4	19000	71		534	
Richardson (1986)	WD5#	0.175	2.2	0.8	2.8	3.6	29.4	19000	55	0.43	334	0.58
	WD7			0.8	2.8	3.6	25.4	18000	123		494	
	WD12#	0.175	2.2	0.8	2.8	3.6	24.2	15500	22	0.50	196	0.74
	WD9				2.8	3.6	24.6	19800	55		267	
Mosalam et al. (1997)	S2-N-II				0.9	1.8	-	-	8.9		42.7	
	S2-SYM#	0.055	0.31	0.3	0.9	1.8	-	-	4.4	0.49	33	0.77
Tasnimi & Mohebkhah (2011)	SW				1.8	2.26	7.4	6290*	20.8		211	
	PW1#	0.061	0.5	0.5	1.8	2.26	7.4	6290*	22.2	1.07	176	0.84
	PW2#	0.138	0.8	0.7	1.8	2.26	7.0	5950*	21.9	1.05	152	0.75
	PW3#	0.177	0.6	1.2	1.8	2.26	7.0	5950*	19.2	0.92	137	0.68
	PW4#	0.25	1.45	0.7	1.8	2.26	8.5	7225*	17.4	0.75	117	0.50
Liu & Soon (2012)	P3NA				1.1	1.36	7.3	10496	58.3		93.8	
	P3WA#	0.103	0.28	0.5	1.1	1.36	10.3	10496	31.2	0.83	89.1	0.67
	P3DA#	0.176	0.64	0.4	1.1	1.36	10.3	10496	13.7	0.45	75.3	0.57

Note: # Specimens with opening * E_m was not reported in the paper, a value of 850 f'_m was assume

Comparisons between $R_{F(exp)}/R_{F(ana)}$ for the proposed method and other empirical methods are listed in Tables 5.4 and 5.5. In the case of stiffness, the proposed stiffness Eqn. (5.14) or general Eq.(5.16) shows the best overall performance with an average $R_{F(exp)}/R_{F(ana)}$ slightly higher than unity and a reasonable COV of 36%. In the case of strength, the proposed strength Eqn. (5.15) provides the reasonably accurate estimate and also on the conservative side with an average $R_{F(exp)}/R_{F(ana)}$ of 1.08 and a COV of 9%. The proposed general Eqn. (5.16) has an average $R_{F(exp)}/R_{F(ana)}$ of 1.14 and a COV of 12%. It should be noted that Eqn. (5.15) was developed based on the P_{net} of FE models. However, it was compared against the total strength of the infilled system from experimental tests. The main reason for this is the net strength of experimental specimens was not reported in the literature. Due to the small displacement of experimental specimens at failure, it is believed that the contribution of the frame to the total strength was negligible in these specimens. And thus, comparing Eqn. (5.15) with the experimental total strength will not cause any major discrepancy in results.

Among the existing methods, the methods by Tasnimi and Mohebkhah (2011) (Eqn. (5.8)) and Mohammadi and Nikfar (2013) (Eqn. (5.11)) provide estimates close to test results where the average $R_{F(exp)}/R_{F(ana)}$ is 0.93 and 0.96 respectively and a COV of 13% for both methods. However, the overestimation of strength is not desirable for design. The method by Mondal and Jain (2008) (Eqn. (5.7)) also provides estimates close to tests results where the average $R_{F(exp)}/R_{F(ana)}$ is 1.04. However it is intended only for stiffness calculation and

for opening area smaller than 38% of the infill area. It should be pointed out that the comparison sample size was small with only 13 for stiffness and 11 for strength, and only two (specimens WC5 and WC6) had an eccentric opening. The majority A_o/A_p ratios were less than 0.2 and the average A_o/A_p ratio was 0.15. The infill-to-frame stiffness ratios λH for specimens was around 6. The capability of dealing with wide range of openings sizes, eccentric openings and a range of infill-to-frame stiffness ratios using the proposed method was not fully reflected by the comparison. Those existing reduction factor equations intended for both stiffness and strength (Eqn. (5.1), (5.5) and (5.6)) show large disparities with test results, making them inferior to the proposed general equation.

Table 5.4: Comparison of $R_{F(exp)}/R_{F(ana)}$ values for stiffness methods

		Eqn (5.1) 1994	Eqn (5.5) 2003	Eqn (5.6) 2006	Eqn (5.7) 2008	Eqn (5.9) 2012	Eqn (5.10) 2014	Eqn (5.14)*	Eqn (5.16)*
Amos (1985)	WC3	1.09	0.64	0.71	0.86	1.32	0.63	0.89	0.89
	WC4	1.02	0.60	0.66	0.81	1.23	0.59	0.83	0.83
	WC5	0.97	0.57	0.63	0.77	1.18	0.56	0.86	0.95
	WC6	1.27	0.74	0.83	1.01	1.54	0.74	0.96	0.89
Richardson (1986)	WD5	1.00	0.58	0.65	0.79	1.20	0.58	0.81	0.81
	WD12	1.16	0.68	0.75	0.92	1.40	0.67	0.94	0.94
Mosalam et al. (1997)	S2-SYM	0.61	0.54	0.65	0.58	0.80	0.54	0.59	0.59
Tasnimi & Mohebkhah (2011)	PW3	1.70	1.25	4.52	1.70	2.60	1.24	1.75	1.75
	PW4	2.12	1.18	1.40	2.14	2.88	1.14	1.71	1.71
Liu & Soon (2012)	P3WA	1.15	0.97	1.85	1.10	1.63	0.97	1.18	1.18
	P3DA	0.85	0.61	0.81	0.81	1.24	0.60	0.85	0.85
AVG		1.18	0.76	1.22	1.04	1.55	0.75	1.03	1.04
COV (%)		35	34	95	44	41	33	36	36

* the proposed analytical method of this study

Table 5.5: Comparison of $R_{F(exp)}/R_{F(ana)}$ values of strength methods

		Eqn (5.1) 1994	Eqn (5.5) 2003	Eqn (5.7) 2006	Eqn (5.9) 2011	Eqn (5.11) 2013	Eqn (5.15)*	Eqn (5.16)*
Amos (1985)	WC3	1.34	0.78	0.87	0.89	0.92	1.04	1.10
	WC4	1.46	0.85	0.95	0.96	1.00	1.13	1.19
	WC5	1.09	0.64	0.71	0.72	0.75	1.10	1.06
	WC6	1.71	1.00	1.11	1.13	1.17	1.08	1.20
Richardson (1986)	WD5	1.34	0.78	0.87	0.89	0.92	1.04	1.10
	WD12	1.71	1.00	1.11	1.13	1.17	1.13	1.40
Mosalam et al. (1997)	S2-SYM	0.96	0.85	1.03	0.88	0.88	0.91	0.92
Tasnimi & Mohebkhah (2011)	PW1	1.04	0.93	1.26	0.97	0.97	1.02	1.03
	PW2	1.20	0.95	1.40	1.04	1.06	1.18	1.22
	PW3	1.26	0.92	3.34	1.05	1.09	1.23	1.30
	PW4	1.42	0.78	0.93	0.94	1.06	1.21	1.32
Liu & Soon (2012)	P3WA	0.93	0.78	1.49	0.83	0.84	0.93	0.95
	P3DA	1.07	0.77	1.02	0.86	0.89	1.03	1.08
AVG		1.27	0.85	1.24	0.93	0.96	1.08	1.14
COV (%)		20	13	54	13	13	9	12

* the proposed analytical method of this study

Chapter 6 Parametric Study on Geometric and Material Properties

6.1 Introduction

As mentioned in Chapter 2, previous studies have shown that the extent of interaction between the infill and its bounding frame largely depends on the geometric and material properties of both components. Although considerable research has been conducted on this general topic, some important factors such as infill grouting extent and configuration, and vertical and joint reinforcement are less researched with only a few studies on limited variation of parameters (Mainstone, 1971; McBride, 1984; Focardi & Manzini, 1984; Zarnic & Tomazevic, 1984; Amos, 1985; Richardson, 1986; Liu & Soon, 2012; Nazief, 2014). Even within the available studies on common parameters such as infill aspect ratio, and infill-to-frame stiffness ratio, an investigation covering a wider range of variation is still needed to provide an in-depth understanding of the interaction of frame and infill of varying material and geometric characteristics. For example, while a decrease in aspect ratio has been shown to result in an increase in stiffness, cracking strength and ultimate strength (Riddington & Stafford-Smith, 1977; Mehrabi et al., 1996; Flanagan & Bennett, 1999; Ng'andu, 2006; Nazief, 2014), some other studies (Dawe et al., 2001) indicated that the highest load was achieved in the infilled frame with aspect ratio 1.0. Nazief (2014) reported that aspect ratio had more impact on steel infilled frames than RC infilled frames. Because of the high stiffness and strength of the bare RC frame, changing the aspect ratio

resulted in a relatively lower change in the strength and stiffness of RC infilled frames. While Ng'andu (2006) reported that the changes in the bounding frame member sizes were influential for the stiffness of infilled frames, Riddington and Stafford-Smith (1977) and Parducci and Mezzi (1980) showed that the stiffness of the columns is much more influential than the beam stiffness. Flanagan (1994) found that although the increases in frame stiffness resulted in stiffer infilled frames, the net infill capacities remained the same.

In light of the above, this study was motivated to investigate the effect of aspect ratio, grouting extent and configuration, vertical and joint reinforcement of the infill, and bounding frame stiffness on the behaviour of infills bounded by steel frames. The Model II was used in this study. A wide range of aforementioned parameters were considered. The validity of design provisions in both CSA S304-14 and MSJC 2013 for the design of masonry infills was examined using the finite element results.

6.2 Parametric Study

6.2.1 Parameter Description

In this study, parameters considered included aspect ratio, masonry compressive strength, grouting extent and configuration, vertical and joint reinforcement of the infill as well as the stiffness of the bounding frame. For the standard model, the bounding frame consisted of W250x58 columns and W200x46 beams. The infill was 2800 mm high by 2800 mm long. The infill compressive strength (f'_m) was assumed to be 15 MPa and the tensile strength was taken as the 1.5 MPa. As the infill panel was assumed to be orthotropic, the

elastic modulus and compressive strength of masonry in head joint direction (x- direction) were taken as 0.7 times that in bed joint direction (y- direction). The boundary conditions, constitutive model, and the analysis and loading procedures described for the Model II in the previous section were used in this study. It is noted that in the case of reinforcement modeling, either vertical or joint reinforcement was modeled using a 2D plastic spar element LINK1, which is a uni-axial tension-compression element with two degrees of freedom at each node, i.e. translations in the nodal x and y directions. For the joint reinforcement, shape of the reinforcement (ladder or truss) was not simulated, and the reinforcement was modelled using the LINK1 element with an equal cross-sectional area.

Table 6.1 summarizes the finite element models reflecting these parameters in this study. In addition to the standard model (h/l=1.0, f'_m =15 MPa, W250x58 columns and W200x46 beams), five additional aspect ratios were considered and they were h/l = 2.33, 1.4, 0.78, 0.62, and 0.5, representing infills ranging from slender to squat. The change in aspect ratio was realized by increasing the length of infill from 1200 mm to 5600 mm while keeping the height of infill at 2800 mm. Three additional f'_m were considered, and they were f'_m = 10 MPa, 20 MPa and 25 MPa, respectively. For the frame member stiffness study, four additional column cross-sections which represent 0.1, 0.5, 5, and 10 times the column stiffness of the standard model and four additional beam cross-sections which represent 0.1, 0.5, 5, and 10 times the beam stiffness of the standard model were considered. Together with the standard model, a total of 25 combinations of beam and column stiffness were

included in the study.

For the grouting and reinforcement study, the standard model was used. Grouting extents including 0%, 30%, 50%, and 100% grouting were considered. For partially grouted cases (30% and 50% grouting), two grouting configurations were considered where either the first column of cells at the loaded side were grouted or ungrouted. For the case of 30% grouting with the first column of cells grouted, three cases of vertical reinforcing were considered including un-reinforced, reinforced with 10M bars, and reinforced with 25M bars, respectively. The configuration of grouting along with the vertical reinforcing cases is plotted in Fig. 6.1. For the joint reinforcement study, as the shape of reinforcement was not modelled, the main parameter selected was the cross-sectional area. Four cases of joint reinforcement were considered, and they were un-reinforced, 3.66 mm gauge wire (21.1 mm^2/course), 4.76 mm gauge wire (46.6 mm^2/course), and a fictitious reinforcement type which has an effective area equal to five times that of 3.66 mm gauge wire (105.3 mm^2/course) to simulate extra heavy reinforced infills. The joint reinforcement was placed in the bed joint of each course.

Table 6.1: Parameters in the study of geometric and material factors and reinforcement

ID	h (m)	l (m)	h/l	f'_m (MPa)	Beam section	Column section
1	2.8	5.6	0.50	10	W200x46	W250x48
2	2.8	4.5	0.62	10		
3	2.8	3.6	0.78	10		
4	2.8	2.8	1.00	10		
5	2.8	2	1.40	10		
6	2.8	1.4	2.00	10		
7	2.8	5.6	0.50	15	W200x46	W250x48
8	2.8	4.5	0.62	15		
9	2.8	3.6	0.78	15		
10*	2.8	2.8	1.00	15		
11	2.8	2	1.40	15		
12	2.8	1.4	2.00	15		
13	2.8	5.6	0.50	20	W200x46	W250x48
14	2.8	4.5	0.62	20		
15	2.8	3.6	0.78	20		
16	2.8	2.8	1.00	20		
17	2.8	2	1.40	20		
18	2.8	1.4	2.00	20		
19	2.8	5.6	0.50	25	W200x46	W250x48
20	2.8	4.5	0.62	25		
21	2.8	3.6	0.78	25		
22	2.8	2.8	1.00	25		
23	2.8	2	1.40	25		
24	2.8	1.4	2.00	25		

*Standard Model

Table 6.1: Parameters in the study of geometric and material factors and reinforcement (Cont'd)

ID	h (m)	l (m)	h/l	f'_m (MPa)	Beam section	Column section	Grouting	Joint reinf. (mm)
grouting and vertical reinforcement								
25	2.8	2.8	1.00	15			30%, conf. 1	
26	2.8	2.8	1.00	15			30%, conf. 2	
27	2.8	2.8	1.00	15			50%, conf. 1	
28	2.8	2.8	1.00	15	W200x46	W250x48	50%, conf. 2	
29	2.8	2.8	1.00	15			100%	
30	2.8	2.8	1.00	15			ID 25 with 10M vert.	
31	2.8	2.8	1.00	15			ID 25 with 25M vert.	
joint reinforcement								
32	2.8	2.8	1.00	15				3.66
33	2.8	2.8	1.00	15				4.76
34	2.8	2.8	1.00	15				5x 3.66
35	2.8	2.8	1.00	15				3.66^{+}
36	2.8	2.8	1.00	15				4.76^{+}
37	2.8	2.8	1.00	15				5x 3.66^{+}

+Anchored joint reinforcement

Table 6.1: Parameters in the study of geometric and material factors and reinforcement (Cont'd)

ID	h (m)	l (m)	h/l	f'_m (MPa)	Beam section	Column section
38	2.8	2.8	1.00	15		W150x24
39	2.8	2.8	1.00	15		W200x42
40	2.8	2.8	1.00	15	W100x19	W250x48
41	2.8	2.8	1.00	15		W310x129
42	2.8	2.8	1.00	15		W460x286
43	2.8	2.8	1.00	15		W150x24
44	2.8	2.8	1.00	15		W200x42
45	2.8	2.8	1.00	15	W150x37	W250x48
46	2.8	2.8	1.00	15		W310x129
47	2.8	2.8	1.00	15		W460x286
48	2.8	2.8	1.00	15		W150x24
49	2.8	2.8	1.00	15		W200x42
50	2.8	2.8	1.00	15	W200x46	W250x48
51	2.8	2.8	1.00	15		W310x129
52	2.8	2.8	1.00	15		W460x286
53	2.8	2.8	1.00	15		W150x24
54	2.8	2.8	1.00	15		W200x42
55	2.8	2.8	1.00	15	W360x79	W250x48
56	2.8	2.8	1.00	15		W310x129
57	2.8	2.8	1.00	15		W460x286
58	2.8	2.8	1.00	15		W150x24
59	2.8	2.8	1.00	15		W200x42
60	2.8	2.8	1.00	15	W460x106	W250x48
61	2.8	2.8	1.00	15		W310x129
62	2.8	2.8	1.00	15		W460x286

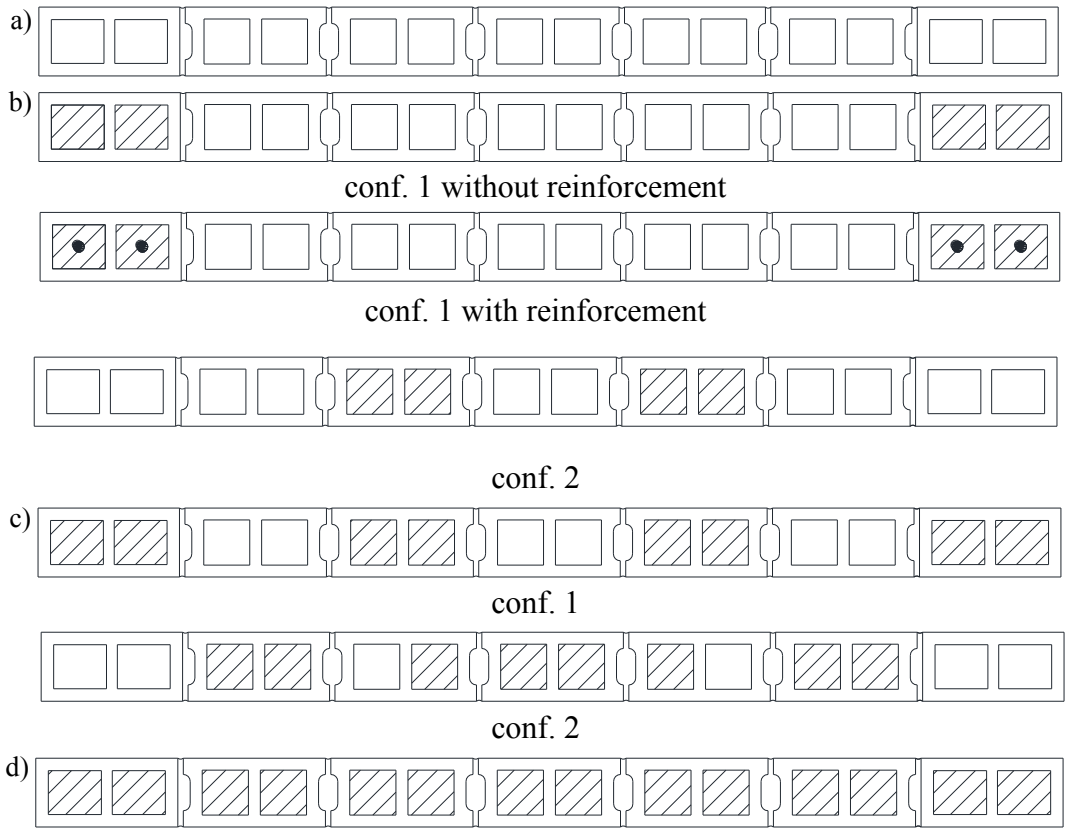

Fig. 6.1: Extent and configuration of grouting: a) 0% grouting, b) 30% grouting (configuration 1: loaded corner column grouted without and with reinforcement; configuration 2: loaded corner column ungrouted), c) 50% grouting (Configuration 1 and 2), d) full grouting

6.2.2 Special Consideration for Reinforcement Modeling

Since the mortar joint between masonry units was modelled using zero-thickness interface elements, to avoid creating a zero-length link element when modelling the joint reinforcement, the reinforcement scheme as shown in Fig. 6.2 (a, b) was adopted. The joint reinforcement at each course was divided equally into three strands of link elements based on the cross-sectional area. In each strand of link elements, each link element connects two nodes which belong to two blocks in adjacent courses and have a horizontal distance of one-half of the block length (Fig. 6.2 (b)). Altogether, three strands of reinforcement cover all the nodes in each course of bed joint. In practice, horizontal reinforcement may be welded to the bounding steel frame or tied to the reinforcement in RC columns. In such cases, the joint reinforcement was considered as anchored to the frame. In order to model the anchorage effect, the end node of each strand of link elements was coupled with the node on the bounding frame which shared the same physical location.

As previously discussed, this study adopted a 2x2 mesh for each masonry block. However, in the case of the vertical reinforcement study, a finer mesh must be adopted to ensure that the vertical reinforcement was located in the middle of a grouted cell. A mesh of 4x2 was then adopted in which, a masonry block was divided into 4 units along its length and 2 units along its height. This meshing scheme (Fig. 6.2 (a, c)) shows that dividing the whole block into 4 units lengthwise creates a middle node for each grouted cell to which the vertical reinforcement is connected. Since the bed joint has zero-thickness, the vertical reinforcement only connects the middle nodes of each grouted cell to avoid creating zero-

length elements.

It should be pointed out that these techniques for reinforcement modeling were used due to the limitations of simplified micro-modelling. For a more accurate simulation of reinforcement, a detailed micro-model would be required where the actual mortar joint with a material constitutive model can be considered, and the reinforcement can then be modelled using a discreet reinforcement model. As the detailed micro-modelling technique is outside the scope of this research, the simplified treatment of reinforcement is reasonable, and it is believed that the key characteristics of reinforcement and its contribution to stiffness and strength can still be captured. Despite some stress concentration at reinforcement connected nodes, the simulation of the overall reinforcing effect on infills was acceptable. Since the physical dimension of mortar joints was not modelled, the failure mechanism of mortar surrounding a rebar such as cracking of mortar, crushing of mortar between steel ribs, and the bond-slip behaviour between rebar and mortar are beyond the capability of this model.

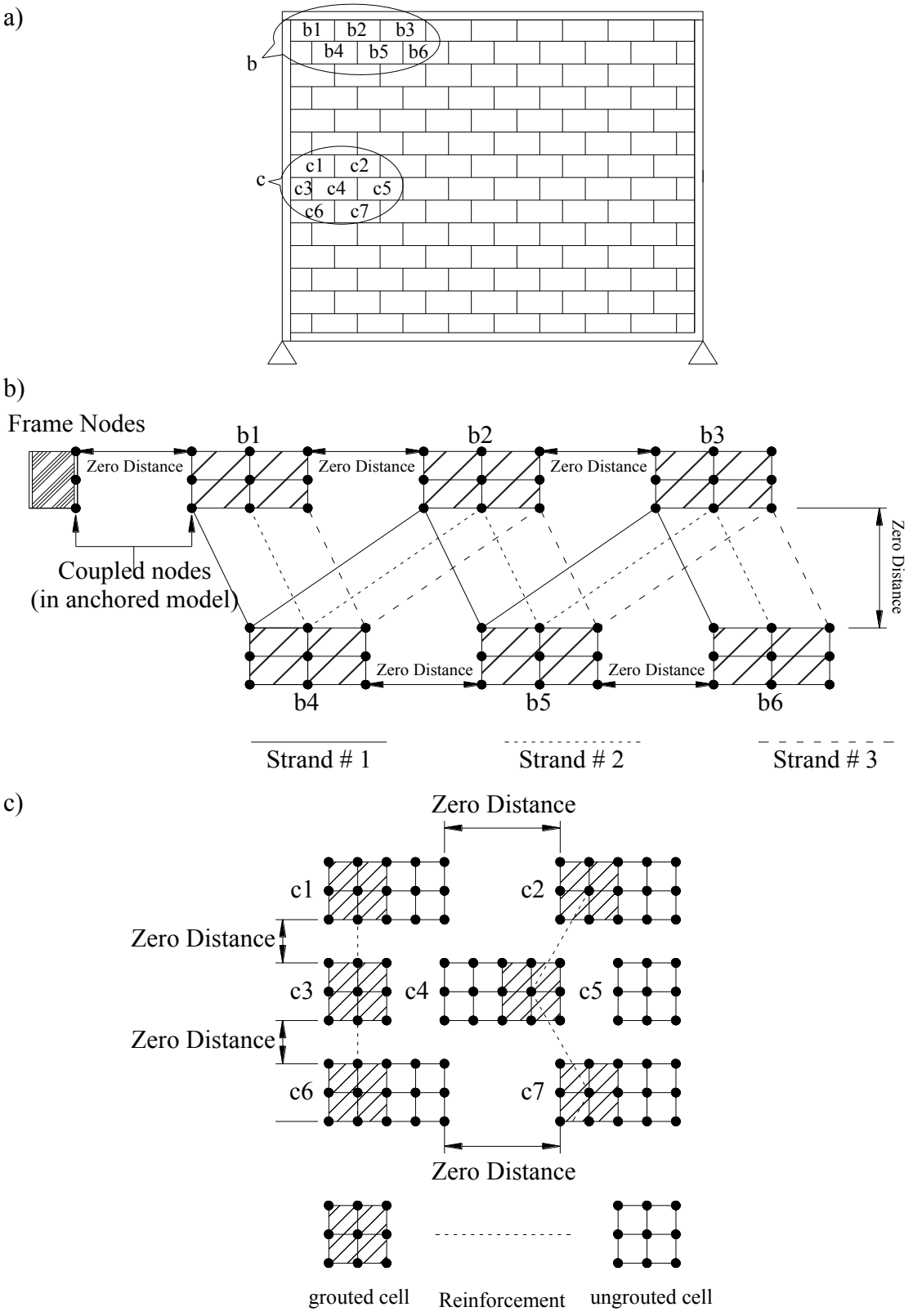

Fig. 6.2: Modeling of reinforcement: a) elevation of the infill b) horizontal joint reinforcement, c) vertical reinforcement

6.3 Discussion of Results

6.3.1 Infill Aspect Ratio and Masonry Compressive Strength

The effects of infill aspect ratio *(h/l*) and masonry compressive strength (f'_m) on the cracking stiffness K_{cr} and net load P_{net} of the infill are collectively illustrated in Fig. 6.3 and 6.4 respectively where the K_{cr} and P_{net} of the infills were normalized with respect to the standard model. Fig. 6.3 shows that for a given aspect ratio, both the K_{cr} and P_{net} increase in an approximately linear manner as the masonry strength f'_m increases. This is reasonable since the elastic modulus of masonry was assumed to be proportional to f'_m (850 f'_m). An increase in f'_m value corresponds to an increase in masonry modulus, which in turn results in an increase in the masonry cracking stiffness, a delay in cracking and thus a higher strength. This trend is true for other all aspect ratios studied.

For a given masonry strength f'_m, an increase in *h/l* results in a reduction in both the K_{cr} and P_{net} and the rate of reduction becomes greater as *h/l* increases. For example, in the case of f'_m =15 MPa, an increase in *h/l* from 1.0 to 2.33 results in reductions in the K_{cr}, and P_{net} of 73%, and 56% respectively while the corresponding reductions in K_{cr} and P_{net} are 20% and 21% for an increase of *h/l* from 0.5 to 1.0. A similar trend can be observed for other f'_m values. The load transferr mechanism of infills can be assumed to be a combination of flexural behaviour and diagonal strut action. The contribution of each in load transferr is largely dependent on the slenderness of the infill. As the infill becomes slender (*h/l* increases), the flexural behaviour of the infill increases and the diagonal strut action diminishes. The infilled frame behaves more like a cantilever member with increasingly

smaller flexural in-plane stiffness. Note that the flexure is not as effective in transferring the load as the strut action, the combined effect of an increase in flexural behaviour and reduction in flexural stiffness is believed to result in reductions in both the stiffness and strength of infills with increasing aspect ratios.

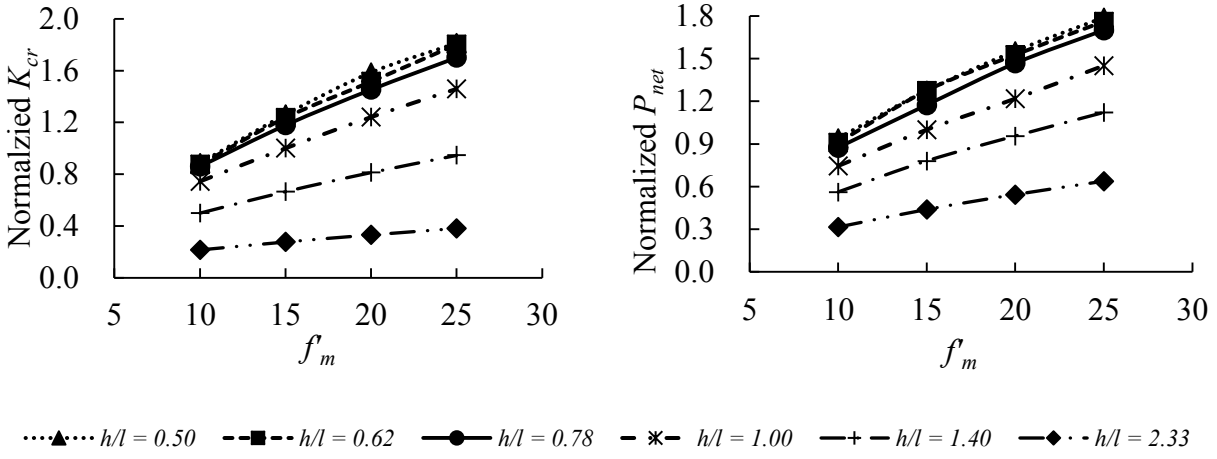

Fig. 6.3: Effect of f'_m on K_{cr} and P_{net}

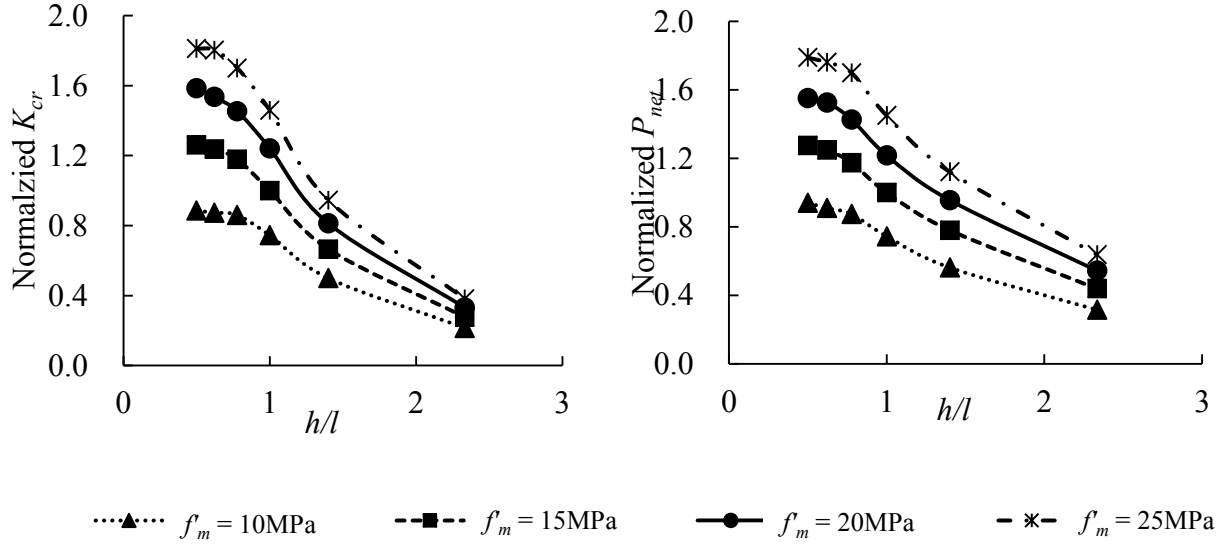

Fig. 6.4: Effect of aspect ratio on K_{cr} and P_{net}

6.3.2 Grouting

The effect of grouting is shown in Fig. 6.5 where the K_{cr} and P_{net} of the infills were normalized with respect to the corresponding ungrouted infill. It can be observed that in

general, grouting is beneficial to the cracking stiffness and infill net load. As shown in Fig. 6.5(a), the increase in the stiffness in relation to the increase in grouting extent is approximately linear, and a fully grouted infill has 1.12 times higher stiffness than an ungrouted infill. However, the degree of the benefit is dependent on the location of the grouting. For example, in the case of cracking stiffness, when the loaded corner column is grouted, the increase from ungrouted infill is 35% for a 30% total grouting area and 54% for a 50% total grouting area. On the other hand, when the loaded corner column is ungrouted, the corresponding increase is 12.3% for 30% total grouting area and 32.9% for 50% total grouting area.

The difference in the degree of benefit due to grouting location is even more evident in P_{net}. As shown in Fig. 6.5(b), when the loaded corner column is grouted, the increase in P_{net} from ungrouted infill is 74.2% for a 30% total grouting area and 94.7% for a 50% total grouting area. When the loaded corner column is ungrouted, the corresponding increase is 18.4% for 30% total grouting area and 20.5% for 50% total grouting area. When the grouting extent reaches 100%, an increase of 124% in P_{net} is achieved.

It is evident that the benefit of grouting can only be realized to the largest degree if the loaded corner column is grouted. Loaded corners of the infill experience the highest compressive stress concentration during loading. If the loaded corner column is not grouted, it would be crushed at the approximately same load as the ungrouted infill which accelerates the loss of strength of the whole system. When the loaded corner column is

grouted, the effective thickness of the infill in the most compressed zone is greatly increased, resulting in a marked increase in strength.

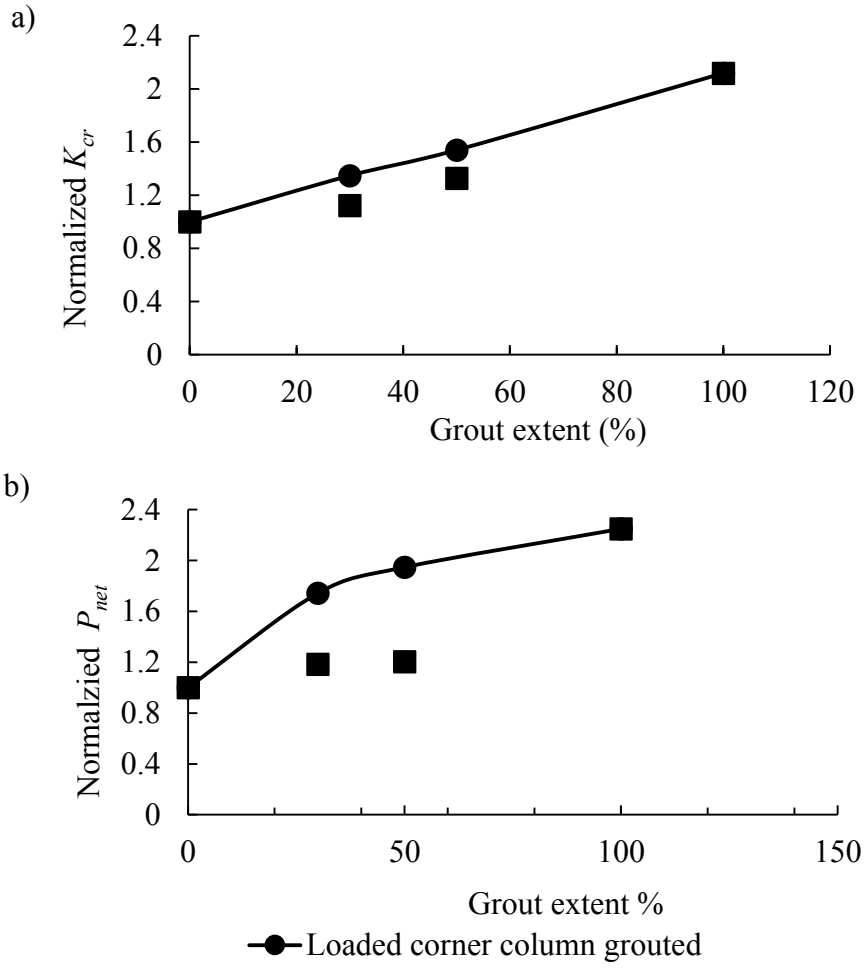

Fig. 6.5: Effect of grouting on behaviour of infills, a) K_{cr}, b) P_{net}

6.3.3 Reinforcement

The effect of vertical reinforcement is found to be insignificant as shown in Fig. 6.6. Regardless of the amount used, reinforcement generally has little to no effect on the K_{cr} or P_u, or behaviour of the system. The K_{cr} or P_u of reinforced infills remains practically the same as un-reinforced ones.

In the case of joint reinforcement, the load vs. lateral displacement curves with varying

joint reinforcement amount are plotted in Fig. 6.7. The Figure shows that the joint reinforcement has some effect on the cracking behaviour of the infill where the presence of joint reinforcement increases the post-cracking stiffness of the infill and reduces the magnitude of load drop after each cracking. As a result, the infill reaches P_u at a lower displacement. However, there is no significant impact on the ultimate strength of the infill system. A greater impact of joint reinforcement is observed when joint reinforcement is anchored to the bounding frame as shown in Fig. 6.7 (b). Fig. 6.8 further plots the normalized K_{cr} and P_{net} curves where values were normalized using un-reinforced infill as the reference. Referring to both figures, comparing with no joint reinforcement case, the use of 3.66 mm gauge wire results in less than 1.5% increase in K_{cr} and about 7% increase in P_{net}. Even increasing the joint reinforcement area to 5 times that of 3.66 mm gauge wire only results in an increase of merely 3% in the K_{cr} and 15% in the P_{net}. When anchored to the bounding frame, joint reinforcement has a greater effect on the stiffness and strength of the infill. The infills with 3.66 mm gauge wire anchored to the frame achieves a K_{cr} that is 8% higher, and a P_{net} that is 24% higher than the unanchored joint reinforcement case.

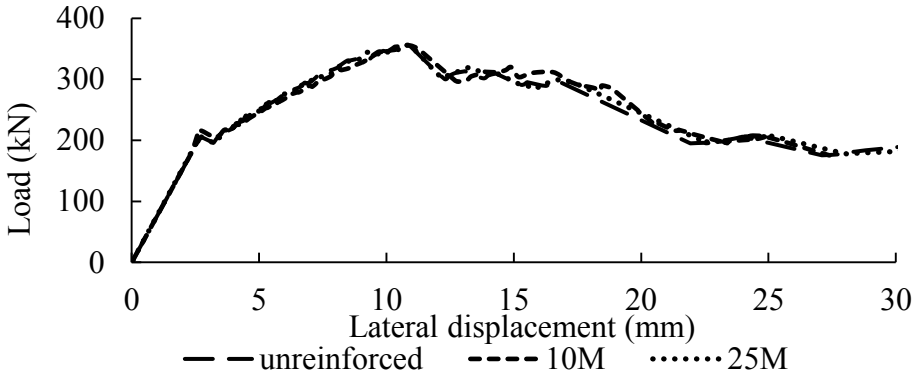

Fig. 6.6: Effect of vertical reinforcement on load vs displacement curve of infills

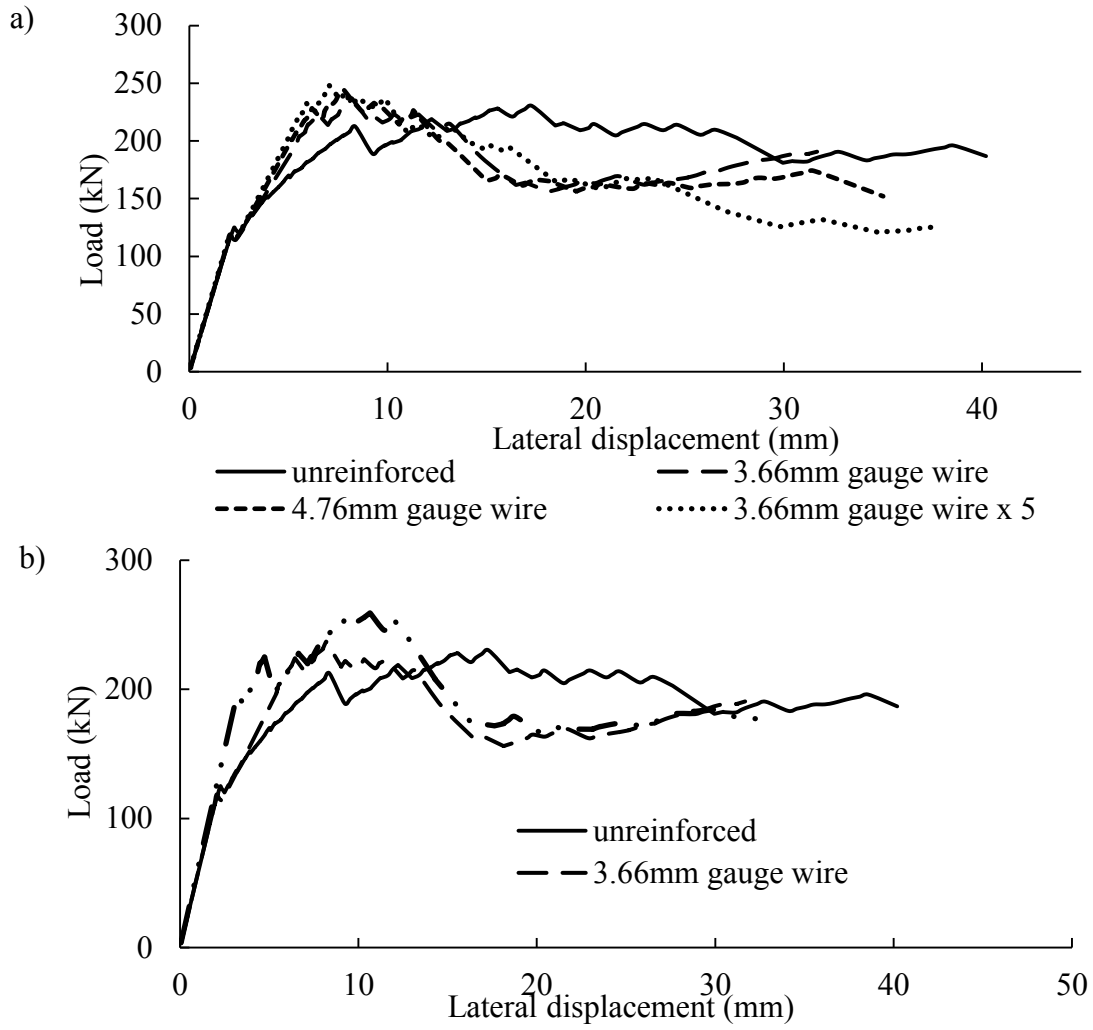

Fig. 6.7: Load vs. lateral displacement curves of infills with different joint reinforcement: a) unanchored joint reinforcement and b) both unanchored and anchored joint reinforcement.

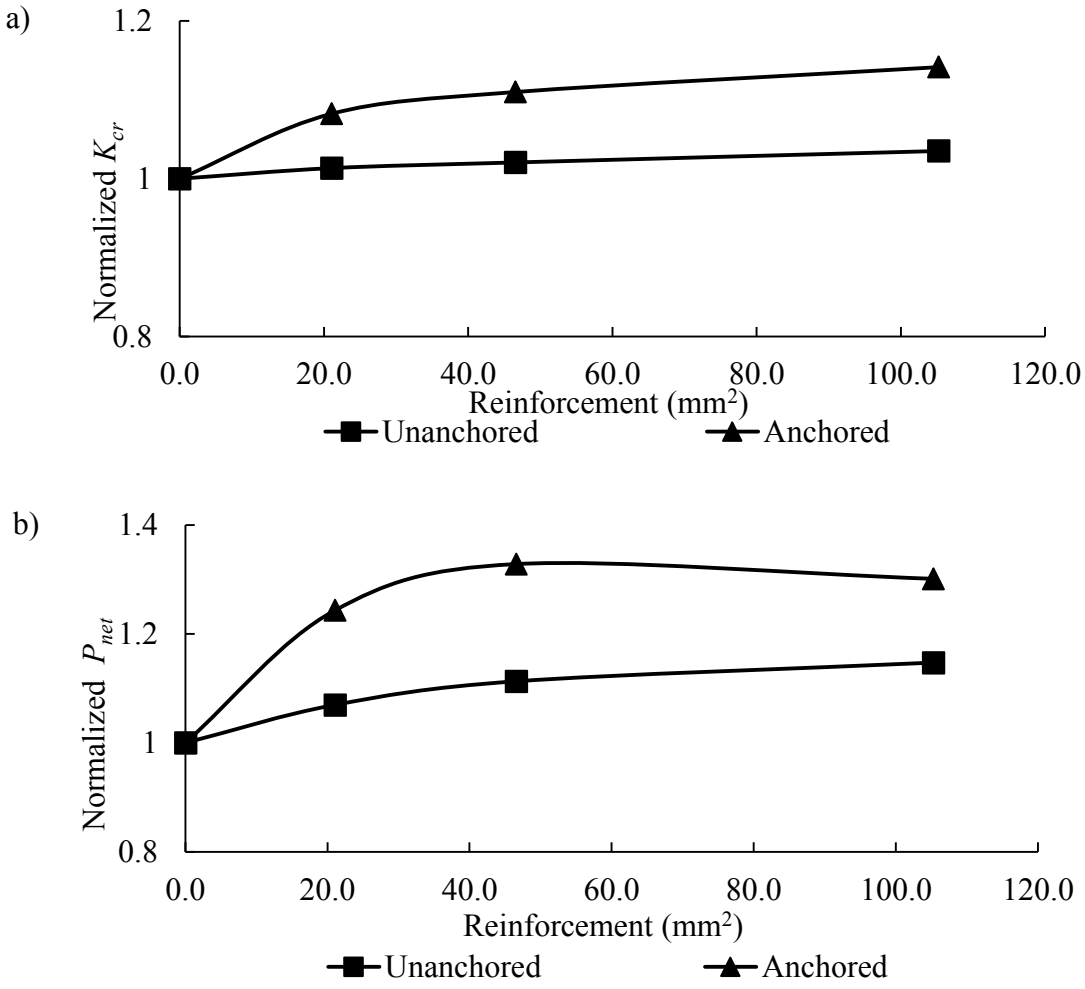

Fig. 6.8: Effect of joint reinforcement on a) K_{cr}, b) P_{net}

Fig. 6.9 compares the FE compressive stress distribution and cracking patterns for infills with and without vertical reinforcement or joint reinforcement prior to failure. It can be seen from Fig. 6.9 (b) and (c) that the presence of vertical reinforcement has no marked impact on the stress distribution or cracking patterns. As shown in Fig. 6.9 (a) and (d), the joint reinforcement reduces the crack width and suppresses the development of cracks. As a result, the integrity of the infill is greatly increased which leads to a smaller load drop after each crack. It can be seen from Fig. 6.9 (e) that when anchored to the bounding frame,

the joint reinforcement prevents the infill from separating from the columns. As a result, the infill is better integrated into the lateral load resisting system which leads to a higher stiffness and strength.

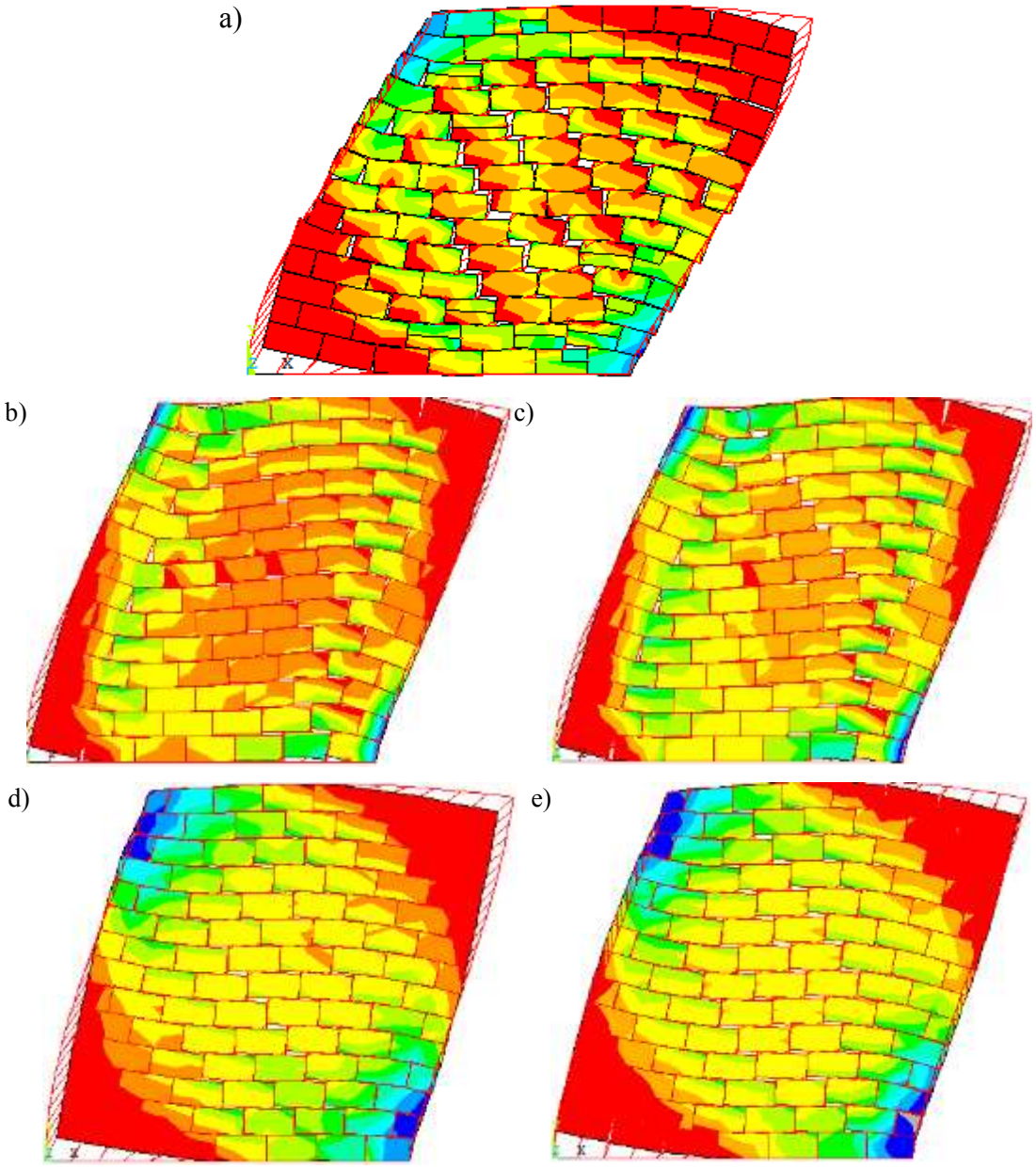

Fig. 6.9: Distribution of compressive stress and cracks in infill (Deformation is exaggerated): a) unreinforced, b) 30% grouting extent without vertical reinforcement, c) 30% grouting extent with 10M vertical reinforcement, d) reinforced with 3.66 mm gauge wire (unanchored), e) reinforced with 3.66 mm gauge wire (anchored)

The insignificant reinforcement effect can be reasoned as follows. According to Moghaddam and Dowling (1987), the vertical reinforcement in infills acts predominately in bending and shear rather than in tension. Due to its low bending and shear stiffness, vertical reinforcement contributes little to the lateral stiffness and strength. The vertical reinforcement may have a greater impact on infills where the bending mode of failure predominates. On the other hand, joint reinforcement acts in tension when controlling the vertical cracks. Its high tensile stiffness contributes to the joint stiffness and, in turn, results in higher overall infill stiffness and strength. When it is anchored to the bounding frame, this effect is more significant.

6.3.4 Frame Stiffness

The load vs. lateral displacement curves of infilled frames with changing columns stiffness and with changing beam stiffness are plotted in Fig. 6.10 (a) and (b) respectively. Although the behaviour trend is similar, column stiffness appears to be more influential in increasing K_{cr} and P_u than beam stiffness. Taking the standard model (I_c/I_{c0} = 1 and I_b/I_{b0} = 1) as a reference, the effect of I_c/I_{c0} ratio on the normalized stiffness and strength of infilled frames with varying I_b is shown in Fig. 6.11. Note that the net stiffness of the infill (K_{net}) is considered in both figures which is calculated as the K_{cr} less the bare frame stiffness. In this section of the study, the contribution of the frame is greatly amplified by increasing of the frame sections and thus the use of K_{net} is necessary for studying the behaviour of the infill itself.

It can be seen that for a given I_b, an increase in I_c/I_{c0} results in a marked increase in K_{cr}. For example, for $I_b = I_{b0,}$ as the I_c/I_{c0} increases from 1 to 9.73, the K_{cr} is increased by 47%. On the other hand, for $I_c = I_{c0}$, increasing beam stiffness from 1 to even 10.75 times I_{b0} results in only 5.3% increase in K_{cr}. It can be concluded that the changing column stiffness has more significant effect on the infill behaviour than changing beam stiffness. From Fig. 6.11, it can also be observed that while K_{cr} is immensely increased by increasing column section, K_{net} and P_{net} are relatively less affected by the change of either column stiffness or beam stiffness. Increasing the stiffness of the column by tenfold results in a maximum of 28% and 18% increase in K_{net} and P_{net}, respectively while increasing the stiffness of the beam by tenfold results in a maximum of 7% and 22% increase in K_{net} and P_{net}, respectively. The use of the strongest beam and the strongest column results in the greatest increase in P_{net}, which is in the order of 40% comparing with the standard model. It can be concluded that the greater variation in the K_{cr} and P_u previously observed is mainly a result of the variation in the stiffness of the frame. The net stiffness and net strength of the infill are affected by the stiffness of frame members to a lesser extent. The stiffness of frame members affected the net stiffness and strength of infill through changing the diagonal strut width in the infill. In general, the stiffer the bounding frame, the greater width of the diagonal strut. Fig. 6.12 shows the distribution of compressive stress in infills with I_c/I_{c0} = 0.1, I_b/I_{b0} = 1 and I_c/I_{c0} = 5, I_b/I_{b0} = 1, respectively. It is evident that the infilled frame with I_c/I_{c0} = 5 has a wider diagonal strut.

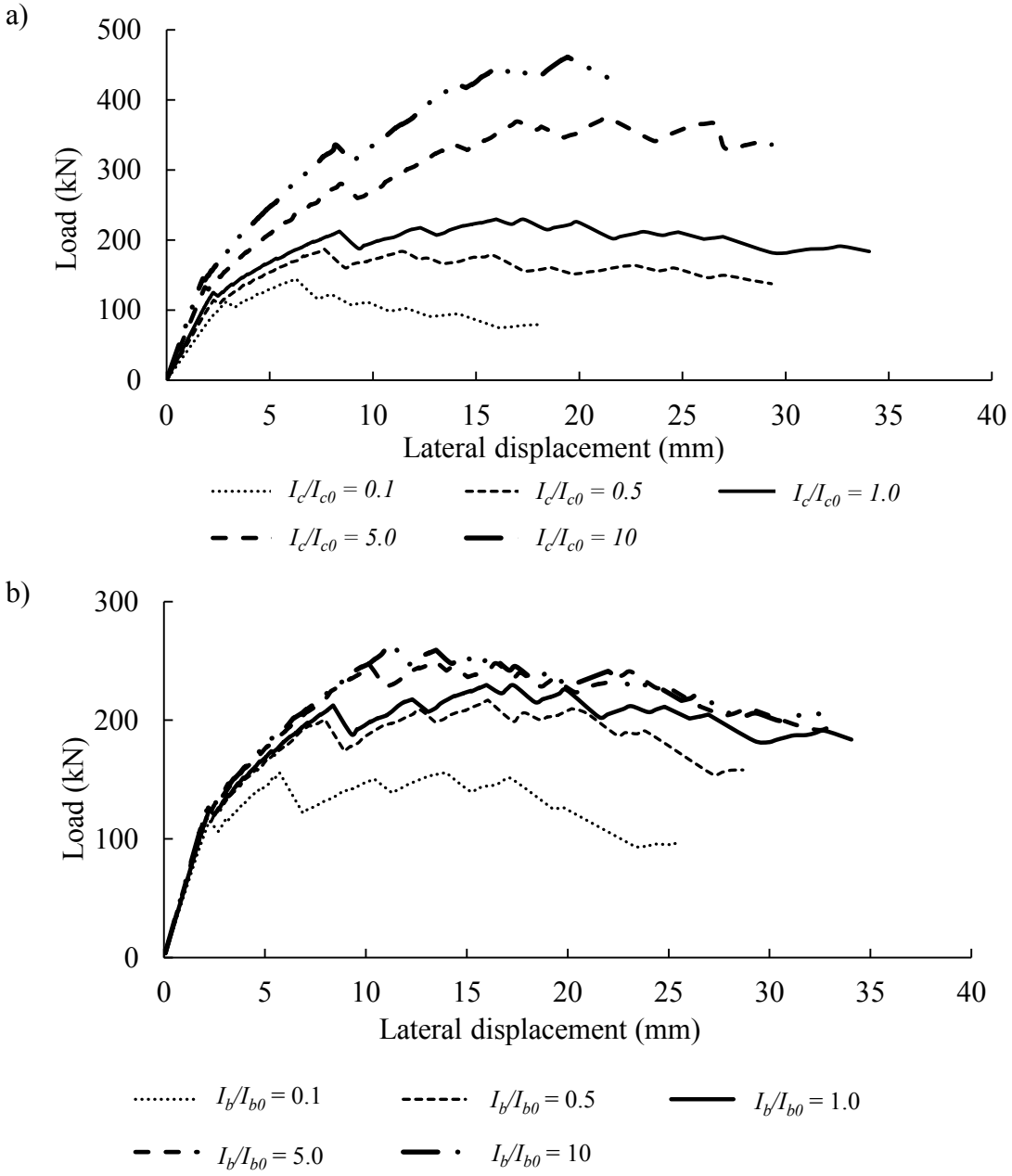

Fig. 6.10: Load vs. lateral displacement curves of infilled frame with a) different column stiffness and b) different beam stiffness

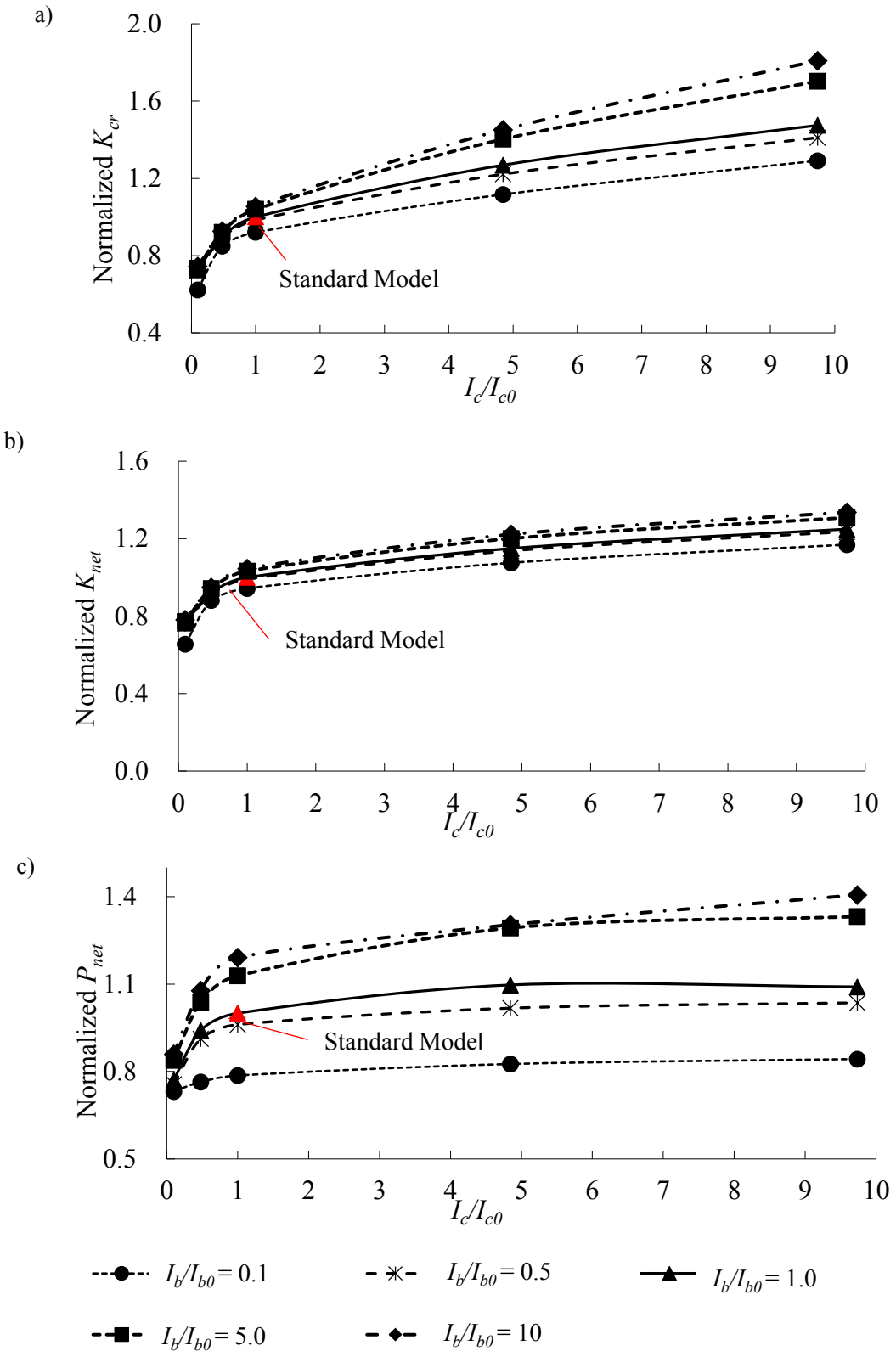

Fig. 6.11: Effect of I_c/I_{c0} ratio on a) K_{cr}, b) K_{net} and c) P_{net}

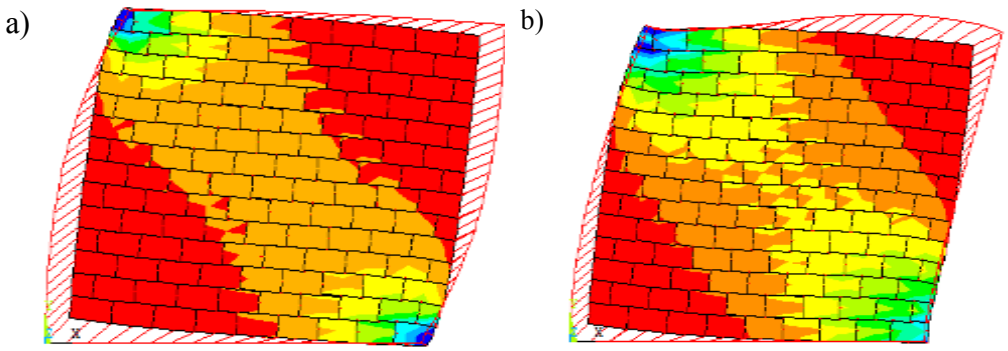

Fig. 6.12: Distribution of compressive stress in infill with: a) I_c/I_{c0} = 0.1 b) I_c/I_{c0} = 5

While changing column stiffness has more effect on the infill behaviour than changing beam stiffness as previously observed, the results also showed that in order to achieve the maximum increase in the frame stiffness, a compatible beam is required to serve as an adequate restraint at the top of columns. A simple frame analysis revealed that if the flexural stiffness of the top beam (EI_b/L) is the same as the flexural stiffness of the column (EI_c/H), the lateral stiffness of the bare frame is 70% of that of a frame which consists of the same columns but a totally rigid beam ($I_b = \infty$). Increasing the top beam flexural stiffness to 10 times column flexural stiffness will increase the bare frame stiffness to 95% of that of a frame with a totally rigid beam. The standard specimen in this study has a beam-to-column flexural stiffness ratio of 1.88. This study suggests that a beam should preferably have greater flexural stiffness than the column to be considered comparable to provide adequate restraints.

6.4 Comparative Study of Standard Equations and FE Results

In this section, the FE results from this study were used to examine the validity of the stiffness and infill strength equations based on both CSA S304-14 and MSJC 2013. The

design provisions from both standards are summarized in Section 2.3 in Chapter 2.

Table 6.2 presents comparison results of design stiffness and strength where K_{CSA} and P_{CSA}, and K_{MSJC} and P_{MSJC} are the design stiffness and strength calculated based on the CSA S304-14, and MSJC 2013, respectively; and K_{cr} and P_{net} represent the finite element values. The design strength refers to as the strength of infill alone calculated based on the abovementioned standards. As shown in the table, the CSA S304-14 in general archives a good agreement with the FE results with a slight overestimation of the stiffness. The overall average K_{cr}/K_{CSA} is 0.91 with a COV of 17%, and the overall average P_{net}/P_{CSA} is 0.99 with a COV of 14%. It can be seen from the table that the effect of infill aspect ratio, masonry f'_m, frame stiffness ratio and grouting extent can be reflected with relatively good accuracy. However, some discrepancies are observed. They are discussed in the following.

Table 6.2: Comparison between FE and design results

ID	CSA				MSJC			
	K_{CSA} (kN/mm)	K_{cr}/K_{CSA}	P_{CSA} (kN)	P_{net}/P_{CSA}	K_{MSJC} (kN/mm)	K_{cr}/K_{MSJC}	P_{MSJC} (kN)	P_{net}/P_{MSJC}
	aspect ratio and f'_m							
1	84.6	0.59	197.8	0.88	18.8	2.66	100.6	1.73
2	69.1	0.72	175.7	0.96	17.5	2.82	100.6	1.67
3	57.0	0.85	156.4	1.03	16.4	2.97	100.6	1.61
4	43.4	0.97	132.5	1.04	15.0	2.82	100.6	1.37
5	28.7	0.99	103.4	1.00	13.0	2.17	100.6	1.03
6	14.6	0.83	66.8	0.87	10.4	1.18	100.6	0.58
7	111.8	0.64	266.9	0.88	24.0	2.98	150.9	1.56
8	90.7	0.77	237.5	0.99	22.2	3.15	150.9	1.56
9	74.3	0.90	211.7	1.02	20.7	3.23	150.9	1.44
10	56.0	1.01	179.8	1.03	18.7	3.03	150.9	1.22
11	36.3	1.04	140.2	1.03	16.1	2.35	150.9	0.96
12	18.0	0.87	91.8	0.88	12.4	1.27	150.9	0.54
13	136.1	0.66	330.2	0.87	28.8	3.12	201.2	1.43
14	109.8	0.78	294.2	0.96	26.5	3.24	201.2	1.40
15	89.6	0.92	262.3	1.03	24.6	3.35	201.2	1.35
16	67.0	1.05	222.9	1.01	22.1	3.18	201.2	1.12
17	43.0	1.07	174.0	1.01	18.8	2.45	201.2	0.88
18	20.7	0.91	113.9	0.88	14.2	1.33	201.2	0.50
19	158.3	0.65	389.5	0.85	33.2	3.09	251.5	1.31
20	127.2	0.80	347.3	0.94	30.5	3.35	251.5	1.29
21	103.3	0.93	309.8	1.01	28.2	3.41	251.5	1.25
22	76.9	1.08	263.3	1.02	25.3	3.27	251.5	1.07
23	48.9	1.10	205.6	1.01	21.3	2.52	251.5	0.82
24	23.2	0.93	134.6	0.87	15.8	1.37	251.5	0.47
AVG		0.88		0.96		2.68		1.17
COV (%)		17		7		27		32

Table 6.2: Comparison between FE and design results(Cont'd)

ID	CSA				MSJC			
	K_{CSA} (kN/mm)	K_{cr}/K_{CSA}	P_{CSA} (kN)	P_{net}/P_{CSA}	K_{MSJC} (kN/mm)	K_{cr}/K_{MSJC}	P_{MSJC} (kN)	P_{net}/P_{MSJC}
grouting and vertical reinforcement								
25	79.8	0.96	273.4	1.18	24.1	3.17	231.8	1.39
26	79.8	0.80	273.4	0.81	24.1	2.64	231.8	0.96
27	101.4	0.86	361.2	1.00	28.9	3.02	312.7	1.15
28	101.4	0.74	361.2	0.61	28.9	2.61	312.7	0.70
29	130.0	0.92	474.6	0.88	35.4	3.39	434.3	0.96
AVG		0.86		0.90		2.97		1.03
COV (%)		10		24		11		25
frame stiffness								
38	28.8	1.22	101.2	1.33	8.5	4.15	150.9	0.90
39	34.2	1.41	109.2	1.29	14.1	3.41	150.9	0.94
40	38.9	1.34	115.4	1.26	18.8	2.78	150.9	0.96
41	64.4	0.98	138.4	1.10	44.1	1.44	150.9	1.01
42	87.0	0.84	151.0	1.03	65.6	1.11	150.9	1.03
43	38.6	1.06	143.9	0.97	8.5	4.82	150.9	0.93
44	44.6	1.13	149.7	1.12	14.1	3.57	150.9	1.12
45	49.4	1.13	154.3	1.15	18.8	2.97	150.9	1.18
46	74.4	0.93	172.4	1.09	44.2	1.56	150.9	1.25
47	97.2	0.82	182.6	1.05	66.2	1.21	150.9	1.27
48	44.2	0.93	170.9	0.83	8.5	4.84	150.9	0.94
49	51.0	1.00	175.9	0.99	14.1	3.60	150.9	1.15
50	56.1	1.01	179.8	1.03	18.8	3.02	150.9	1.22
51	81.0	0.89	195.2	1.04	44.3	1.62	150.9	1.34
52	103.9	0.80	204.3	0.99	66.3	1.26	150.9	1.33
53	55.8	0.75	232.8	0.67	8.5	4.90	150.9	1.03
54	64.0	0.81	232.8	0.83	14.1	3.70	150.9	1.27
55	69.2	0.85	232.8	0.90	18.8	3.14	150.9	1.38
56	91.4	0.87	232.8	1.03	44.3	1.79	150.9	1.58
57	112.4	0.86	232.8	1.06	66.4	1.45	150.9	1.63
58	55.8	0.75	232.8	0.68	8.5	4.95	150.9	1.05
59	64.0	0.82	232.8	0.85	14.1	3.72	150.9	1.32
60	69.2	0.86	232.8	0.94	18.8	3.18	150.9	1.46
61	91.4	0.90	232.8	1.03	44.3	1.86	150.9	1.60
62	112.4	0.91	232.8	1.11	66.4	1.54	150.9	1.72
AVG		0.95		1.01		2.86		1.22
COV (%)		18		16		45		20
Overall								
AVG		0.91		0.99		2.80		1.18
COV (%)		17		14		36		26

In the case of infill aspect ratio, the CSA S304-14 significantly overestimates the K_{cr} of infills with low aspect ratios (h/l=0.5 and 0.64) but accurately predicts the K_{cr} of infills with higher aspect ratios ($h/l \geq 0.78$). The CSA S304-14 shows an approximately linear relationship between the K_{CSA} and h/l while this relationship from the FE results is nonlinear. Such discrepancy can be attributed to the fact that CSA S304-14 overestimates the contact length between the infill and beam (α_l) for low aspect ratio infills. According to Eqn (2.59) provided by the CSA S304-14, an increase in the length of infill (l) results in a proportional increase in α_l. However, the FE model shows that α_l does not have such a linearly increasing relationship with l, rather, as the length of infill increases, the rate of increase in α_l slows down due to the diminishing diagonal compression action and increasing shear action of the infill. The over-prediction of the α_l results in an over-prediction of the diagonal strut width and K_{cr} for infills with low aspect ratios. As the infill aspect ratio increases, the length of the infill decreases and so does the contribution of α_l to the diagonal strut width. Thus for infills with high or medium aspect ratios, the over-prediction of α_l by CSA S304-14 is not as pronounced. Considering the fact that squat infills (aspect ratio < 1) are more often encountered in practice, the over-prediction of the K_{cr} for squat infills is a significant drawback of the Canadian masonry standard.

In the case of bounding frame stiffness where the aspect ratio is kept as 1, a noted discrepancy is observed in P_{net} in the cases of infills bounded by strong beams ($I_b/I_{b0} \geq 5.0$). When the strong beams are combined with weak columns ($I_c/I_{c0} \leq 1.0$), the P_{CSA} values are

markedly greater than P_{net} values. This over-prediction in P_{net} for infills bounded by a strong beam combined with weak columns is attributed to the over-prediction of the contact length. According to the Eqn (2.58) and (2.59), an increase in I_c or I_b results in an independent increase in either α_h or α_l, respectively. However, a strong beam needs compatible columns to provide end restraints in order for the contact length to develop. For those infills which are bounded by a strong beam and weak columns, the increases from FE results in α_h or α_l were far less than the values predicted by CSA S304-14. In addition, CSA S304-14 overemphasizes the contribution of beam stiffness. As discussed in the previous section, the beam stiffness has less effect on the behaviour of the infill system than column stiffness. However, according to Eqn (2.58) and (2.61), the beam stiffness has twice the amount of influence on the diagonal strut as column stiffness. It should be noted that, for all infills bounded by strong beams ($I_b/I_{b0} \geq 5.0$), the P_{CSA} predicted by CSA S304-14 was the same (232.8kN). This can be attributed to the upper limit (*d/4*) of *w* imposed by Eqn (2.60). For all these infills, the term $\frac{1}{2}\sqrt{\alpha_h^{\,2} + \alpha_l^{\,2}}$ in Eqn (2.60) far exceeds the cap value (*d/4*) and thus all design strengths are calculated based on the same strut width $w = d/4$. If $w = \frac{1}{2}\sqrt{\alpha_h^{\,2} + \alpha_l^{\,2}}$ is used instead, the resulted P_{CSA} and K_{CSA} values for these infills would be higher which will in turn lead to a more severe over-prediction of P_{net} and K_{cr}.

It is noted that for the grouting study, the infill thickness used in the standard is the face-shell thickness for hollow infills and the weighted average thickness for partially grouted infills. The K_{CSA} and P_{CSA} obtained from the CSA S304-14 using these thicknesses are close

to FE results except for those with the loaded corner column ungrouted. It should be recommended that if grouting is used in infills, the loaded corner columns be grouted.

In contrast to CSA S304-14, MSJC 2013 generally underestimates stiffness with the average K_{cr}/K_{MSJC} of 2.80 with a COV of 36%. The diagonal strut width equation in MSJC 2013 does not take into account of the influence of beam stiffness, and the effect of the length of infill is only accounted for through the direction angle θ. As a result, the underestimation of K_{cr} becomes most severe for infills with great length ($l \geq 2.8$m) and infill with strong beams ($I_b/I_{b0} \geq 5.0$). A much-improved performance of MSJC 2013 in predicting strength is observed with an average P_{net}/P_{MSJC} of 1.18 with a COV of 26%. However, in the calculation of P_{MSJC}, MSJC 2013 assigns a constant (6 inches) to w. As a result, a constant P_{MSJC} is obtained for infills bounded by various frame members and infills with various aspect ratios. Although this design strength obtains a reasonable overall average P_{net}/P_{MSJC} ratio, it should be noted that the P_{MSJC} fails to capture changes caused by any parameters other than f'_m. The simple treatment of w in MSJC 2013 works moderately well for infills with intermediate aspect ratios ($0.78 \leq h/l \leq 1.4$) and infills with low to moderate frame members ($I_b/I_{b0} \leq 5.0$ and $I_c/I_{c0} \leq 5.0$). However, in an infill with a parameter which can cause a drastic change in w ($I_b/I_{b0} > 5.0$, $I_c/I_{c0} > 5.0$, $h/l < 0.78$ or $h/l > 1.4$), a great discrepancy in P_{net} and P_{MSJC} is found.

The difference between CSA S304-14 and MSJC 2013 design stiffness results from the difference in the diagonal width value. For all specimens considered, the average strut

width in the stiffness calculation determined by CSA S304-14 is 394.5 mm (with φ_{st}=0.5 applied), which is about 2.47 times the width determined by MSJC 2013; the average strut width determined by CSA S304-14 in strength calculation is 789 mm, which is about 5.18 times the width determined by MSJC 2013.

In summary, the results obtained from CSA S304-14 achieve better agreement with the FE results and is able to reflect reasonably the effects of several parameters. The exception are that for an infill with a great length or bounded by a strong beam, the CSA S304-14 overestimates the contact length especially between the beam and the infill (α_l) which results in an overestimation of the stiffness and strength. On the other hand, MSJC 2013 significantly underestimates the K_{cr} for all cases. The MSJC 2013 diagonal width equation is unable to reflect accurately the effect of infill length and frame beam stiffness. Moreover, the P_{MSJC} equation by MSJC 2013 is unable to capture the influence of any parameters other than f'_m.

Chapter 7 Parametric Study on Vertical Loading

7.1 Introduction

The presence of vertical loading on the bounding beam or columns could be a common occurrence in practice. If the bounding frame is an integral part of the gravity loading system, the vertical load can be either applied through columns or beams depending on the framing plan. Fiorato et al. (1970), Mehrabi et al. (1996), Manos et al. (2012) and Stylianidis (2012) conducted experimental tests on masonry infilled RC frames under lateral load along with vertical load applied on the frame columns. Test results showed that the vertical load applied to the frame columns resulted in an increase in the lateral stiffness and strength of the infilled system. As mentioned in Chapter 2, Amato et al. (2008) and Campione et al. (2015) derived a vertical load factor k (Eqn 2.17 and 2.18) based on the work conducted by Cavaleri et al. (2004) and by Papia et al. (2003) (Eqn 2.13) to account for the presence of vertical loads applied at the beam-column joints. Asteris et al. (2015) integrated the work of Papia et al. (2003) and Amato et al. (2008) and proposed an analytical equation taking into account the effect of both the opening in the infill wall and the vertical load applied at the beam-column joints as well as the interaction between the two. The aforementioned studies were all on masonry infilled RC frames where the k factors in these studies were developed for determination of only the initial stiffness of the infilled systems. Due to different characteristics between RC and steel frames, it is believed that the extent of interaction between the infill and its bounding frame is affected by the

material of the frames. The results obtained for RC bounding frames may not be directly applicable to steel bounding frames. Comparing to infilled RC frames, the research on infilled steel frames was limited in the available literature. One such study was conducted by Stafford-Smith (1968) nearly 50 years ago where infills made of just mortar and bounded by steel bar frames were tested under a lateral load and a uniformly distributed vertical load imposed on the upper beam of the frame. The study found that vertical load up to a certain level increased the lateral stiffness and strength of the infill. This finding was also supported by experimental work of Liu and Manesh (2013) where thirteen concrete masonry infilled steel frames subjected to either in-plane lateral loading or combined lateral and axial loading were tested. However, no quantified correlation between the vertical load and the lateral stiffness and strength was provided in either studies.

Noting that most analytical equations for estimating the stiffness and strength of infills were developed for infilled frames subjected to in-plane lateral loading only, this chapter focused on the investigation of vertical load effect on the lateral stiffness and strength of the infills. The main objective was to determine the correlation between the vertical load and the lateral stiffness and strength of the infills. The effects of a wide range of geometric and material properties of the infilled frame, vertical load levels as well as manners of application were included in the study.

7.2 Parametric Study

The Model II was used for this study. For the standard model, the bounding frame was

made of W250x58 columns and W200x46 beams. The infill was 2800 mm high by 2800 mm long. The infill compressive strength, f'_m, was assumed to be 25 MPa and the tensile strength was taken as the 1/10th of f'_m. The parameters considered included the magnitude of vertical loading and the manner of its application; infill aspect ratio; infill compressive strength; and bounding frame stiffness.

Table 7.1 summarizes the finite element models used in this study. Five vertical load levels, V, representing 10, 20, 30, 40, and 50% of the axial capacity of 350W W250x58 (CSA S16-14, 2014) columns were studied. It is recognized that in practice, the vertical load may be applied directly through frame columns or some of it may be applied through the frame beam. Thus, for each vertical load level, three different manners of application were considered including: 1) applied as a uniformly distributed load (UDL) on the top beam of the frame; 2) applied as point loads at the top of two columns; and 3) half of the vertical load applied as UDL on the top beam and the other half as point loads at the top of two columns, referred to as 50-50 manner. Also included in the parametric studies were four aspect ratios of the infill (h/l=0.78, 1.00, 1.40, 2.33) covering a range of stocky to slender infills; three masonry compressive strengths (f'_m =10, 15 and 25 MPa); and in addition to the standard model, a strong frame (SF,W310x129 columns and W360x79 beam) and a weak frame (WF, W200x42 columns and W150x37 beam). Columns of the strong and weak frame had an EI/L approximately 5 and 0.5 times respectively those of the standard model frame which is referred to as the normal frame (NF).

Table 7.1: Summary of finite element models in the study of vertical load effect

No. of models	Vertical load level (%)	h (m)	l (m)	Aspect ratio	f'_m (MPa)	Appl. method	Frame type	λL	p
24	0-50	2.8	1.2~3.6	0.78~2.33	25	UDL	NF	2.66~8.58	0~0.37
24	0-50	2.8	1.2~3.6	0.78~2.33	25	Point load	NF	2.66~8.58	0~0.37
24	0-50	2.8	1.2~3.6	0.78~2.33	25	50-50	NF	2.66~8.58	0~0.37
10	0-40	2.8	2~2.8	1.00~1.40	15	UDL	NF	4.17~5.92	0~0.29
6	0-50	2.8	3.6	0.78	15	UDL	NF	7.55	0~0.30
5	0-40	2.8	2.8	1	10	UDL	NF	5.35	0~0.30
18	0-50	2.8	2~3.6	0.78~2.33	25	UDL	SF	3.19~5.78	0~0.19
18	0-50	2.8	2~3.6	0.78~2.33	25	UDL	WF	5.70~10.32	0~0.37

7.3 Discussion of Results

7.3.1 Effect of Vertical Load Level

In this case, the material and geometric properties of the standard model were used, and the vertical load was assumed to be applied as a UDL on the frame beam. The finite element results showed that the effect of the vertical load level on K_{cr} and P_{net} of the infilled system are also dependent on the aspect ratio of the infill. This collective effect can be seen in Fig. 7.1 where the applied vertical load V versus normalized K_{cr} and P_{net} are plotted. The K_{cr} and P_{net} values were normalized with respect to the model of each aspect ratio but without vertical load. Fig. 7.1 shows that the presence of vertical load affects both the stiffness and strength of infilled systems to various degrees depending on infill aspect ratios. Overall, there seems to exist an optimal vertical load level up to which an increase in the vertical load results in an increase in both K_{cr} and P_{net} of the system. A further increase above this level, however, K_{cr} and P_{net} begin to decrease gradually. This optimal load level varies for different infill aspect ratio, and this is discussed in more detail in the next section.

The increase in stiffness and strength due to the presence of vertical load is believed to be attributed to the increase in diagonal strut width caused by the vertical load. This is qualitatively shown in Fig. 7.2. The strut width of the infill without vertical loading (Fig. 7.2 (a.i)) is much narrower than that of the infill with vertical load (Fig. 7.2 (b.i)) during the loading. For the latter case, even after localized corner crushing of the infill, there is still a relatively large region in contact between the beam and the infill at failure (Fig. 7.2 (b.ii)), which enables possible loading paths for lateral load transfer thus achieving a higher

strength. However, as the vertical load increases, local crushing at the loaded corners occurs increasingly earlier. It is reasonable to deduce that at some vertical load level, the occurrence of crushing will outweigh the increase in the contact length. This is believed to be the reason that the lateral strength of the infilled frame begins to decrease beyond the optimal load level.

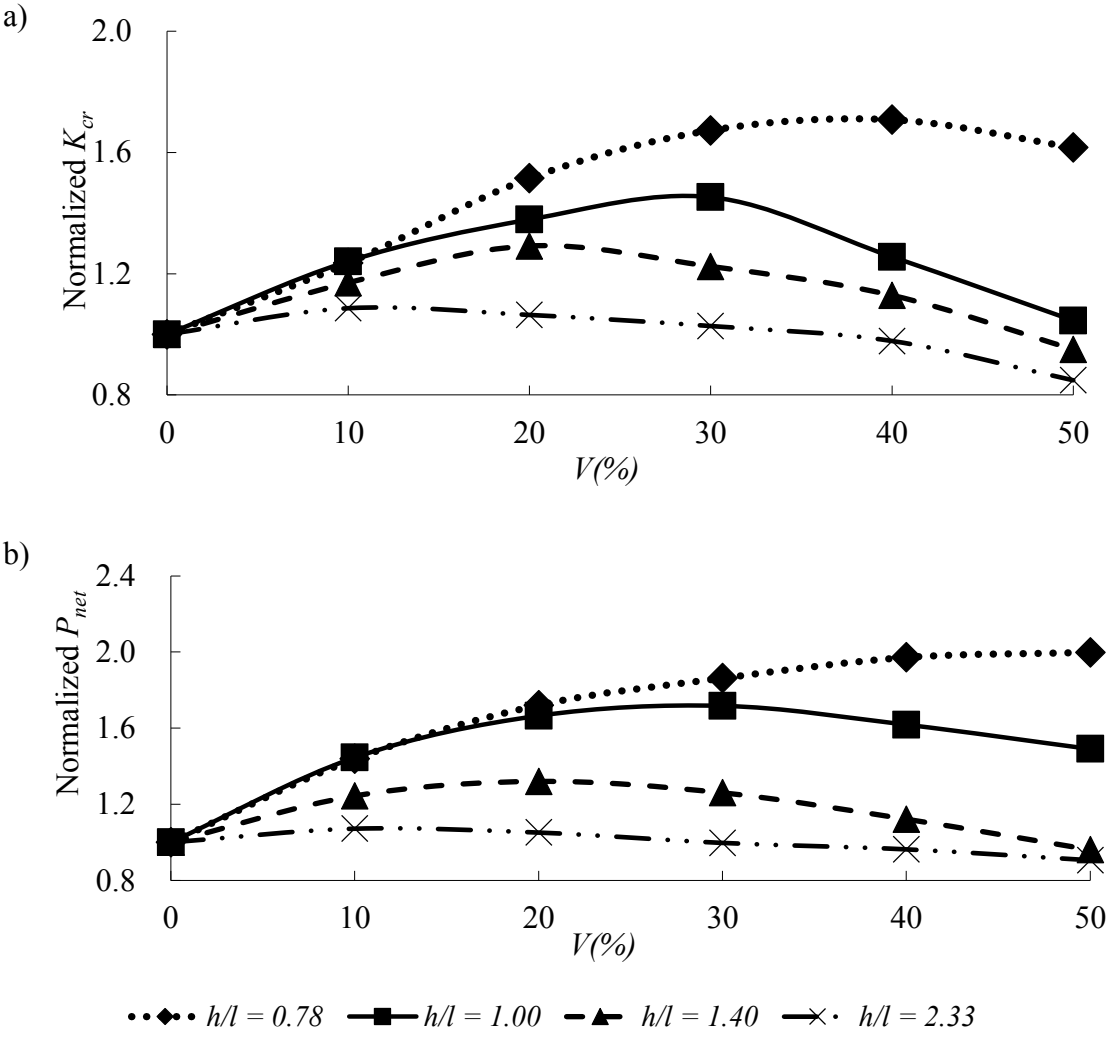

Fig. 7.1: Effect of vertical load level on a) K_{cr} and b) P_{net} of the infilled frame for varying infill aspect ratios

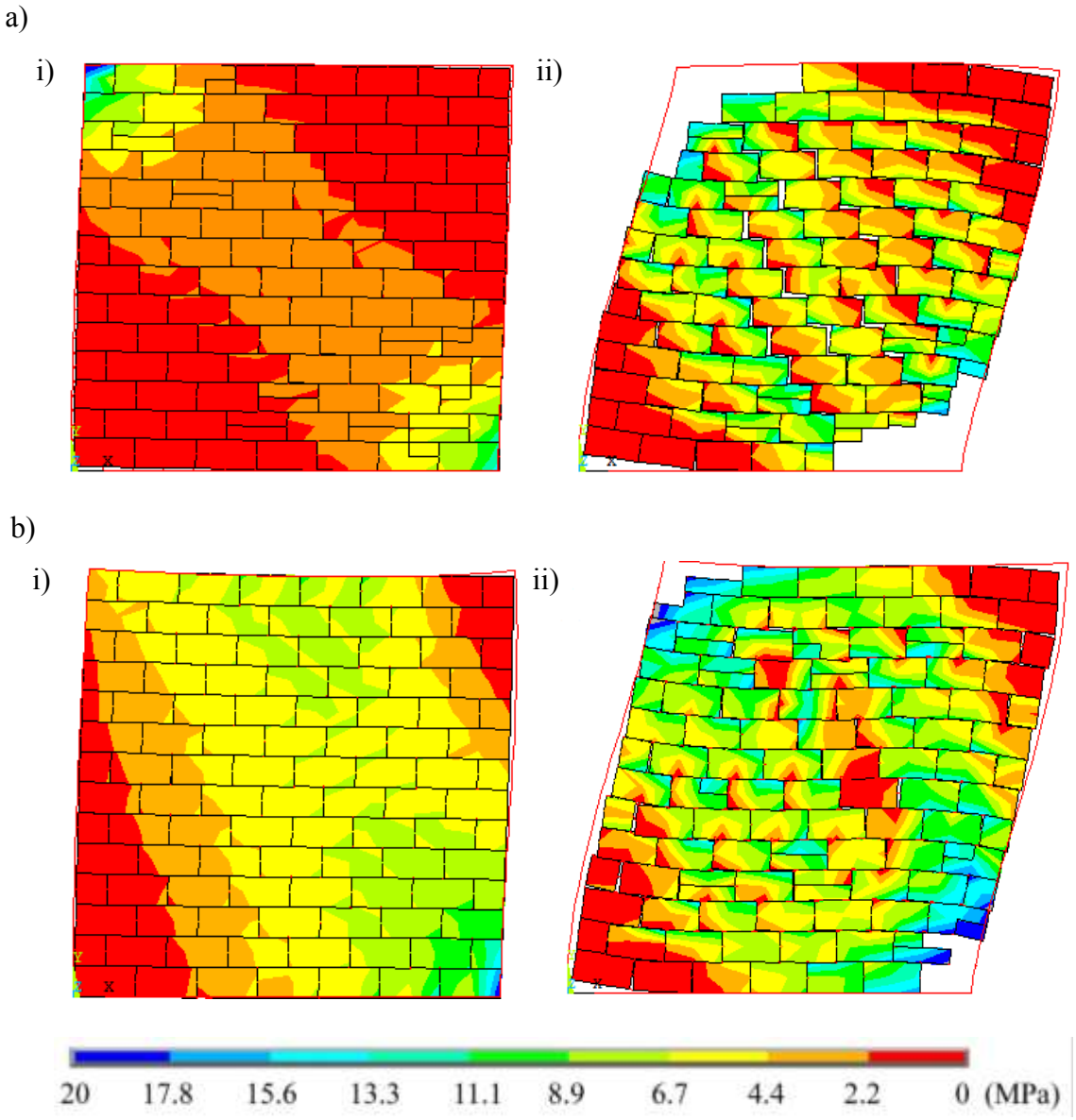

Fig. 7.2: FE distribution of compressive stress in the infill a) subjected to only lateral load, b) subject to combined loading: i) early stage of loading, ii) at failure

7.3.2 Effect of Aspect Ratio

Referring to Fig. 7.1, it can be observed that the percentage increase in K_{cr} and P_{net} caused by the vertical load is increasingly significant as the infill becomes stockier. The behaviour of the most slender infill (h/l = 2.33) seems to be least affected by the presences of vertical load. Shown in Fig. 7.3 is a plot of optimal vertical load level versus infill aspect ratio. It

shows that in general, an increase in slenderness of the infill corresponds to a decrease in the optimal load level. The lateral load transfer mechanism for infills consists of flexure characterized by the overall bending of the infill and shear characterized by the diagonal strut action. It is reasonable to assume that more forces are transferred through flexural behaviour than the diagonal strut action as infills become more slender. The benefit of vertical load on increasing K_{cr} and P_{net} by increasing the width of the diagonal strut is thus not significant for slender infills. Slender infills have smaller lengths than other infills and consequently lower axial capacities. As a result, the vertical load induced masonry crushing happens at a lower vertical load levels in slender infills. On the other hand, the combined lateral and vertical loading results in second-order effects by magnifying the bending moment the infill experiences. This secondary effect is more pronounced for the slender infill than for the stocky infill. The decrease of optimal load level as the aspect ratio of the infill increases is attributed to the combination of these two factors.

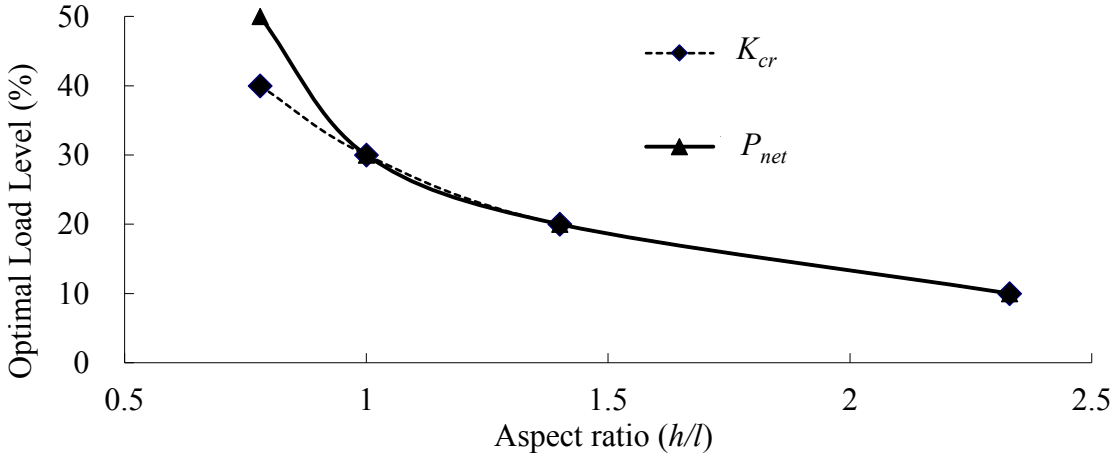

Fig. 7.3: Optimal load level vs. aspect ratio for K_{cr} and P_{net}

7.3.3 Effect of Infill Compressive Strength

The effect of varying masonry compressive strengths on infilled frames subjected to combined loading is presented in Fig. 7.4 for infill with an aspect ratio of 1.0 as an example. A similar trend is observed for other aspect ratios. The figure shows that the presence of the vertical load on increasing the K_{cr} and P_{net} up to a certain level is true for all masonry compressive strengths studied. However, the optimal vertical load level decreases as the compressive strength of the infill decreases, from 30% for f'_m = 25 MPa to about 10% for f'_m = 10 MPa. At 40% vertical load level, infill with f'_m = 10 MPa failed directly by crushing even without any lateral load since the vertical load at this level is greater than (1.1 times) the compressive capacity of the infill. It is hence concluded that the benefit of vertical load is better realized for strong infills than for weak infills.

7.3.4 Effect of Frame Stiffness

The effect of frame stiffness on infilled frames subjected to combined loading is presented in Fig. 7.5 for the infill with an aspect ratio of 1.0 as an example. A similar trend is observed for other aspect ratios. As shown in the figure, the stiffness of the frame does influence the optimal load level and degree of increase in K_{cr} and P_{net} due to the vertical load. As the frame stiffness increases, the optimal load level increases while the percentage increase due to vertical load decreases. This suggests that strong frames can sustain a higher level of vertical load up to which the increase in K_{cr} and P_{net} exists, however, the rate of this increase is less than the weak frame. For a given infill, at a same applied vertical load level, less vertical load is transferred to the infill in a strong frame than in a weak frame. Thus, a

strong frame can sustain a higher applied vertical load prior to the infill failure. However, the strong frame experiences less deformation due to its high rigidity and thus less increase in contact length than a relatively weak frame. This is attributed to its lower rate of increase in stiffness and strength as the vertical load increases than weak frames.

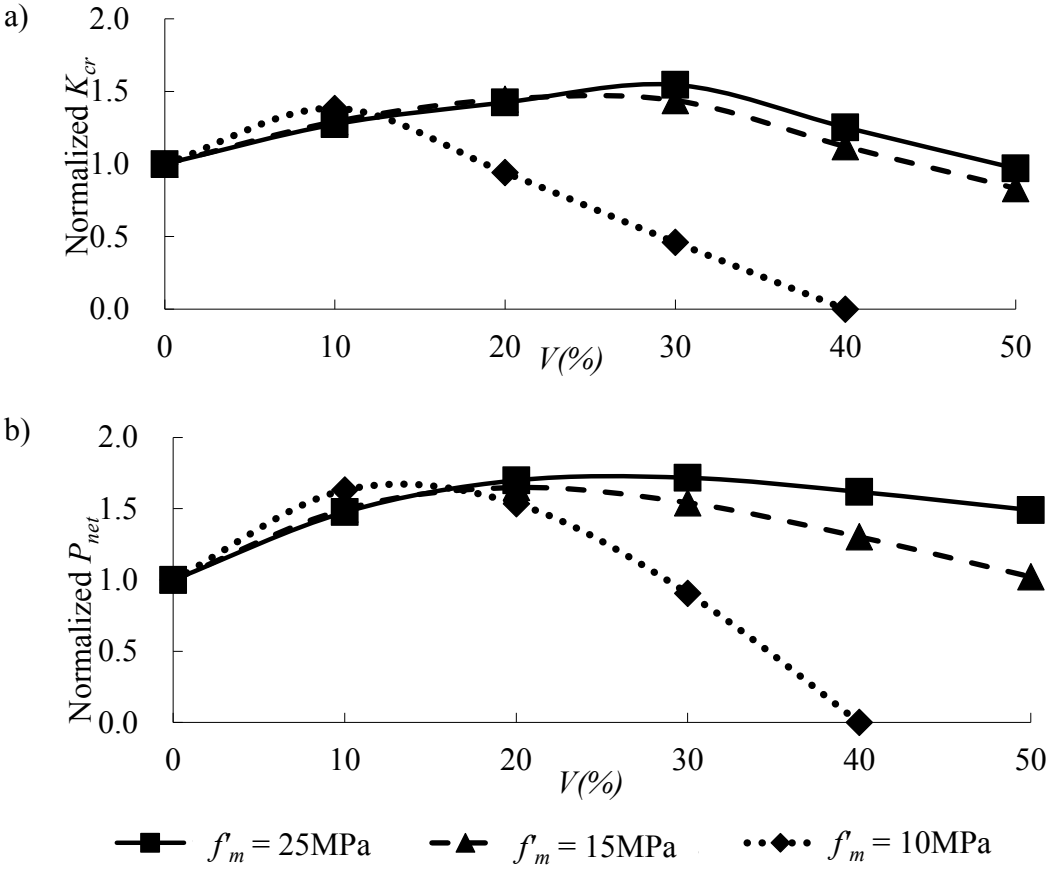

Fig. 7.4: Effect of masonry compressive strength on a) K_{cr} and b) P_{net} of the infilled frame

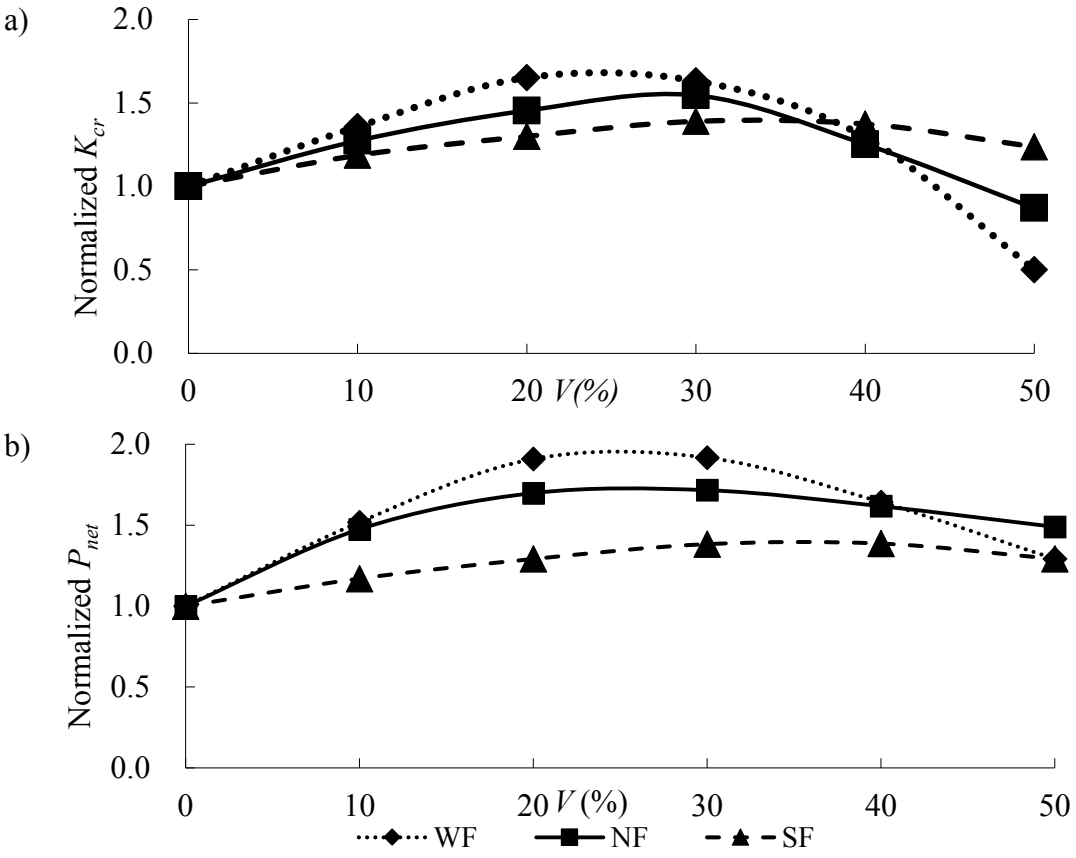

Fig. 7.5: Effect of frame stiffness on a) K_{cr} and b) P_{net} of the infilled frame

7.3.5 Effect of Vertical Load Application Methods

Fig. 7.6 shows the effect of vertical load application methods for infills using an aspect ratio of 1.0 as an example. The manner of vertical load application significantly affects the behaviour of the infilled system especially between the cases of applying through the frame beam and through the frame columns. When the vertical load is applied through columns, the K_{cr} shows a continuous increase trend as the vertical load level increases while the P_{net} showed an approximately linear decrease. When the vertical load is applied in the 50-50 manner, both the K_{cr} and P_{net} seem to increase in a linear relationship with the increase in vertical load. This suggests that the benefit of the vertical load applied through the beam

outweighs the detrimental effect of the vertical load applied through columns, resulting in a net result of a beneficial effect on the K_{cr} and P_{net} of the infill.

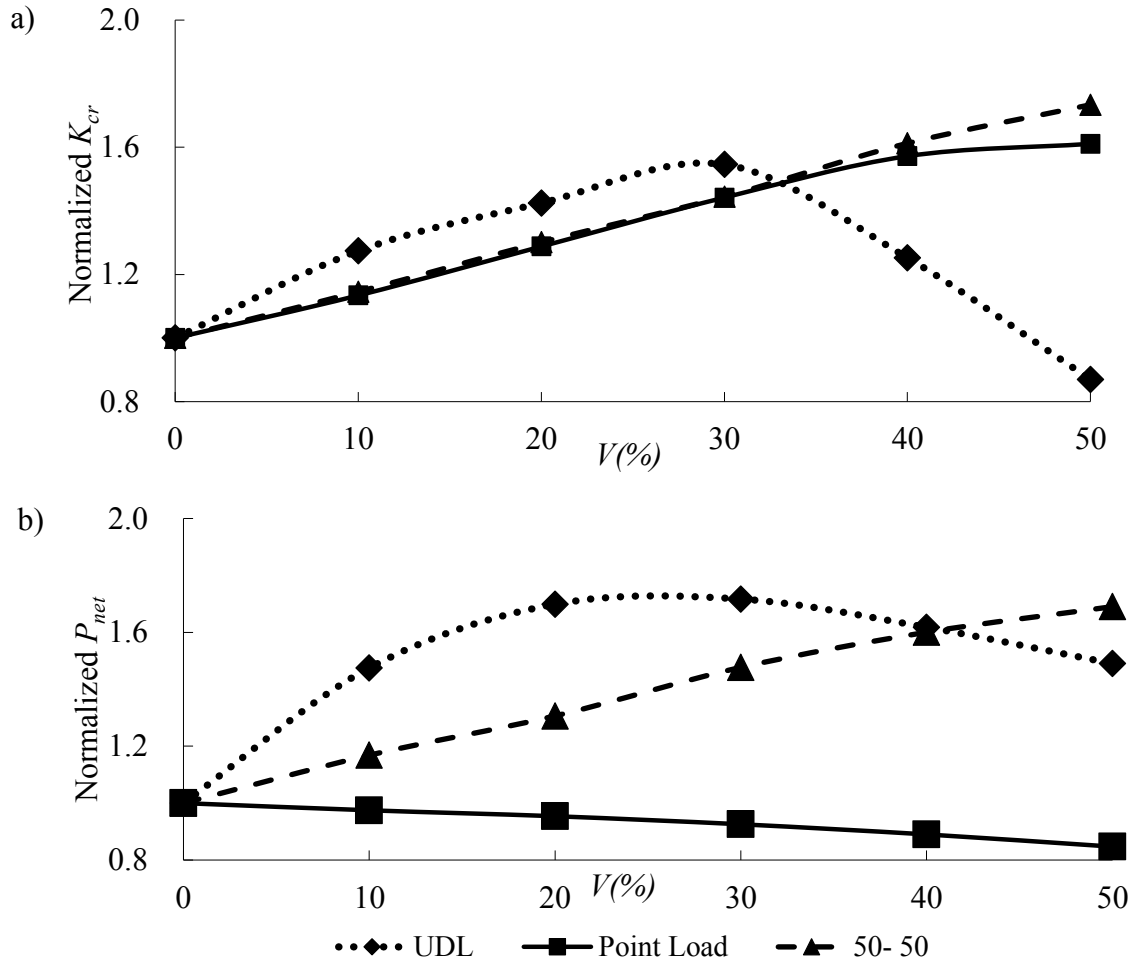

Fig. 7.6: Effect of vertical loading application methods on a) K_{cr} and b) P_{net} of the infilled frame

The difference in behaviour due to the manner of vertical load application is believed to be a result of the load sharing between the infill and the frame. Table 7.2 lists the loads transferred through two columns, V_c, and the ratio of this load to the total applied vertical load, V, for the case of V equal to the 10% of the axial capacity of columns. The table shows that the columns experience the significantly different amounts of load among the three

application methods. When the vertical load is applied as a UDL on the frame beam, the amount of load transferred through columns depends on the infill aspect ratio and more load is transferred to infills as the aspect ratio increases. The load transferred to the infill will effectively increase the contact regions between the beam and the infill. When the vertical load is applied through the columns, the majority of this load is directly transferred into columns (about 83%) which leaves a small portion (about 17%) transferred through the infills. Thus, the contact regions developed between the beam and the infill are less than the former case. Instead, the shortening of the columns makes the loaded corner highly stressed. The already stressed corner crushes much earlier and more extensively as the lateral load is applied than the case when no vertical load is present. This is believed to be the reason of the negative impact on the lateral strength caused by the vertical load applied directly through the columns. It is important to note that this observation is different from that for RC frames where the vertical load applied to the columns is shown to increase the strength of the infilled frame. For RC frames, the vertical load applied through the columns delays cracking and thus results in increases in stiffness and ultimately the moment capacity of the columns. For steel columns, these beneficial effects of vertical load do not exist. Instead, the vertical load through columns reduces their moment capacity.

Table 7.2: Vertical load transferred through columns for different load application methods (V=10% of axial capacity of column W250x28)

h/l	UDL		Point load		50-50	
	V_c (kN)	V_c/V(%)	V_c (kN)	V_c/V (%)	V_c (kN)	V_c/V (%)
2.33	331.4	63.8	447.6	86.2	395.6	76.2
1.40	209.6	40.4	434.0	83.6	337.4	65.0
1.00	150.4	28.9	430.4	82.9	307.0	59.1
0.78	117.4	22.6	430.0	82.8	288.4	55.5

7.4 Analytical Model

7.4.1 Development of Modification Factor

Based on the diagonal strut approach, the effect of vertical loading on the K_{cr} and P_{net} of the infilled frame may be considered through a modification factor M_F to the K_{cr} and P_{net} of the infill subjected to lateral load only. Due to the complexity of the problem, this study focused on the vertical load applied as a UDL to the frame beam. To develop an analytical model that incorporates effects of the aforementioned factors and is also simple to use, this study adopted the use of the unit-less factor λL to account for effects of both infill aspect ratio and relative infill and frame stiffness on the sharing of vertical load between columns and infill, and proposed the use of a vertical load ratio p as a measurement of vertical load level. The term λ was commonly used in previous studies and was defined in Eqn (2.2) while L is the length of the frame beam. Unlike previous studies (Stafford-Smith, 1962; Stafford-Smith & Carter 1969; Mainstone, 1971; Wood 1978; Liauw & Kwan 1984), this study adopted factor λL instead of λH because the change in the length of the infill panel/frame beam is more crucial to the sharing of vertical load between the infill and the bounding frame than the change in height. A change in the infill length results in a

significant change in the lateral stiffness of the infill panel and thus, changes the load sharing between the infill and the columns. However, a change in infill/frame height affects the lateral stiffness of both the infill panel and the columns in equal proportion, and thus, the load sharing between the frame and the infill will not be affected.

The ratio p is defined as the applied vertical load divided by the combined axial capacity of the columns and the infill and can be expressed as:

$$p = \frac{V}{f'_m tL + 2A_c f_y} \tag{7.1}$$

where V is the applied vertical load, f'_m is the infill strength, A_c is the column cross-sectional area, and f_y is the yield strength of steel columns. The resulting λL and p values for all model specimens ranged from around 3 to 10.5 and 0 to 0.37 respectively as summarized in Table 7.1.

This study proposes that the modification factor M_F be expressed as follows where $f(p)$ and $g(\lambda L)$ are two independent functions:

$$M_F = 1 + f(p)g(\lambda L) \tag{7.2}$$

Fig. 7.7 plots the relationship between p and normalized stiffness and strength of infilled model specimens. For clarity, three λL scenarios are shown in the figure. The details of each scenario are described as follows: 1) λL=2.66 corresponds to an infill with an aspect ratio of 2.33 and f'_m = 25 MPa and bounded by the standard frame; 2) λL=4.53 corresponds to an infill with an aspect ratio of 1.00 and f'_m = 25 MPa and bounded by the strong frame;

3) λL=7.55 corresponds to an infill with an aspect ratio of 0.78 and f'_m = 15 MPa and bounded by the standard frame. These three scenarios cover different combinations of infill aspect ratio, f'_m and frame stiffness, therefore, were chosen as examples for demonstration. Fig. 7.7 shows that the relationship between p and the increase in K_{cr} and P_{net} is approximately parabolic. This observation is also true for other λL values in this study. Fig. 7.8 plots the λL values vs. maximum increase of normalized K_{cr} and P_{net} of infilled frames as a result of the vertical load increase. It can be seen that the maximum increase in both K_{cr} and P_{net} has an approximately linear relationship with λL values.

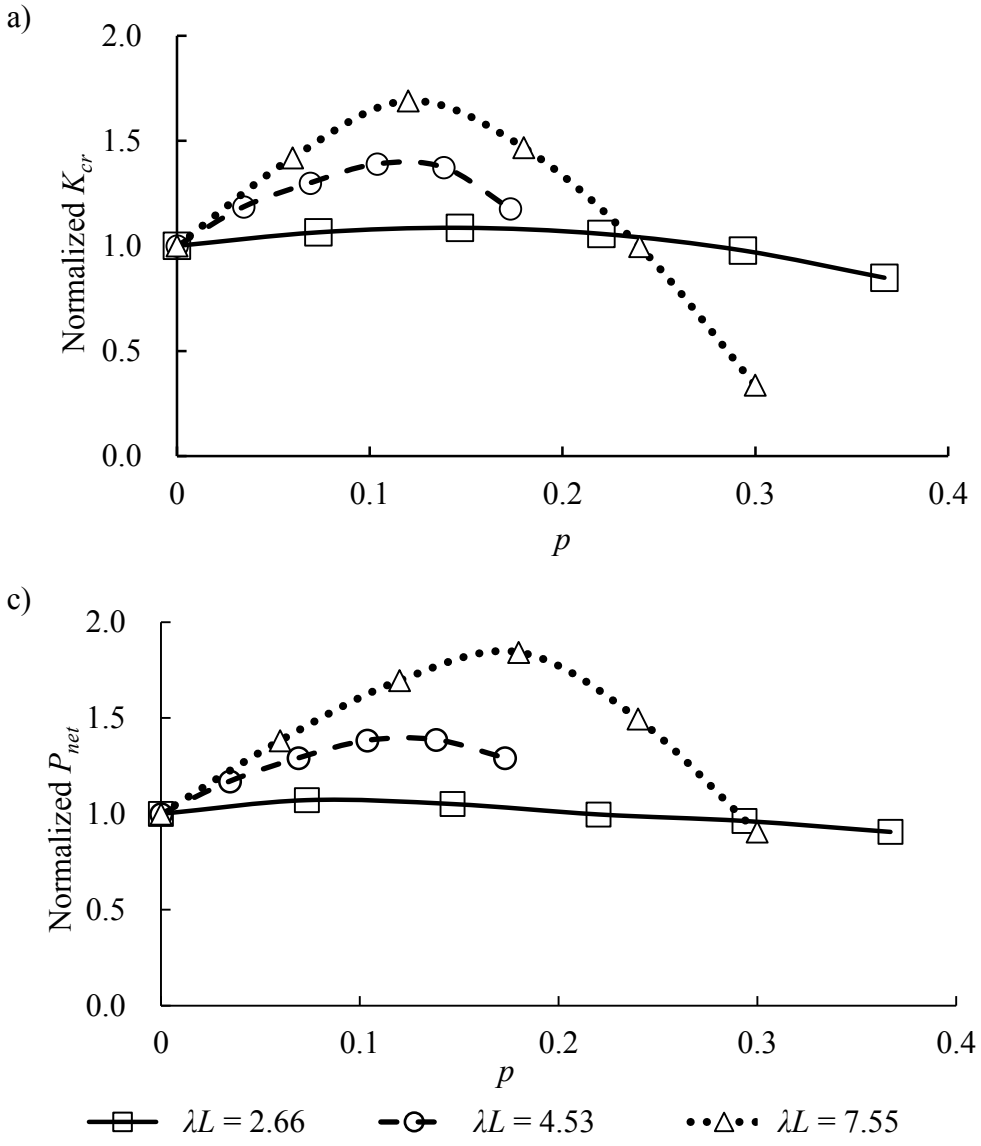

Fig. 7.7: Vertical load ratio p vs. a) normalized K_{cr} and b) normalized P_{net}

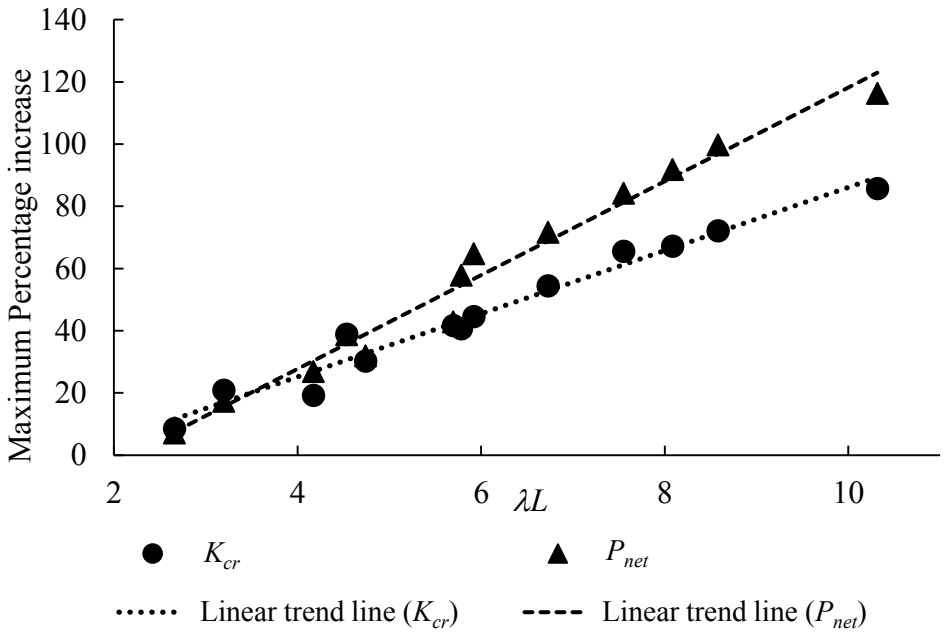

Fig. 7.8: λL vs. maximum increase in stiffness and strength

7.4.2 Equation of Modification Factor and Comparison with FE Results

Based on the above discussion and through nonlinear regression analysis on results of finite element models, the expressions of *f(p)* and *g(λL)* are then determined as follows:

For stiffness:

$$f(p) = -4.635p^2 + 1.180p \tag{7.3}$$

$$g(\lambda L) = 1.406\lambda L - 2.690 \tag{7.4}$$

For strength:

$$f(p) = -2.941p^2 + 0.955p \tag{7.5}$$

$$g(\lambda L) = 1.912\lambda L - 4.417 \tag{7.6}$$

The comparison of these sets of equations with FE results is illustrated in Fig. 7.9 where three scenarios of λL are illustrated. It can be seen that the proposed analytical equations achieve a good agreement with the FE results. When the FE results were compared with

the equation values for all models, the stiffness Eqns (7.3) and (7.4) obtained an $R^2=0.967$ while the strength Eqns (7.5) and (7.6) obtained an $R^2=0.984$, indicating a good performance of the analytical model over a wide range of parameters. It is noted though that the failure mode of all FE models was by corner crushing and hence Eqns (7.5) and (7.6) should be used corresponding to this failure mode.

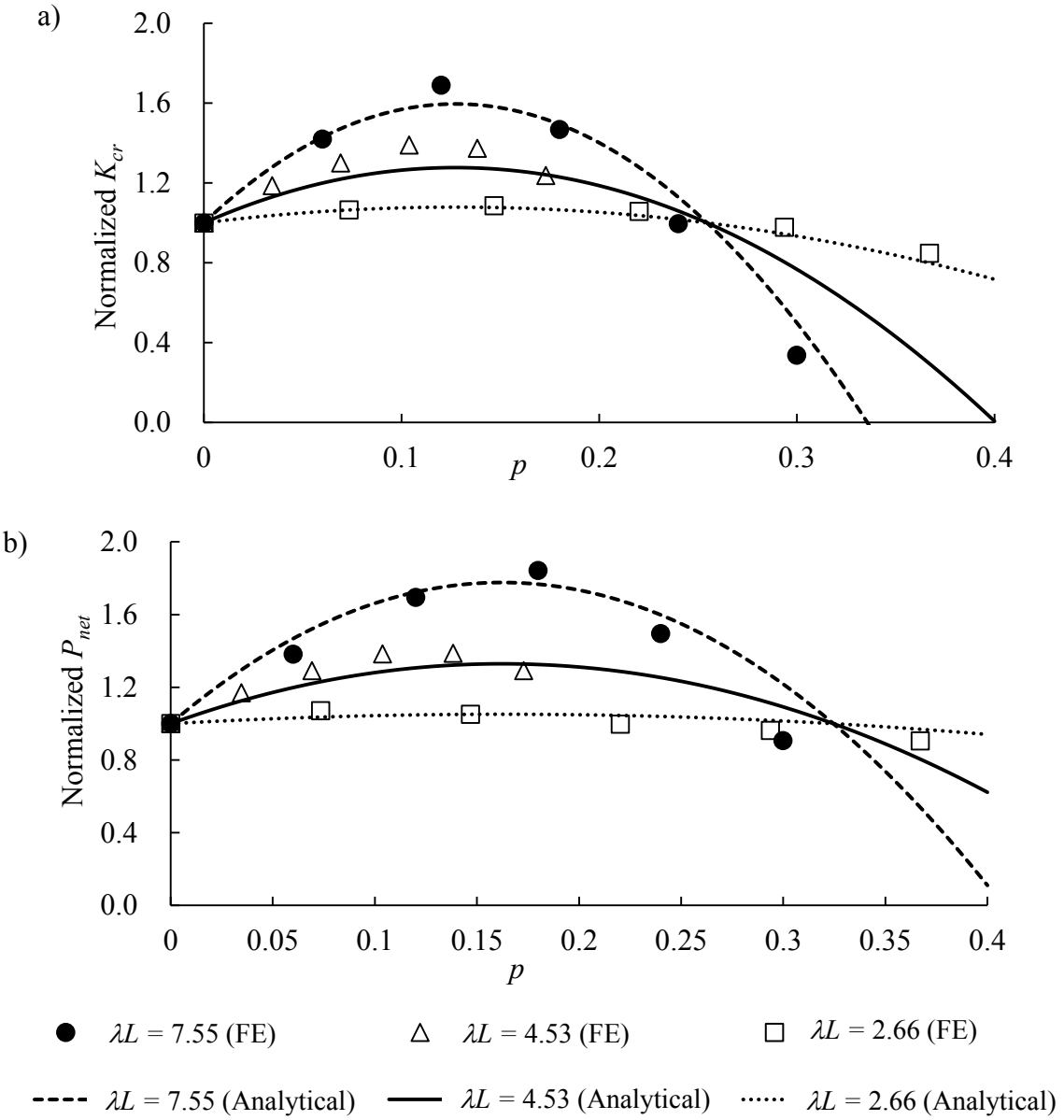

Fig. 7.9:Analytical model values vs. FE results: a) K_{cr} and b) P_{net}

The modification factor developed based on normalized K_{cr} and P_{net} trend as described above, is intended to be used to modify the stiffness and strength of the infills subjected to only lateral load. It is noted though that this modification factor equation was developed for infills bounded by steel frames with the vertical load applied through frame beams. For other bounding frame materials or vertical load applied in different manners, this set of equations is not directly applicable.

Chapter 8 Parametric Study on Interfacial Gaps

8.1 Introduction

In practice, initial gaps between the infill and its bounding frame are common occurrences due to shrinkage and settlement of the infill or defects in workmanship. These gaps could be located either at the beam-infill interface, or column-infill interface, or both. Since the total elimination of gaps is not practical, it is thus important to understand the effect of gaps on the infill contribution to the behaviour and strength of an infilled system.

Despite a large amount of research available to address the infill behaviour in general, studies focusing on the effect of gaps were limited. Within the few available studies on gaps, the common findings showed that gapped infilled frames exhibited a much lower stiffness in early loading stage regardless of whether gaps were present at the column-infill interface or the beam-infill interface. Once the gap was closed at the loaded corner, a sudden increase in stiffness was observed. The detrimental effect of frame-infill interfacial gaps on both the strength and stiffness of the infilled system has been reported (Yong, 1984; Dawe & Seah, 1989; Liu & Soon, 2012; Riddington, 1984). However, the range of reduction observed in these studies was scattered and due to limited data points, no correlation between the gap and the infill stiffness and strength was defined. For example, the experiment program of Yong (1984) and Dawe and Seah (1989) showed that a 20 mm gap at the roof beam and infill interface reduced both the cracking strength and ultimate strength of the infilled steel frame by 50 and 60% respectively. Flanagan (1994) reported

that a 25.4 mm gap at the column-infill interface resulted in nearly no reduction in the infilled steel frame ultimate capacity but a nonsymmetrical cracking pattern where more cracks developed in the lower portion of the panel. In the study conducted by Kadir (1974) showed that a gap of 1.6 mm between the top beam and the infill did not significantly affect the ultimate strength, but it reduced the cracking strength. In the experimental study conducted by Ng'andu (2006) on infilled steel frames, a 12 mm gap at the beam-infill interface was found to reduce the system stiffness by about 20% but had no significant effect on the cracking load or ultimate strength. Nazief (2014) conducted a finite element study where the effect of the beam-infill gap and full separation gap (around the three infill-frame interfaces) was studied. Both steel and RC frames were considered. Results showed that a top beam-infill gap or a full separation gap up to 5 mm did not have a significant impact on the infill ultimate strength while the lateral stiffness was reduced by around 30%. A top beam-infill gap of 10 to 15 mm resulted in a reduction in the ultimate strength of 24% while a full separation gap of the same size resulted in a reduction of 50%. Nazief (2014) also reported that a large gap (15mm at the top beam-infill interface) width may result in a change in failure modes. In the studies mentioned above, the gap scenarios were often limited to the top beam-infill gap (Yong, 1984; Dawe & Seah, 1989; Kadir, 1974; Ng'andu, 2006); the magnitudes of gaps studied were limited; and no systematic comparison between different gap locations was made.

The treatment of the effect of interfacial frame-infill gaps in the various design standards is either non-existent or incomplete. For example, both the Canadian masonry design standard S304-14 (2014) and Eurocode 8 (2004) require that there are no interfacial gaps for infills to be considered as participating infills while no guidelines are provided for the treatment of interfacial gaps in either document. The American masonry standard MSJC 2013 (2013) states that infills can be considered as participating infills provided that the top beam-infill gap is less than 9.5 mm (3/8″), but in such a case, a factor of 0.5 must be applied to the stiffness and strength of the infill. However, there was no sufficient background information provided on the given gap size limit or the reduction factor in stiffness and strength.

In light of the above, this study was motivated to investigate the effect of gaps on the behaviour of infills bounded by steel frames. The objective of the study is to determine correlations between the gap size and location and the lateral stiffness and strength of the infilled frame and to assess the validity of design provisions on gapped infills contained in the American design standard MSJC 2013. To this end, various gap magnitudes and arrangement scenarios were considered as main parameters. The effect of bounding frame stiffness, as well as the friction coefficient, was also included in the study.

8.2 Parametric Study

The Model II was used in this study. The model specimens and associated parameters used in this parametric study are summarized in Table 8.1. Parameters considered included the

gap size and location, bounding frame stiffness, and friction coefficient at the frame-infill interface. The gap size and location were two main parameters where the gap sizes ranging from 0 to 60 mm were considered in three location scenarios. These scenarios were 1) gap present at the top beam-infill interface (labeled as BB); 2) gaps present at two column-infill interfaces (labeled as BC); and 3) full separation gap with equal width at three interfaces (labeled as AA). The model of the infill with no gaps was considered as the control model (labeled as N0). The infill was taken to be 2800 mm high by 2800 mm long. The infill compressive strength was assumed to be 15 MPa, and the tensile strength was taken as the $1/10^{th}$ of that value.

Three types of bounding frames, representing normal, strong and weak frames, were considered. They were 1) the normal frame (NF) which consisted of W250x58 columns and W200x46 beam; 2) the strong frame (SF) which consisted of W310x129 columns and W360x79 beam; and 3) the weak frame (WF) which consisted of W150x24 columns and W100x19 beam. Members of the strong and weak frame have an *EI/L* approximately 5 and 0.1 times respectively those of the normal frame. The analysis for all gap location and sizes was performed for all three types of frames.

The gap width and its arrangement are indicated in the specimen label. For instance, specimen BB-10 stands for a model with a 10 mm gap at the top beam-infill interface (total width = 10 mm); specimen BC-15-30 stands for a model with a 15 mm gap at each of the column-infill interfaces with a total width of 30 mm; whereas specimen AA-10-30

indicates a model with a separation gap of 10 mm between the infill and three members of the frame with a total width of 30 mm. In the case of column-infill gap scenario for specimen BC-10-20, two different arrangements of gaps were also considered where specimens L0R20 and L20R0 indicate that the total 20 mm gap was located between either the right column or the left column whereas the other column-infill interface was assumed in tight contact.

The default friction coefficient (μ) at the frame-infill interface was chosen as 0.4 since it was recommended for concrete on steel surfaces by King and Pandey (1978) and it provided a reasonably good agreement with experimental results. For specimens BC-10-20, L20R0 and L0R20, two additional μ values of 0.7 and 1.0 were considered. The value of 0.7 is suggested by CSA S304-14 for sliding shear between masonry and bare steel while the value of 1.0 was selected to represent sliding on very rough surfaces.

A finite element analysis conducted on the bare frame showed that for the normal frame (NF), yielding of columns occurred when the lateral displacement reached 28 mm. For the weak (WF) and the strong frame (SF), the yielding commenced at a lateral displacement of 62 mm and 23 mm, respectively. When the column-infill gap size exceeds the elastic limit for lateral displacement, yielding is expected to initiate in the columns before the gap is closed. As can be seen, some gap sizes studied place the frame in the yielding region. These cases are identified in Table 8.1.

Table 8.1: Parameters in the study of gap

Gap location	ID	Gap size		Frame type	Fric. coef.
		Per side	total		
None	C0	0		NF, SF, WF	0.4, 0.7, 1.0
Full separation	AA-1-3	1	3	NF, SF, WF	0.4
	AA-5-15	5	15		
	AA-10-30①②	10	30		
	AA-15-45①②	15	45		
	AA-20-60①②	20	60		
Beam-infill	BB-1	1	1	NF, SF, WF	0.4
	BB-5	5	5		
	BB-10	10	10		
	BB-15	15	15		
	BB-20	20	20		
	BB-30①②	30	30		
Column-infill	BC-1-2	1	2	NF, SF, WF	0.4
	BC-5-10	5	10		0.4
	BC-10-20	10	20		0.4, 0.7, 1.0
	L0R20	0, 20	20	NF	0.4, 0.7,1.0
	L20R0	20, 0	20		0.4, 0.7, 1.0
	BC-15-30①②	15	30	NF, SF, WF	0.4
	BC-20-40①②	20	40		

① total gap magnitude exceeds the maximum elastic lateral displacement of a normal frame (NF).

② total gap magnitude exceeds the maximum elastic lateral displacement of a strong frame (SF).

8.3 Numerical Study Results

8.3.1 General Discussion

The typical load vs. lateral displacement curves are presented in Fig. 8.1 using specimen

AA-10-30 bounded by the normal frame as an example. It can be seen that before the gap is closed, the gapped infill system behaves similarly to a bare frame, and a sudden increase in stiffness is observed upon closure of the gap. The specimen reaches failure at a larger displacement and thus higher member forces would be developed in the frame. Note that in this section, in addition to the previously defined lateral cracking stiffness (K_{cr}), the ultimate lateral strength of the infill system (P_u) and the net lateral strength (P_{net}) carried by the infill, the following terms are introduced to evaluate the infill behaviour. As illustrated in Fig. 8.1, the initial stiffness, K_i, is defined as the initial slope of the response curve of the gapped infill frame; and the tangent cracking stiffness K_t, is defined as the slope of the straight line connecting the point of the sudden stiffness increase and the cracking load point. For the infilled frame without gaps (C0), the initial stiffness is denoted as K_s.

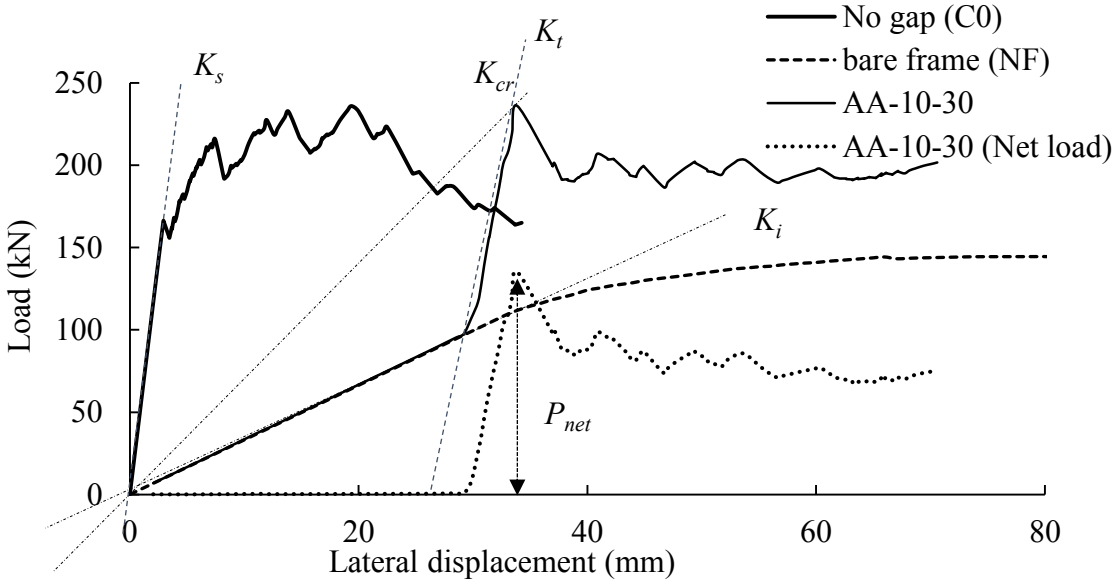

Fig. 8.1: Definition of K_s, K_i, K_{cr}, K_t and P_{net} in this study

Fig. 8.2 compares the load vs. lateral displacement curves of specimens with the same total gap size (AA-10-30, BB-30, and BC-15-30) bounded by the normal frame. As shown in Fig. 8.2(a), the initial stiffnesses of specimens AA-10-30 and BC-15-30 are similar, and they are more or less the same as that of the bare frame. This is expected since the gap present between the infill and the columns will enable some "free" deformation of the frame before the infill is engaged. In the case of specimen BB-30, the initial stiffness is slightly higher than that of a bare frame. In this case, although there is no bearing at the beam-infill interface, the infill is engaged at the initial loading stage through bearing at the two column-infill interfaces. Fig. 8.2(b) shows that before the gaps are closed, only the infill of specimen BB-30 shows noticeable load carrying which further confirms the above observation of loading transfer at the onset of loading. The general trend of all three specimens is similar where an elastic linear behaviour is observed before engagement of the infill indicating the frame deformed elastically up to the closure of the gap(s) and after which point, the infill system behaves similarly to the control specimen C0. The development of cracking is reflected through small drops in the load but with an immediate increase in the curve. After the ultimate strength, the system still shows marked ductility maintaining about 80% of the ultimate strength with increasing lateral deflection.

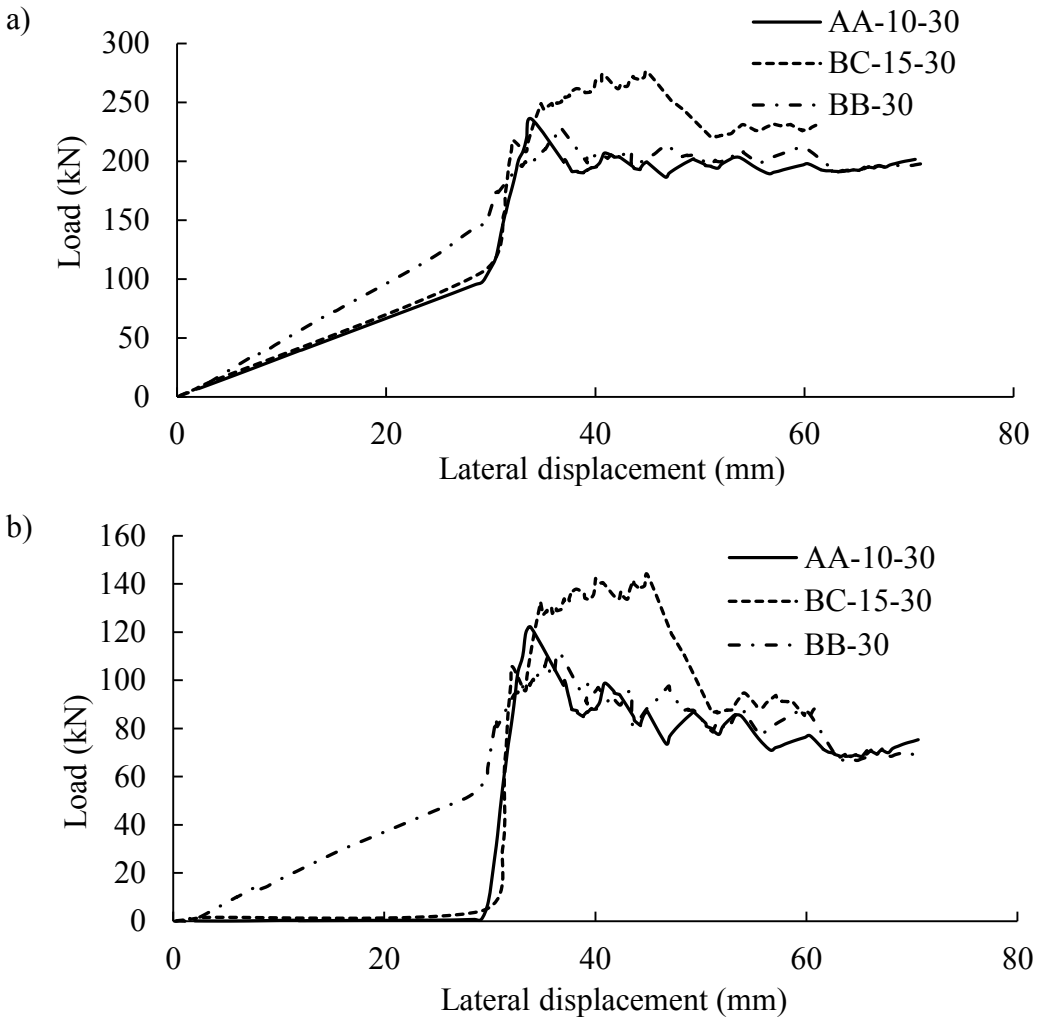

Fig. 8.2: Load vs. lateral displacement curves of infill with gaps: a) Pu of the infill system, b) Pnet of infill

8.3.2 Failure Mode

The finite element results show that for all gapped specimens bounded by the normal or weak frames, once the gap(s) is closed, the diagonal strut forms in the infill, and failure is still predominated by crushing of the masonry at the loaded corners, which is the same as the failure mode for the infill without gaps. One such failure mode is shown in Fig. 8.3(a). For specimens with gap sizes exceeding the elastic lateral displacement of the frame (28 mm), the frame begins to yield at column bases and beam-column joints before gap(s) is closed. However, the FE model shows that the diagonal strut action is still developed in the inelastic stage of the frame.

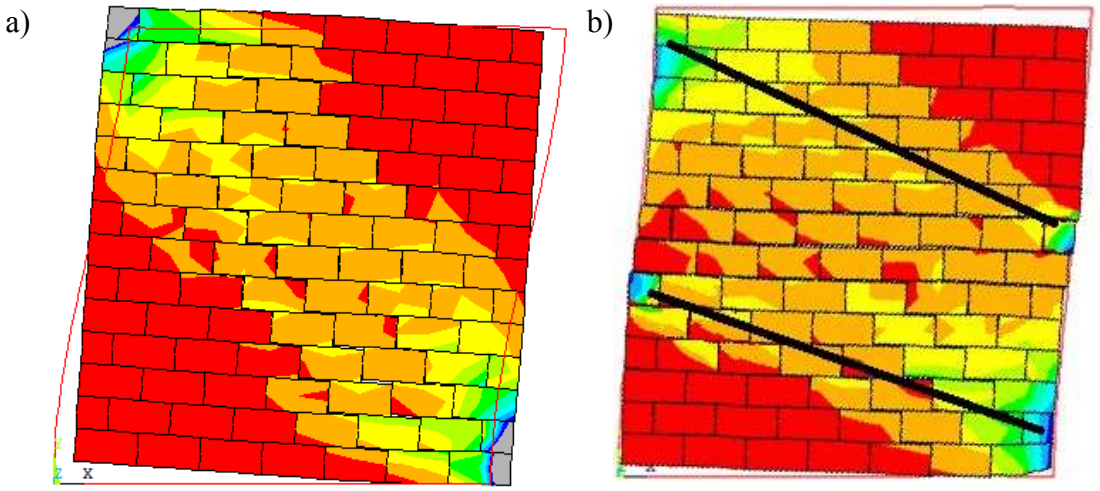

Fig. 8.3: Compressive stress distribution in specimen: a) AA-5-15, b) BB-10 bounded by the strong frame (where grey areas indicate crushing failure of masonry)

For specimens with BB gap scenario and bounded by strong frames, however, failure is initiated by sliding shear where the resistance is mainly achieved through bearing at column-infill interfaces. The high rigidity of beam-column connection of strong frame yielded smaller rotation at a given lateral displacement and thus the contact area achieved

between the top beam and the infill is less than that in the normal or weak frame, resulting in the majority of the lateral load being transferred through the contact at the columns-infill interfaces. The mode of failure of specimen BB-10 is shown in Fig. 8.3(b) as an example. As the figure shows, the load is transferred through two alternative struts developed between the mid-height of the column and the two diagonal corners, which results in sliding of the two portion of the infill with respect to each other along the mortar joints. It should be pointed out that this failure mechanism is only observed in specimens with BB gap scenario and bounded by strong frames.

8.3.3 Effect of Gap Size

Fig. 8.4 shows the normalized stiffness (K_{cr} and K_t) and normalized strength (P_{net}) of infills plotted against the gap size for specimens with the normal frame for all three gap scenarios. The stiffness and strength values are normalized using the corresponding values of the control specimen C0 without gaps. Since specimen C0 behaves linearly to the first cracking load, the K_{cr} and K_t for specimen C0 are identical and they are essentially the initial stiffness K_s (Fig. 8.1). It is evident that both K_{cr} and K_t show a significant decrease as gap size increases and also the reduction in K_{cr} is more severe than in K_t. For example, for a given gap location (BB for example), the normalized K_{cr} is reduced to 0.11 while K_t is about 0.56 with a beam-infill gap size of 30 mm (specimen BB-30). This is reasonable since K_{cr} is largely dependent on the lateral displacement of the system before the infill engagement whereas K_t is a measure of stiffness after the infill engagement. The increase in gap size has more impact on K_{cr} as the frame needs to deform a greater amount before the infill

becomes engaged. The infill strength P_{net} also shows significant reduction as a result of an increase in the gap size where specimen BB-30 has a P_{net} of 54% of that of specimen C0. The general trend described above also applies to gap scenarios AA and BC. The reduction in infill strength is believed to be attributed to the reduction in contact area developed between the infill and the frame. According to the diagonal strut concept, as the lateral loading increases, the flexural deformation of the frame causes the frame to separate from the infill and at failure with only two loaded corners remaining in contact with the infill to provide the resistance. For a gapped specimen, as gap size increases, the flexural deformation required to engage the infill is increasingly greater. The larger deformation of frame members leads to less contact area between the infill and the frame, which ultimately reduces the effective width of the diagonal strut for the load transfer.

Referring to Fig. 8.4 (a), while the yielding reduces K_{cr} significantly, e.g. K_{cr} for specimen AA-20-60 is reduced below the stiffness of a bare frame, the P_{net} seems less affected by yielding of the frame since there is no sudden change in the rate of reduction as shown in Fig. 8.4 (c). In practice, the gap size should be maintained within the elastic limit of the frame deformation. In the case that the gap size exceeds the elastic deformation of the frame, this study suggests that the diagonal strut can still develop and a large portion of the infill strength can still be achieved, provided that the frame is allowed to develop its full plastic capacity.

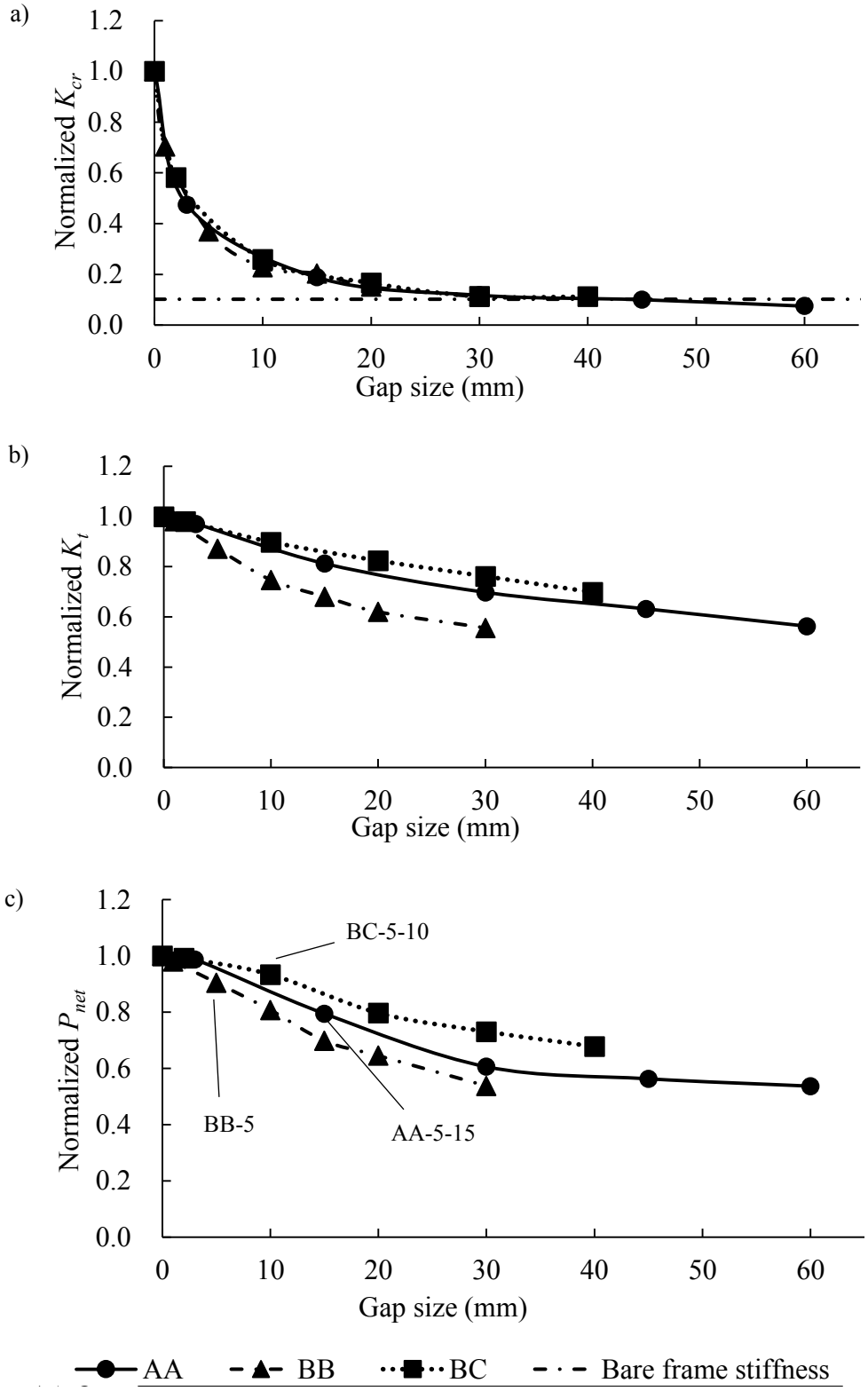

Fig. 8.4: Normalized stiffness and strength of infills with varying gap sizes and locations: a) K_{cr}, b) K_t and c) P_{net}

8.3.4 Effect of Gap Location

It can also be observed in Fig. 8.4 that with the same total size of the gap, the gap scenario BB results in the greatest reduction in both the stiffness and strength while the BC scenario shows the least reduction. It suggests that for a given total gap size, the beam-infill gap has a more detrimental effect on infill strength than the column-infill gap. The load transfer mechanism for an infill without gaps is a combination of direct bearing and friction between the infill and frame members. In the case of top beam-infill gap, the load transfer can only rely on the direct bearing between the infill and frame columns; whereas in the case of column-infill gaps, the load is transferred initially through friction between the infill and the top beam and after the gaps closes, the bearing between the infill and the frame members also partakes in loading transfer. Therefore, the presence of the top gap is more disruptive in establishing an effective loading path. Fig. 8.4(c) also shows that the reduction in stiffness or strength for the case of full separation gap is not simply the addition of the reduction due to the beam-infill gap (BB) and the column-infill gap (BC). For example, specimen AA-5-15 scenario is equivalent to the superposition of specimen BB-5 and specimen BC-5-10 scenarios. The reduction in strength in specimen AA-5-15 (21%) is greater than the summation of reduction in the latter two specimens (10% + 7% = 17%).

8.3.5 Effect of Frame Stiffness

The effect of gaps on infills bounded by different frames is presented in Fig. 8.5 using gap scenario AA as an example. It can be seen that the decreasing trend on K_{cr}, K_t, and P_{net} as a result of an increase in gap size remains true for varying frame stiffness. However, as the

stiffness of the bounding frame increases, reductions in K_t and P_{net} increases. In other words, weak frames results in smaller reductions whereas strong frames results in larger reductions in stiffness (K_t) and strength (P_{net}) than those bounded by the normal frame. This may be attributed to the fact that a weak frame, especially a weak beam allows more rotation to develop at beam-column joints which can accommodate the presence of gap better than a stiffer frame. A stiff beam remains relatively horizontal during loading with little end rotation at beam-column joints. This leads to small contact regions at the loaded corners. In the case of K_{cr}, it is greatly influenced by the bare frame stiffness. As a result, a weak frame has a low K_{cr} while a strong frame has a high K_{cr}.

The above findings are also valid for BB and BC gap scenarios in general. However, a noted difference is that the normalized strength P_{net} of infills bounded by strong frames for the BB gap scenario shows a more drastic decrease than those bounded by normal or weak frames. This is shown in Fig. 8.6. This may be attributed to the change in failure mechanism in specimens with BB gap scenario and bounded by strong frames. As previously discussed, for these specimens, the failure is initiated by sliding shear where the top left portion of the infill tends to slide with respect to the bottom right portion of the infill. This load transfer mechanism is much less efficient than the original diagonal strut which ultimately leads to a lower strength.

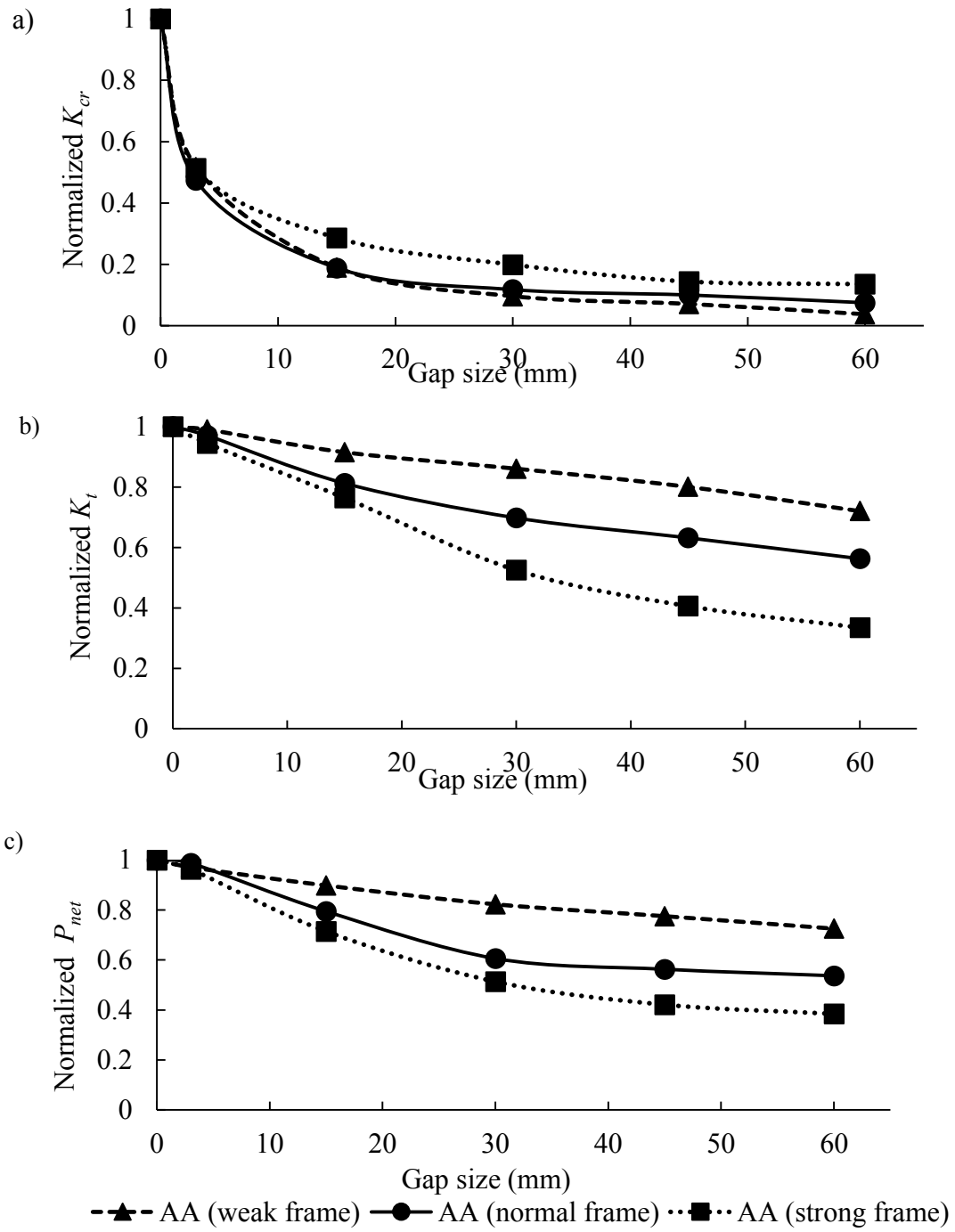

Fig. 8.5: Normalized stiffness and strength of infills bounded by different frames (AA scenario): a) K_{cr}, b) K_t and c) P_{net}

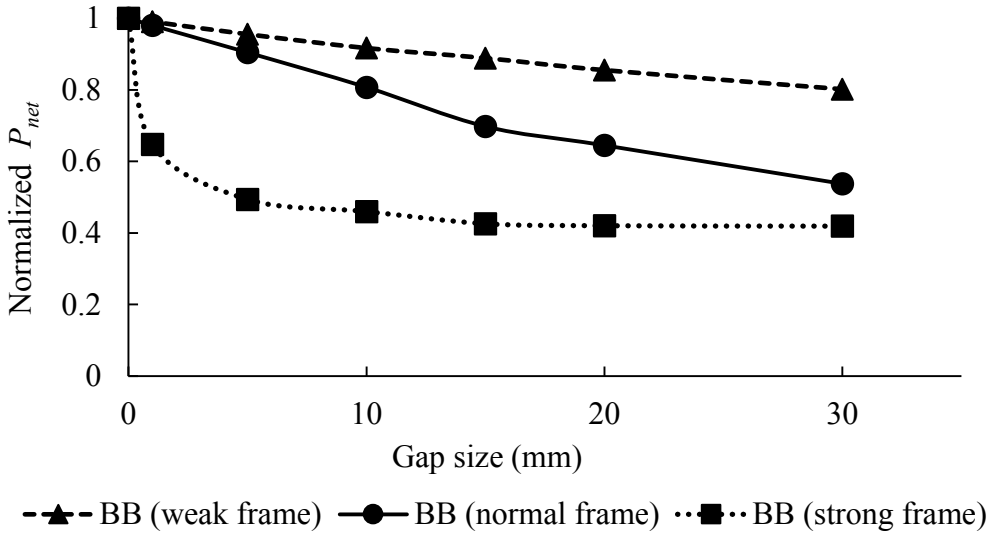

Fig. 8.6: Normalized P_{net} of infills bounded by different frame with BB scenario gaps

8.3.6 Effect of Column-Infill Gaps

In practice, the gap may be present at either side of the column-infill interface. The effect of location of the column-infill gap along with friction coefficient is discussed in this section. Fig.8.7 compares the net load vs. lateral displacement curves of specimens L20R0, BC-10-20, and L0R20 for different μ values. It shows that increasing μ from 0.4 to 0.7 has little to no impact on the behaviour of the specimen except for a slight increase in the net strength of the infill. Further, the initial infill behaviour of infills with μ = 0.4 and 0.7 are non-participating. After the lateral displacement of the frame reaches about 20 mm, the infill becomes engaged and the system had a sudden increase in stiffness.

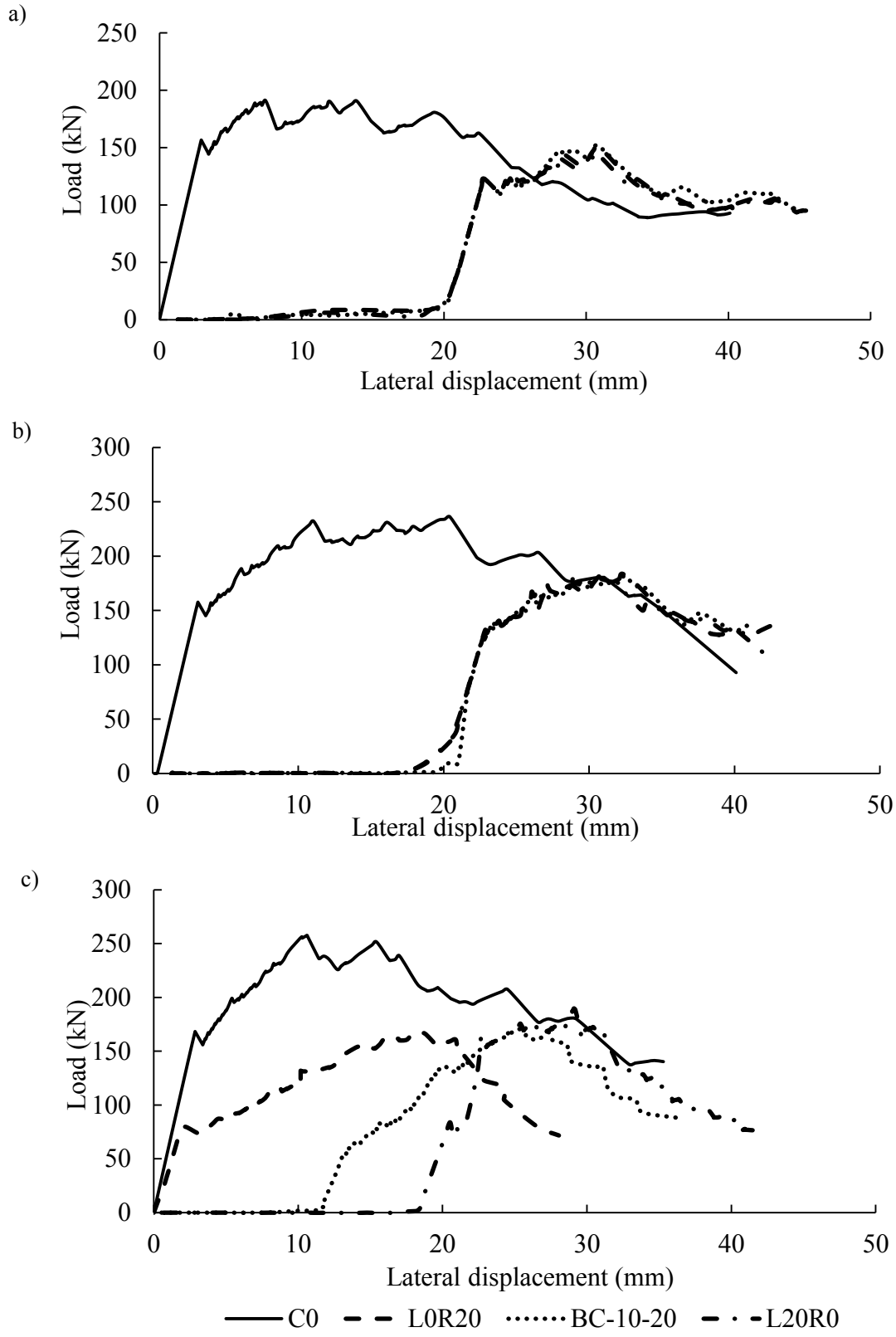

Fig. 8.7: Net load vs. lateral displacement curves of infill with different μ: a) μ =0.4, b) μ =0.7 and c) μ =1.0

When μ is 1.0, however, different column-infill gap locations result in different infill behaviour. Fig. 8.7(c) shows that when μ = 1.0, L0R20 is participating from the beginning with the highest K_i of 44.6 kN/mm, albeit still lower than that of specimen C0 (62.6 kN/mm). Since in this case the gap on the loaded column side is non-existent, the diagonal strut began to develop at the onset of loading. For both specimens BC-10-20 and L20R0, due to the gap at the loaded column side, the initial infill behaviour is non-participating until the displacement reached 10 and 20 mm respectively.

In terms of strength, when μ = 0.4 and 0.7, there is little variation in the net strength of the three gapped frames. When μ = 1.0, the lowest net strength (166 kN) occurs in specimen L0R20 while the highest net strength (189 kN) occurs in specimen L20R0 and specimen BC-10-20 has a strength (172 kN) in between. The finding that the infill (specimen L0R20) with the highest initial stiffness but lowest strength may be attributed to the following reason. Due to the high friction coefficient, the right side of the column-infill gap in specimen L0R20 was never fully closed. This can be seen in the finite element failure mode comparison shown in Fig.8.8. The direct bearing of the right column at the bottom right corner was absent for specimen L0R20, and the transfer of lateral load relied solely on the beam-infill interface. For specimen L20R0, the left gap was closed through frame deformation and thus the lateral load was transferred through both the column-infill interface and beam-infill interface at both loaded corners. As a result, specimen L20R0 has a better-developed diagonal strut than specimens L0R20 and BC-10-20 and thus achieves

higher strength.

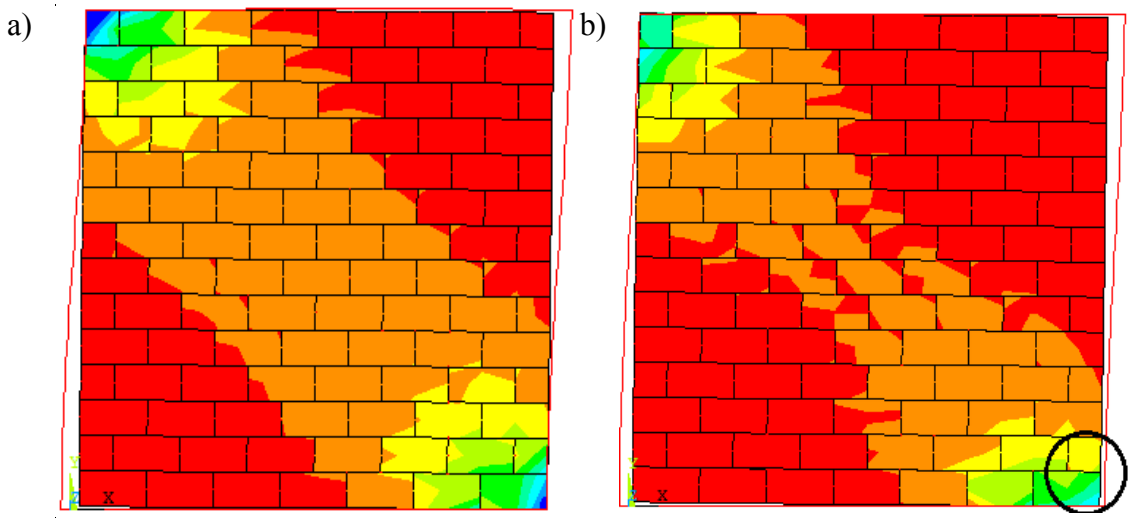

Fig. 8.8: Distribution of compressive stress prior to failure in a) specimen L20R0 and b) specimen L0R20

In summary, when the friction coefficient is less than 1.0 which is commonly the case for masonry on steel surfaces, the effect of friction coefficient to the infill stiffness and strength for gapped frames is negligible. When the friction coefficient is greater than 1.0 which may be considered for very rough surface contact, the infill stiffness and strength are noticeably affected by the column-infill gap location.

8.3.7 Discussion of Gap-Related Clauses in MSJC 2013

As mentioned earlier, the guidelines contained in the MSJC 2013 on the treatment of interfacial gaps in the design of masonry infills specifies a 9.5 mm limit for the beam-infill gap along with a 0.5 reduction factor for the infill stiffness and strength. In practice, most steel frames have an elastic deformation greater than 10 mm. Therefore, it is safe to assume that for most practical frames, the compressive diagonal strut can be developed without resulting in plastic strains at column bases or beam-column joints if the gap is within 10

mm. The finite element results of the entire parametric study in terms of normalized stiffness and strength are plotted against the gap size (total width) in Fig. 8.9. The lower bound of all results is also shown in the figure together with the 0.5 reduction factor line.

It can be seen that, in the case of K_{cr}, the 0.5 reduction factor becomes un-conservative when gap size reaches 3 mm. In the case of K_t, the reduction factor is adequate up to a gap size of 20 mm and beyond that, the reduction factor is only un-conservative for a few infills bounded by the strong frame, as identified in Fig. 8.9(b). This suggests that the stiffness referred to in the MSJC 2013 should be intended for the tangent stiffness after the infill engagement. In the case of infill strength, up to a total gap size of 10 mm, the 0.5 reduction factor provides a markedly conservative estimate for cases with normal and weak bounding frames. The average reduction factor for a gap size of 10 mm is around 0.83. For strong bounding frames, however, the 0.5 reduction factor is closer to the FE results for a gap size of 10 mm but on the un-conservative side for a few cases beyond 10 mm. Note that these specimens were infills with BB gap scenario and bounded by strong frames, it suggests that the reduction factor should be used with caution with strong bounding frames. In the case of a normal and weak frame, the 0.5 reduction factor was conservative up to 30 mm.

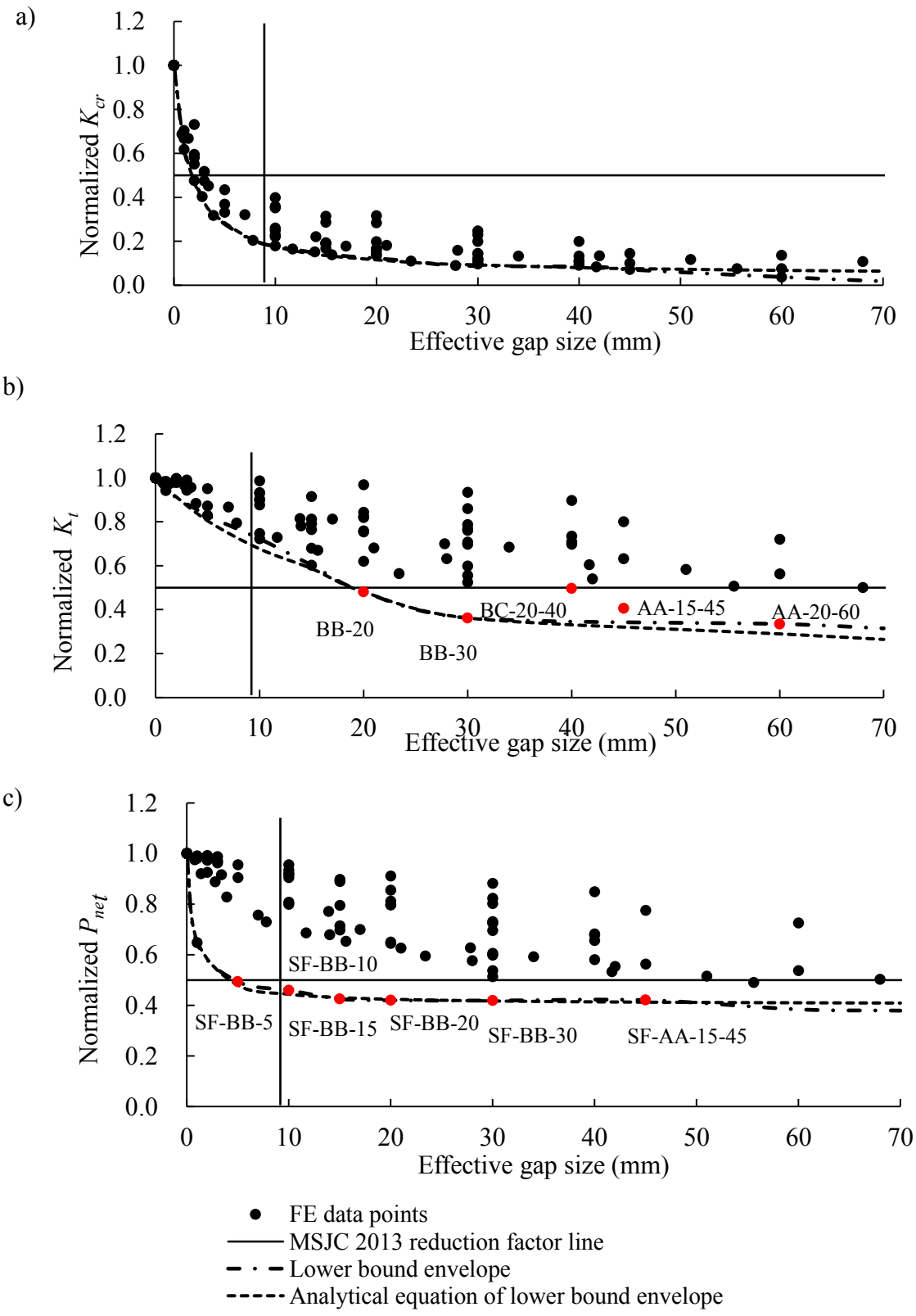

Fig. 8.9: Comparison of the lower bound envelope from FE results and the MSJC reduction factor: a) K_{cr}, b) K_t ,and, c) P_{net}

To obtain overall reduction factor expressions that may cover all parameters as discussed previously, a linear regression analysis of the finite element results was conducted. A term "effective gap size" is introduced and labeled as "x". As shown in Fig.8.10 (a), to fully close the side gaps with a total magnitude of δ_{BC}, the amount of lateral displacement needed simply equals δ_{BC} provided that slippage of infill is allowed. However, to close a top gap with the magnitude of δ_{BB}, the infill needs to undergo a certain amount of rigid body rotation to close the top gap. And this rigid body rotation can be calculated as $(h/l) \times \delta_{BB}$, where h/l is the aspect ratio of infill. Thus, the effective gap size (x) is defined as:

$$x = \delta_{BC} + (h/l) \times \delta_{BB}. \tag{8.1}$$

Adopting this effective gap size, a set of analytical equations was then proposed as follows for the lower bound curves of normalized K_{cr}, K_t, and P_{net}.

$$R_{F,\mathrm{cr}} = \frac{0.0324x + 1.42}{0.817x + 1.42}, R^2 = 0.996 \tag{8.2a}$$

$$R_{F,t} = \frac{0.0103x + 2.97}{0.157x + 2.97}, R^2 = 0.981 \tag{8.2b}$$

$$R_{F,net} = \frac{0.202x + 0.37}{0.501x + 0.37}, R^2 = 0.996 \tag{8.2c}$$

where "$R_{F,\mathrm{cr}}$" , "$R_{F,t}$" and "$R_{F,net}$" are reduction factors for K_{cr}, K_t, and P_{net}, respectively, and R^2 is the coefficient of determination of the regression analysis.

The comparison of these equations with FE results is illustrated in Fig. 8.9. It can be seen that all proposed analytical equations obtained an R^2>0.98, indicating a good performance of the equations against FE results.

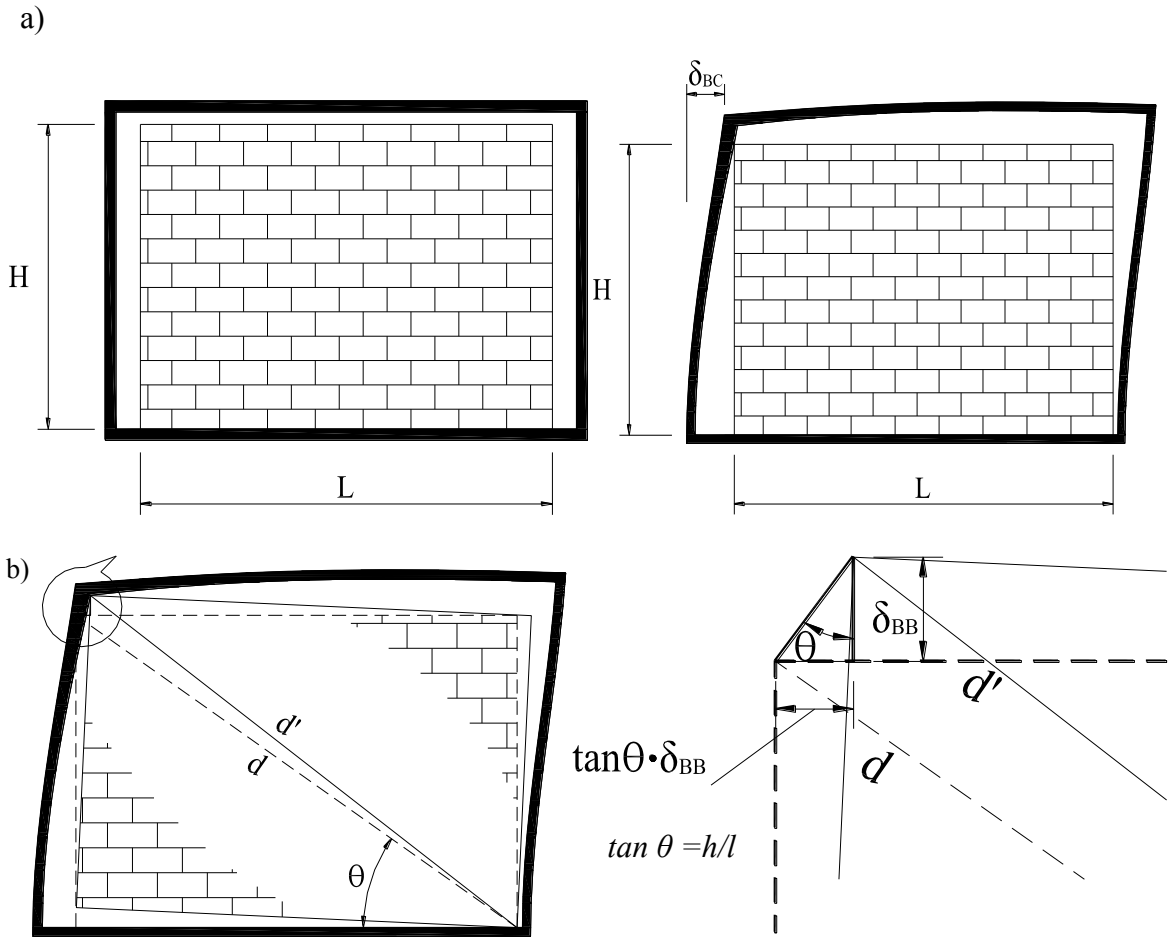

Fig. 8.10: The calculation of the lateral displacement required to close gaps a) side gaps, b) top gaps

8.3.8 Application of Reduction Factors and Limitations

These reduction factors (Eqn (8.2a)-(8.2c)), developed based on normalized stiffness and strength trend, and are intended to be used to modify the stiffness and strength of the infills without gaps. Although the study suggests that some yielding in frame members does not adversely impact the infill strength, it is recommended that the gap size be kept within the elastic limit of the frame deformation to ensure the frame integrity in the event of infill failure. It is also noted that while the previous discussion was presented for aspect ratio equal to 1.0, other aspect ratios (h/l =1.4 and 0.78) were also investigated and the results

were included in the development of the reduction factors. It can then be reasonably assumed that the proposed reduction factor equations are also valid for other aspect ratios. It is noted that these equations were developed for infills bounded by steel frames. For other bounding frame materials, it is believed that the general trend presented is still valid while the set of equations may not be directly applicable.

Chapter 9 Conclusions

9.1 Summary

This research was conducted to investigate the in-plane behaviour of concrete masonry infills bounded by steel frames using the finite element modeling technique. The thesis is divided into two sections. The first section is dedicated to a comparative study including a summarization and compilation of existing experimental results on the in-plane stiffness and strength of masonry infilled frames in their specific infill and frame material categories, and a performance assessment of several analytical methods and standard design equations based on these results. The second section of the thesis focuses on the finite element modeling and subsequent parametric studies using the model. To this end, two finite element models were developed where the Model I adopted the self-defined joint elements to simulate the mortar effect between masonry units whereas the Model II implemented the cohesive zone interface contact pairs for simulation of the mortar effect. Both models were validated with experimental results obtained from the available literature. Following the validation of the models, a series of studies was conducted to investigate the effect of several influential parameters on the in-plane behaviour and strength of masonry infills and to propose analytical models for stiffness and strength prediction. These parameters included the material and geometric properties of the infilled system; the infill opening; the presence of vertical loading; and the frame-to-infill interfacial gaps.

Conclusions drawn from the results of this research are summarized in the following sections organized according to each parametric study.

9.2 Section 1: Comparative Study

1. The comparison analysis shows that the Canadian masonry standard CSA S304.1 markedly overestimates the stiffness to 2 to 2.5 times the test results for all infill materials investigated and for both the steel and concrete bounding frames. A reduced strut width by a factor of 0.5 shows a much-improved estimate of stiffness. Contrary to CSA S304.1, the MSJC 2013, on average, underestimates the stiffness by approximately 40% for all results considered.
2. In the case of strength comparison, both the S304.1 and MSJC 2013 provide a conservative estimate of strength for steel infilled frames with S304.1 showing a better test-to-design average. In the case of infills bounded by concrete frames, the current strength equations in both standards result in high COVs in test-to-design ratios. The validity of the standard equations for infilled concrete frame needs further investigation.
3. The comparison with multiple analytical methods shows that there is no one method that performs well for all infill specimens in predicting stiffness or strength. The existing analytical strength method that provides the best comparison with the stiffness or strength of test results for each infill type or frame type was identified.

9.3 Section 2: Parametric Study

9.3.1 Infill Opening

1. An increase in the opening area results in a reduction in both stiffness and strength of infills. However, the rate of this reduction is associated with the location of the opening. Openings offsets away from the loaded side have lesser reduction effect than openings located toward the loaded side. The reduction factor R_F has an approximately linear relationship with e_c/L and a parabolic relationship with opening-to-infill area ratio.
2. Of the material and geometric properties studied, the variation in opening aspect ratios and several key masonry infill material properties do not have a significant effect on the reduction factor while the variation in infill-to-frame stiffness ratio shows a noticeable impact on the reduction factor.
3. The proposed equations for calculating the reduction factor consider a wide range of masonry infill properties and frame-to-infill stiffness ratios, and they compare well with test results of infills bounded by steel frames. In comparison with other existing methods, the proposed equations provide slightly conservative and overall the best performance in both stiffness and strength predictions.

9.3.2 Material and Geometric Properties of Infill and Frame

1. As the infill aspect ratio increases, the cracking stiffness and infill strength decrease and the rate of this decrease increases as aspect ratio increases. The change in aspect ratio affects infills with different compressive strength almost equally in terms of the cracking stiffness and infill strength.

2. The stiffness of the infill is affected by both grouting extent and configuration while the strength of the infill is primarily influenced by grouting configuration.
3. The vertical reinforcement is ineffective in strengthening the infills. By comparison, joint reinforcement shows a greater benefit in strengthening infills especially when it is anchored to the bounding frame.
4. Column stiffness has a greater effect on the behaviour of the infilled system than beam stiffness. The stiffness and strength of infills alone are less affected by the change in frame stiffness.
5. Comparison between the design values and FE results shows that CSA S304-14 achieves good agreement with FE results and is able to reflect the effects of various parameters with reasonable accuracy. However, the CSA S304-14 tends to overestimate the beam-to-infill contact length and thus the infill stiffness and strength for infills with low aspect ratios and infills bounded by strong beams. The MSJC 2013 significantly underestimates the cracking stiffness and infill strength in most cases. This is attributed to the fact that MSJC 2013 method is unable to take into account of the effect of frame stiffness and infill aspect ratios in the diagonal strut width calculation.

9.3.3 Vertical Load

1. When applied as a UDL on the frame beam, the presence of a vertical load, up to a certain level, results in an increase in the stiffness and the strength of the infills. And beyond that level, the benefit of vertical load begins to diminish. Defined as the optimal

load level, it is found to be dependent on the infill aspect ratio, infill strength, and bounding frame stiffness.

2. When the vertical load is applied on columns, the cracking stiffness of infilled system is increased with an increase in the vertical load level. However, the strength of the infill shows a decrease. When the vertical load is applied in a 50-50 manner on both the frame beam and columns, infilled systems show almost linearly increasing cracking stiffness and strength as the load level increases.
3. A set of equations for calculating modification factor M_F for vertical load effect is proposed for the vertical load applied to the frame beam case. The equations are shown to produce results in good agreement with FE values for a wide range of vertical load levels. The development of M_F also considered the effect of aspect ratio and material strength of infills as well as frame stiffness.

9.3.4 Interfacial Gaps

1. For all specimens considered, an increase in gap size results in a reduction in infill secant cracking stiffness and tangent cracking stiffness, as well as in the infill strength. The degree of reduction is dependent on the gap location and the bounding frame stiffness. When comparing beam-infill and column-infill gap scenarios for a given total gap size, the beam-infill gap results in the greater reduction in both the stiffness and strength than the column-infill gap scenario. The reduction in stiffness or strength for the full separation gap is not simply the addition of the reduction of the cases of beam-infill and column-infill gaps. It is greater than the summation of reduction in the

latter two cases.

2. For varying bounding frame stiffness, results show that gap(s) has less effects on infills bounded by weak frames than on those bounded by stronger frames. In the case of a beam-infill gap on infills bounded by strong frames, sliding shear failure was observed which resulted in a significant reduction in infill strength.
3. For the friction coefficient, results show that increasing friction coefficient from 0.4 to 0.7 has no significant effect on the column-infill gap, regardless of whether the gap is located on both column-infill interfaces or only on one side. However, when friction coefficient = 1.0, the infill stiffness and strength are noticeably affected by the column-infill gap location.
4. The examination of MSJC 2013 shows that in the case of infill strength, up to a total gap size of 10 mm, the 0.5 reduction factor provides a markedly conservative estimate for cases with normal and weak bounding frames. For strong bounding frames, however, the 0.5 reduction factor is adequate and even slightly on the high side. In the case of tangent cracking stiffness, the reduction factor provides marked underestimates for a gap size up to 10 mm for all bounding frame cases.
5. A set of equations was proposed for calculating reduction factors for stiffness and strength over a wide range of gap size and locations and they are shown to achieve a good agreement with FE results.

9.4 Recommendations for Future Research

While this research has contributed to the advancement of knowledge of the in-plane behaviour of masonry infills bounded by steel frames, it is recognized that some aspects of the behaviour need further investigations. The following is recommended for future research:

1. A detailed 3-D micro-modelling technique should be further studied and implemented. With the advancement of computer technology, it is expected that a 3-D model may become more cost effective as an analysis tool. In that case, the actual geometry of the masonry units, grouting, and reinforcement can be more accurately simulated.
2. The proposed equations for openings were developed based on FE results and calibrated with experimental results. They are intended for window openings. Further validation of the analytical model for door openings with high aspect ratios is needed.
3. It is also noted that this study used a single frame configuration, the applicability of conclusions and proposed analytical equations on multi-storey, multi-bay infilled steel frames needs further investigation. Moreover, the proposed equations are only intended for steel bounding frames, their applicability to reinforced concrete bounding frames needs validation. It is recommended as a supplement to this research, a study on the masonry infilled RC frames should be carried out.
4. The current model was developed to simulate the static loading. For evaluating the seismic behaviour of masonry infills, the development of material models capable of

simulating the cumulative damage and cracks development in the masonry infill wall and the bounding frame is needed.

5. Due to the lack of experimental data, the proposed analytical equations in Chapter 5, 7, 8 are not calibrated or verified against experimental results. Further experimental tests are required to verify the efficacy of these equations. It is recommended that experimental tests on the following aspects be conducted: tests on infills with large ($A_o/A_p > 0.2$) and eccentric openings are needed to examined the efficacy of Eqn (5.14-5.16) in dealing with large openings and openings with eccentricities; tests on infills with openings that bounded by frames with various stiffnesses are needed to examine the lower bound envelope proposed in Section5.4.5; tests on steel infilled frames with vertical load applied as an UDL or multiple point loads on the top beam are needed to examine the efficacy of Eqn (7.3-7. 6); tests on infills with effective gaps size greater than 20 mm are needed to examine the capability of equation Eqn (8.2) in dealing with large gap(s); and tests on infills bounded by strong frames with a gap at top beam-infill interface are needed to verify the theory that sliding shear failure mode will be initiated by the gap in strong frame bounded infills.

References

Al-Chaar, G., Lamb, G. E., & Issa, M. A. (2003). Effect of openings on structural performance of unreinforced masonry infilled frames. *American Concrete Institute, 211*, 247-261. doi:10.14359/12593

Al-Chaar, G., & Mehrabi, A. (2008). *Constitutive models for nonlinear finite element analysis of masonry prisms and infill walls.* (No. Report ERDC/CERL TR-08-19).US Army Corps of Engineers.

Al-Chaar, G. K. (1998). *Nonductile behavior of reinforced concrete frames with masonry infill panels subjected to in-plane loading.* (Ph.D.). Available from ProQuest Dissertations & Theses Global. (304492653). Retrieved from http://search.proquest.com.ezproxy.library.dal.ca/docview/304492653?accountid=10406

Amato, G., Cavaleri, L., Fossetti, M., & and Papia, M. (2008). Infilled frames: Influence of vertical load on the equivalent diagonal strut model. *The 14th World Conference on Earthquake Engineering (WCEE),* Beijing, China.

Amos, K. A. (1985). *The shear strength of masonry infilled steel frames*. (M.Sc.E.). Available from ProQuest Dissertations & Theses Global. (303433817). Retrieved from http://search.proquest.com.ezproxy.library.dal.ca/docview/303433817?accountid=10406

Angel, R. E. (1994). *Behavior of reinforced concrete frames with masonry infill walls*. (Ph.D.). Available from ProQuest Dissertations & Theses Global. (304117403). Retrieved from http://search.proquest.com.ezproxy.library.dal.ca/docview/304117403?accountid=10406

Asteris, P. G., Cavaleri, L., Di Trapani, F., & Sarhosis, V. A. (2015). A macro-modelling approach for the analysis of infilled frame structures considering the effects of openings and vertical loads. *Structure and Infrastructure Engineering,* (5), 551. doi:10.1080/15732479.2015.1030761

Asteris, P. G., Giannopoulos, I. P., & Chrysostomou, C. Z. (2012). Modeling of infilled frames with openings. *The Open Construction and Building Technology Journal, 6*, 81-91. doi:10.2174/1874836801206010081]

Barua, H. K., & Mallick, S. K. (1976). Behavior of mortar infilled steel frames under lateral load. *Building and Environment, 12*(4), 263-272. doi:10.1016/0360-1323(77)90028-2

Campione, G., Cavaleri, L., Macaluso, G., Amato, G., & Di Trapani, F. (2015). Evaluation

of infilled frames: An updated in-plane-stiffness macro-model considering the effects of vertical loads. *Bulletin of Earthquake Engineering, 13*(8), 2265-2281. doi:10.1007/s10518-014-9714-x

CAN/CSA. (2004). *Design of masonry structures (S304.1-04)*. ON, Canada: Canadian Standard Association.

CAN/CSA. (2014). *Design of masonry structures (S304-14)*. ON, Canada: Canadian Standard Association.

CAN/CSA. (2014). *Design of steel structures (S16-14)*. ON, Canada: Canadian Standard Association.

Cavaleri, L., Fossetti, M., & Papia, M. (2004). Effect of vertical loads on lateral response of infilled frames. *Proceedings 13th World Conference on Earthquake Engineering,* Vancouver, Canada. 2931.

Chen, X., & Liu, Y. (2015). Numerical study of in-plane behaviour and strength of concrete masonry infills with openings. *Engineering Structures, 82*, 226-235. doi:http://dx.doi.org/10.1016/j.engstruct.2014.10.042

Chen, X., & Liu, Y. (2016). A finite element study of the effect of vertical loading on the in-plane behavior of concrete masonry infills bounded by steel frames. *Engineering Structures, 117*, 118-129. doi:http://dx.doi.org/10.1016/j.engstruct.2016.03.010

Chrysostomou, C. Z., Gergely, P., & Abel, J. F. (2002). A six-strut model for nonlinear dynamic analysis of steel infilled frames. *International Journal of Structural Stability and Dynamics, 02*(03), 335-353. doi:10.1142/S0219455402000567

Commission of the European Communities. (1988). *Eurocode 8: Structures in seismic regions, design, part 1, general and building.* Luxembourg: EUROPEAN COMMITTEE FOR STANDARDIZATION.

Commission of the European Communities. (2004). *Design of structures for earthquake resistance -part 1: General rules, seismic actions and rules for buildings.* Brussels: EUROPEAN COMMITTEE FOR STANDARDIZATION.

Commission of the European Communities. (2005). *Eurocode 6: Design of masonry structures -part 1-1: General rules for reinforced and unreinforced masonry structures*. Brussels: EUROPEAN COMMITTEE FOR STANDARDIZATION.

Crisafulli, F. (1997). *Seismic behaviour of reinforced concrete structures with masonry infills.* (Ph.D.). University of Canterbury, Christchurch, New Zealand.

Dawe, J. L., Liu, Y., & Seah, C. K. (2001). A parametric study of masonry infilled steel frames. *Canadian Journal of Civil Engineering, 28*(1), 149-157. Retrieved from http://search.proquest.com.ezproxy.library.dal.ca/docview/213329999?accountid=10

406

Dawe, J. L., & Seah, C. K. (1989). Behaviour of masonry infilled steel frames. *Canadian Journal of Civil Engineering, 16*(6), 865-876. doi:10.1139/l89-129

Durrani, A. J., & Luo, Y. H. (1994). *Seismic retrofit of flat-slab buildings with masonry infills.* (No. Technical Report NCEER-94-0004, 1-8). San Francisco, California. National Center for Earthquake Engineering Research.

El-Dakhakhni, W., Elgaaly, M., & Hamid, A. (2003). Three-strut model for concrete masonry-infilled steel frames. *Journal of Structural Engineering, 129*(2), 177-185. doi:10.1061/(ASCE)0733-9445(2003)129:2(177)

El-Dakhakhni, W. W. (2002). *Experimental and analytical seismic evaluation of concrete masonry -infilled steel frames retrofitted using GFRP laminates* (Ph.D.). Drexel University, Philadelphia, United States. Available from ProQuest Dissertations & Theses Global. (304803971). Retrieved from http://search.proquest.com.ezproxy.library.dal.ca/docview/304803971?accountid=10406

Federal Emergency Management Agency. (1997). *NEHRP guidelines for the seismic rehabilitation of buildings (FEMA-273).* Washington, D.C, United States. Building Seismic Safety Council (BSSC).

Federal Emergency Management Agency. (1998). *Evaluation of earthquake damaged concrete and masonry wall buildings (FEMA-306).* Redwood, California, United States. Applied Technology Council (ATC).

Federal Emergency Management Agency. (2000). *Prestandard and commentary for the seismic rehabilitation of buildings (FEMA-356).* Washington, D.C, United States. Building Seismic Safety Council (BSSC).

Fiorato, A. E., Sozen, M. A., & Gamble, W. L. (1970). *An investigation of the interaction of reinforced concrete frames with masonry filler walls.* (Technical Report No. Civil Engineering Studies SRS- 370).University of Illinois Engineering Experiment Station. College of Engineering. University of Illinois at Urbana-Champaign.

Flanagan, R. D. (1994). *Behavior of structural clay tile infilled frames* (Ph.D.). Available from ProQuest Dissertations & Theses Global. (304121732). Retrieved from http://search.proquest.com.ezproxy.library.dal.ca/docview/304121732?accountid=10406

Flanagan, R., & Bennett, R. (1999). In-plane behavior of structural clay tile infilled frames. *Journal of Structural Engineering, 125*(6), 590-599. doi:10.1061/(ASCE)0733-9445(1999)125:6(590)

Flanagan, R., & Bennett, R. (2001). In-plane analysis of masonry infill materials. *Practice*

Periodical on Structural Design and Construction, 6(4), 176-182. doi:10.1061/(ASCE)1084-0680(2001)6:4(176)

Focardi, F., & Manzini, E. (1984). Diagonal tension tests on reinforced and non-reinforced brick panels. *Proceeding of 8th World Conference on Earthquake Engineering.* San Francisco, California, USA. *, VI* 839-846.

Hamburger, R. O., & Chakradeo, A. S. (1993). Methodology for seismic-capacity evaluation of steel-frame buildings with infill unreinforced masonry. *Proc., National Earthquake Conf,* Central U.S. Earthquake Consortium, Memphis, TN., *2* 173-191.

Henderson, R. C. (1994). *Experimental and analytical investigation of out-of-plane and in-plane seismic drift in un-reinforced masonry infilled frames* (Ph.D.). The University of Tennessee, Knoxville.

Hendry, A. W. (Ed.). (1981). *Structural brickwork*. London: Macmillan press.

Hendry, A. W. and Liauw, T. C. (1991). Tests on steel frames with reinforced masonry infillings. *Proceedings of the 3rd international masonry conference*, 1991. 108-114.

Holmes, M. (1961). Steel frames with brickwork and concrete infilling. *Proceedings of the Institution of Civil Engineers, 19*(4), 473-478. doi:10.1680/iicep.1961.11305

Kadir, M. R. A. (1974). *The structural behavior of masonry infill panels in framed structures* (Ph.D). University of Edinburgh, Edinburgh, Scotland, UK.

Kakaletsis, D. J., & Karayannis, C. G. (2008). Influence of masonry strength and openings on infilled R/C frames under cycling loading. *Journal of Earthquake Engineering, 12*(2), 197-221. doi:10.1080/13632460701299138

King, G. K. W., & Pandey, P. C. (1978). The analysis of infilled frames using finite elements. *Proceedings of the Institution of Civil Engineers, 65*(4), 749-760. doi:10.1680/iicep.1978.2707

Liauw, T. C., & Kwan, K. H. (1983). Plastic theory of non integral infilled frames. *Proceedings of the Institution of Civil Engineers, 75*(3), 379-396. doi:10.1680/iicep.1983.1437

Liauw, T., & Kwan, K. (1985). Unified plastic analysis for infilled frames. *Journal of Structural Engineering, 111*(7), 1427-1448. doi:10.1061/(ASCE)0733-9445(1985)111:7(1427)

Liu, Y., & Manesh, P. (2013). Concrete masonry infilled steel frames subjected to combined in-plane lateral and axial loading – an experimental study. *Engineering Structures, 52*, 331-339. doi:http://dx.doi.org/10.1016/j.engstruct.2013.02.038

Liu, Y., & Soon, S. (2012). Experimental study of concrete masonry infills bounded by steel frames. *Canadian Journal of Civil Engineering, 39*(2), 180-190. doi:10.1139/l11-

Lotfi, H., & Shing, P. (1994). Interface model applied to fracture of masonry structures. *Journal of Structural Engineering, 120*(1), 63-80. doi:10.1061/(ASCE)0733-9445(1994)120:1(63)

Lotfi, H. R., & Shing, P. B. (1991). An appraisal of smeared crack models for masonry shear wall analysis. *Computers & Structures, 41*(3), 413-425. doi:http://dx.doi.org/10.1016/0045-7949(91)90134-8

Lourenço, P. B., & Rots, J. G. (1997). A solution for the macro-modelling of masonry structures. *Proceedings of the 11th International Brick/Block Masonry Conference,* Tongji University, Shanghai, China. 1239-1249.

Lourenço, P. B. (1994). *Analysis of masonry structures with interface elements: Theory and applications*. (No. report no.03-21-22-0-01). Delft, Netherlands: Delft University of Technology. . (TNO Building and Construction Research Report)

Lourenço, P. B. (1995). *An orthotropic continuum model for the analysis of masonry structures*. (No. report no. 03-21-1-31-27). Delft, Netherlands: Delft University of Technology. . (TNO Building and Construction Research Report)

Lourenço, P. B. (1996). *Computational strategies for masonry structures* (Ph.D.).

Mainstone, R. J., Weeks, G. A. Building Research Station (Great Britain) (1972). *The influence of a bounding frame on the racking stiffness and strengths of brick walls*. Garston, Eng.: Building Research Station.

Mainstone, R. J. (1971). Summary of paper 7360. on the stiffness and strengths of infilled frames. *Proceedings of the Institution of Civil Engineers, 49*(2), 230. doi:10.1680/iicep.1971.6267

Mallick, D. V., & Garge, R. P. (1971). Effect of openings on the lateral stiffness of infilled frames. *Proceedings of the Institution of Civil Engineers, 49*(2), 193-209. doi:10.1680/iicep.1971.6263

Manos, G. C., Soulis, V. J., & Thauampteh, J. (2012). The behavior of masonry assemblages and masonry-infilled R/C frames subjected to combined vertical and cyclic horizontal seismic-type loading. *Advances in Engineering Software, 45*(1), 213-231. doi:http://dx.doi.org/10.1016/j.advengsoft.2011.10.017

Masonry Standards Joint Committee. (2013). *Building code requirements and specification for masonry structures*. ACI 530-13/ASCE 5-13/TMS 402-13, American Concrete Institute, the American Society of Civil Engineers and the Masonry Society Portland, United States: Ringgold Inc. Retrieved from http://search.proquest.com.ezproxy.library.dal.ca/docview/894457499?accountid=10406

McBride, R. T. (1984). *The behavior of masonry infilled steel frames subjected to racking* (M.Sc.E.). Available from ProQuest Dissertations & Theses Global. (303346105). Retrieved from http://search.proquest.com/docview/303346105?accountid=10406

Mehrabi, A., Benson Shing, P., Schuller, M., & Noland, J. (1996). Experimental evaluation of masonry-infilled RC frames. *Journal of Structural Engineering, 122*(3), 228-237. doi:10.1061/(ASCE)0733-9445(1996)122:3(228)

Mehrabi, A., & Shing, P. (1997). Finite element modeling of masonry-infilled RC frames. *Journal of Structural Engineering, 123*(5), 604-613. doi:10.1061/(ASCE)0733-9445(1997)123:5(604)

Moghaddam, H. A., & Dowling, P. J. (1987). *The state of the art in infilled frames.* (No. Rep. No. 87-2). London, England.: Imperial College of Science and Technology, Civil Engineering Dept. . (ESEE Res)

Mohammadi, M., & Nikfar, F. (2013). Strength and stiffness of masonry-infilled frames with central openings based on experimental results. *Journal of Structural Engineering, 139*(6), 974-984. doi:10.1061/(ASCE)ST.1943-541X.0000717

Mondal, G., & Jain, S. K. (2008). Lateral stiffness of masonry infilled reinforced concrete (RC) frames with central opening. *Earthquake Spectra, 24*(3), 701-723. doi:0.1193/1.2942376

Mosalam, K., White, R., & Gergely, P. (1997). Static response of infilled frames using quasi-static experimentation. *Journal of Structural Engineering, 123*(11), 1462-1469. doi:10.1061/(ASCE)0733-9445(1997)123:11(1462)

Nazief, M. A. (2014). *Finite element characterization of the behaviour of masonry infill shear walls with and without openings* (Ph.D.). University of Alberta, Alberta, Canada

New Zealand Society for Earthquake Engineering. (June 2006). *Assessment and improvement of the structural performance of buildings in earthquakes* New Zealand Society for Civil Engineering.

Ng'andu, B. M. (2006). *Bracing steel frames with calcium silicate element walls* (Ph.D.). Available from ProQuest Dissertations & Theses Global. (304959494). Retrieved from http://search.proquest.com/docview/304959494?accountid=10406

Page, A. W. (1979). a non-linear analysis of the composite action of masonry walls on beams. *Proceedings of the Institution of Civil Engineers, 67*(1), 93-110. doi:10.1680/iicep.1979.2319

Papia, M., Cavaleri, L., & Fossetti, M. (2003). Infilled frames: Developments in the evaluation of the stiffening effect of infills. *Structural Engineering and Mechanics, 16*(6), 675-693. doi:http://dx.doi.org/10.12989/sem.2003.16.6.675

Parducci, A., & Mezzi, M. (1980). Repeated horizontal displacement of infilled frames having different stiffness and connection systems – experimental analysis. *Proceeding of 7th World Conference on Earthquake Engineering,* California, USA. *, 7* 193-196.

Polyakov, S. V. (1963). *Masonry in framed buildings (an investigation into the strength and stiffness of masonry infilling).* [Gosudarstvennoe izdatel'stvo Literatury po stroitel'stvu iarkhitekture] (G. L. Cairns Trans.). Boston, Yorkshire, England: National Lending Library for Science and Technology.

Priestley, M. J. N., and Elder, D. M. (1983). Stress-strain curves for unconfined and confined concrete masonry. *American Concrete Institute*, 80(3), 192-201.doi: 10.14359/10834

Richardson, J. (1986). *The behaviour of masonry infilled steel frames* (M.Sc.E.). Available from ProQuest Dissertations & Theses Global. (303570768). Retrieved from http://search.proquest.com/docview/303570768?accountid=10406

Riddington, J., & Stafford-Smith, B. (1977). Analysis of infilled frames subject to racking with design recommendations. *Structure Engineering, 55*(6), 263-268.

Riddington, J. R. (1984). The influence of intial gaps on infilled frame behaviour. *Proceedings of the Institution of Civil Engineers, 77*(3), 295-310. doi:10.1680/iicep.1984.1185

Saneinejad, A., & Hobbs, B. (1995). Inelastic design of infilled frames. *Journal of Structural Engineering, 121*(4), 634-650. doi:10.1061/(ASCE)0733-9445(1995)121:4(634)

Schneider, S., Zagers, B., & Abrams, D. (1998). Lateral strength of steel frames with masonry infills having large openings. *Journal of Structural Engineering, 124*(8), 896-904. doi:10.1061/(ASCE)0733-9445(1998)124:8(896)

Seah, C. K. (1999). *A universal approach for the analysis and design of masonry infilled frame structures* (Ph.D.). Available from ProQuest Dissertations & Theses Global. (304572731). Retrieved from http://search.proquest.com/docview/304572731?accountid=10406

Stafford-Smith, B. (1962). Lateral stiffness of infilled frames. *Journal of the Structural Division, ASCE, 88*(6), 183-199.

Stafford-Smith, B. (1966). Behaviour of square infilled frames. *Journal of the Structural Division, ASCE, 92*(1), 381-404.

Stafford-Smith, B. (1968). Model test results of vertical and horizontal loading of infilled frames. *Journal Proceedings, 65*(8) doi:10.14359/7499

Stafford-Smith, B., & Carter, C. (1969). a method of analysis for infilled frames. *Proceedings of the Institution of Civil Engineers, 44*(1), 31-48.

doi:10.1680/iicep.1969.7290

Stafford-Smith, B., & Coull, A. (Eds.). (1991). *Tall building structures: Analysis and design.* New York: Wiley-Interscience.

Stavridis, A., & Shing, P. (2010). Finite-element modeling of nonlinear behavior of masonry-infilled RC frames. *Journal of Structural Engineering, 136*(3), 285-296. doi:10.1061/(ASCE)ST.1943-541X.116

Stylianidis, K.C. (2012). Experimental Investigation of Masonry Infilled R/C Frames. *The Open Construction and Building Technology Journal*, 6, (Suppl 1-M13) 194-212. doi: 10.2174/1874836801206010194]

Tasnimi, A. A., & Mohebkhah, A. (2011). Investigation on the behavior of brick-infilled steel frames with openings, experimental and analytical approaches. *Engineering Structures, 33*(3), 968-980. doi:http://dx.doi.org/10.1016/j.engstruct.2010.12.018

Thiruvengadam, V. (1985). On the natural frequencies of infilled frames. *Earthquake Engineering & Structural Dynamics, 13*(3), 401-419. doi:10.1002/eqe.4290130310

Tucker, C. J. (2007). *Predicting the in-plane capacity of masonry infilled frames* (Ph.D.). Available from ProQuest Dissertations & Theses Global. (304766338). Retrieved from http://search.proquest.com/docview/304766338?accountid=10406

Vasconcelos, G. &, Lourenço, P.B. (2009). Experimental characterization of stone masonry in shear and compression. *Construction and Building Materials*, 23, 3337 – 3345. doi:10.1016/j.conbuildmat.2009.06.045

Wood, R. H. (1978). Plasticity, composite action and collapse design of unreinforced shear wall panels in frames. *Proceedings of the Institution of Civil Engineers, 65*(2), 381-411. doi:10.1680/iicep.1978.2952

Yong, T. C. (1984). *Shear strength of masonry infilled panels in steel frames* (M.Sc.E.). Available from ProQuest Dissertations & Theses Global. (303344572). Retrieved from http://search.proquest.com/docview/303344572?accountid=10406

Zarnic, R., & Tomazevic, M. (1984). The behaviour of masonry infilled reinforced concrete frames subjected to seismic loading. *Proceeding of 8th World Conference on Earthquake Engineering,* San Francisco, California, USA. *, VI* 863-870.

Zucchini, A., & Lourenço, P. B. (2002). A micro-mechanical model for the homogenisation of masonry. *International Journal of Solids and Structures, 39*(12), 3233-3255. doi:http://dx.doi.org/10.1016/S0020-7683(02)00230-5

Zucchini, A., & Lourenço, P. B. (2004). A coupled homogenisation–damage model for masonry cracking. *Computers & Structures, 82*(11–12), 917-929. doi:http://dx.doi.org/10.1016/j.compstruc.2004.02.020

Zucchini, A., & Lourenço, P. B. (2007). Mechanics of masonry in compression: Results from a homogenisation approach. *Computers & Structures, 85*(3–4), 193-204. doi:http://dx.doi.org/10.1016/j.compstruc.2006.08.054

APPENDIX A Copyright Permission

September 29, 2016

Engineering Structures:

I am preparing my PhD thesis for submission to the Faculty of Graduate Studies at Dalhousie University, Halifax, Nova Scotia, Canada. I am seeking your permission to include a manuscript version of the following paper(s) as a chapter in the thesis:

Numerical study of in-plane behaviour and strength of concrete masonry infills with openings
A finite element study of the effect of vertical loading on the in-plane behavior of concrete masonry infills bounded by steel frames

Canadian graduate theses are reproduced by the Library and Archives of Canada (formerly National Library of Canada) through a non-exclusive, world-wide license to reproduce, loan, distribute, or sell theses. I am also seeking your permission for the material described above to be reproduced and distributed by the LAC(NLC). Further details about the LAC(NLC) thesis program are available on the LAC(NLC) website (www.nlc-bnc.ca).

Full publication details and a copy of this permission letter will be included in the thesis.

Yours sincerely,

Xi Chen

Permission is granted for:

a) the inclusion of the material described above in your thesis.

b) for the material described above to be included in the copy of your thesis that is sent to the Library and Archives of Canada (formerly National Library of Canada) for reproduction and distribution.

Name: Xi Chen Title: _____

Signature: _____ Date: September 29, 2016

RightsLink | Copyright Clearance Center

Thank You For Your Order!

Dear Xi Chen,

Thank you for placing your order through Copyright Clearance Center's RightsLink service. Elsevier has partnered with RightsLink to license its content. This notice is a confirmation that your order was successful.

Your order details and publisher terms and conditions are available by clicking the link below:
http://s100.copyright.com/CustomerAdmin/PLF.jsp?ref=96e6e6ee-1ad7-4154-9ae0-2f449bc205e3

Order Details
Licensee: Xi Chen
License Date: Oct 3, 2016
License Number: 3961390409062
Publication: Engineering Structures
Title: Numerical study of in-plane behaviour and strength of concrete masonry infills with openings
Type Of Use: reuse in a thesis/dissertation
Total: 0.00 CAD

To access your account, please visit https://myaccount.copyright.com.

Please note: Online payments are charged immediately after order confirmation; invoices are issued daily and are payable immediately upon receipt.

To ensure that we are continuously improving our services, please take a moment to complete our customer satisfaction survey.

B.1:v4.2

+1-855-239-3415 / Tel: +1-978-646-2777
customercare@copyright.com
http://www.copyright.com

RightsLink | Copyright Clearance Center

Thank You For Your Order!

Dear Xi Chen,

Thank you for placing your order through Copyright Clearance Center's RightsLink service. Elsevier has partnered with RightsLink to license its content. This notice is a confirmation that your order was successful.

Your order details and publisher terms and conditions are available by clicking the link below:
http://s100.copyright.com/CustomerAdmin/PLF.jsp?ref=058e0391-471d-4902-80ce-86bd92c5f3b9

Order Details
Licensee: Xi Chen
License Date: Oct 3, 2016
License Number: 3961390292836
Publication: Engineering Structures
Title: A finite element study of the effect of vertical loading on the in-plane behavior of concrete masonry infills bounded by steel frames
Type Of Use: reuse in a thesis/dissertation
Total: 0.00 USD

To access your account, please visit https://myaccount.copyright.com.

Please note: Online payments are charged immediately after order confirmation; invoices are issued daily and are payable immediately upon receipt.

To ensure that we are continuously improving our services, please take a moment to complete our customer satisfaction survey.

B.1:v4.2

+1-855-239-3415 / Tel: +1-978-646-2777
customercare@copyright.com
http://www.copyright.com

ELSEVIER LICENSE
TERMS AND CONDITIONS

Oct 04, 2016

This Agreement between Xi Chen ("You") and Elsevier ("Elsevier") consists of your license details and the terms and conditions provided by Elsevier and Copyright Clearance Center.

License Number	3961390409062
License date	Oct 03, 2016
Licensed Content Publisher	Elsevier
Licensed Content Publication	Engineering Structures
Licensed Content Title	Numerical study of in-plane behaviour and strength of concrete masonry infills with openings
Licensed Content Author	Xi Chen,Yi Liu
Licensed Content Date	1 January 2015
Licensed Content Volume Number	82
Licensed Content Issue Number	n/a
Licensed Content Pages	10
Start Page	226
End Page	235
Type of Use	reuse in a thesis/dissertation
Intended publisher of new work	other
Portion	full article
Format	both print and electronic
Are you the author of this Elsevier article?	Yes
Will you be translating?	No
Order reference number	
Title of your thesis/dissertation	NUMERICAL STUDY OF THE IN-PLANE BEHAVIOUR OF CONCRETE MASONRY INFILLS BOUNDED BY STEEL FRAMES
Expected completion date	Oct 2016
Estimated size (number of pages)	200
Elsevier VAT number	GB 494 6272 12
Requestor Location	Xi Chen 1094 Wellington Street Apt.1102 Halifax, Nova Scotia, NS B3H2Z9 Canada Attn: Xi Chen
Total	0.00 CAD

Terms and Conditions

INTRODUCTION

1. The publisher for this copyrighted material is Elsevier. By clicking "accept" in connection with completing this licensing transaction, you agree that the following terms and conditions apply to this transaction (along with the Billing and Payment terms and conditions established by Copyright Clearance Center, Inc. ("CCC"), at the time that you opened your Rightslink account and that are available at any time at http://myaccount.copyright.com).

GENERAL TERMS

2. Elsevier hereby grants you permission to reproduce the aforementioned material subject to the terms and conditions indicated.

3. Acknowledgement: If any part of the material to be used (for example, figures) has appeared in our publication with credit or acknowledgement to another source, permission must also be sought from that source. If such permission is not obtained then that material may not be included in your publication/copies. Suitable acknowledgement to the source must be made, either as a footnote or in a reference list at the end of your publication, as follows:

"Reprinted from Publication title, Vol /edition number, Author(s), Title of article / title of chapter, Pages No., Copyright (Year), with permission from Elsevier [OR APPLICABLE SOCIETY COPYRIGHT OWNER]." Also Lancet special credit - "Reprinted from The Lancet, Vol. number, Author(s), Title of article, Pages No., Copyright (Year), with permission from Elsevier."

4. Reproduction of this material is confined to the purpose and/or media for which permission is hereby given.

5. Altering/Modifying Material: Not Permitted. However figures and illustrations may be altered/adapted minimally to serve your work. Any other abbreviations, additions, deletions and/or any other alterations shall be made only with prior written authorization of Elsevier Ltd. (Please contact Elsevier at permissions@elsevier.com)

6. If the permission fee for the requested use of our material is waived in this instance, please be advised that your future requests for Elsevier materials may attract a fee.

7. Reservation of Rights: Publisher reserves all rights not specifically granted in the combination of (i) the license details provided by you and accepted in the course of this licensing transaction, (ii) these terms and conditions and (iii) CCC's Billing and Payment terms and conditions.

8. License Contingent Upon Payment: While you may exercise the rights licensed immediately upon issuance of the license at the end of the licensing process for the transaction, provided that you have disclosed complete and accurate details of your proposed use, no license is finally effective unless and until full payment is received from you (either by publisher or by CCC) as provided in CCC's Billing and Payment terms and conditions. If full payment is not received on a timely basis, then any license preliminarily granted shall be deemed automatically revoked and shall be void as if never granted. Further, in the event that you breach any of these terms and conditions or any of CCC's Billing and Payment terms and conditions, the license is automatically revoked and shall be void as if never granted. Use of materials as described in a revoked license, as well as any use of the materials beyond the scope of an unrevoked license, may constitute copyright infringement and publisher reserves the right to take any and all action to protect its copyright in the materials.

9. Warranties: Publisher makes no representations or warranties with respect to the licensed material.

10. Indemnity: You hereby indemnify and agree to hold harmless publisher and CCC, and their respective officers, directors, employees and agents, from and against any and all claims arising out of your use of the licensed material other than as specifically authorized pursuant to this license.

11. No Transfer of License: This license is personal to you and may not be sublicensed, assigned, or transferred by you to any other person without publisher's written permission.

12. No Amendment Except in Writing: This license may not be amended except in a writing signed by both parties (or, in the case of publisher, by CCC on publisher's behalf).
13. Objection to Contrary Terms: Publisher hereby objects to any terms contained in any purchase order, acknowledgment, check endorsement or other writing prepared by you, which terms are inconsistent with these terms and conditions or CCC's Billing and Payment terms and conditions. These terms and conditions, together with CCC's Billing and Payment terms and conditions (which are incorporated herein), comprise the entire agreement between you and publisher (and CCC) concerning this licensing transaction. In the event of any conflict between your obligations established by these terms and conditions and those established by CCC's Billing and Payment terms and conditions, these terms and conditions shall control.
14. Revocation: Elsevier or Copyright Clearance Center may deny the permissions described in this License at their sole discretion, for any reason or no reason, with a full refund payable to you. Notice of such denial will be made using the contact information provided by you. Failure to receive such notice will not alter or invalidate the denial. In no event will Elsevier or Copyright Clearance Center be responsible or liable for any costs, expenses or damage incurred by you as a result of a denial of your permission request, other than a refund of the amount(s) paid by you to Elsevier and/or Copyright Clearance Center for denied permissions.

LIMITED LICENSE

The following terms and conditions apply only to specific license types:
15. **Translation**: This permission is granted for non-exclusive world **English** rights only unless your license was granted for translation rights. If you licensed translation rights you may only translate this content into the languages you requested. A professional translator must perform all translations and reproduce the content word for word preserving the integrity of the article.
16. **Posting licensed content on any Website**: The following terms and conditions apply as follows: Licensing material from an Elsevier journal: All content posted to the web site must maintain the copyright information line on the bottom of each image; A hyper-text must be included to the Homepage of the journal from which you are licensing at http://www.sciencedirect.com/science/journal/xxxxx or the Elsevier homepage for books at http://www.elsevier.com; Central Storage: This license does not include permission for a scanned version of the material to be stored in a central repository such as that provided by Heron/XanEdu.
Licensing material from an Elsevier book: A hyper-text link must be included to the Elsevier homepage at http://www.elsevier.com . All content posted to the web site must maintain the copyright information line on the bottom of each image.

Posting licensed content on Electronic reserve: In addition to the above the following clauses are applicable: The web site must be password-protected and made available only to bona fide students registered on a relevant course. This permission is granted for 1 year only. You may obtain a new license for future website posting.
17. **For journal authors:** the following clauses are applicable in addition to the above:
Preprints:
A preprint is an author's own write-up of research results and analysis, it has not been peer-reviewed, nor has it had any other value added to it by a publisher (such as formatting, copyright, technical enhancement etc.).
Authors can share their preprints anywhere at any time. Preprints should not be added to or enhanced in any way in order to appear more like, or to substitute for, the final versions of articles however authors can update their preprints on arXiv or RePEc with their Accepted Author Manuscript (see below).
If accepted for publication, we encourage authors to link from the preprint to their formal publication via its DOI. Millions of researchers have access to the formal publications on ScienceDirect, and so links will help users to find, access, cite and use the best available

version. Please note that Cell Press, The Lancet and some society-owned have different preprint policies. Information on these policies is available on the journal homepage.
Accepted Author Manuscripts: An accepted author manuscript is the manuscript of an article that has been accepted for publication and which typically includes author-incorporated changes suggested during submission, peer review and editor-author communications.
Authors can share their accepted author manuscript:

- immediately
  - via their non-commercial person homepage or blog
  - by updating a preprint in arXiv or RePEc with the accepted manuscript
  - via their research institute or institutional repository for internal institutional uses or as part of an invitation-only research collaboration work-group
  - directly by providing copies to their students or to research collaborators for their personal use
  - for private scholarly sharing as part of an invitation-only work group on commercial sites with which Elsevier has an agreement
- after the embargo period
  - via non-commercial hosting platforms such as their institutional repository
  - via commercial sites with which Elsevier has an agreement

In all cases accepted manuscripts should:

- link to the formal publication via its DOI
- bear a CC-BY-NC-ND license - this is easy to do
- if aggregated with other manuscripts, for example in a repository or other site, be shared in alignment with our hosting policy not be added to or enhanced in any way to appear more like, or to substitute for, the published journal article.

Published journal article (JPA): A published journal article (PJA) is the definitive final record of published research that appears or will appear in the journal and embodies all value-adding publishing activities including peer review co-ordination, copy-editing, formatting, (if relevant) pagination and online enrichment.
Policies for sharing publishing journal articles differ for subscription and gold open access articles:
Subscription Articles: If you are an author, please share a link to your article rather than the full-text. Millions of researchers have access to the formal publications on ScienceDirect, and so links will help your users to find, access, cite, and use the best available version.
Theses and dissertations which contain embedded PJAs as part of the formal submission can be posted publicly by the awarding institution with DOI links back to the formal publications on ScienceDirect.
If you are affiliated with a library that subscribes to ScienceDirect you have additional private sharing rights for others' research accessed under that agreement. This includes use for classroom teaching and internal training at the institution (including use in course packs and courseware programs), and inclusion of the article for grant funding purposes.
Gold Open Access Articles: May be shared according to the author-selected end-user license and should contain a CrossMark logo, the end user license, and a DOI link to the formal publication on ScienceDirect.
Please refer to Elsevier's posting policy for further information.
18. **For book authors** the following clauses are applicable in addition to the above:
Authors are permitted to place a brief summary of their work online only. You are not allowed to download and post the published electronic version of your chapter, nor may you scan the printed edition to create an electronic version. **Posting to a repository:** Authors are permitted to post a summary of their chapter only in their institution's repository.

19. **Thesis/Dissertation**: If your license is for use in a thesis/dissertation your thesis may be submitted to your institution in either print or electronic form. Should your thesis be published commercially, please reapply for permission. These requirements include permission for the Library and Archives of Canada to supply single copies, on demand, of the complete thesis and include permission for Proquest/UMI to supply single copies, on demand, of the complete thesis. Should your thesis be published commercially, please reapply for permission. Theses and dissertations which contain embedded PJAs as part of the formal submission can be posted publicly by the awarding institution with DOI links back to the formal publications on ScienceDirect.

Elsevier Open Access Terms and Conditions

You can publish open access with Elsevier in hundreds of open access journals or in nearly 2000 established subscription journals that support open access publishing. Permitted third party re-use of these open access articles is defined by the author's choice of Creative Commons user license. See our open access license policy for more information.

Terms & Conditions applicable to all Open Access articles published with Elsevier:

Any reuse of the article must not represent the author as endorsing the adaptation of the article nor should the article be modified in such a way as to damage the author's honour or reputation. If any changes have been made, such changes must be clearly indicated.

The author(s) must be appropriately credited and we ask that you include the end user license and a DOI link to the formal publication on ScienceDirect.

If any part of the material to be used (for example, figures) has appeared in our publication with credit or acknowledgement to another source it is the responsibility of the user to ensure their reuse complies with the terms and conditions determined by the rights holder.

Additional Terms & Conditions applicable to each Creative Commons user license:

CC BY: The CC-BY license allows users to copy, to create extracts, abstracts and new works from the Article, to alter and revise the Article and to make commercial use of the Article (including reuse and/or resale of the Article by commercial entities), provided the user gives appropriate credit (with a link to the formal publication through the relevant DOI), provides a link to the license, indicates if changes were made and the licensor is not represented as endorsing the use made of the work. The full details of the license are available at http://creativecommons.org/licenses/by/4.0.

CC BY NC SA: The CC BY-NC-SA license allows users to copy, to create extracts, abstracts and new works from the Article, to alter and revise the Article, provided this is not done for commercial purposes, and that the user gives appropriate credit (with a link to the formal publication through the relevant DOI), provides a link to the license, indicates if changes were made and the licensor is not represented as endorsing the use made of the work. Further, any new works must be made available on the same conditions. The full details of the license are available at http://creativecommons.org/licenses/by-nc-sa/4.0.

CC BY NC ND: The CC BY-NC-ND license allows users to copy and distribute the Article, provided this is not done for commercial purposes and further does not permit distribution of the Article if it is changed or edited in any way, and provided the user gives appropriate credit (with a link to the formal publication through the relevant DOI), provides a link to the license, and that the licensor is not represented as endorsing the use made of the work. The full details of the license are available at http://creativecommons.org/licenses/by-nc-nd/4.0.

Any commercial reuse of Open Access articles published with a CC BY NC SA or CC BY NC ND license requires permission from Elsevier and will be subject to a fee.

Commercial reuse includes:

- Associating advertising with the full text of the Article
- Charging fees for document delivery or access
- Article aggregation
- Systematic distribution via e-mail lists or share buttons

Posting or linking by commercial companies for use by customers of those companies.

20. **Other Conditions**:

v1.8

Questions? customercare@copyright.com or +1-855-239-3415 (toll free in the US) or +1-978-646-2777.

ELSEVIER LICENSE
TERMS AND CONDITIONS

Oct 04, 2016

This Agreement between Xi Chen ("You") and Elsevier ("Elsevier") consists of your license details and the terms and conditions provided by Elsevier and Copyright Clearance Center.

License Number	3961390292836
License date	Oct 03, 2016
Licensed Content Publisher	Elsevier
Licensed Content Publication	Engineering Structures
Licensed Content Title	A finite element study of the effect of vertical loading on the in-plane behavior of concrete masonry infills bounded by steel frames
Licensed Content Author	Xi Chen,Yi Liu
Licensed Content Date	15 June 2016
Licensed Content Volume Number	117
Licensed Content Issue Number	n/a
Licensed Content Pages	12
Start Page	118
End Page	129
Type of Use	reuse in a thesis/dissertation
Portion	full article
Format	both print and electronic
Are you the author of this Elsevier article?	Yes
Will you be translating?	No
Order reference number	
Title of your thesis/dissertation	NUMERICAL STUDY OF THE IN-PLANE BEHAVIOUR OF CONCRETE MASONRY INFILLS BOUNDED BY STEEL FRAMES
Expected completion date	Oct 2016
Estimated size (number of pages)	200
Elsevier VAT number	GB 494 6272 12
Requestor Location	Xi Chen 1094 Wellington Street Apt.1102 Halifax, Nova Scotia, NS B3H2Z9 Canada Attn: Xi Chen
Total	0.00 USD
Terms and Conditions	

INTRODUCTION

1. The publisher for this copyrighted material is Elsevier. By clicking "accept" in connection with completing this licensing transaction, you agree that the following terms and conditions apply to this transaction (along with the Billing and Payment terms and conditions established by Copyright Clearance Center, Inc. ("CCC"), at the time that you opened your Rightslink account and that are available at any time at http://myaccount.copyright.com).

GENERAL TERMS

2. Elsevier hereby grants you permission to reproduce the aforementioned material subject to the terms and conditions indicated.

3. Acknowledgement: If any part of the material to be used (for example, figures) has appeared in our publication with credit or acknowledgement to another source, permission must also be sought from that source. If such permission is not obtained then that material may not be included in your publication/copies. Suitable acknowledgement to the source must be made, either as a footnote or in a reference list at the end of your publication, as follows:

"Reprinted from Publication title, Vol /edition number, Author(s), Title of article / title of chapter, Pages No., Copyright (Year), with permission from Elsevier [OR APPLICABLE SOCIETY COPYRIGHT OWNER]." Also Lancet special credit - "Reprinted from The Lancet, Vol. number, Author(s), Title of article, Pages No., Copyright (Year), with permission from Elsevier."

4. Reproduction of this material is confined to the purpose and/or media for which permission is hereby given.

5. Altering/Modifying Material: Not Permitted. However figures and illustrations may be altered/adapted minimally to serve your work. Any other abbreviations, additions, deletions and/or any other alterations shall be made only with prior written authorization of Elsevier Ltd. (Please contact Elsevier at permissions@elsevier.com)

6. If the permission fee for the requested use of our material is waived in this instance, please be advised that your future requests for Elsevier materials may attract a fee.

7. Reservation of Rights: Publisher reserves all rights not specifically granted in the combination of (i) the license details provided by you and accepted in the course of this licensing transaction, (ii) these terms and conditions and (iii) CCC's Billing and Payment terms and conditions.

8. License Contingent Upon Payment: While you may exercise the rights licensed immediately upon issuance of the license at the end of the licensing process for the transaction, provided that you have disclosed complete and accurate details of your proposed use, no license is finally effective unless and until full payment is received from you (either by publisher or by CCC) as provided in CCC's Billing and Payment terms and conditions. If full payment is not received on a timely basis, then any license preliminarily granted shall be deemed automatically revoked and shall be void as if never granted. Further, in the event that you breach any of these terms and conditions or any of CCC's Billing and Payment terms and conditions, the license is automatically revoked and shall be void as if never granted. Use of materials as described in a revoked license, as well as any use of the materials beyond the scope of an unrevoked license, may constitute copyright infringement and publisher reserves the right to take any and all action to protect its copyright in the materials.

9. Warranties: Publisher makes no representations or warranties with respect to the licensed material.

10. Indemnity: You hereby indemnify and agree to hold harmless publisher and CCC, and their respective officers, directors, employees and agents, from and against any and all claims arising out of your use of the licensed material other than as specifically authorized pursuant to this license.

11. No Transfer of License: This license is personal to you and may not be sublicensed, assigned, or transferred by you to any other person without publisher's written permission.

12. No Amendment Except in Writing: This license may not be amended except in a writing signed by both parties (or, in the case of publisher, by CCC on publisher's behalf).

13. Objection to Contrary Terms: Publisher hereby objects to any terms contained in any purchase order, acknowledgment, check endorsement or other writing prepared by you, which terms are inconsistent with these terms and conditions or CCC's Billing and Payment terms and conditions. These terms and conditions, together with CCC's Billing and Payment terms and conditions (which are incorporated herein), comprise the entire agreement between you and publisher (and CCC) concerning this licensing transaction. In the event of any conflict between your obligations established by these terms and conditions and those established by CCC's Billing and Payment terms and conditions, these terms and conditions shall control.

14. Revocation: Elsevier or Copyright Clearance Center may deny the permissions described in this License at their sole discretion, for any reason or no reason, with a full refund payable to you. Notice of such denial will be made using the contact information provided by you. Failure to receive such notice will not alter or invalidate the denial. In no event will Elsevier or Copyright Clearance Center be responsible or liable for any costs, expenses or damage incurred by you as a result of a denial of your permission request, other than a refund of the amount(s) paid by you to Elsevier and/or Copyright Clearance Center for denied permissions.

LIMITED LICENSE

The following terms and conditions apply only to specific license types:

15. **Translation**: This permission is granted for non-exclusive world **English** rights only unless your license was granted for translation rights. If you licensed translation rights you may only translate this content into the languages you requested. A professional translator must perform all translations and reproduce the content word for word preserving the integrity of the article.

16. **Posting licensed content on any Website**: The following terms and conditions apply as follows: Licensing material from an Elsevier journal: All content posted to the web site must maintain the copyright information line on the bottom of each image; A hyper-text must be included to the Homepage of the journal from which you are licensing at http://www.sciencedirect.com/science/journal/xxxxx or the Elsevier homepage for books at http://www.elsevier.com; Central Storage: This license does not include permission for a scanned version of the material to be stored in a central repository such as that provided by Heron/XanEdu.

Licensing material from an Elsevier book: A hyper-text link must be included to the Elsevier homepage at http://www.elsevier.com . All content posted to the web site must maintain the copyright information line on the bottom of each image.

Posting licensed content on Electronic reserve: In addition to the above the following clauses are applicable: The web site must be password-protected and made available only to bona fide students registered on a relevant course. This permission is granted for 1 year only. You may obtain a new license for future website posting.

17. **For journal authors:** the following clauses are applicable in addition to the above:

Preprints:

A preprint is an author's own write-up of research results and analysis, it has not been peer-reviewed, nor has it had any other value added to it by a publisher (such as formatting, copyright, technical enhancement etc.).

Authors can share their preprints anywhere at any time. Preprints should not be added to or enhanced in any way in order to appear more like, or to substitute for, the final versions of articles however authors can update their preprints on arXiv or RePEc with their Accepted Author Manuscript (see below).

If accepted for publication, we encourage authors to link from the preprint to their formal publication via its DOI. Millions of researchers have access to the formal publications on ScienceDirect, and so links will help users to find, access, cite and use the best available version. Please note that Cell Press, The Lancet and some society-owned have different preprint policies. Information on these policies is available on the journal homepage.

Accepted Author Manuscripts: An accepted author manuscript is the manuscript of an article that has been accepted for publication and which typically includes author-incorporated changes suggested during submission, peer review and editor-author communications.
Authors can share their accepted author manuscript:

- immediately
  - via their non-commercial person homepage or blog
  - by updating a preprint in arXiv or RePEc with the accepted manuscript
  - via their research institute or institutional repository for internal institutional uses or as part of an invitation-only research collaboration work-group
  - directly by providing copies to their students or to research collaborators for their personal use
  - for private scholarly sharing as part of an invitation-only work group on commercial sites with which Elsevier has an agreement
- after the embargo period
  - via non-commercial hosting platforms such as their institutional repository
  - via commercial sites with which Elsevier has an agreement

In all cases accepted manuscripts should:

- link to the formal publication via its DOI
- bear a CC-BY-NC-ND license - this is easy to do
- if aggregated with other manuscripts, for example in a repository or other site, be shared in alignment with our hosting policy not be added to or enhanced in any way to appear more like, or to substitute for, the published journal article.

Published journal article (JPA): A published journal article (PJA) is the definitive final record of published research that appears or will appear in the journal and embodies all value-adding publishing activities including peer review co-ordination, copy-editing, formatting, (if relevant) pagination and online enrichment.
Policies for sharing publishing journal articles differ for subscription and gold open access articles:
Subscription Articles: If you are an author, please share a link to your article rather than the full-text. Millions of researchers have access to the formal publications on ScienceDirect, and so links will help your users to find, access, cite, and use the best available version.
Theses and dissertations which contain embedded PJAs as part of the formal submission can be posted publicly by the awarding institution with DOI links back to the formal publications on ScienceDirect.
If you are affiliated with a library that subscribes to ScienceDirect you have additional private sharing rights for others' research accessed under that agreement. This includes use for classroom teaching and internal training at the institution (including use in course packs and courseware programs), and inclusion of the article for grant funding purposes.
Gold Open Access Articles: May be shared according to the author-selected end-user license and should contain a CrossMark logo, the end user license, and a DOI link to the formal publication on ScienceDirect.
Please refer to Elsevier's posting policy for further information.
18. **For book authors** the following clauses are applicable in addition to the above:
Authors are permitted to place a brief summary of their work online only. You are not allowed to download and post the published electronic version of your chapter, nor may you scan the printed edition to create an electronic version. **Posting to a repository:** Authors are permitted to post a summary of their chapter only in their institution's repository.
19. **Thesis/Dissertation**: If your license is for use in a thesis/dissertation your thesis may be submitted to your institution in either print or electronic form. Should your thesis be

published commercially, please reapply for permission. These requirements include permission for the Library and Archives of Canada to supply single copies, on demand, of the complete thesis and include permission for Proquest/UMI to supply single copies, on demand, of the complete thesis. Should your thesis be published commercially, please reapply for permission. Theses and dissertations which contain embedded PJAs as part of the formal submission can be posted publicly by the awarding institution with DOI links back to the formal publications on ScienceDirect.

Elsevier Open Access Terms and Conditions

You can publish open access with Elsevier in hundreds of open access journals or in nearly 2000 established subscription journals that support open access publishing. Permitted third party re-use of these open access articles is defined by the author's choice of Creative Commons user license. See our open access license policy for more information.

Terms & Conditions applicable to all Open Access articles published with Elsevier:

Any reuse of the article must not represent the author as endorsing the adaptation of the article nor should the article be modified in such a way as to damage the author's honour or reputation. If any changes have been made, such changes must be clearly indicated.

The author(s) must be appropriately credited and we ask that you include the end user license and a DOI link to the formal publication on ScienceDirect.

If any part of the material to be used (for example, figures) has appeared in our publication with credit or acknowledgement to another source it is the responsibility of the user to ensure their reuse complies with the terms and conditions determined by the rights holder.

Additional Terms & Conditions applicable to each Creative Commons user license:

CC BY: The CC-BY license allows users to copy, to create extracts, abstracts and new works from the Article, to alter and revise the Article and to make commercial use of the Article (including reuse and/or resale of the Article by commercial entities), provided the user gives appropriate credit (with a link to the formal publication through the relevant DOI), provides a link to the license, indicates if changes were made and the licensor is not represented as endorsing the use made of the work. The full details of the license are available at http://creativecommons.org/licenses/by/4.0.

CC BY NC SA: The CC BY-NC-SA license allows users to copy, to create extracts, abstracts and new works from the Article, to alter and revise the Article, provided this is not done for commercial purposes, and that the user gives appropriate credit (with a link to the formal publication through the relevant DOI), provides a link to the license, indicates if changes were made and the licensor is not represented as endorsing the use made of the work. Further, any new works must be made available on the same conditions. The full details of the license are available at http://creativecommons.org/licenses/by-nc-sa/4.0.

CC BY NC ND: The CC BY-NC-ND license allows users to copy and distribute the Article, provided this is not done for commercial purposes and further does not permit distribution of the Article if it is changed or edited in any way, and provided the user gives appropriate credit (with a link to the formal publication through the relevant DOI), provides a link to the license, and that the licensor is not represented as endorsing the use made of the work. The full details of the license are available at http://creativecommons.org/licenses/by-nc-nd/4.0.

Any commercial reuse of Open Access articles published with a CC BY NC SA or CC BY NC ND license requires permission from Elsevier and will be subject to a fee.

Commercial reuse includes:

- Associating advertising with the full text of the Article
- Charging fees for document delivery or access
- Article aggregation
- Systematic distribution via e-mail lists or share buttons

Posting or linking by commercial companies for use by customers of those companies.

20. **Other Conditions**:

v1.8

Questions? customercare@copyright.com or +1-855-239-3415 (toll free in the US) or +1-978-646-2777.